PROJECT ADMINISTRATION DATA SHEET

[X] ORIGINAL   [ ] REVISION NO. _____

Project No. __E-25-M13 (R6184-0A0)__   GTRC/~~GIT~~ DATE _9 / 16/ 86_

Project Director: __Dr. David L. McDowell__   School/~~Lab~~ _MECH ENG_

Sponsor: __General Motor Corporation, Allison Gas Turbine Operations__

Type Agreement: __Purchase Order No. H636356 and Std. Research Agreement__

Award Period: From __7/1/86__ To __~~6/30/87~~__ (Performance) __6/30/87__ (Reports)

Sponsor Amount: This Change _7/30/88_   Total to Date

  Estimated: $ _____ $ __211,818__

  Funded: $ _____ $ __59,825 (through 6/30/87__

Cost Sharing Amount: $ __17,985__   Cost Sharing No: __E-25-335__

Title: __Damage Rate Approaches for Thermomechanical Fatigue of Superalloys.__

ADMINISTRATIVE DATA   OCA Contact __E. Faith Gleason__

1) Sponsor Technical Contact: 2) Sponsor Admin/Contractual Matters:

__Dr. W. E. Schneider/T-10__   __Darrell L. Mackey/U02__

__Allison ~~Motors Corporation~~__   ⟶   __Allison Gas Turbine Operations__

__General Motors Corporation__   __General Motors Corporation__

__2001 South Tibbs Avenue__   __P. O. Box 420__

__Indianapolis, IN 46241__   __Indianapolis, IN 46206-0420__

                                __(317)242-6954__

Defense Priority Rating: __N/A__   Military Security Classification: _____

                                (or) Company/Industrial Proprietary: __N/A__

RESTRICTIONS

See Attached _____ Supplemental Information Sheet for Additional Requirements.

Travel: Foreign travel must have prior approval — Contact OCA in each case. Domestic travel requires sponsor

  approval where total will exceed greater of $500 or 125% of approved proposal budget category.

Equipment: Title vests with __Sponsor, however none proposed__

COMMENTS:

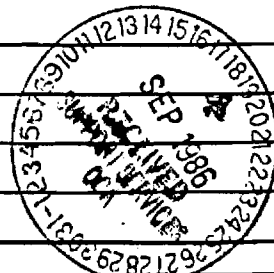 1st year of anticipated 3 year program.

COPIES TO: SPONSOR'S I. D. NO. _____

Project Director   Procurement/GTRI Supply Services   GTRC
Research Administrative Network   Research Security Services   Library
Research Property Management   Reports Coordinator (OCA)   Project File
Accounting   Research Communications (2)   Other _____

GEORGIA INSTITUTE OF TECHNOLOGY
OFFICE OF CONTRACT ADMINISTRATION

NOTICE OF PROJECT CLOSEOUT

Date __4/17/89__

Project No. __E-25-M13__   Center No. __R6184-0A0__

Project Director __D. L. McDowell__   School/Lab __ME__

Sponsor __General Motors Corporation__

Contract/Grant No. __H636356 and Mod H723543__   GTRC __XX__ GIT ____

Prime Contract No. ____

Title __Damage Rate Approaches for Thermomechanical Fatigue of Superalloys__

Effective Completion Date __9/30/88__ (Performance) __9/30/88__ (Reports)

Closeout Actions Required:

- __ None
- __ Final Invoice or Copy of Last Invoice
- __ Final Report of Inventions and/or Subcontracts
- __ Government Property Inventory & Related Certificate
- __ Classified Material Certificate
- __ Release and Assignment
- __ Other ____

Includes Subproject No(s). ____

Subproject Under Main Project No. ____

Continues Project No. ____   Continued by Project No. __E-25-M77__

Distribution:

Project Director	X Reports Coordinator (OCA)
Administrative Network	X GTRC
Accounting	X Project File
Procurement/GTRI Supply Services	2 Contract Support Division (OCA)
Research Property Management	__ Other ____
Research Security Services	

LETTER REPORT

"DAMAGE RATE APPROACHES FOR THERMOMECHANICAL FATIGUE
OF SUPERALLOYS"

By David L. McDowell
Principal Investigator
Project # E-25-M13
General Motors PO# H636356

Submitted to Allison Gas Turbine Operations, General Motors
Corporation

Sponsor Technical Contact:

Dr. W.E. Schneider/T-10
Allison Gas Turbine Operations
General Motors Corporation
2001 South Tibbs Ave.
Indianapolis, IN 46241
(317) 242-7703

Sponsor Administration and Contractual Matters:

Darrell L. Mackey/U02
Allison Gas Turbine Operations
General Motors Corporation
P.O. Box 420
Indianapolis, IN 46206-0420
(317) 242-6954

October 31, 1986

Dr. W.E. Schneider/T-10
Allison Gas Turbine Operations
General Motors Corp.
2001 South Tibbs Avenue
Indianapolis, IN 46241

Dear Dr. Schneider:

This report summarizes the activities of our effort on GM PO#H636356, "Damage Rate Approaches for Thermomechanical Fatigue of Superalloys" from the contract starting date to October 31, 1986.

As you know, the MAR-M 246 specimens have not yet been received from Allison by this date due to problems with micro-porosity in the castings. In spite of these difficulties with specimen manufacture, the research team at Georgia Tech has been fully organized to begin the testing program. A Ph.D. level research engineer has been assigned to the project at 1/3 time and is aiding in planning, supervision and timely completion of the overall experimental program in addition to data analysis. In addition, an M.S. student, supported by matching funds from Georgia Tech, is engaged in the fatigue component of the experimental program. A third student, supported by funds from the State of Georgia, has worked on the creep component of the experimental program of this project in addition to another project. It should be noted that no direct charges were made to this project prior to September 15, 1986.

A November 1, 1986 starting date for testing was requested and granted in the Georgia Tech Fracture and Fatigue Research Laboratory (FFRL). Delay in specimen manufacture, however, has postponed this starting date. I would again like to stress that timely acquistion of the specimens is important, since the FFRL has a heavy scheduling demand and too lengthy a delay may result in a corresponding 1-3 month delay in test starting date.

The following tasks have been accomplished in the program to date:

(1)   A Ph.D. research engineer and 1-2 graduate students have been brought into the program.

(2)   The students are engaged in reading the literature concerning damage rate approaches, creep-fatigue interaction, and behavior of Ni-base alloys including MAR-M 246.

(3)   We are engaged in modification of an existing creep frame
        in the FFRL for testing the button-end specimens, and
        pursuing data acquisition and control algorithms for long-
        range use in this project.
(3)   The research engineer has spent a significant amount of
        time organizing the test matrix and scheduling laboratory
        use. Initial testing will be confined to the baseline test
        matrix in the original proposal and will consist of the
        high temperature creep tests, step-stress creep tests,
        monotonic tests, and some of the fatigue tests at two
        strain rates in air.

        I will continue to contact you regarding the status of the
specimens.

                                Sincerely,

                                David L. McDowell
                                Principal Investigator

LETTER REPORT

"DAMAGE RATE APPROACHES FOR THERMOMECHANICAL FATIGUE
OF SUPERALLOYS"

By David L. McDowell
Principal Investigator
Project # E-25-M13
General Motors PO# H636356

Submitted to Allison Gas Turbine Operations, General Motors
Corporation

Sponsor Technical Contact:

Dr. W.E. Schneider/T-10
Allison Gas Turbine Operations
General Motors Corporation
2001 South Tibbs Ave.
Indianapolis, IN   46241
(317) 242-7703

Sponsor Administration and Contractual Matters:

Darrell L. Mackey/U02
Allison Gas Turbine Operations
General Motors Corporation
P.O. Box 420
Indianapolis, IN   46206-0420
(317) 242-6954

November 30, 1986

Dr. W.E. Schneider/T-10
Allison Gas Turbine Operations
General Motors Corp.
2001 South Tibbs Avenue
Indianapolis, IN 46241

Dear Dr. Schneider:

This report summarizes the activities of our effort on GM PO#H636356, "Damage Rate Approaches for Thermomechanical Fatigue of Superalloys" for the period November 1, 1986 to November 30, 1986.

The MAR-M 246 specimens have not yet been received from Allison. The team of graduate students have been working on experimental methodology, design of the creep grip adaptor, developing an induction coil with a uniform temperature distribution for this specimen geometry, and reading the literature on the effects of environmental fatigue in Ni-base superalloys. We have machined several stainless steel specimens with the same design as the MAR-M 246 specimens we will receive from GM to develop consistent baseline test matrix procedures among the students involved and to proceed with induction coil development.

Sincerely,

David L. McDowell
Principal Investigator

LETTER REPORT

"DAMAGE RATE APPROACHES FOR THERMOMECHANICAL FATIGUE
OF SUPERALLOYS"

By David L. McDowell
Principal Investigator
Project # E-25-M13
General Motors PO# H636356

February 10, 1987

Submitted to Allison Gas Turbine Operations, General Motors
Corporation

Sponsor Technical Contact:

Dr. W.E. Schneider/T-10
Allison Gas Turbine Operations
General Motors Corporation
2001 South Tibbs Ave.
Indianapolis, IN 46241
(317) 242-7703

Sponsor Administration and Contractual Matters:

Darrell L. Mackey/U02
Allison Gas Turbine Operations
General Motors Corporation
P.O. Box 420
Indianapolis, IN 46206-0420
(317) 242-6954

February 10, 1987

Dr. W.E. Schneider/T-10
Allison Gas Turbine Operations
General Motors Corp.
2001 South Tibbs Avenue
Indianapolis, IN 46241

Dear Dr. Schneider:

This report summarizes the activities of our effort on GM PO#H636356, "Damage Rate Approaches for Thermomechanical Fatigue of Superalloys" for the period December 1, 1986 to January 29, 1987.

A total of 19 MAR-M 246 specimens were received in January 1987 along with a 2" diameter cast billet for machining adaptors for the creep machine grips. Currently, we are electro-polishing the specimens to achieve a surface finish appropriate for fatigue testing. A drawing of the creep grip adaptor has been sent out for a quote; we have fabricated an identical type 304 stainless steel adaptor in our shop, but do not have the equipment in-house to machine the MAR-M 246.

We have constructed an induction coil that we think will result in a suitably uniform temperature field within the specimens. As soon as the polishing is completed, we will begin high temperature baseline fatigue tests in air at two different strain rates in addition to several monotonic tests at different strain rates. We propose that the higher isothermal test temperature be 1652°F (900°C) to permit comparison with existing data at that temperature*, but would appreciate your feedback regarding rationale for any other temperature at this time. The strain rates will be in the range of $10^{-3} - 10^{-5}$ sec^{-1}.

Sincerely,

David L. McDowell
Principal Investigator

---

* Harrison, G.F., Tilly, G.P., "The Static and Cyclic Creep Properties of Three Forms of a Cast Nickel Alloy," Proc. Int. Conf. on Creep and Fatigue in Elevated Temperature Applications, ASME, Philadelphia, PA, Vol. 1, 1975.

LETTER REPORT

"DAMAGE RATE APPROACHES FOR THERMOMECHANICAL FATIGUE
OF SUPERALLOYS"

By David L. McDowell
Principal Investigator
Project # E-25-M13
General Motors PO# H636356

March 6, 1987

Submitted to Allison Gas Turbine Operations, General Motors
Corporation

Sponsor Technical Contact:

Dr. W.E. Schneider/T-10
Allison Gas Turbine Operations
General Motors Corporation
2001 South Tibbs Ave.
Indianapolis, IN 46241
(317) 242-7703

Sponsor Administration and Contractual Matters:

Darrell L. Mackey/U02
Allison Gas Turbine Operations
General Motors Corporation
P.O. Box 420
Indianapolis, IN 46206-0420
(317) 242-6954

March 6, 1987

Dr. W.E. Schneider/T-10
Allison Gas Turbine Operations
General Motors Corp.
2001 South Tibbs Avenue
Indianapolis, IN 46241

Dear Dr. Schneider:

This report summarizes the activities of our effort on GM PO#H636356, "Damage Rate Approaches for Thermomechanical Fatigue of Superalloys" for the period January 30, 1987 to February 28, 1987.

A total of 24 MAR-M 246 specimens were received in January 1987 along with a 2" diameter cast billet for machining adaptors for the creep machine grips. It should be noted that the last report for January indicated we received only 19 specimens; some packages, though, contained two specimens. The specimens as-received had rather severe circumferential machining/polishing marks which almost certainly would have significantly degraded fatigue life. We attempted to electro-polish the specimens, but found it extremely difficult to find a current level which would not preferentially etch either the grain boundaries or the inter-dendritic regions. Electro-polishing of these specimens may prove to be a viable way of etching the microstructure for post-test examination of damage. Instead of the electro-polishing process, we went to a sequence of mechanical polishing steps, starting at a somewhat coarse grit (400 grit paper dry, 600 wet, 6 micron diamond paste, 1 micron diamond paste) and finishing with diamond paste. Each specimen requires approximately 1-2 hrs.

In view of the time required for polishing each specimen, I would like to request that all specimens cast by Allison in the future be polished there, at least to the 6 micron diamond paste stage. We can do the finish polishing, but the condition of the gage sections of the first 24 as-received specimens was not appropriate for fatigue testing.

As you know, a quote was obtained on the machining of the creep grip adaptor; we have fabricated an identical type 304 stainless steel adaptor in our shop, and have tried to do the same with the MAR-M 246 with little success. Our carbide tip tools have failed. Hence, we are going to send the adaptor out for machining at a cost of $900.

We have initiated the testing program, having just completed one monotonic and three LCF tests at 900°C at a strain rate of

10^{-3} sec^{-1}. In these early tests, we have had some problems with fracture in the fillet region of the specimens, though the Coffin-Manson behavior is quite consistent with results others have obtained on DS MAR-M 246 in our lab. Since we did not previously polish the fillets to the same extent as the gage section, we suspect small circumferential scratches in the fillet region contributed to the fillet cracking. We are taking two steps to correct the problem. Firstly, we are now polishing the fillets to the same extent as the gage section (we would request Allison to do the same); secondly, we have put great effort into accurate alignment of the machine, and are now in the process of strain gaging a dummy steel specimen to ensure that all grip surfaces are flat to within tolerance.

Please note the test matrix for the first 20 specimens shown in the attached Table. The results of a number of these experiments will be reported in detail in the next report.

Sincerely,

David L. McDowell
Principal Investigator

900°C Test Matrix for First Set of Specimens
Environment: Laboratory Air

Strain-Controlled:

Test Type	$\dot{\epsilon}$ (sec^{-1})	$\Delta\epsilon/2$	ϵ_{max}
Monotonic			
M1	10^{-3}		.05
M2	10^{-2}		.10 or failure
M3	10^{-5}		.10 or failure
M4	10^{-4}		.10 or failure
Fatigue			
F1	10^{-3}	.01	
F2		.008	
F3		.006	
F4		.004	
F5		Sequence: .002 followed by .004	
F6	10^{-2}	.01	
F7		.008	
F8		.006	
F9		.004	
F10		.003	
F11	10^{-4}	.01	
F12		.008	
F13		.006	
F14		.004	

Creep tests:

Test type	Engr. Stress
Constant Load Creep	
F15	60 ksi to rupture.
F16	43.5 ksi to rupture.
Sequence Creep	
F17	1/2 rupture time at 60 ksi; switch to 43.5 ksi and hold to rupture.

LETTER REPORT

"DAMAGE RATE APPROACHES FOR THERMOMECHANICAL FATIGUE
OF SUPERALLOYS"

By David L. McDowell
Principal Investigator

R.L.T. Oehmke
Research Engineer

Project # E-25-M13
General Motors PO# H636356

April 8, 1987

Submitted to Allison Gas Turbine Operations, General Motors
Corporation

Sponsor Technical Contact:

Dr. W.E. Schneider/T-10
Allison Gas Turbine Operations
General Motors Corporation
2001 South Tibbs Ave.
Indianapolis, IN 46241
(317) 242-7703

Sponsor Administration and Contractual Matters:

Darrell L. Mackey/U02
Allison Gas Turbine Operations
General Motors Corporation
P.O. Box 420
Indianapolis, IN 46206-0420
(317) 242-6954

April 8, 1987

Dr. W.E. Schneider/T-10
Allison Gas Turbine Operations
General Motors Corp.
2001 South Tibbs Avenue
Indianapolis, IN 46241

Dear Dr. Schneider:

This report summarizes the activities of our effort on GM PO#H636356, "Damage Rate Approaches for Thermomechanical Fatigue of Superalloys" for the period March 1, 1987 to March 31, 1987.

The MAR-M 246 adaptor for the creep tests is being machined by an external agency. Completion of this task should take 2-3 weeks. Concurrently, we are modifying one of the existing creep frames so we can run some long-term, uninterrupted creep tests. The creep tests should begin in the next month or so.

In this report, we present the data from the first monotonic test of the matrix in Table I in addition to five of the fatigue tests at 900°C. It should be noted that specimen F8 (GM ID 942-5) buckled at 118 cycles; this buckling event occurred by virtue of extensometer instability after the failure crack had formed. As mentioned in the last report, we have had some problems with fracture in the fillet or near-fillet region of the specimens in these early tests. To correct this situation, we have designed and machined a restraining collar with a teflon bushing for the servohydraulic ram in the low pressure seal region to maintain less than one mil lateral deflection under compressive load. Though such a modification is somewhat unusual for routine fatigue testing, this material has very high strength and low ductility, and as a result is quite unforgiving in terms of misalignment. Hopefully, this procedure will correct problems with cracking in the fillet or near-fillet region.

Attached please find plots of some of the hysteresis loops acquired at various cycle numbers for each specimen in addition to a monotonic test run to approximately 5% strain at a rate of 0.001 sec^{-1} (specimen M1). It is apparent that the cyclic stress-strain response is immediately stable; negligible cyclic hardening or softening is observed to occur, even for a total strain range as high as 2%. This result is somewhat surprising given the very high temperature of these tests. We are not yet fully able to assess strain rate sensitivity, since these experiments were conducted predominately at a single strain rate. Note that the hysteresis loops for specimen F8 indicate a control instability in the unloading regimes of the loops, which may have contributed to the eventual buckling problem.

Also attached please find strain-life and stress-life curves for the three specimens tested to date at a strain rate of 0.001

sec^{-1}; though two of the specimens broke in the fillet region, the scatter about a best linear log-log fit is quite small. Additionally, the slope of the regression fit stress-life curve is within 7% of published values for conventionally cast MAR-M 246 [1]. The lives at the same strain amplitudes are comparable to those obtained by Dr. Antolovich and his students in our lab on DS MAR-M 246 at a similar temperature level. Hence, we suspect that the data may be useful.

It is interesting to note that the transition fatigue life ($\Delta \epsilon^{e} = \Delta \epsilon^{p}$) for this material at this strain rate and temperature is less than 36 reversals; hence, the problem is one of resistance based on strength, i.e. predominately "high cycle" fatigue. This feature may ultimately lead us to cast the fatigue damage rate (microcrack initiation/growth) in terms of stresses rather than strains, as has been done (albeit in a different framework) by the French for similar materials.

We are also continuously measuring the stress amplitude in each test with a strip chart recorder. These measurements reveal that the specimen stiffness does not change appreciably until very near the end of each test. Hence, propagation of small cracks across the specimen occurs rapidly and the great majority of the life is spent in the development of short cracks, as expected for this material.

Sincerely,

David L. McDowell
Principal Investigator

1. Harrison, G.F. and Tilly, G.P., "The Static and Cyclic Creep Properties of Three Forms of a Cast Nickel Alloy," Creep and Fatigue in Elevated Temperature Applications, International Conf. of ASME, Vol. 1, Philadelphia, 1973, Sheffield, 1974, 1975.

TABLE I

900°C Test Matrix for First Set of Specimens
Environment: Laboratory Air

Strain-Controlled:

Test Type		ϵ rate (sec^{-1})	$\Delta\epsilon/2$	ϵ_{max}	$\Delta\sigma/2$ (MPa)	$2N_f$
Monotonic						
	M1*	10^{-3}		.0475		
	M2	10^{-2}		.10 or failure		
	M3	10^{-3}		.10 or failure		
	M4	10^{-4}		.10 or failure		
Fatigue						
	F1*	10^{-3}	.0097		863	36
	F2*		.0076		725	90
	F3		.006			
	F4*		.004		550	1166
	F5*		Sequence:0.002 followed by 0.004		284	144724
	F6	10^{-2}	.01			
	F7		.008			
	F8*		.0063		780	236**
	F9		.004			
	F10		.003			
	F11	10^{-4}	.01			
	F12		.008			
	F13		.006			
	F14		.004			

Creep tests:	
Test type	**Engr. Stress**
Constant Load Creep	
F15	60 ksi to rupture.
F16	43.5 ksi to rupture.
Sequence Creep	
F17	1/2 rupture time at 60 ksi; switch to 43.5 ksi and hold to rupture.

* Denotes completed experiment.
** Buckled after failure crack formed.

MAR-M 246   900 DEG C   RATE .001 /SEC
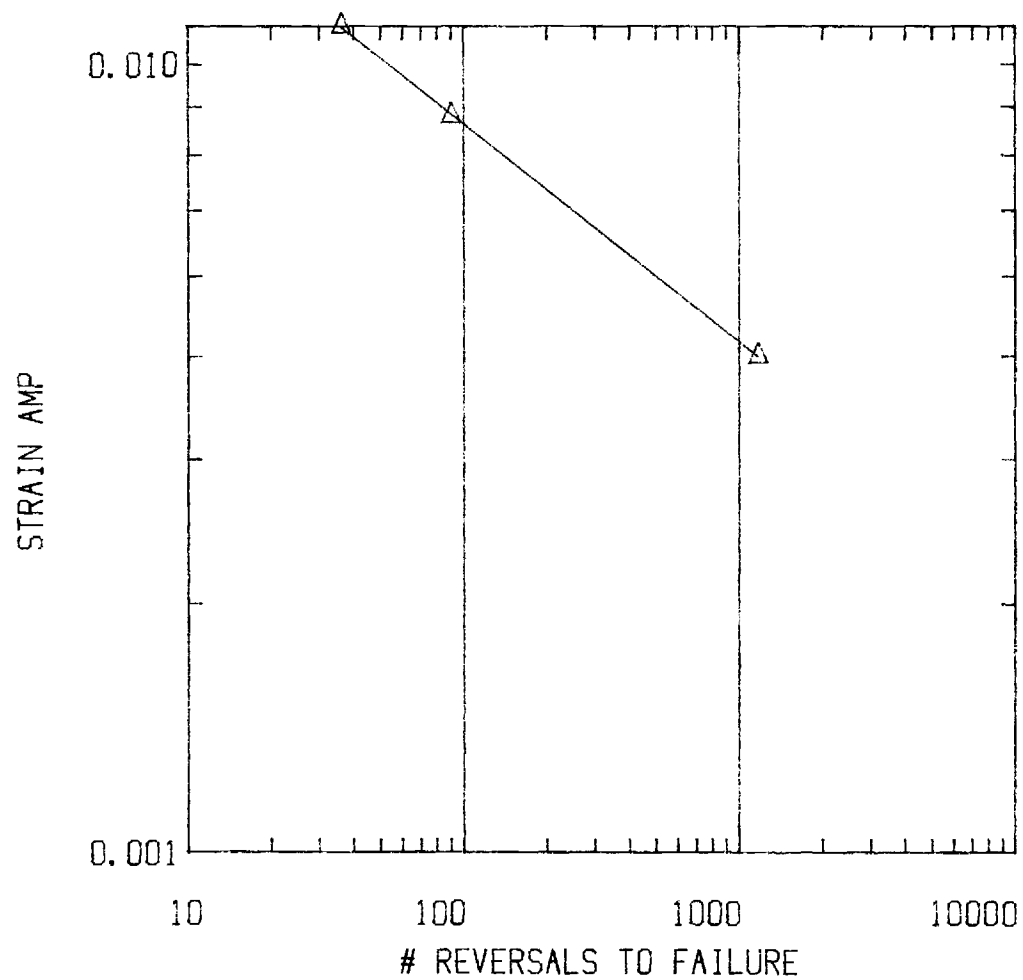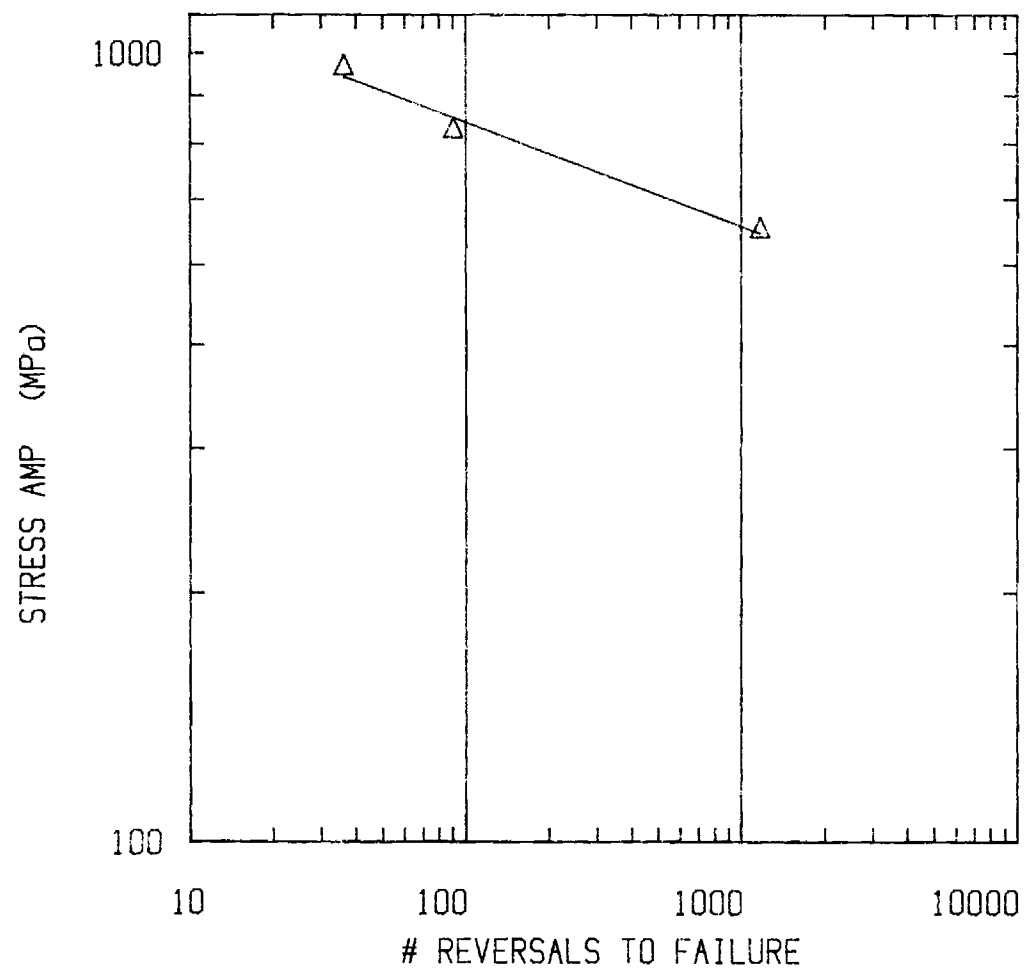
MAR-M 246   900 DEG C   RATE .001 /SEC

MONOTONIC   SPECIMEN M1   RATE .001 /SEC
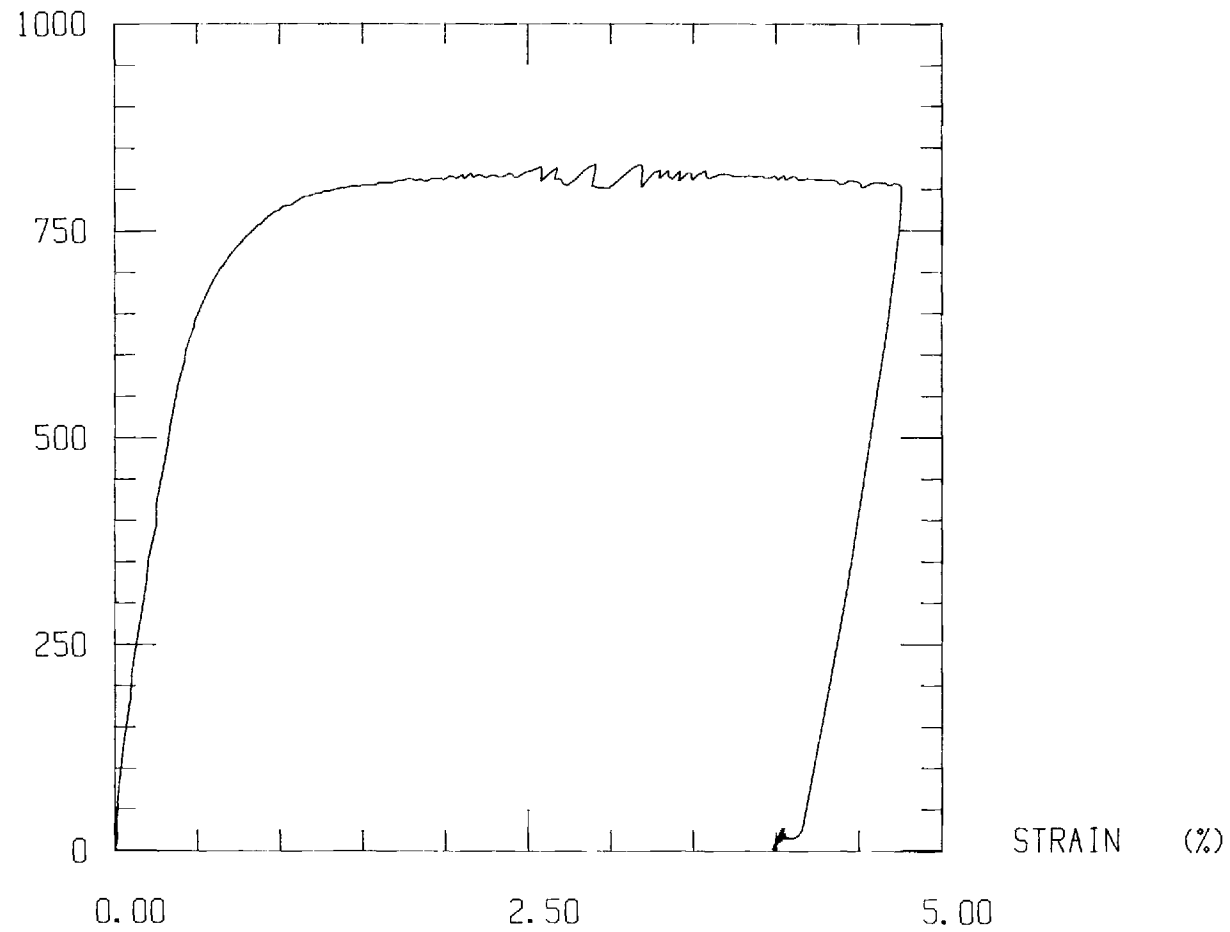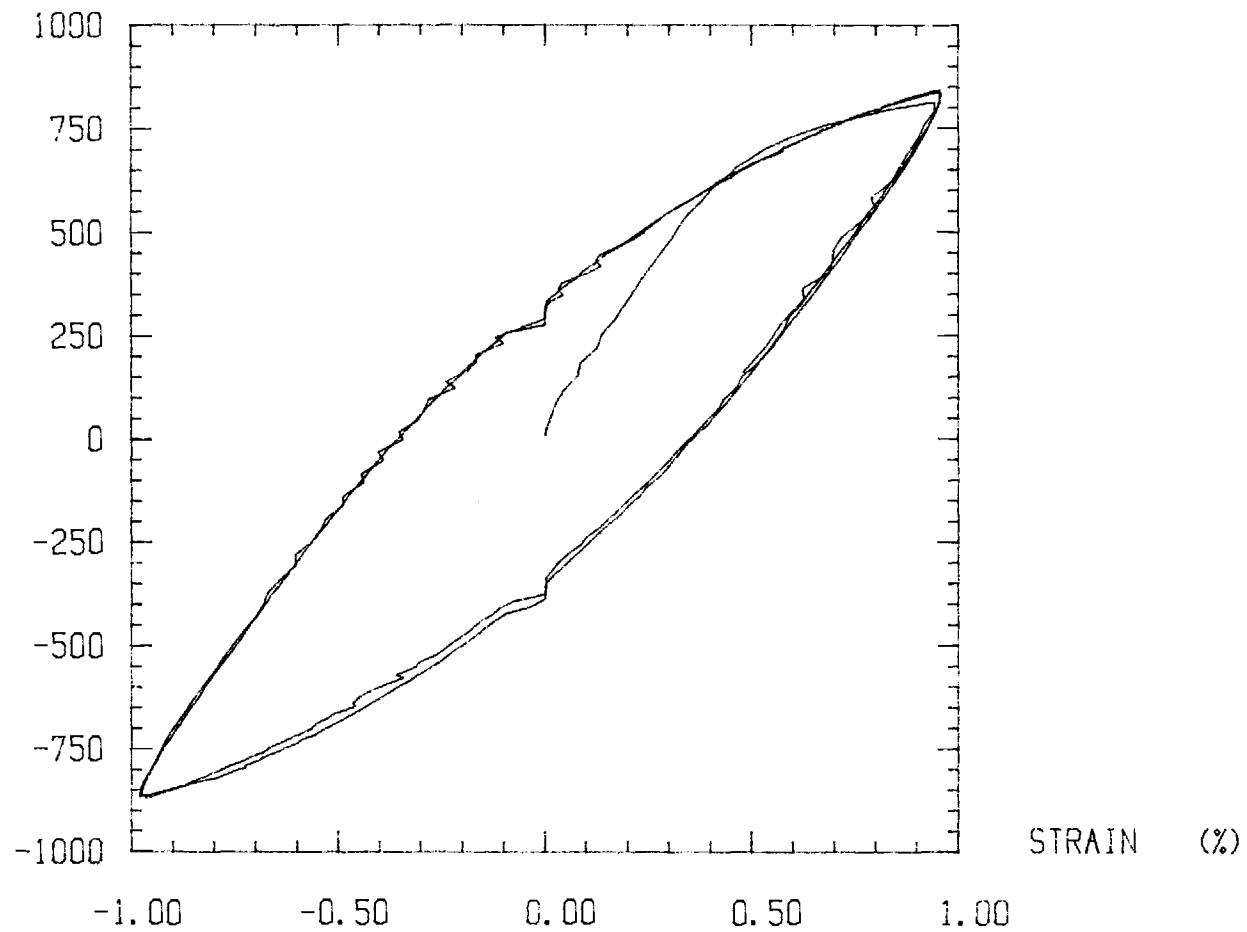
STRESS   (MPa)

CYCLE #1-2   SPECIMEN F1   RATE = .001 /SEC

STRESS   (MPa)

STRAIN   (%)

CYCLE #16-17   SPECIMEN F1   RATE =   .001 /SEC
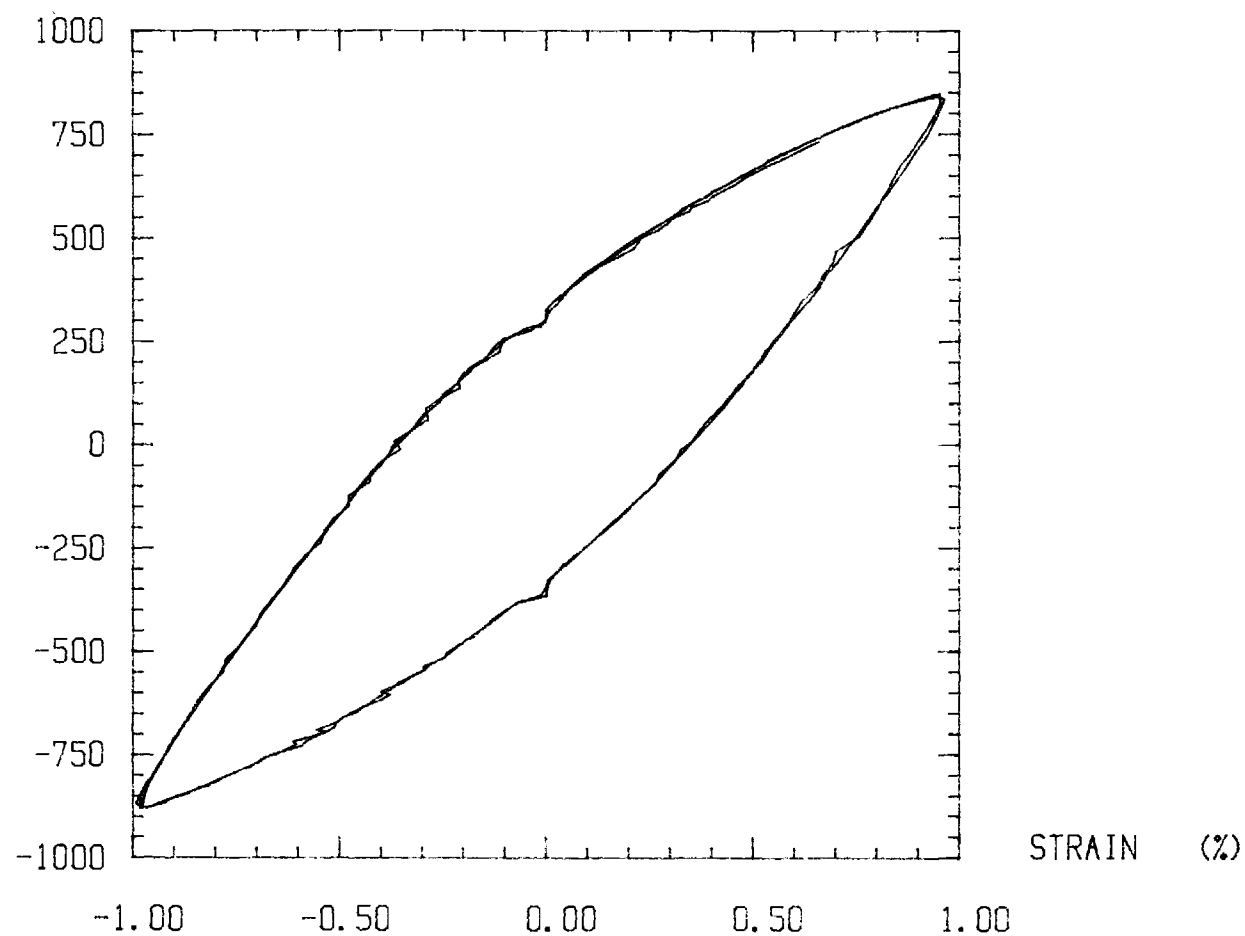
CYCLE #1-2   SPECIMEN F2   RATE =   .001 /SEC
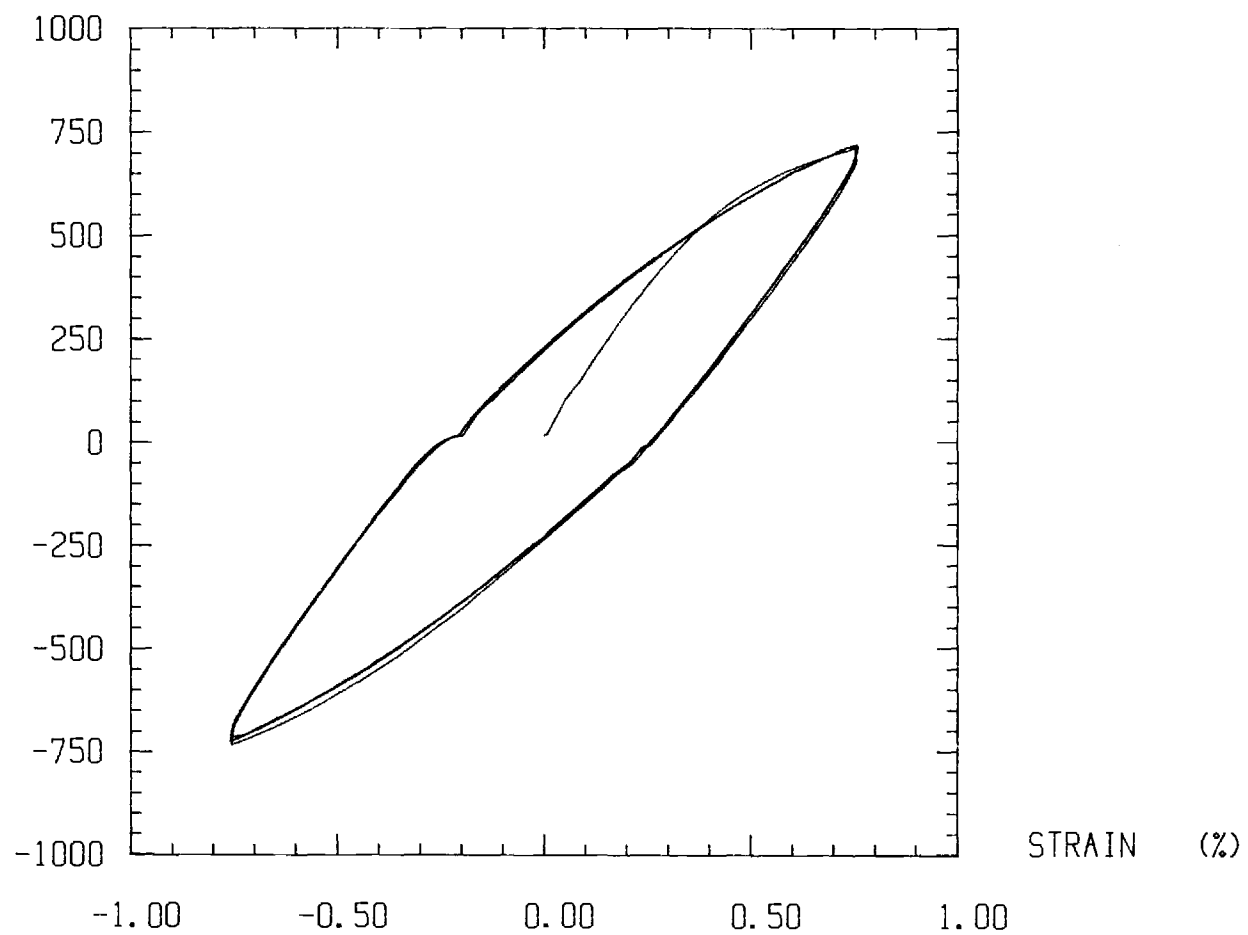
STRESS   (MPa)

CYCLE #8-9   SPECIMEN F2   RATE =   .001 /SEC
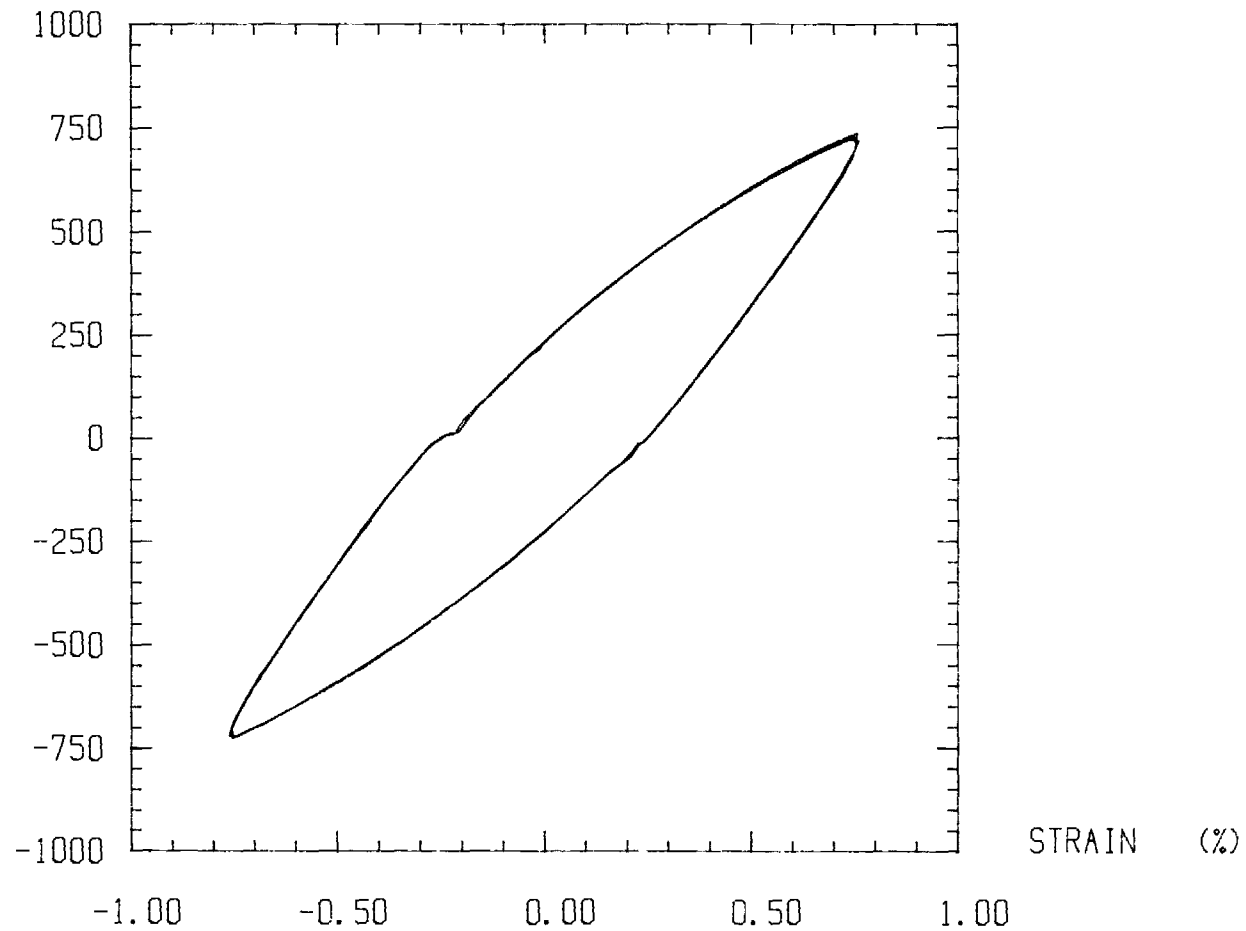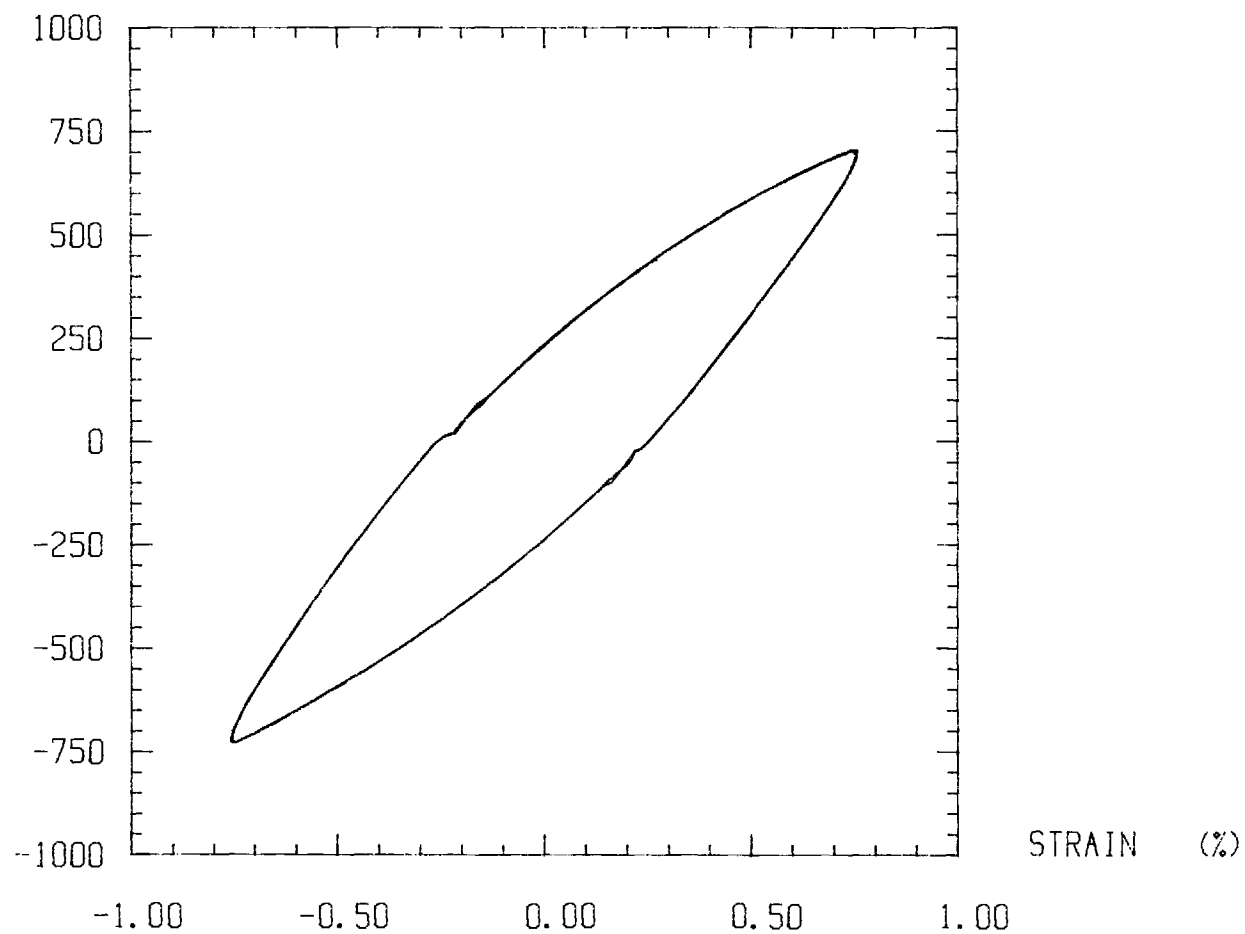
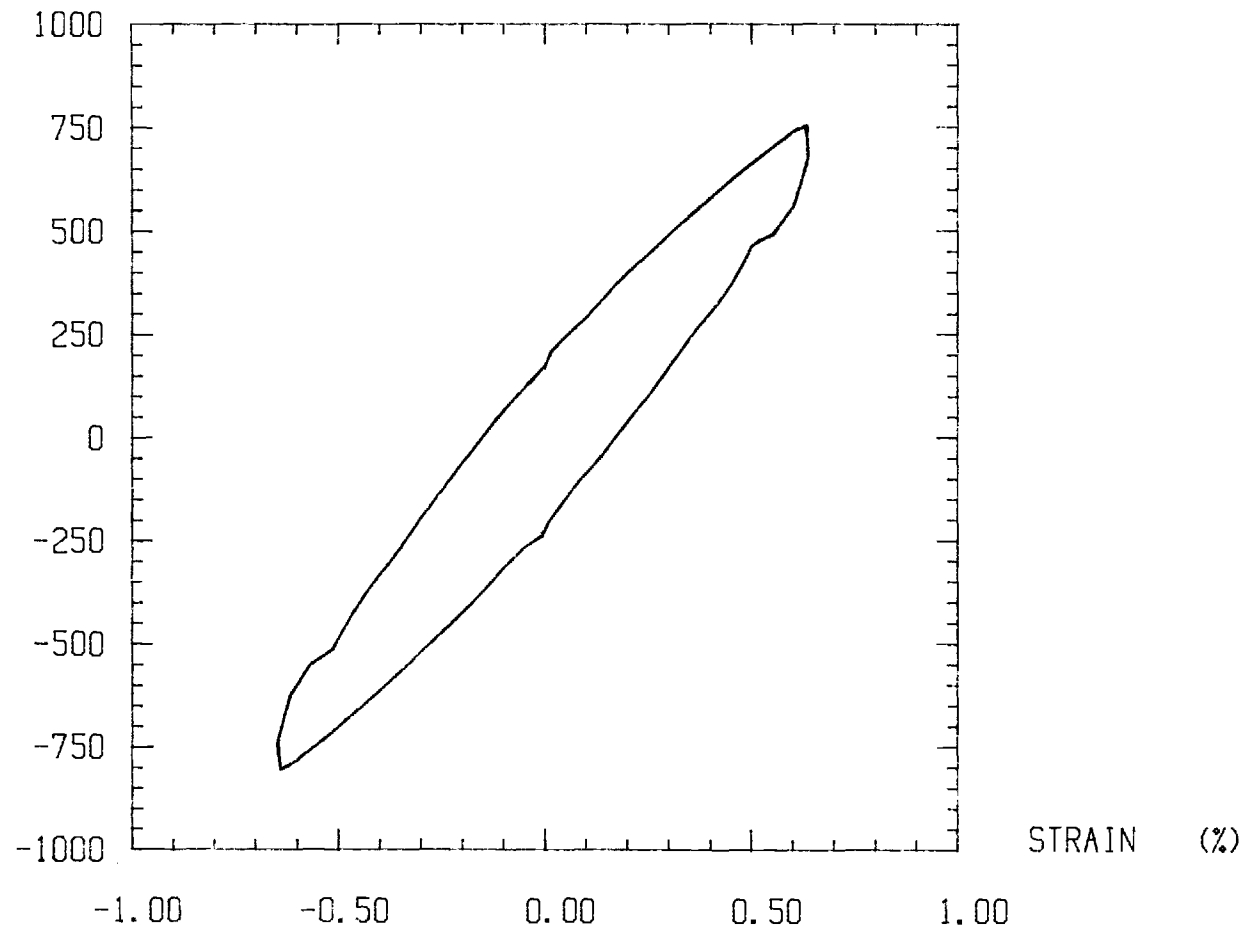CYCLE #32-33   SPECIMEN F2   RATE =   .001 /SEC

STRESS   (MPa)

CYCLE #2   SPECIMEN F4   RATE = .001 /SEC
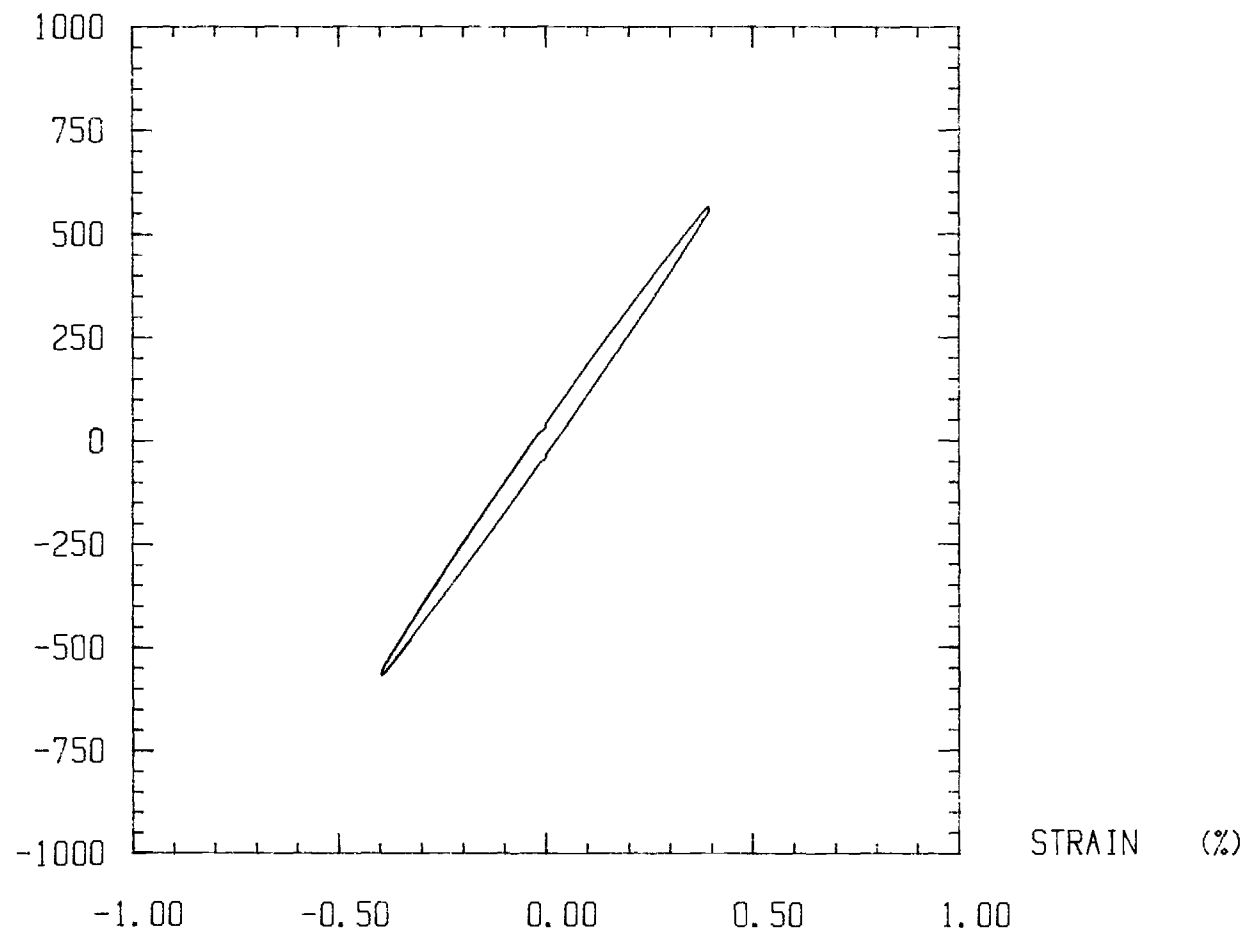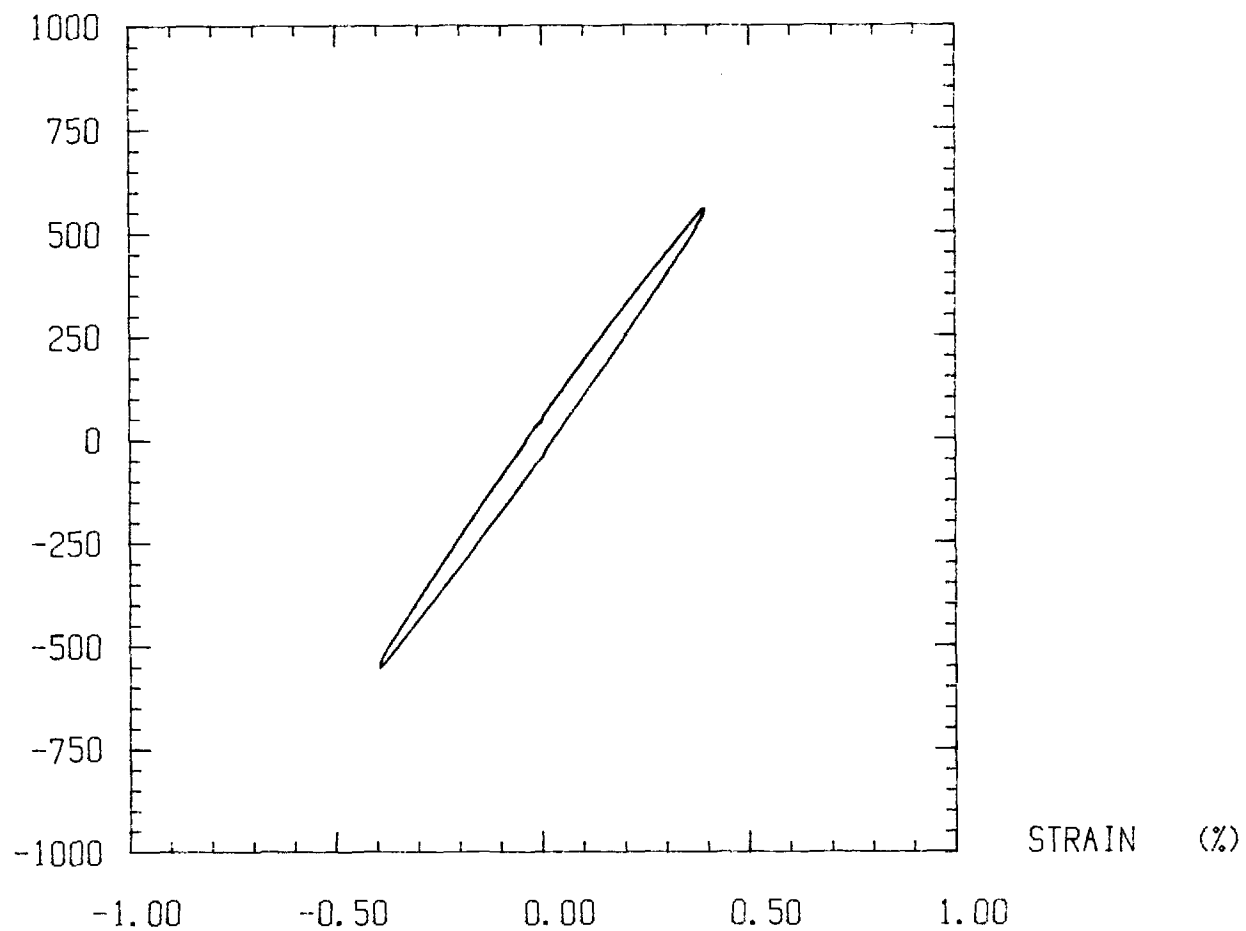
CYCLE #16-17 SPECIMEN F4 RATE = .001 /SEC

STRESS (MPa)

CYCLE #64-65   SPECIMEN F4   RATE = .001 /SEC
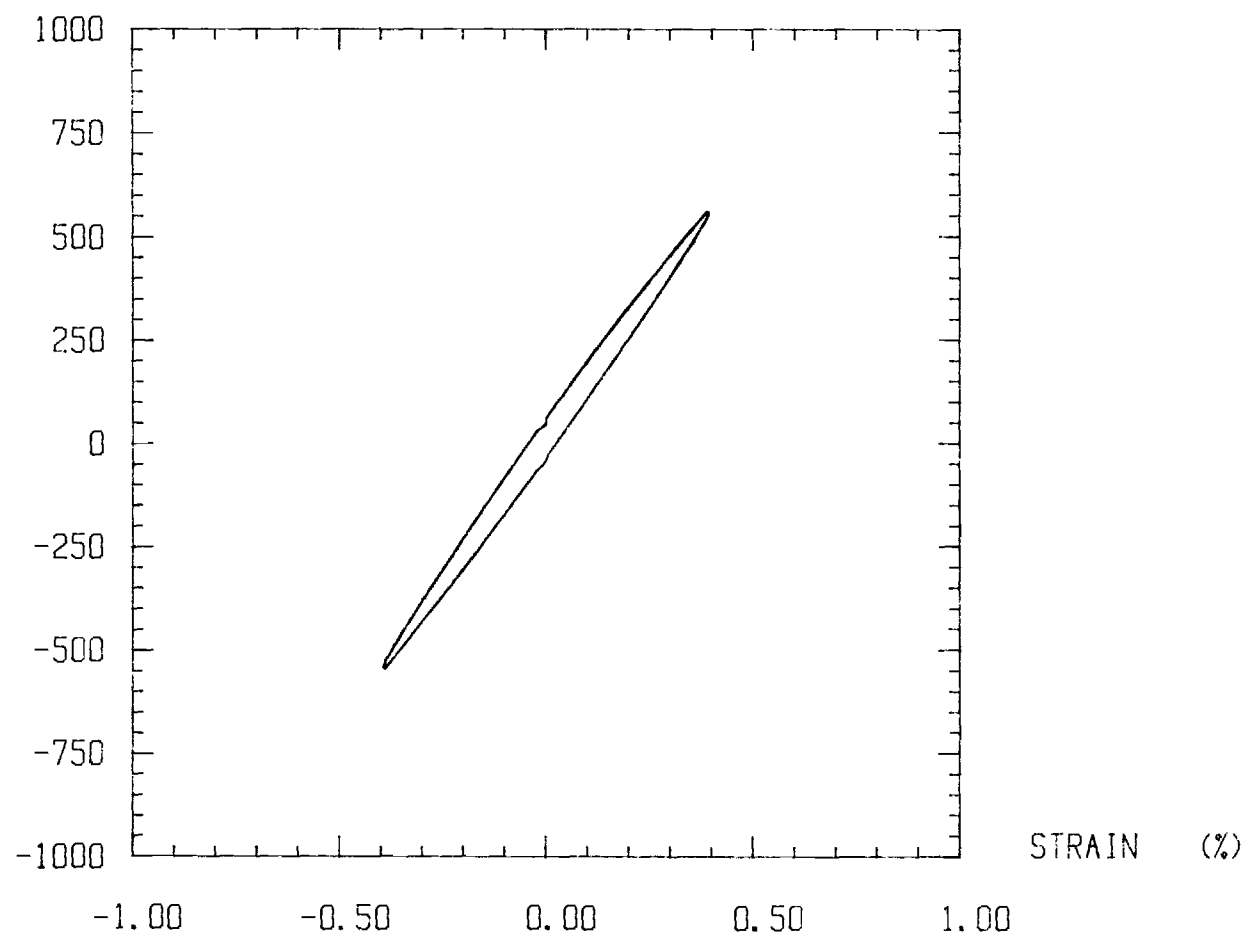
STRESS   (MPa)

STRAIN   (%)

CYCLE #550-551   SPECIMEN F4   RATE = .001 /SEC

STRESS   (MPa)

STRAIN   (%)
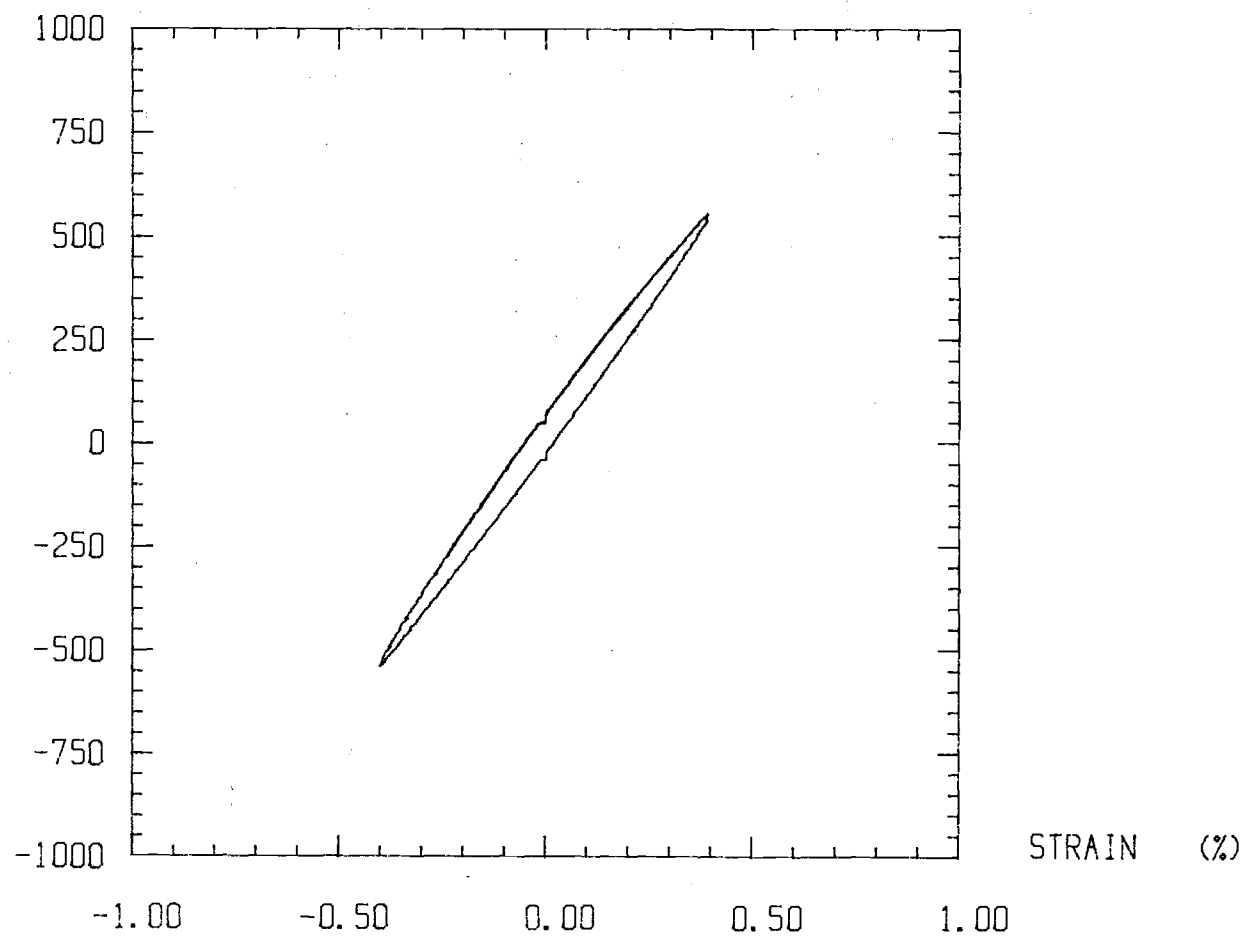
CYCLE #1-2 SPECIMEN F5 RATE = .001 /SEC
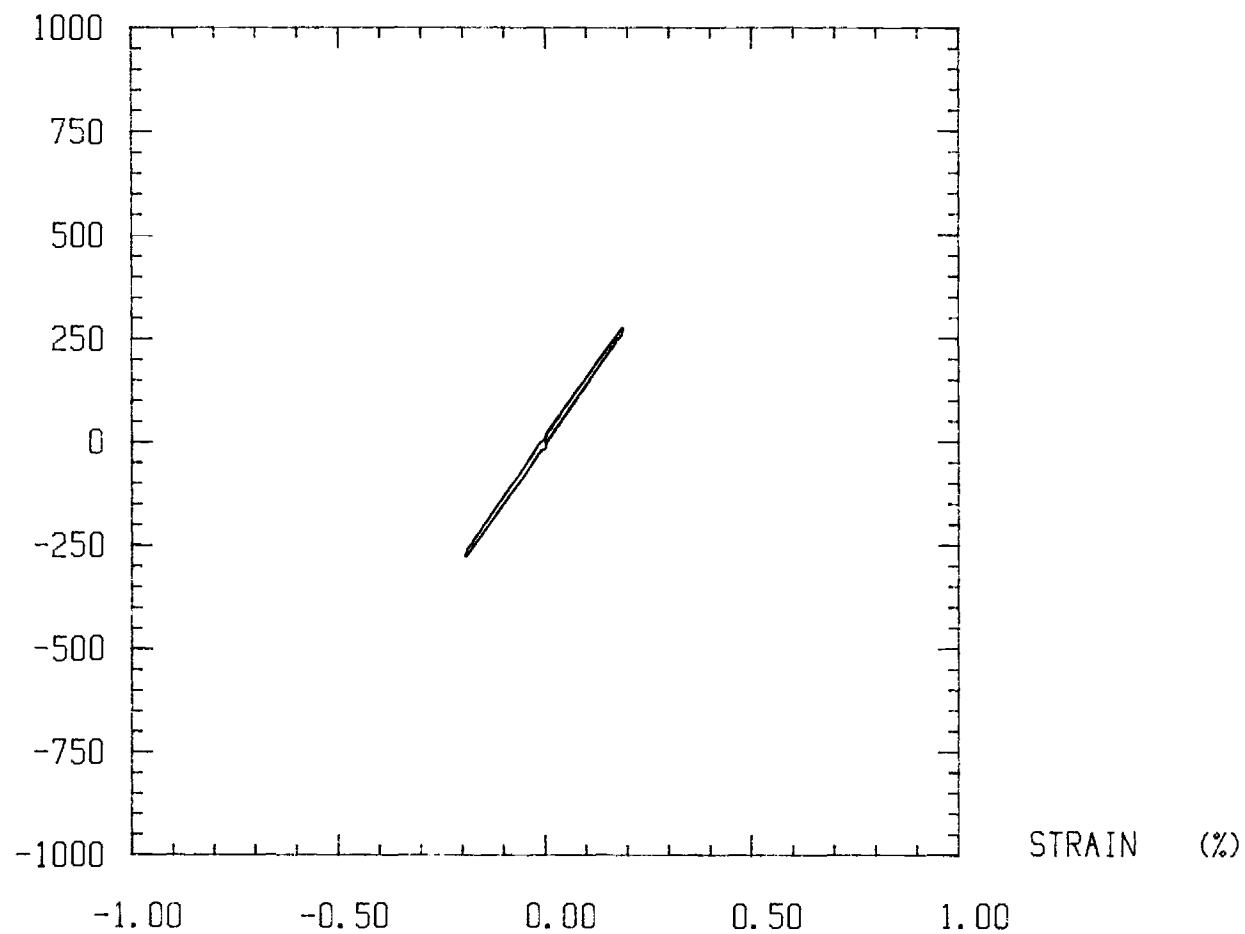
CYCLE #10936   SPECIMEN F5   RATE =   .001 /SEC

STRESS   (MPa)

CYCLE #1-4   SPECIMEN F8   RATE =   .01 /SEC

STRESS   (MPa)

STRAIN   (%)
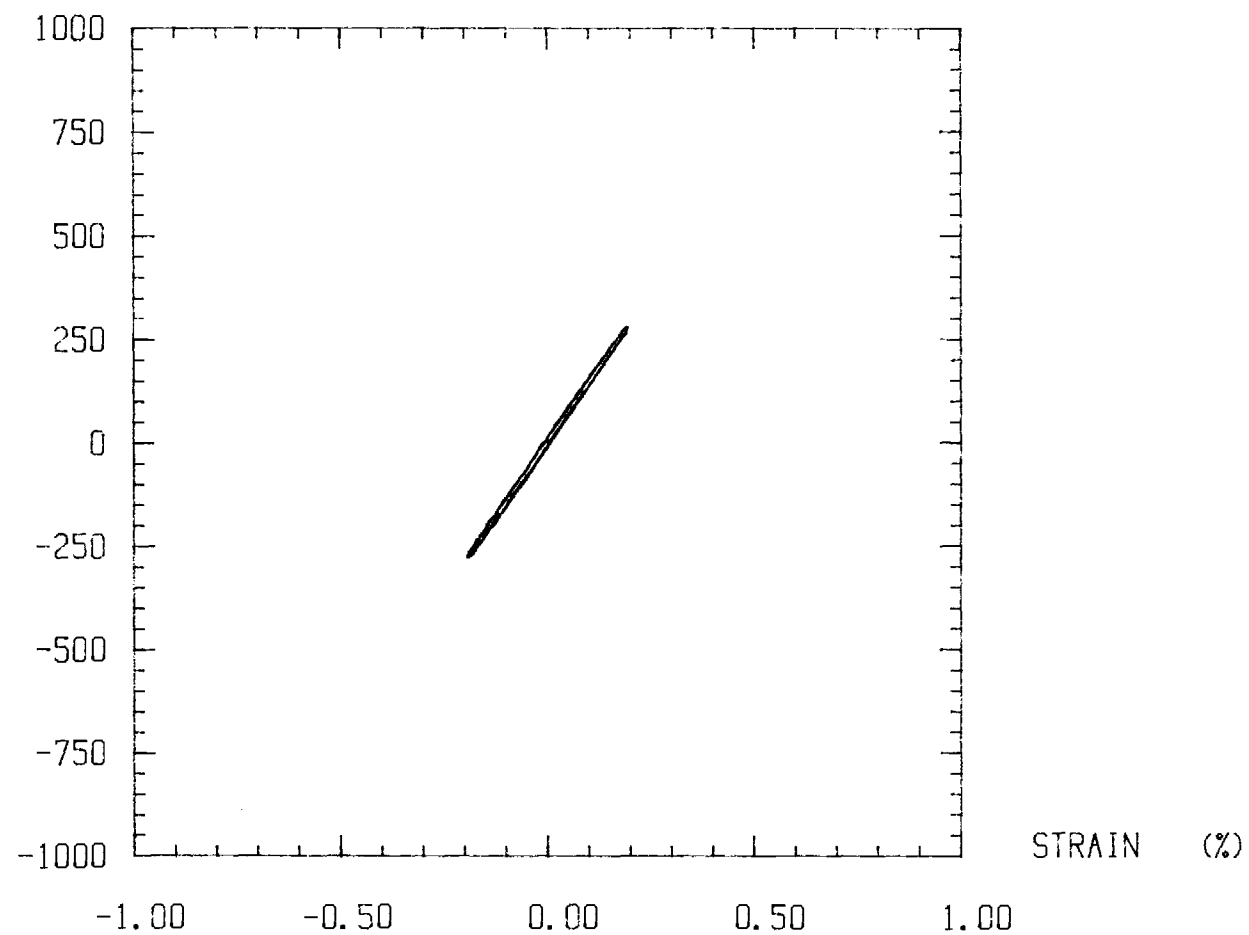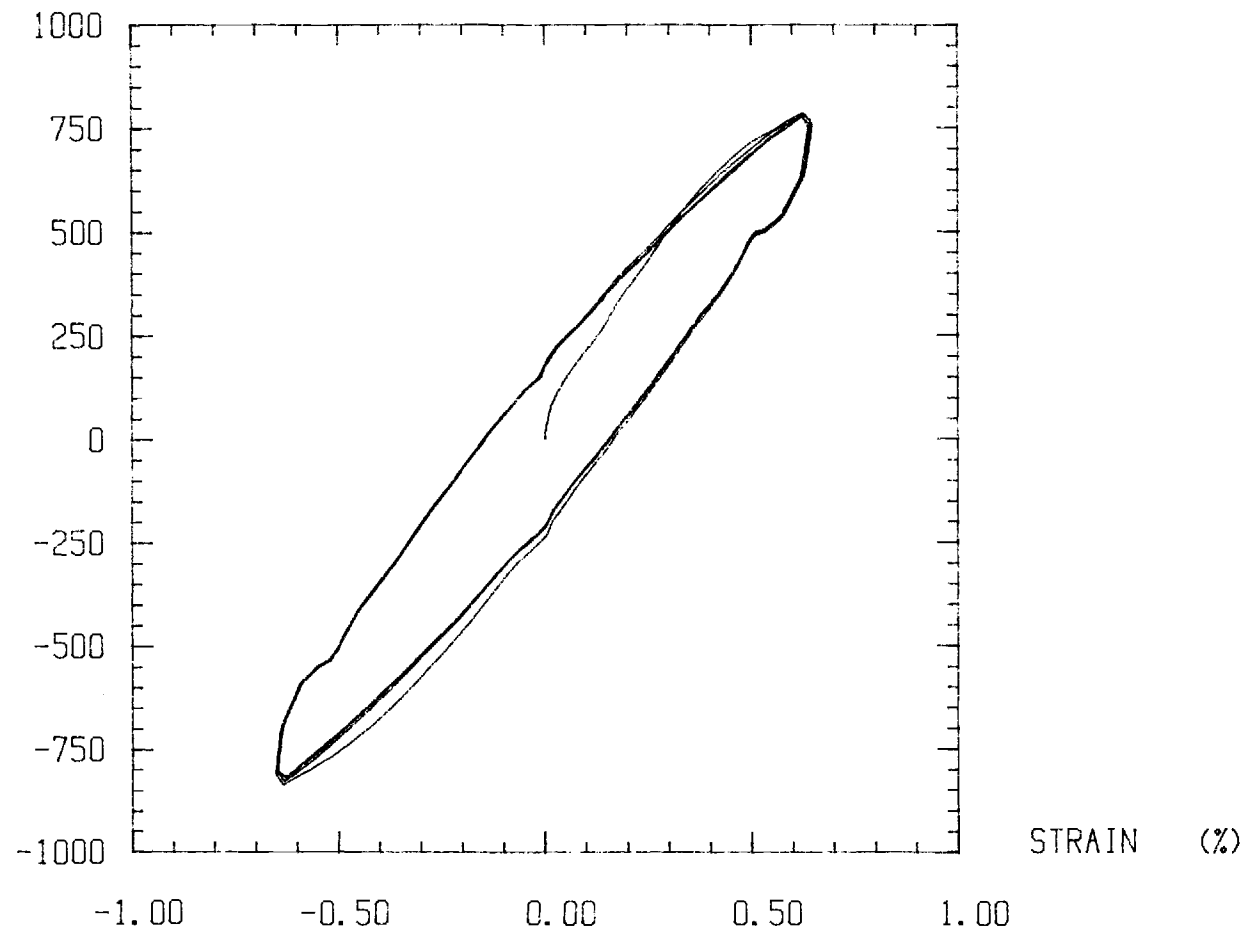
CYCLE #16-19   SPECIMEN F8   RATE = .01 /SEC

STRESS   (MPa)

CYCLE #100-107   SPECIMEN F8   RATE = .01 /SEC
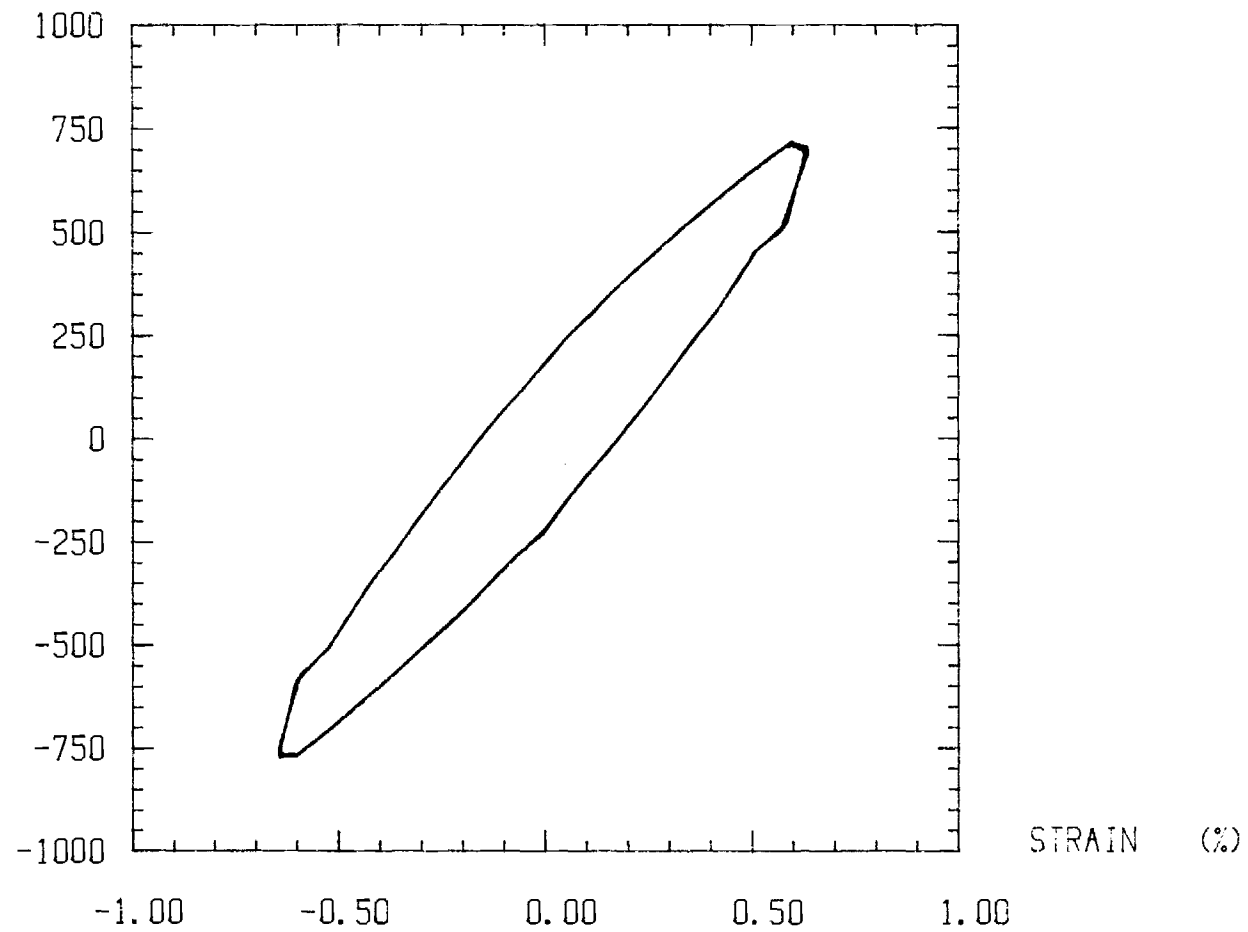
LETTER REPORT

"DAMAGE RATE APPROACHES FOR THERMOMECHANICAL FATIGUE
OF SUPERALLOYS"

By David L. McDowell
Principal Investigator

R.L.T. Oehmke
Research Engineer

Project # E-25-M13
General Motors PO# H636356

May 31, 1987

Submitted to Allison Gas Turbine Operations, General Motors
Corporation

Sponsor Technical Contact:

Dr. W.E. Schneider/T-10
Allison Gas Turbine Operations
General Motors Corporation
2001 South Tibbs Ave.
Indianapolis, IN 46241
(317) 242-7703

Sponsor Administration and Contractual Matters:

Darrell L. Mackey/U02
Allison Gas Turbine Operations
General Motors Corporation
P.O. Box 420
Indianapolis, IN 46206-0420
(317) 242-6954

May 31, 1987

Dr. W.E. Schneider/T-10
Allison Gas Turbine Operations
General Motors Corp.
2001 South Tibbs Avenue
Indianapolis, IN 46241

Dear Dr. Schneider:

This report summarizes the activities of our effort on GM PO#H636356, "Damage Rate Approaches for Thermomechanical Fatigue of Superalloys" for the period April 1, 1987 to May 31, 1987.

In this report, we update the database which has been previously reported with the remainder of the monotonic tests in air at 900°C and fatigue tests at several strain rates.

We have made a concerted effort to accurately align our machine, including construction of a teflon restraining collar for the servohydraulic ram near the low pressure seal region to maintain less than one mil lateral deflection under compressive and tensile loading. This was done, as discussed previously to alleviate persistent cracking in the specimen fillet region.

After a cursory dimensional inspection of the first lot of specimens shipped to us, most of which we have tested, we have determined that some are significantly out of tolerance with respect to the parallel button-end surfaces. These surfaces must be perpendicular to the specimen centerline and all of the four surfaces (A,B,C and D in the attached drawing) must be parallel to within 0.001" as specified in the original drawing. This parallelism is very important since we may associate a bending strain of approximately 5% of the uniform strain with each 0.001" out of tolerance. We suspect that some of our problems with fillet cracking may be related to specimen geometry errors.

Due to the machining tolerance problems, we will re-run at least a few of the previous experiments to validate the results with more accurately machined specimens. It should be noted that the failure cracks occurred seemingly at random in the uniform section near the top or bottom fillets or in the gage section; however, the data is consistent in all cases when plotted as log strain or stress vs. log life as seen in the attached plots. Hence, we have confidence at this point that the data is valid.

A second lot of specimens was received the week of May 10-17. Inspection of several of these specimens using gage blocks revealed significant deficiencies in machining tolerances; errors in both the parallelism of the button-end surfaces and the radius of the button-end fillets were quite in excess of tolerance.
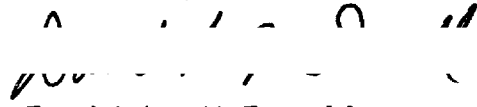
Note the attached memorandum from Roger Oehmke, the research engineer on the project. Errors in parallelism exceed tolerance by as much as a factor of four. A number of button-end fillets were machined with a radius of 0.10" instead of the specified 0.05" and hence will not fit into our grips. One of the specimens had a severe longitudinal "scrape" down the entire length of the gage section. The machining job on the most recently received batch of specimens was noticeably inferior to that of the initial batch, even though the gage sections were more appropriately polished as requested. We greatly appreciate the polishing job done by your machine shop.

In view of these specimen tolerance problems, the most recently received batch of specimens require modification prior to testing. Hence, as we discussed in our telephone conversation on May 22, we will undertake specimen preparation necessary to meet the tolerance specifications on the button-end surfaces and the button-end fillet radii.

Attached please find an updated table of data and plots of some of the hysteresis loops acquired at various cycle numbers for each specimen. Note that the monotonic tensile tests at four strain rates at 900°C reveal significant strain rate sensitivity.

Also attached please find updated strain-life and stress-life curves.

Sincerely,

David L. McDowell
Principal Investigator

900°C Test Matrix for First Set of Specimens
Environment: Laboratory Air

Strain-Controlled:

Test Type	$\dot{\epsilon}$ rate (sec^{-1})	$\Delta\epsilon/2$	ϵ_{max}	$\Delta\sigma/2$ (MPa)	$2N_f$
Monotonic					
M1*	10^{-3}		.0475 then unload		
M2*	10^{-2}		.072 at failure		
M3*	10^{-5}		.0315 at failure		
M4*	10^{-4}		.043 at failure		
M5*	10^{-1}		.059 at failure		
Fatigue					
F1*	10^{-3}	.0097		863	36
F2*		.0076		725	90
F3*		.006		710	192
F4*		.004		550	1166
F5*		Sequence:0.002 followed by 0.004		284	144724
F6*	10^{-2}	.01		1019	48
F7		.008			
F8*		.0063		780	236**
F9		.004			
F10		.003			
F11*	10^{-4}	.01		745	28
F12*		.008		752	50
F13*		.004		516	748
F14		.004			

Creep tests:

Test type	Engr. Stress
Constant Load Creep	
F15	60 ksi to rupture.
F16	43.5 ksi to rupture.
Sequence Creep	
F17	1/2 rupture time at 60 ksi; switch to 43.5 ksi and hold to rupture.

* Denotes completed experiment.
** Buckled after failure crack formed.

MEMORANDUM   MAY 18,1987

TO: Dr. Dave McDowell

FROM: Roger Oehmke

SUBJECT: New specimens from GM

The most recent batch of specimens received from General Motors are
not suitable for use in our testing machines. Most of them will not
fit into the specimen grips because the button end radius is too
large. Instead of a .050 inch radius it is closer to .100 inches. The
excess material interferes with the specimen holders.

A quick check of the specimens with a machinists square indicates that
the button ends on most of the specimens are not flat as is absolutely
essential for this type of specimen. If the .001 inch tolerance for
surfaces A, B, C, and D (see attached drawing) is not met, the
specimen will bend.

Two randomly selected specimens were taken to the GTRI machine shop
for inspection. Neither of the specimens was within specifications.
One of them (#T010-3) varied between 0 and .004 inches on only one
surface (A). Another of the specimens (#T010-5) has a flat spot about
.050 inches wide that runs the length of the gage section.

Attached is a table of specimen discrepencies noted during a simple
visual inspection with a machinists square and radius gage. The table
is not complete. I am sure that a more detailed inspection would
reveal many more serious deviations.

I encourage you to return these specimens to General Motors and
request that they provide us with specimens that meet specifications.
It is the only way to ensure the integrity of our tests and the
validity of the results.

Specimen	radius	ends	comments
T010-5	bad		end out .0025. Flat in gage section.
T010-3	bad		end out .004.
T001-5		bulged	sharp edges
T016-1		bulged	
T015-3		bulged	
T001-3		not ground	
T011-2	bad	bulged	
T015-5	bad	bulged	
S999-1	bad	not ground	
T011-3	bad	1/32" too long. scratches in gage section.	
T001-4	bad	bulged	
T010-4	bad	bulged	
S999-5	bad	bulged	
S999-4	double shoulder		short ends
T010-2		bulged	circumferential scratches
T010-1	bad		
T015-1	bad	bulged	
T011-5	bad	bulged	
T011-1	bad	not ground	
T016-4	bad	bulged	

Surfaces A, B, C and D Must Be Parallel Within .001
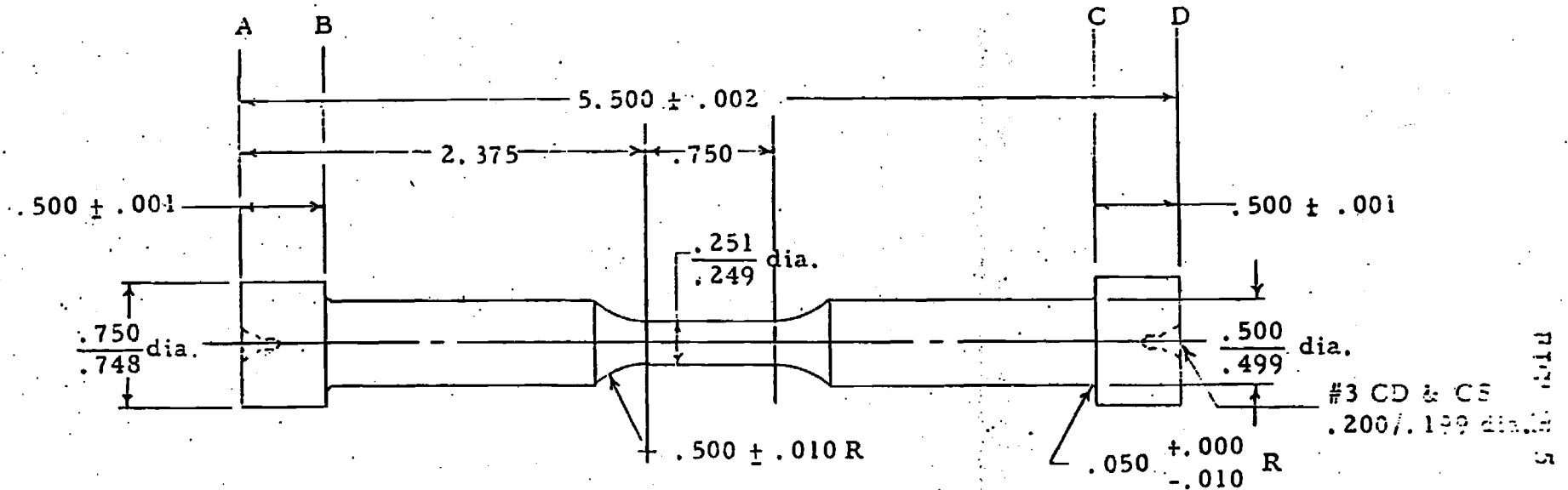
	LOW CYCLE FATIGUE SPECIMEN	METCUT RESEARCH ASSOCIATES INC.
		CINCINNATI, OHIO 45209
		DWG. NO. 720303-1

MONOTONIC   SPECIMEN M5   RATE .1 /SEC

STRESS   (MPa)

strain to failure = 5.9%

1250 —

1000 —

750 —

500 —

250 —

0 —

STRAIN   (%)

0.00   2.50   5.00   7.50
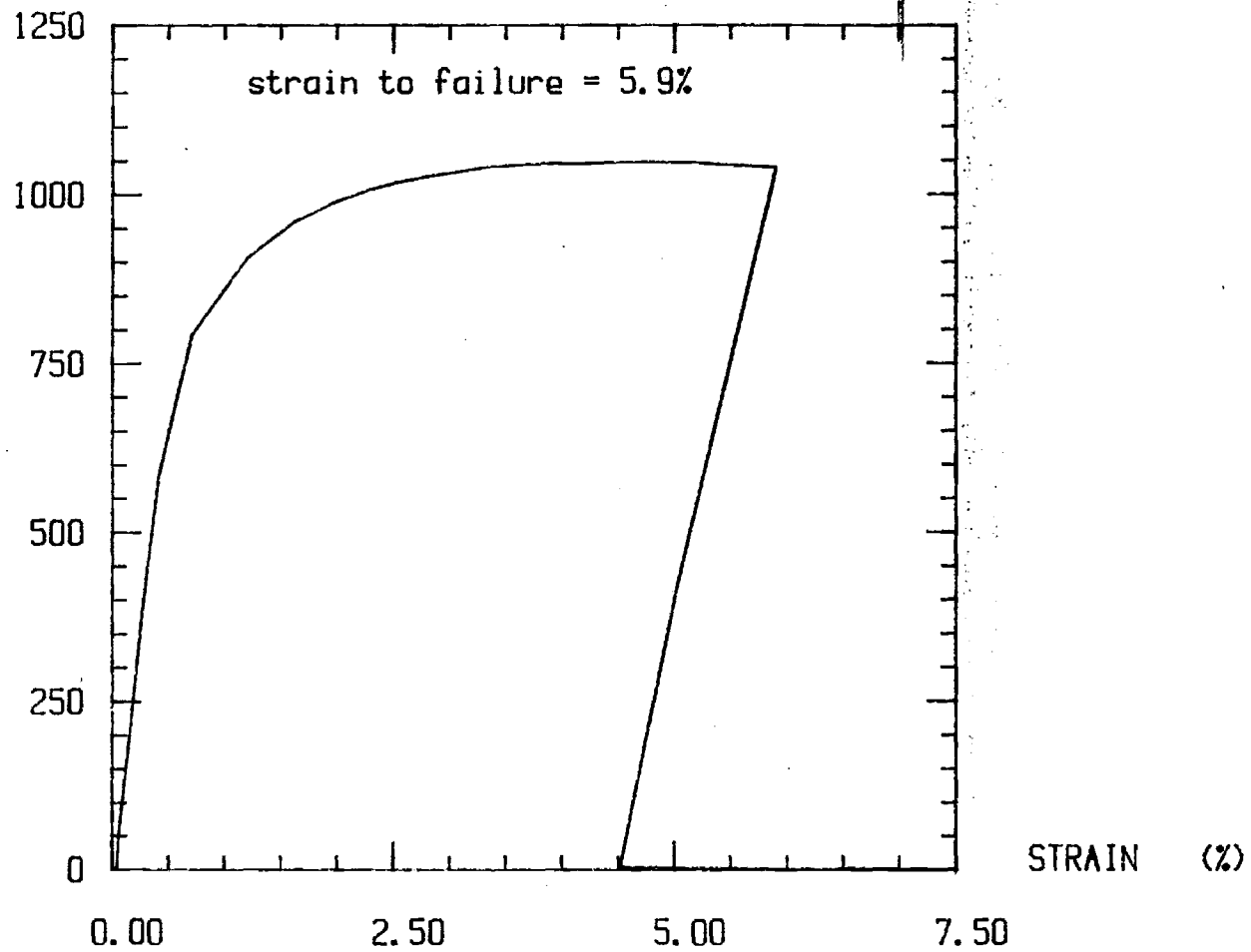
MONOTONIC   SPECIMEN M2   RATE .01 /SEC

STRESS   (MPa)

strain to failure = 7.2%

STRAIN   (%)

MONOTONIC   SPECIMEN M1   RATE .001 /SEC

STRESS   (MPa)

1000 ┤

     │

 750 ┤

                    (no failure)

 500 ┤

 250 ┤

   0 ┤   STRAIN   (%)

   0.00   2.50   5.00
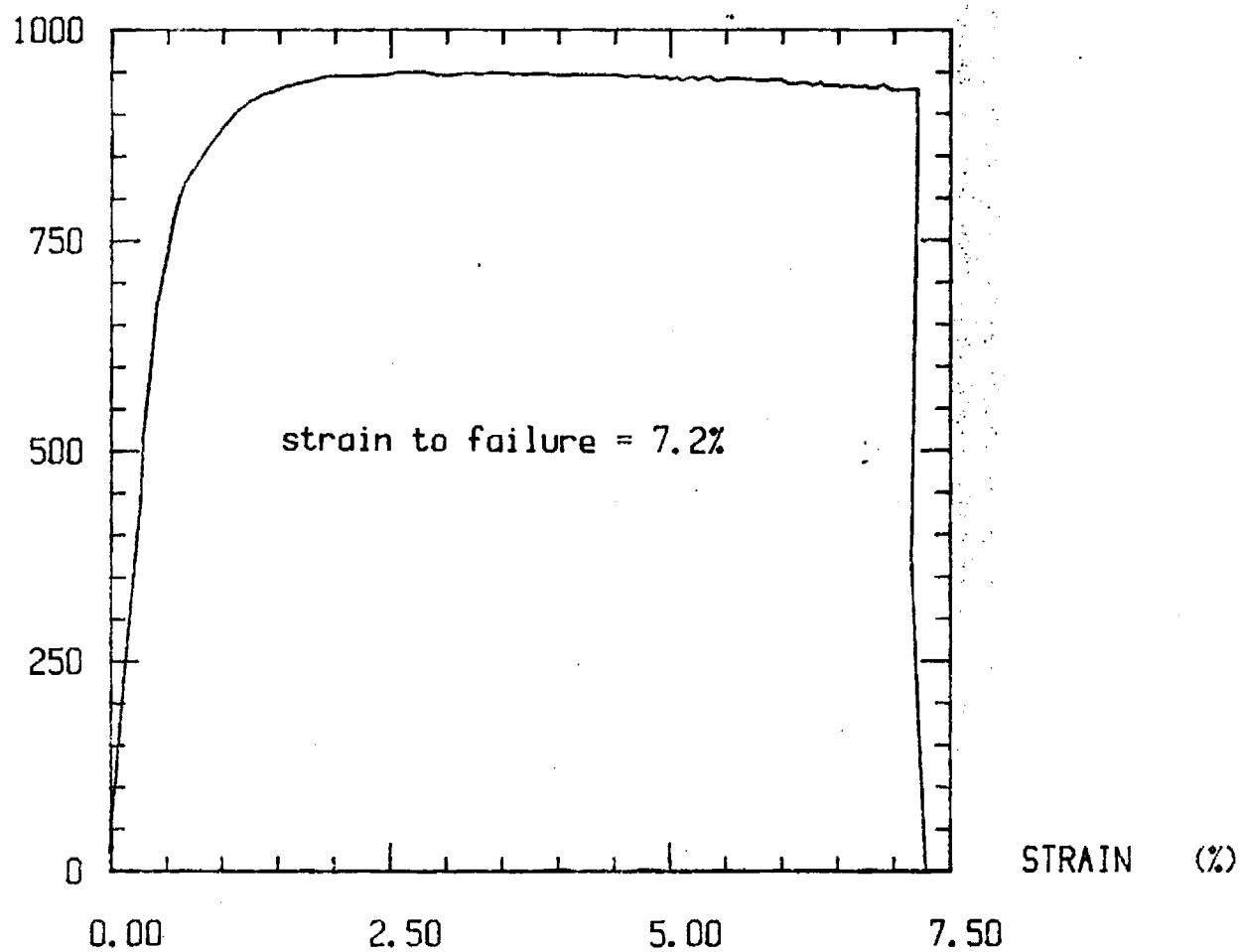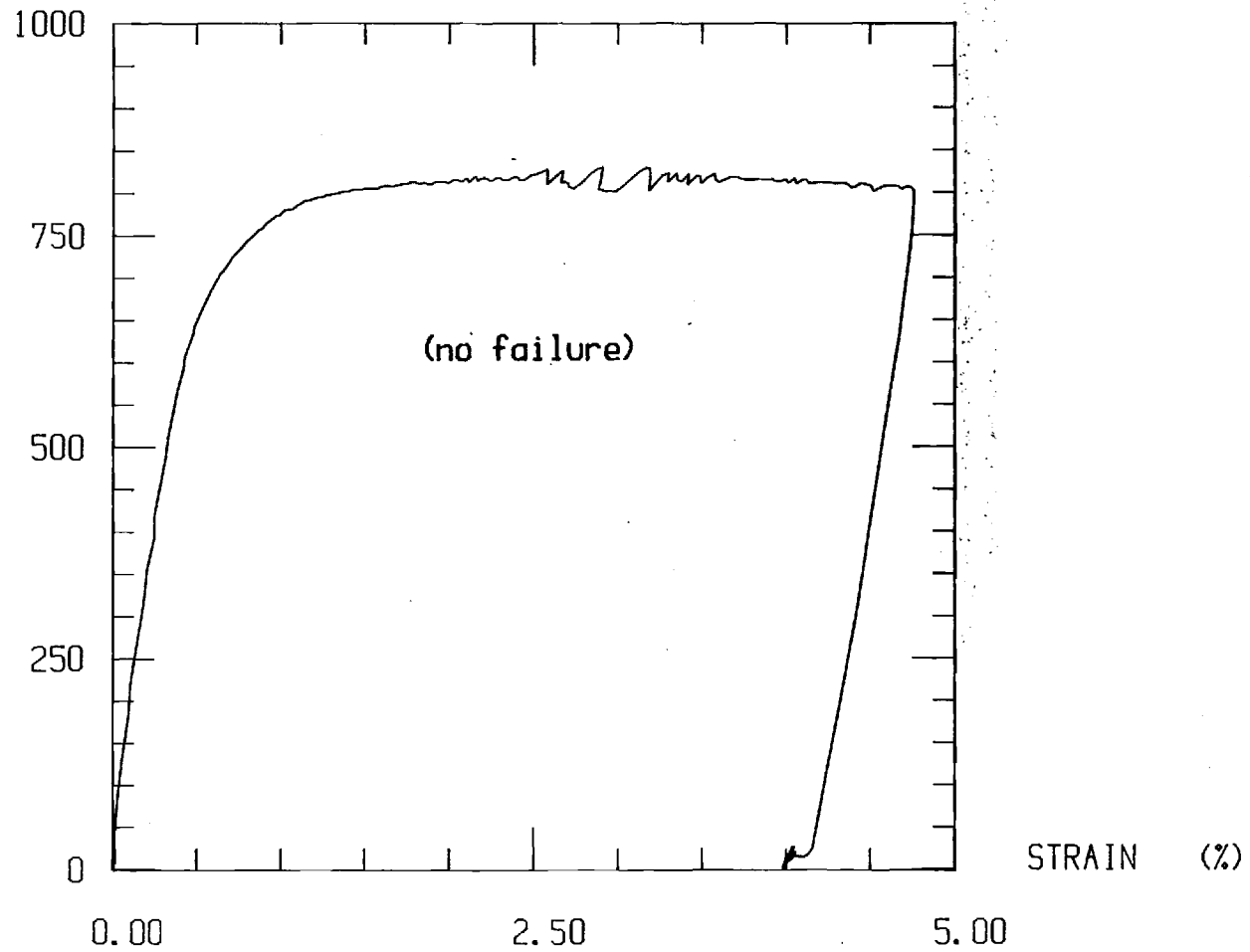
MONOTONIC   SPECIMEN M4   RATE .0001 /SEC

STRESS   (MPa)

strain to failure = 4.3%

STRAIN   (%)
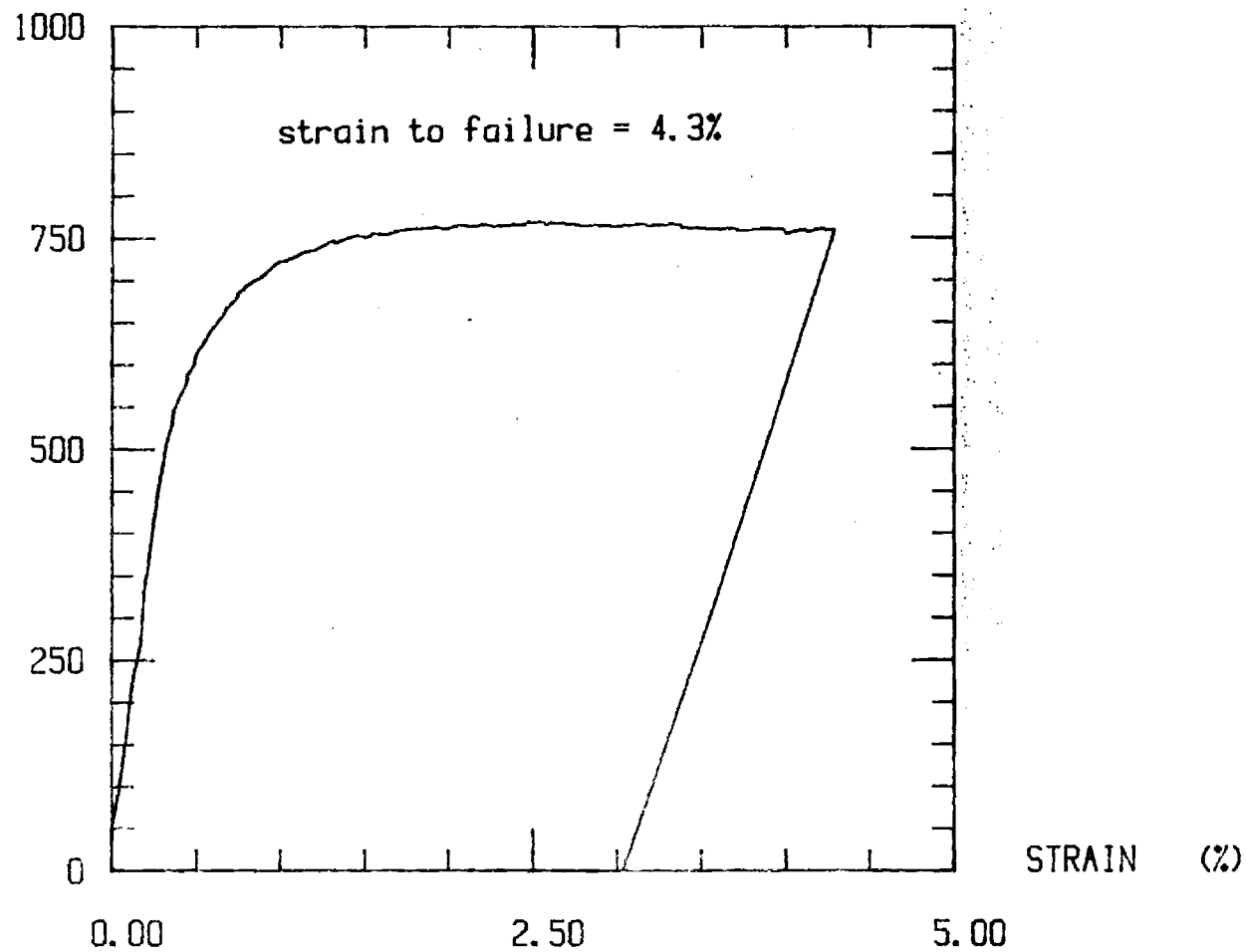
MONOTONIC   SPECIMEN M3   RATE .00001 /SEC

STRESS   (MPa)

strain to failure = 3.15%

STRAIN   (%)
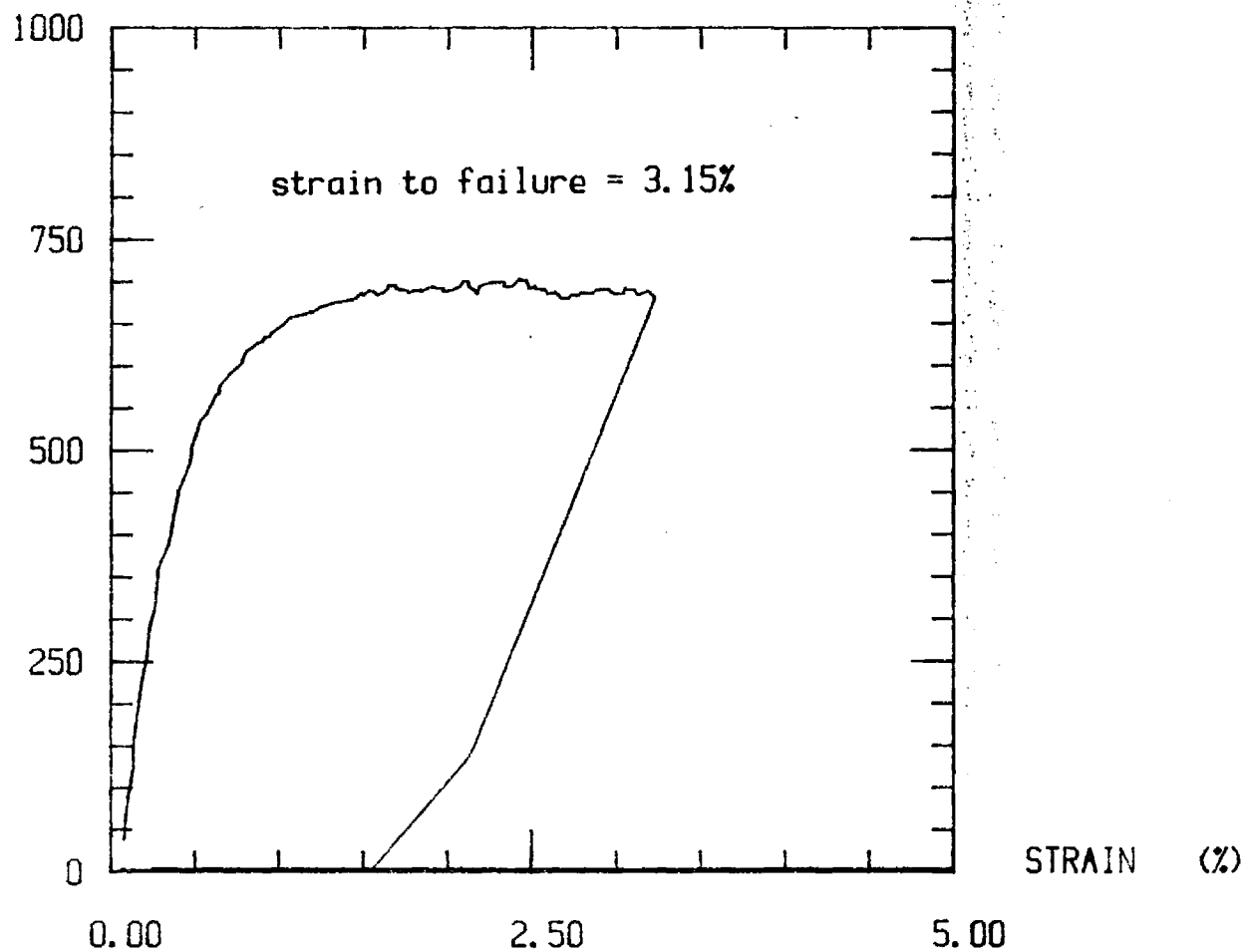
MONOTONIC TESTS AT 900 DEG C

STRESS   (MPa)
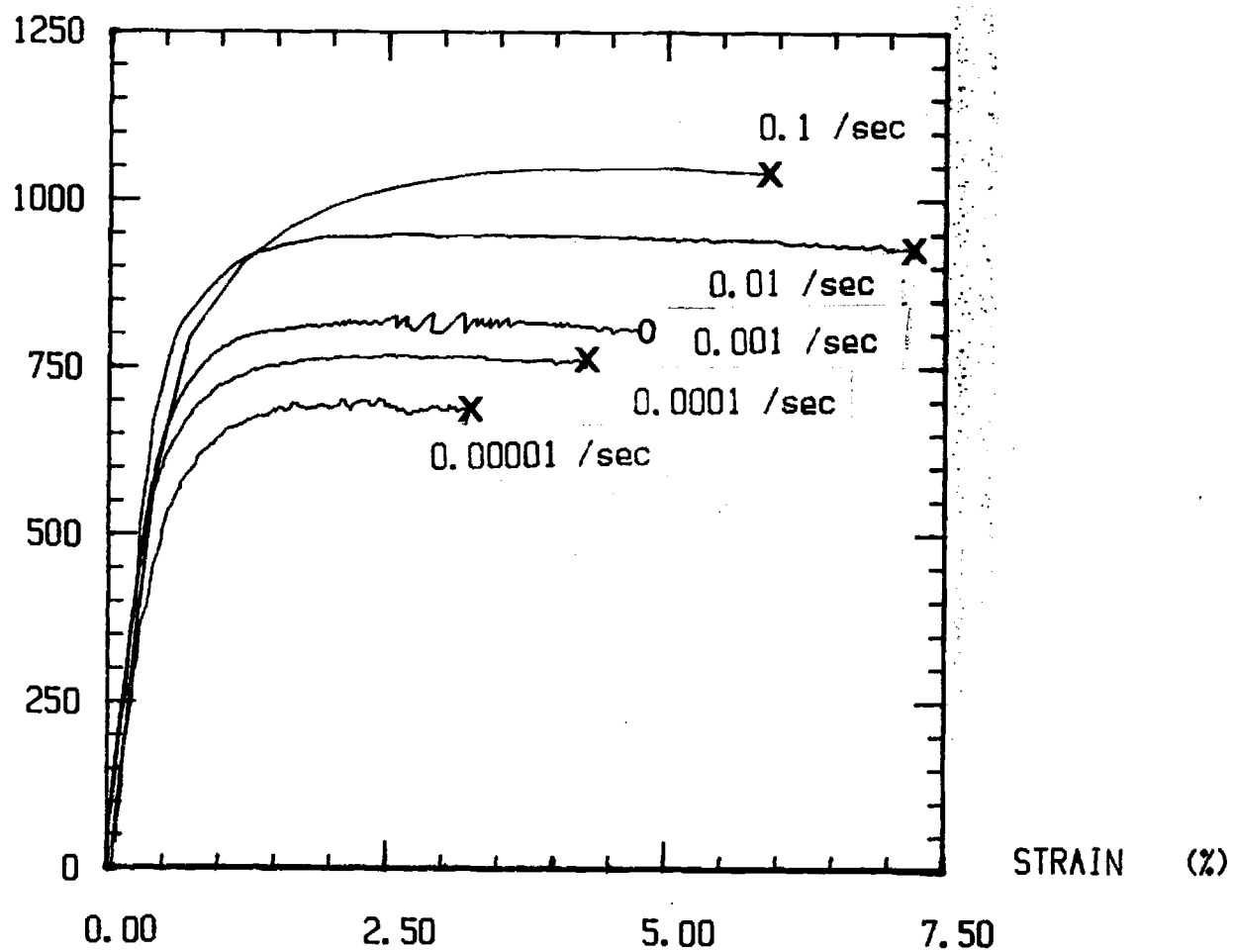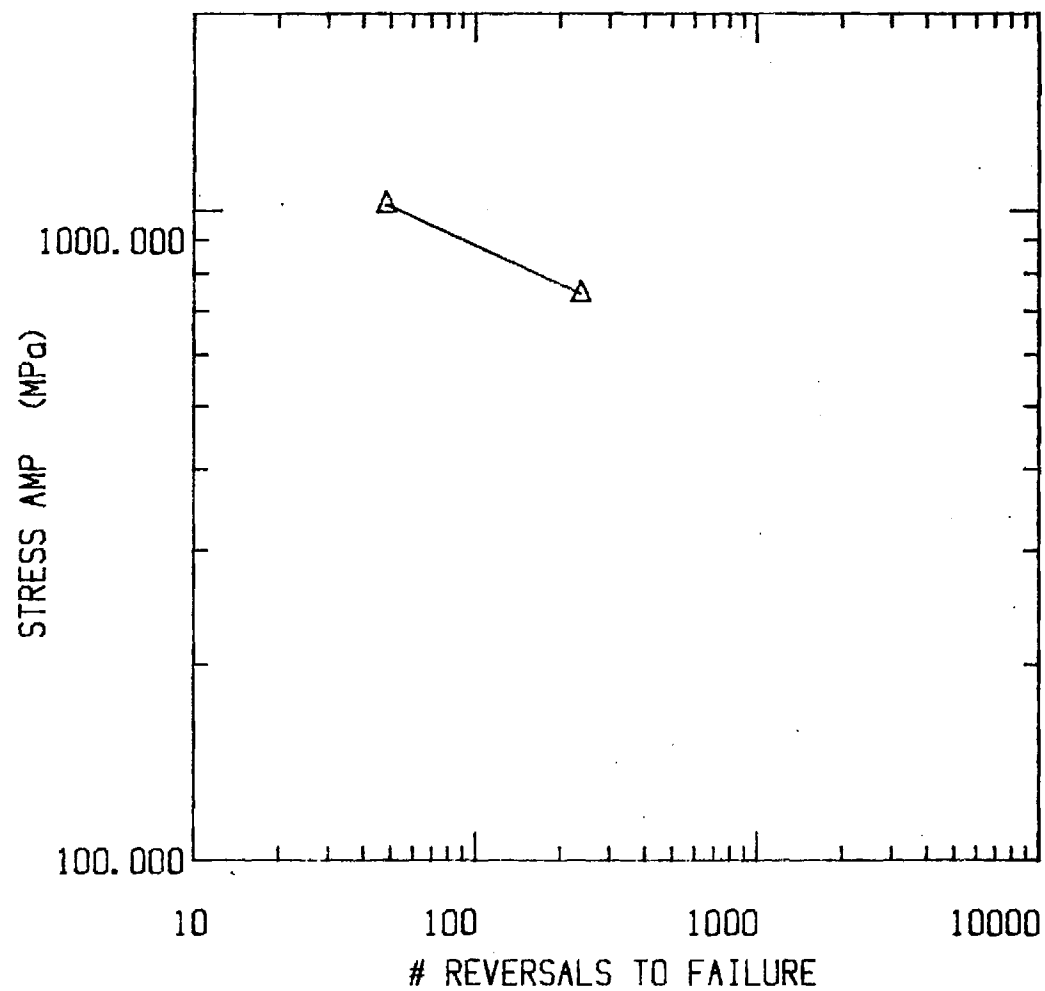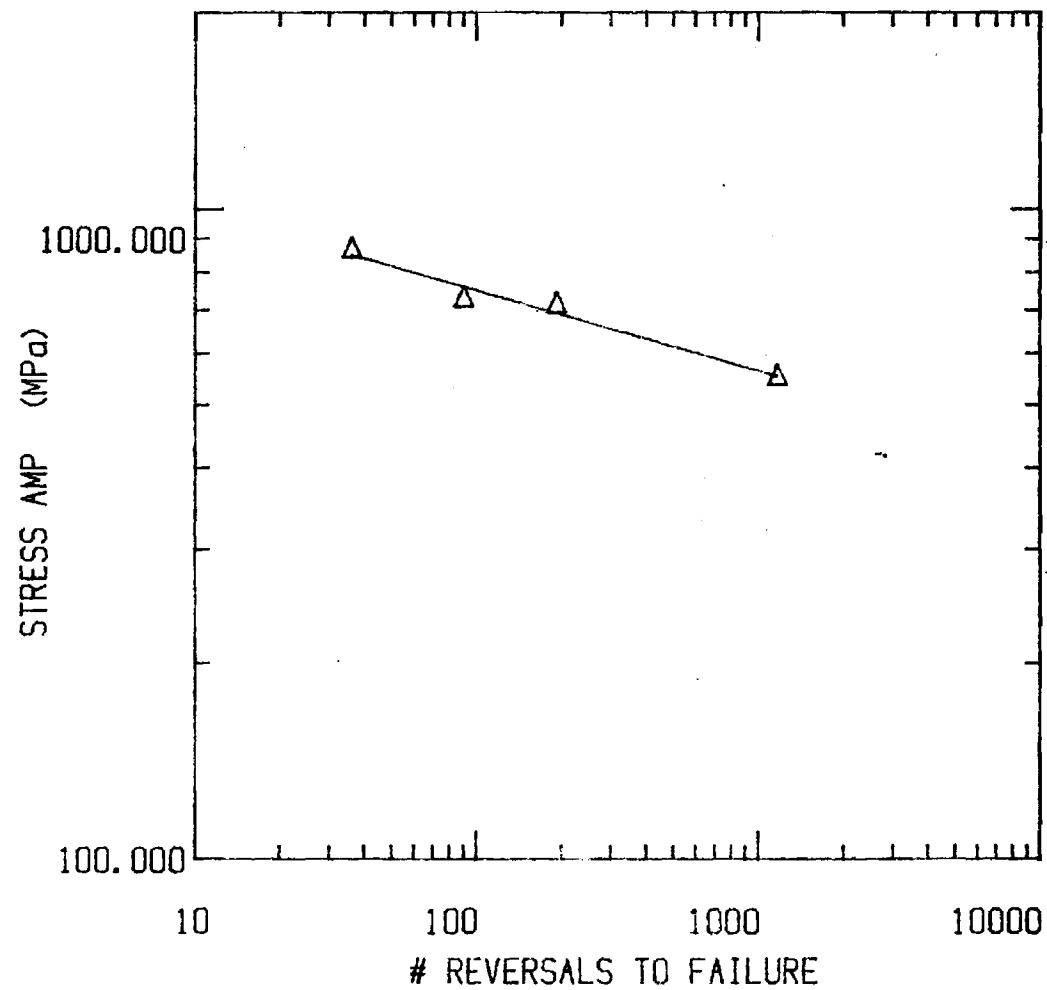
1250	
	0.1 /sec
1000	
	0.01 /sec
750	0.001 /sec
	0.0001 /sec
500	0.00001 /sec
250	
0	

0.00   2.50   5.00   7.50

STRAIN   (%)

MAR-M 246   900 DEG C   RATE .01 /SEC

MAR-M 246 900 DEG C RATE .001 /SEC

MAR-M 246   900 DEG C   RATE .0001 /SEC

STRESS AMP (MPa)

1000.000

100.000

10   100   1000   10000

REVERSALS TO FAILURE

MAR-M 246   900 DEG C

STRESS AMP (MPa)

1000.000

100.000

▲ 0.0001 /sec
● 0.001 /sec
⬭0.01 /sec

10   100   1000   10000

REVERSALS TO FAILURE

MAR-M 246   900 DEG C   RATE .01 /SEC

MAR-M 246   900 DEG C   RATE .001 /SEC

STRAIN AMP

0.010

0.001

10   100   1000   10000

REVERSALS TO FAILURE
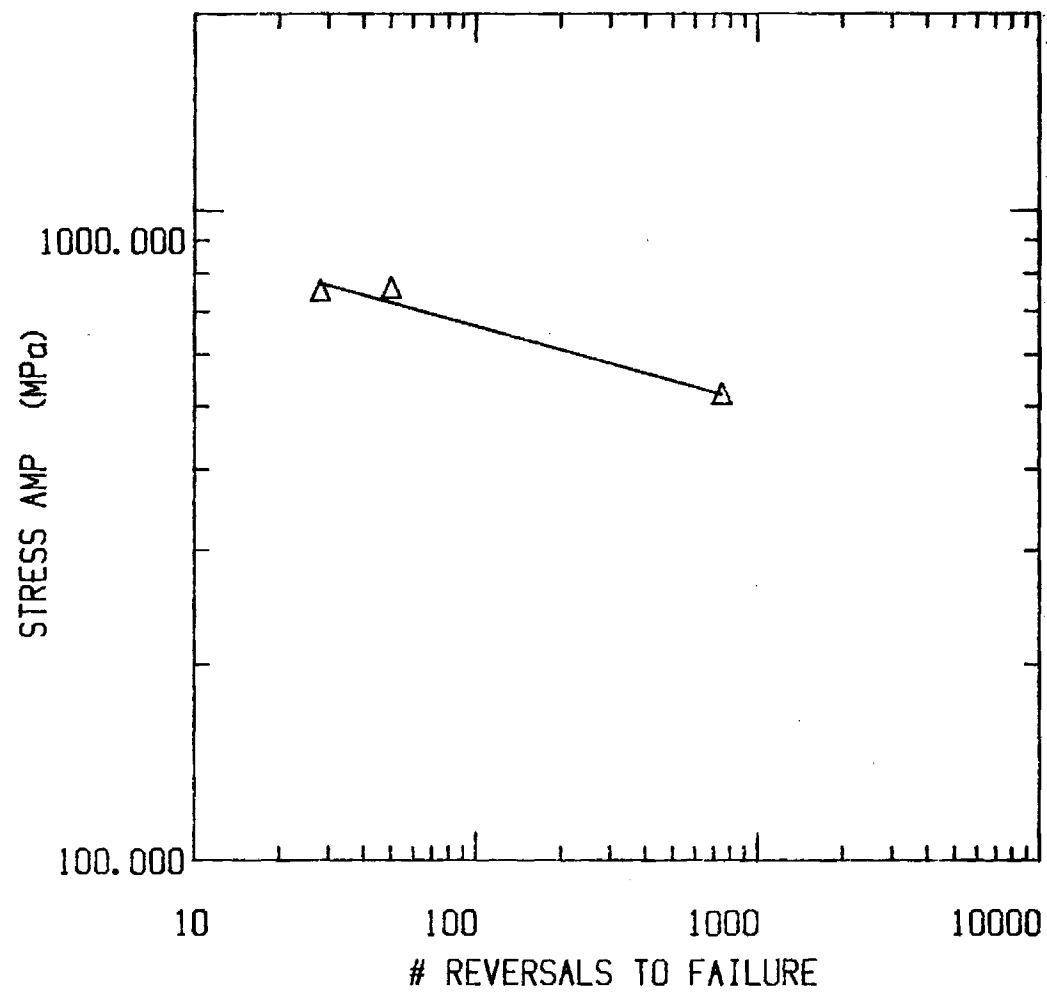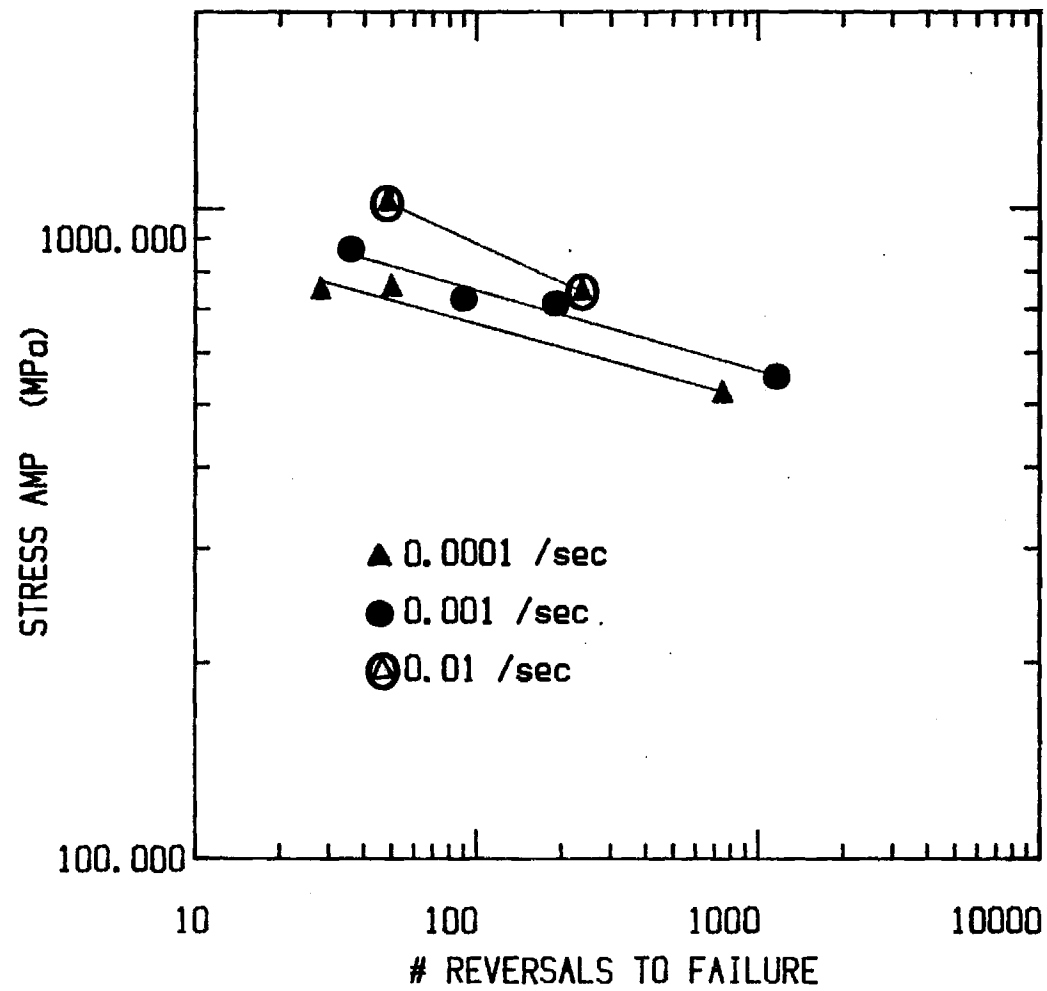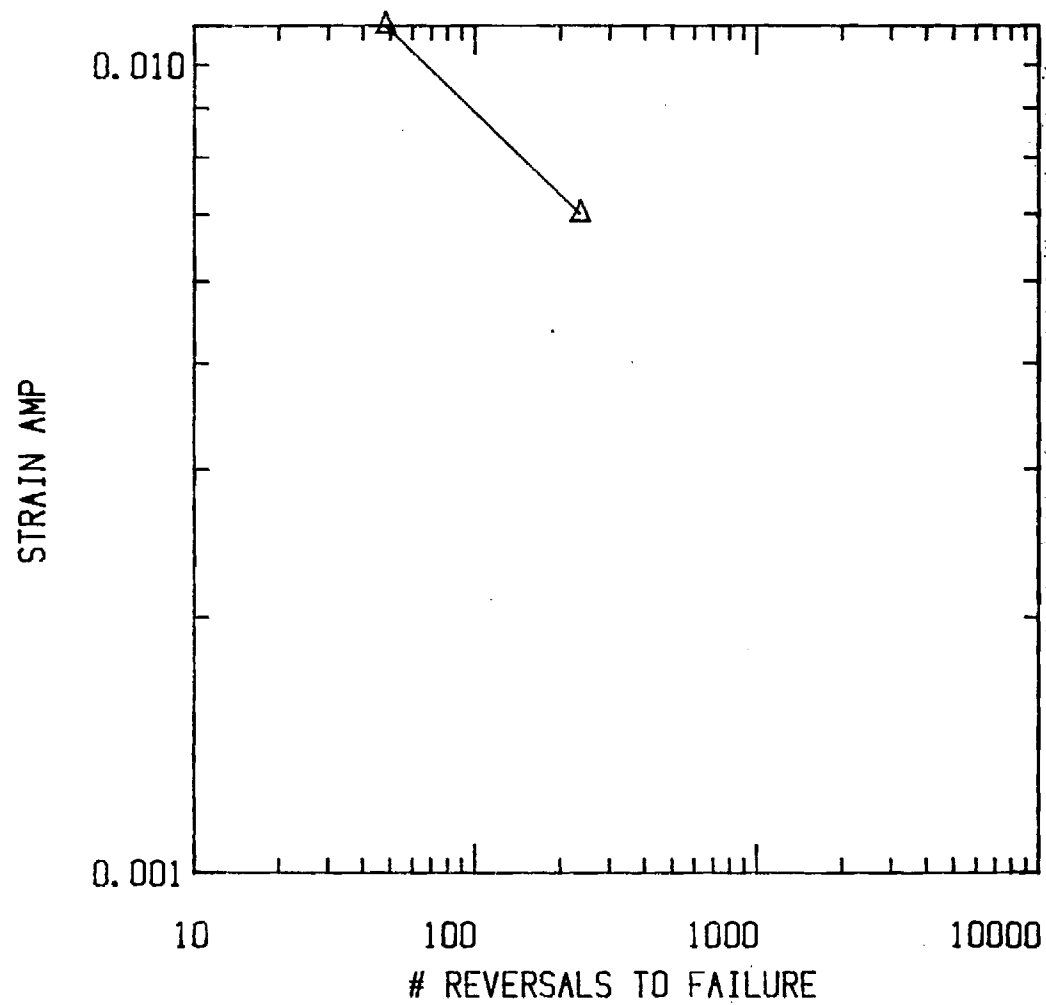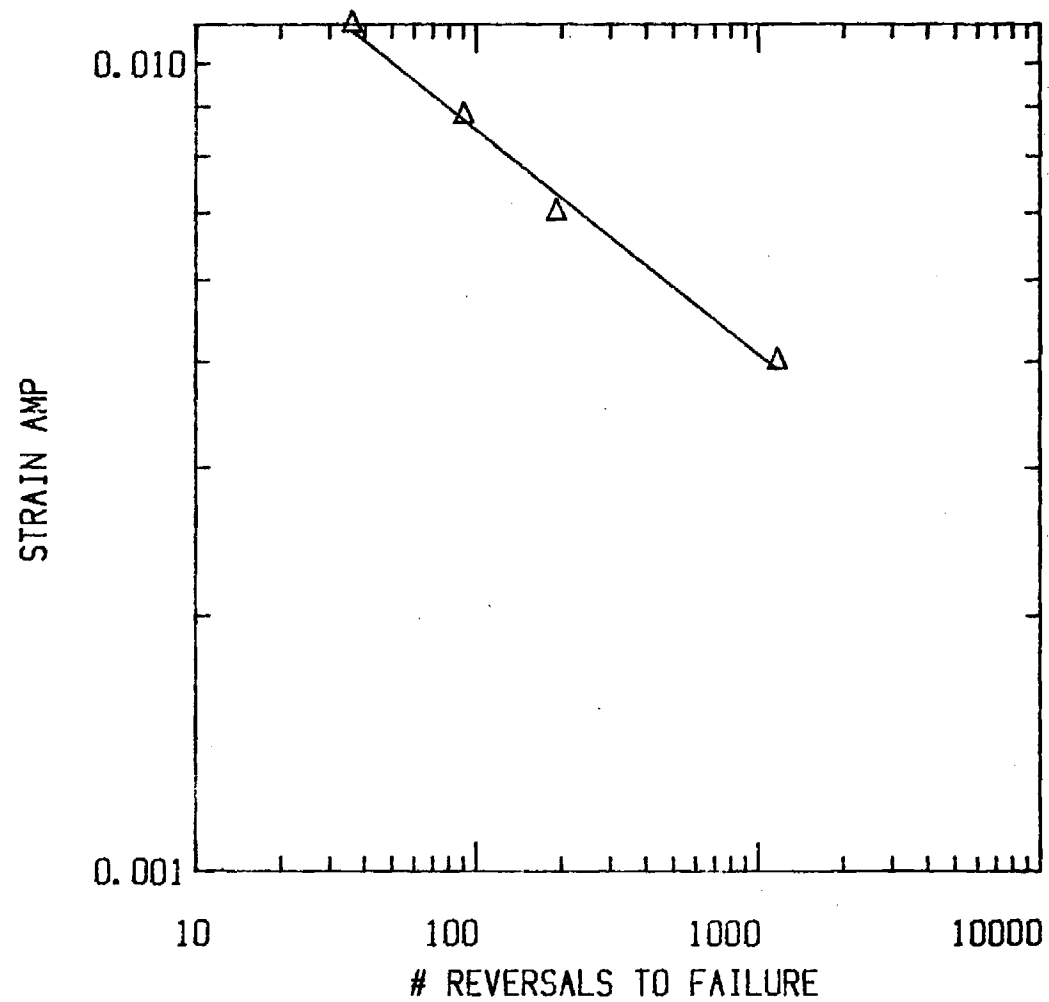
MAR-M 246   900 DEG C   RATE .0001 /SEC
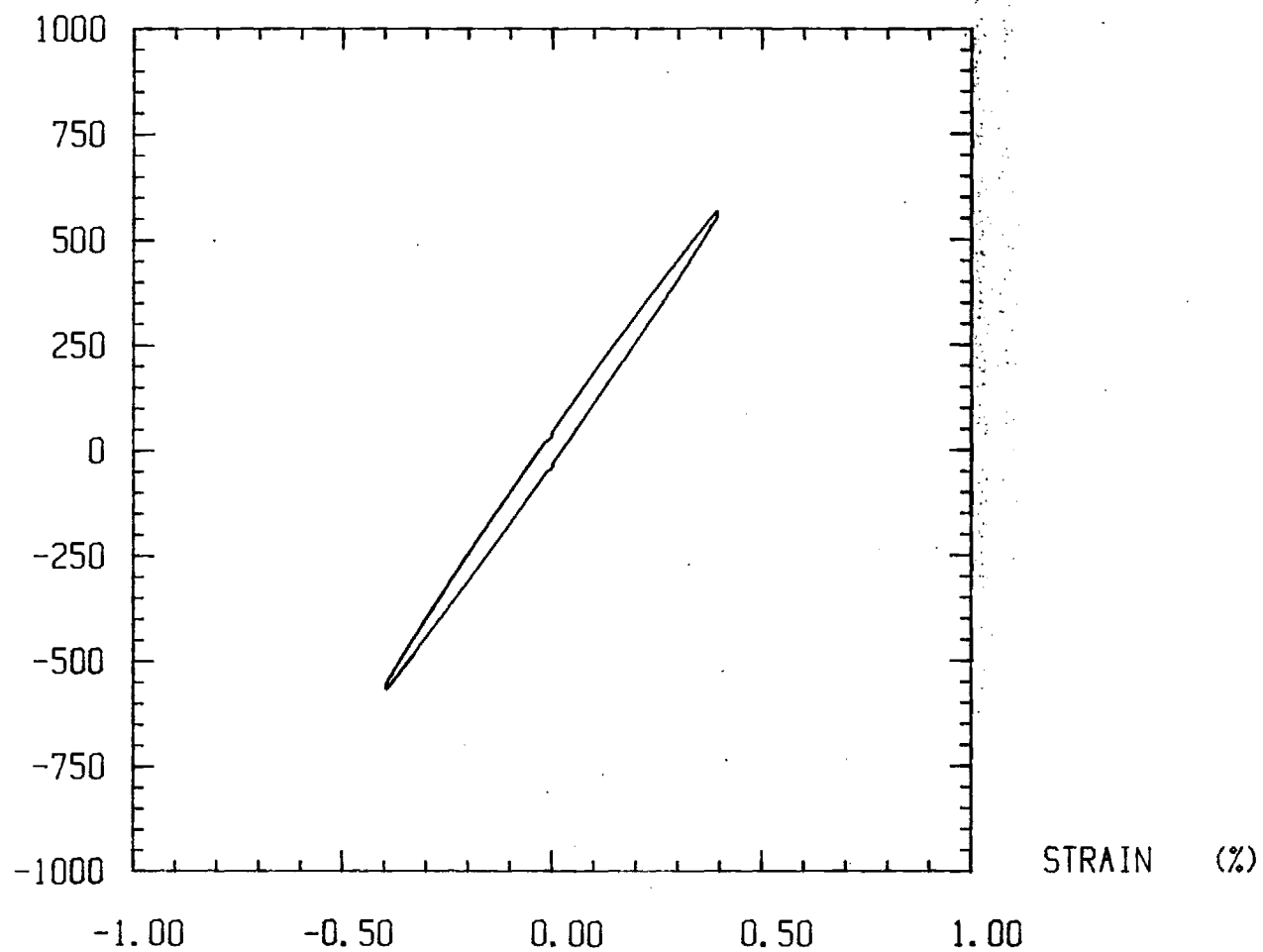
CYCLE #1-2   SPECIMEN F1   RATE = .001 /SEC
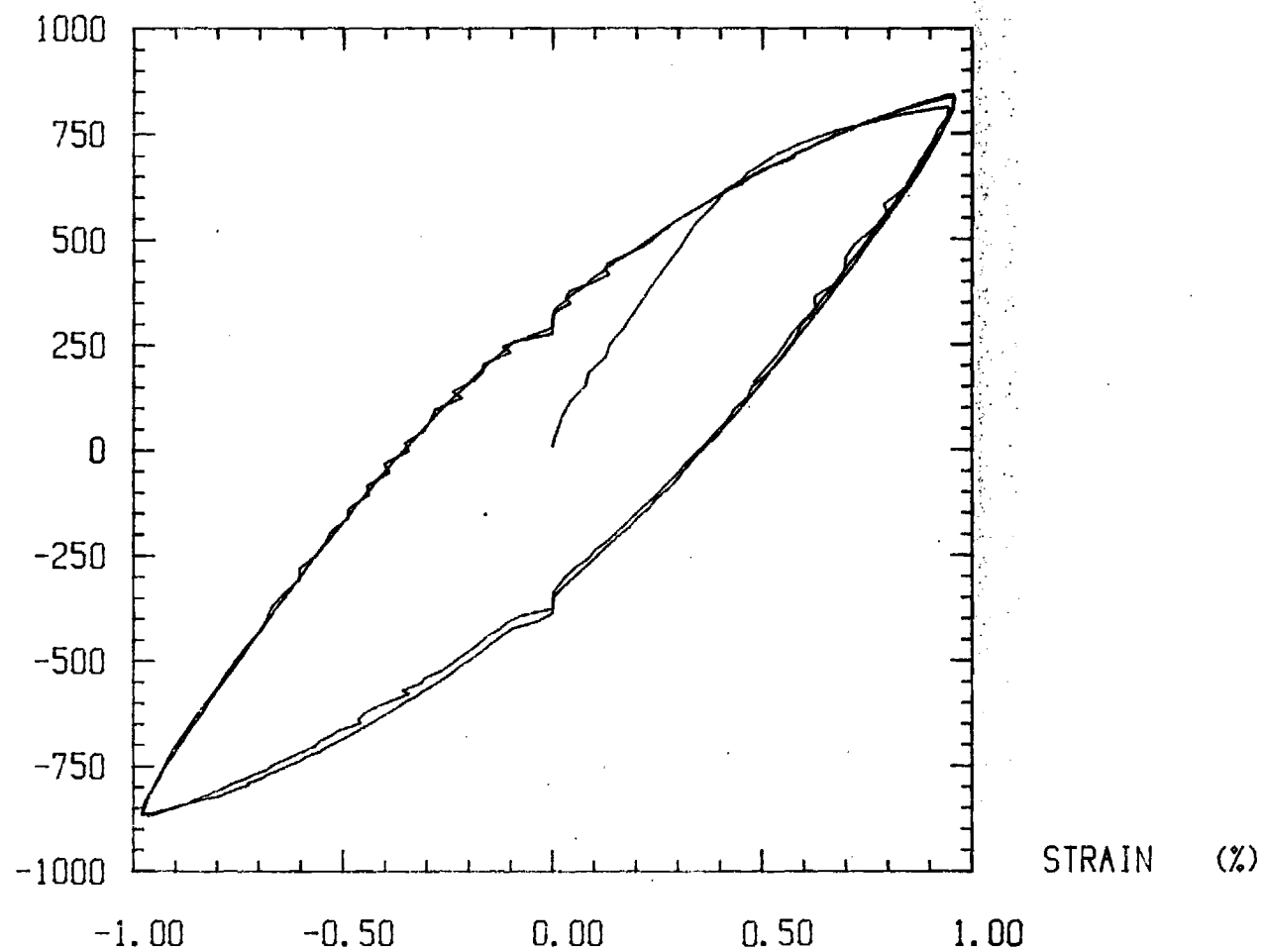
CYCLE #16-17   SPECIMEN F1   RATE =   .001 /SEC

STRESS   (MPa)

CYCLE #1-2 SPECIMEN F2 RATE = .001 /SEC

CYCLE #8-9 SPECIMEN F2 RATE = .001 /SEC

CYCLE #32-33 SPECIMEN F2 RATE = .001 /SEC

STRESS (MPa)

STRAIN (%)
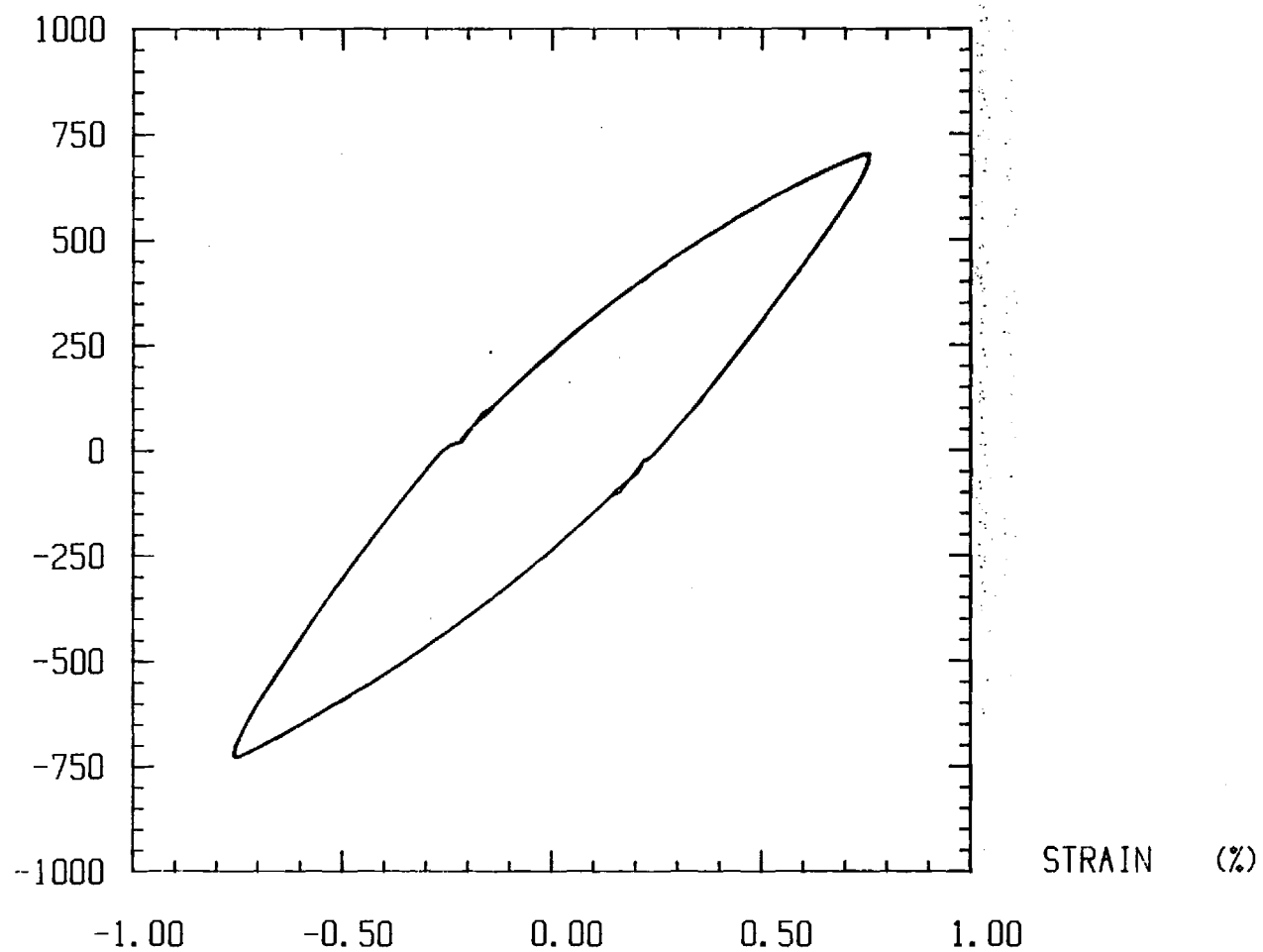
CYCLE #16-19 SPECIMEN F3 RATE = .001 /SEC
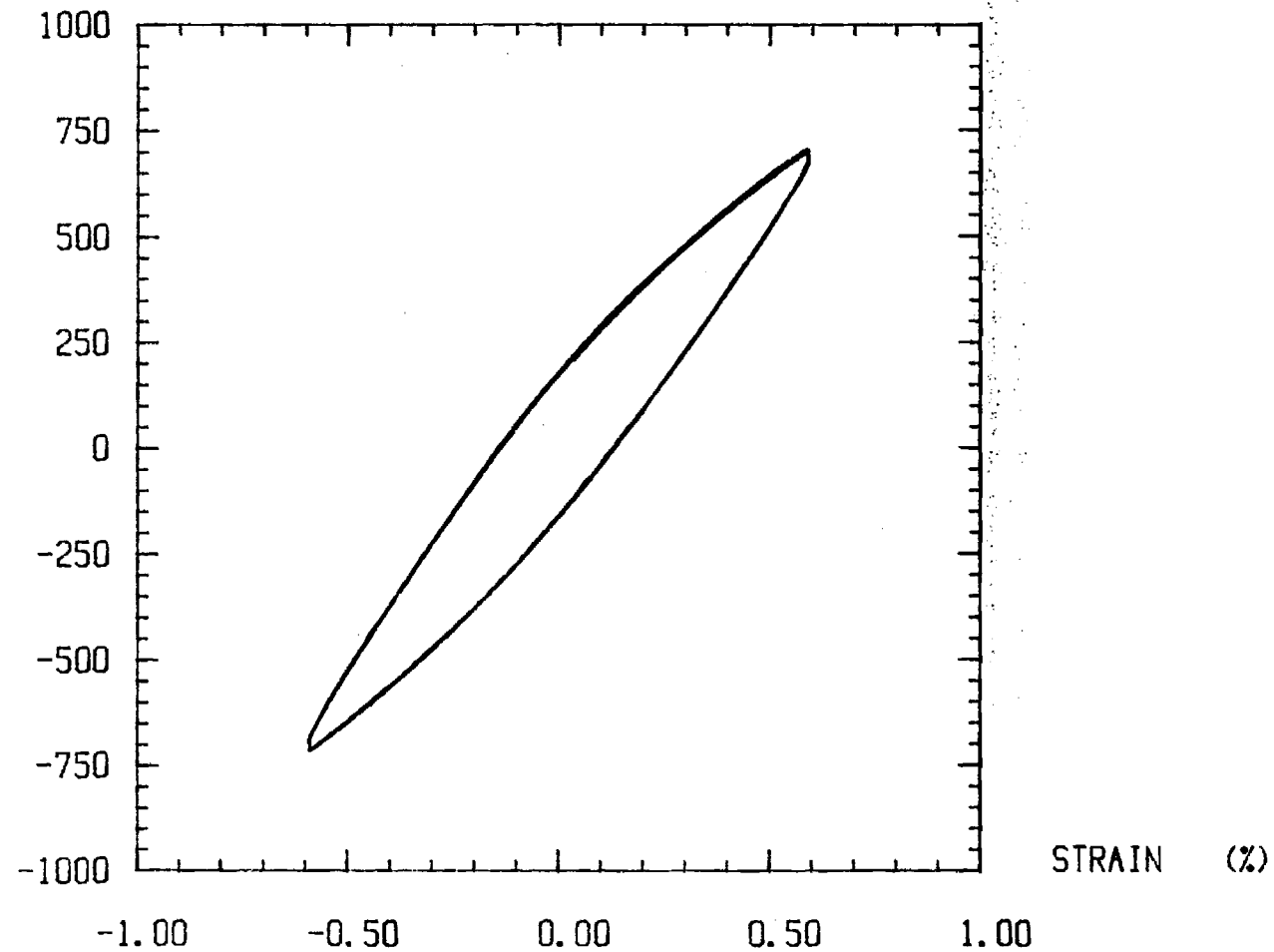
CYCLE #1-4 SPECIMEN F3 RATE = .001 /SEC

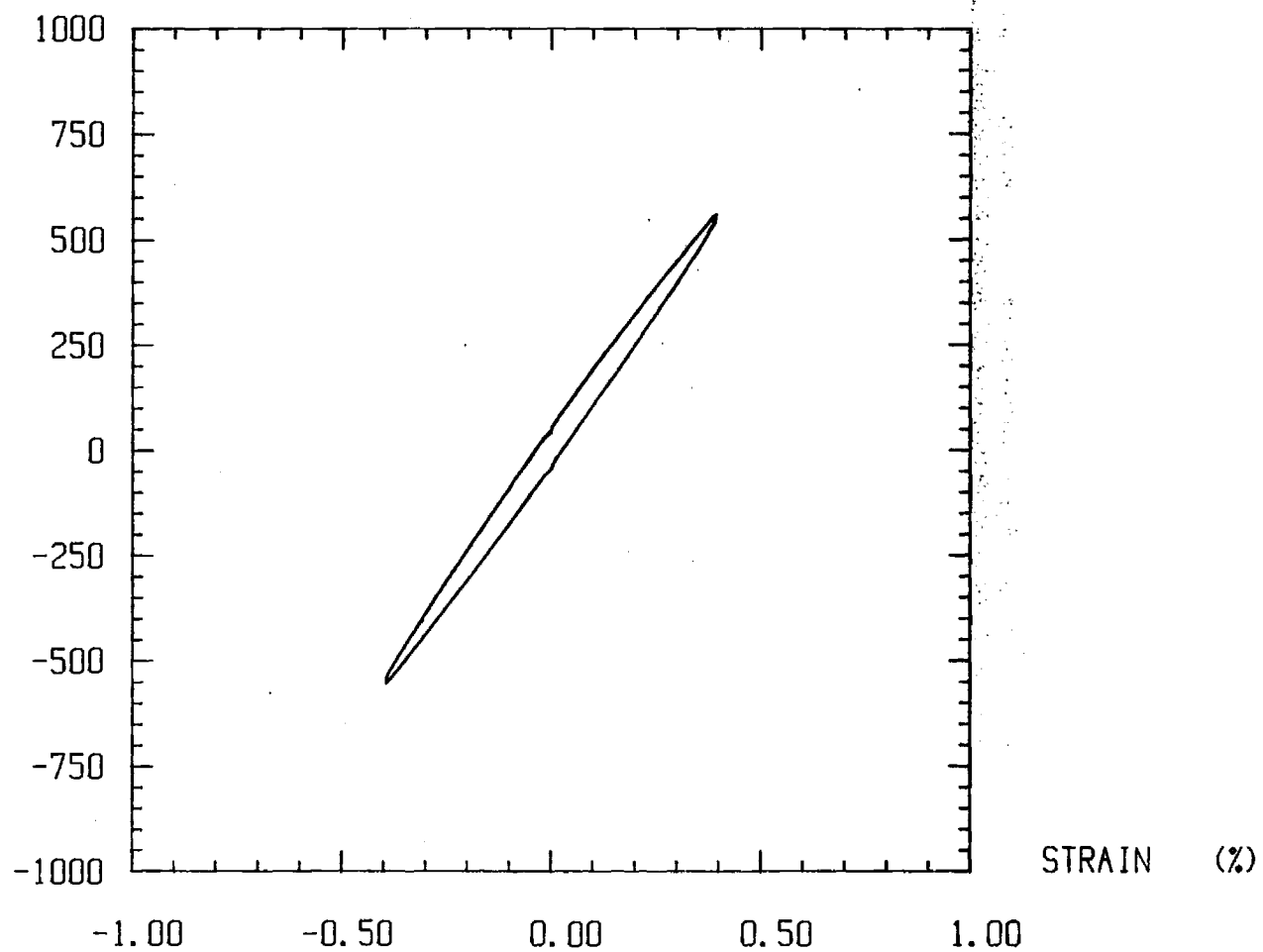CYCLE #95-96   SPECIMEN f3   RATE =   .001 /SEC

STRESS   (MPa)
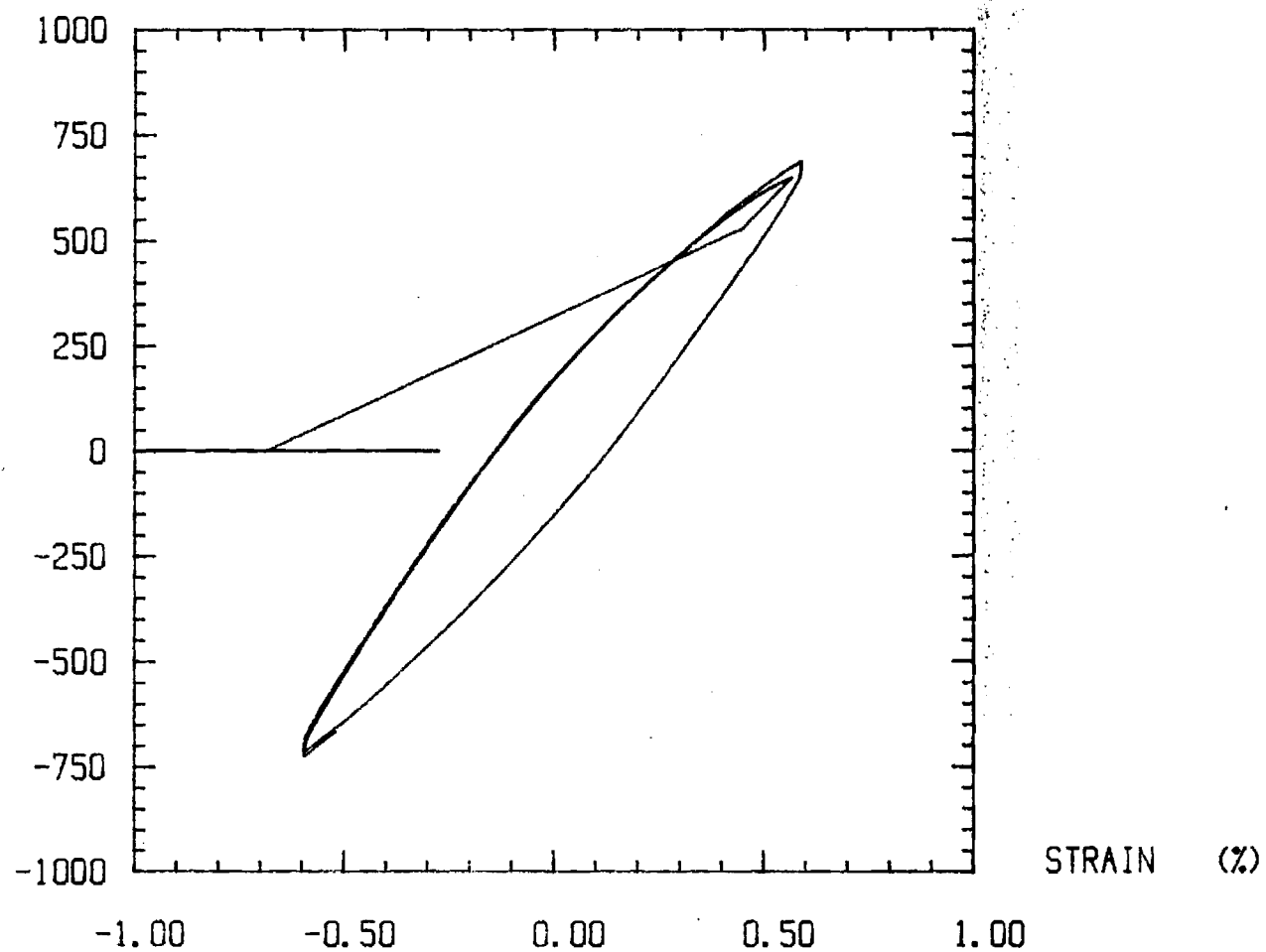
STRAIN   (%)

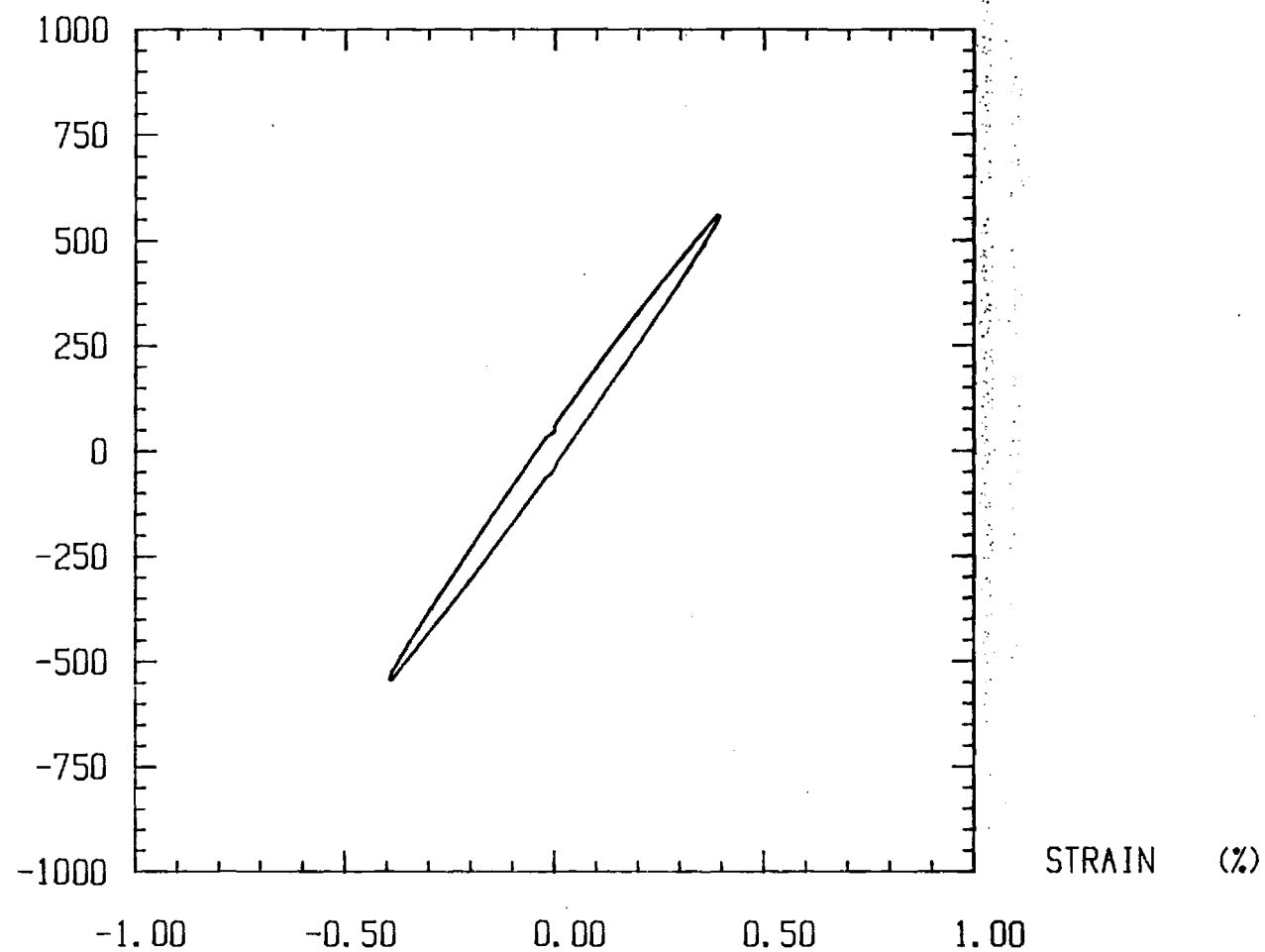CYCLE #2   SPECIMEN F4   RATE = .001 /SEC
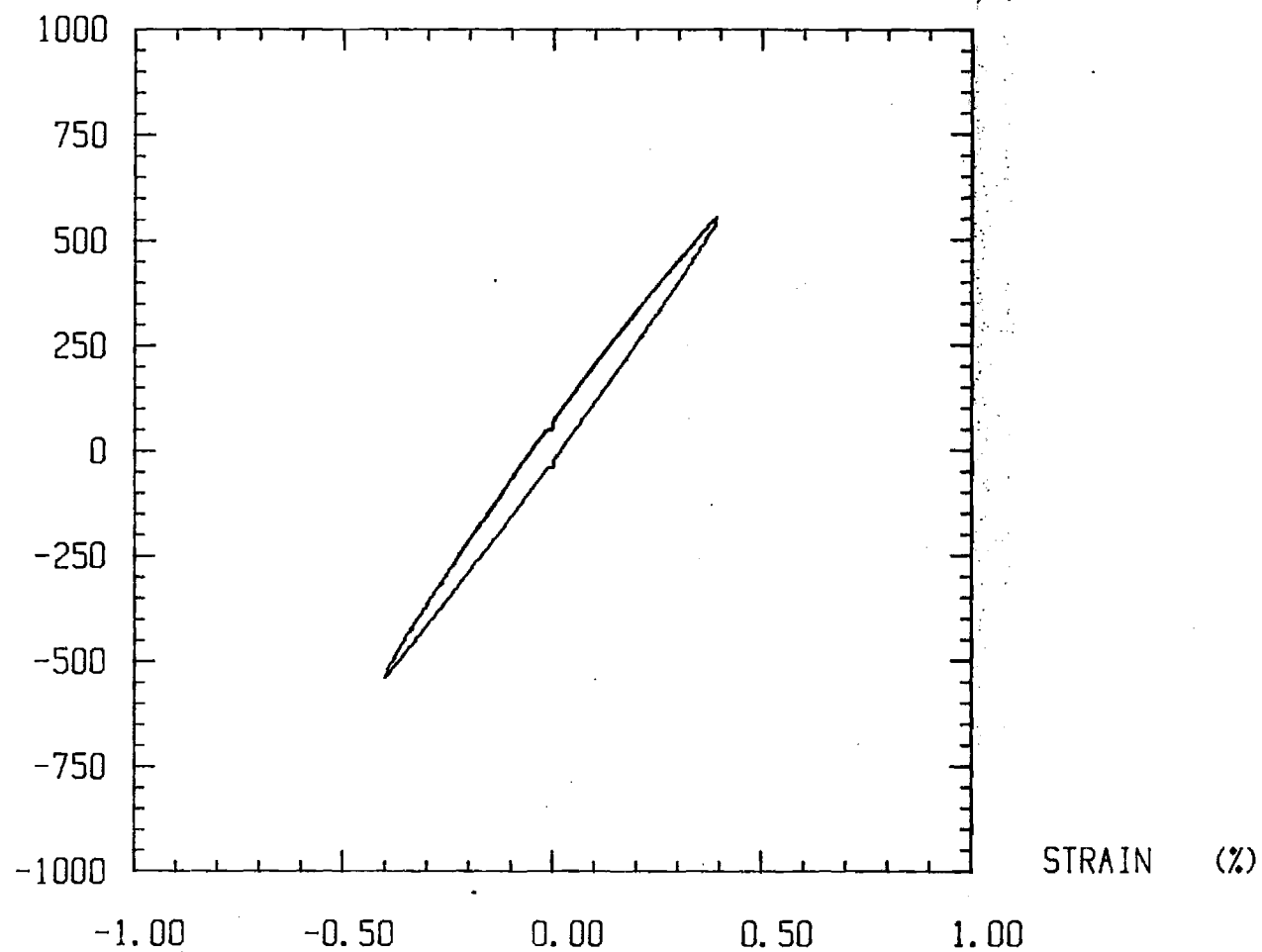
CYCLE #16-17   SPECIMEN F4   RATE = .001 /SEC

CYCLE #64-65   SPECIMEN F4   RATE =   .001 /SEC

STRESS   (MPa)

STRAIN   (%)

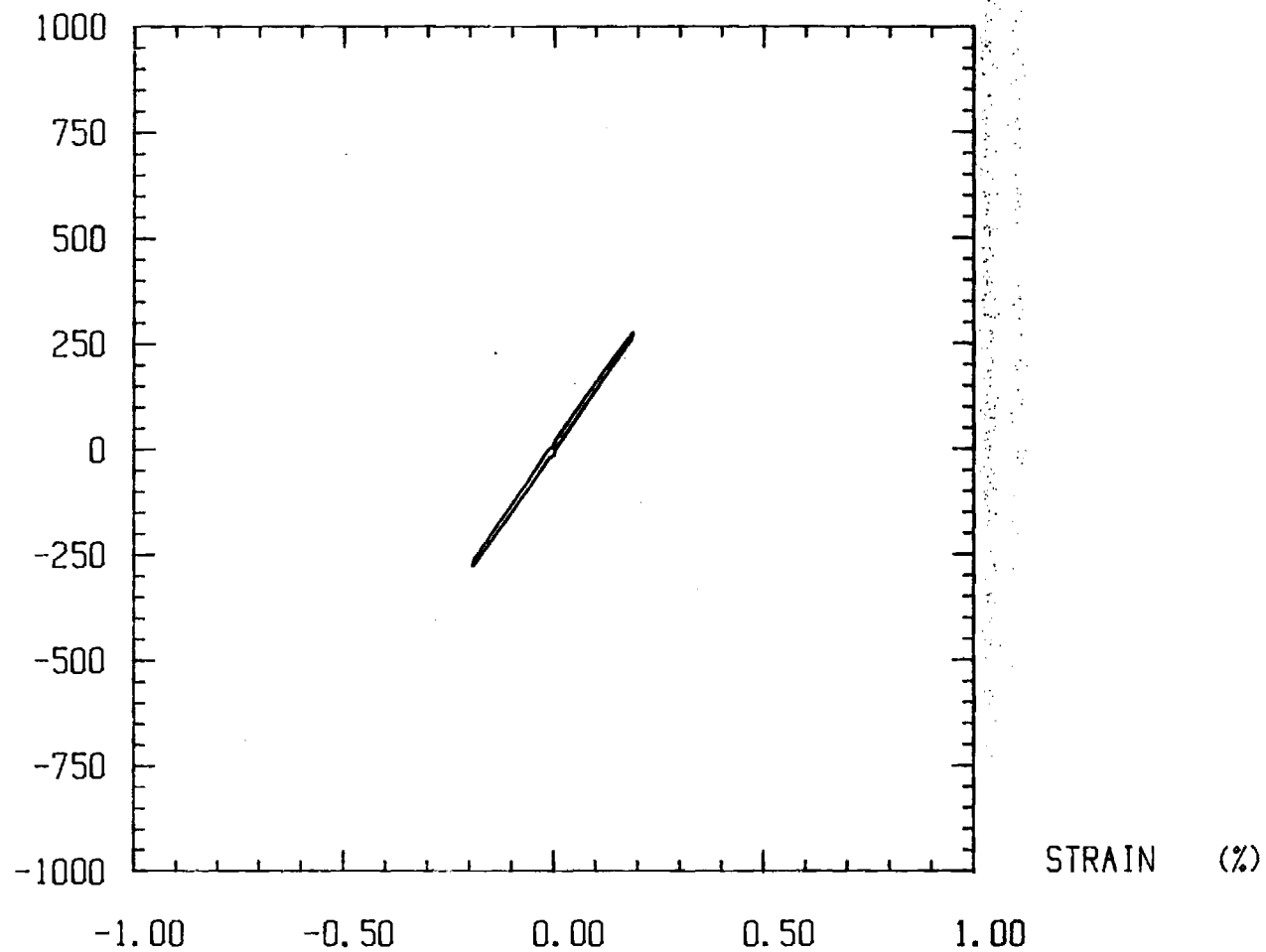CYCLE #550-551   SPECIMEN F4   RATE = .001 /SEC
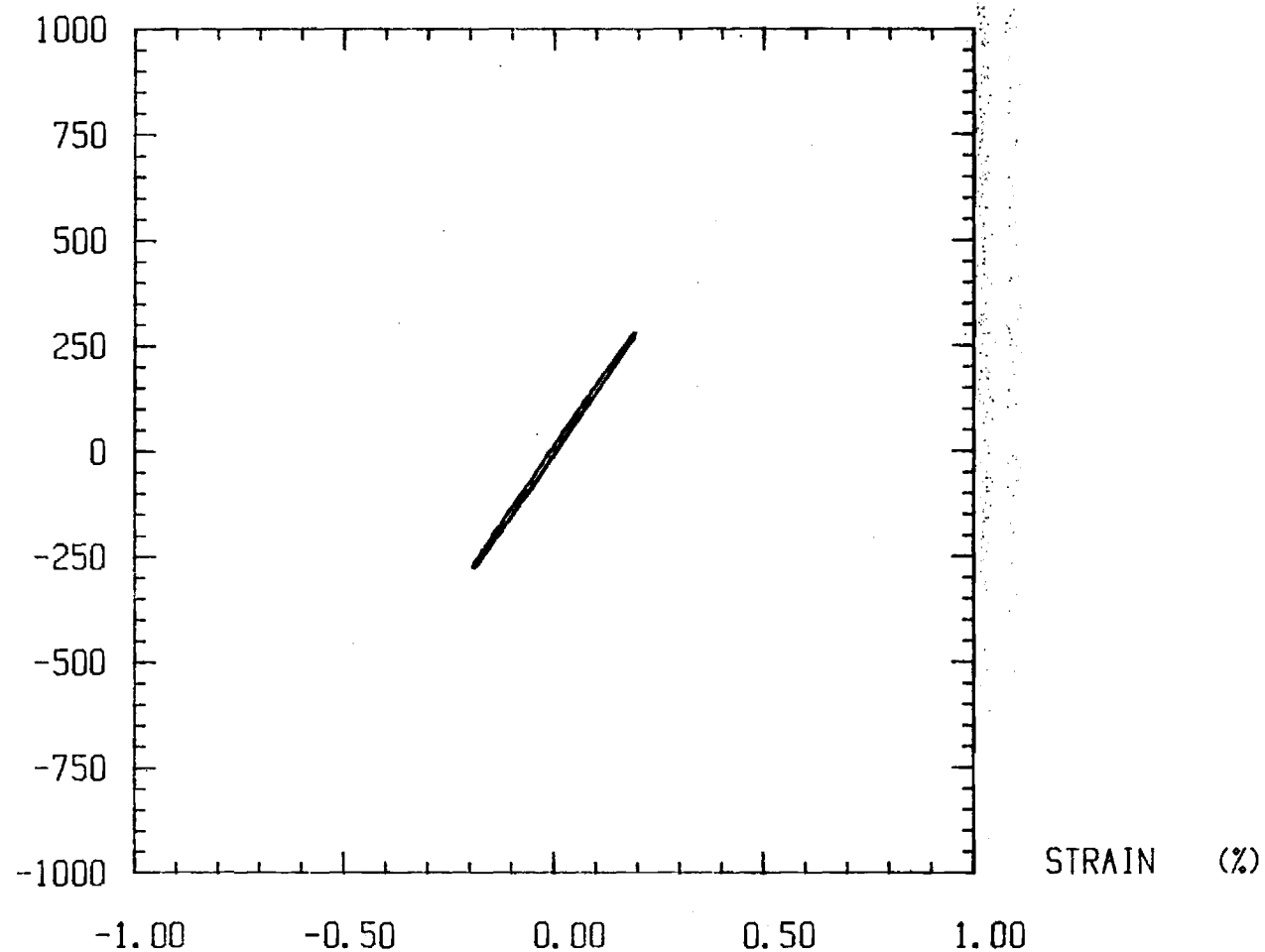
STRESS   (MPa)

STRAIN   (%)

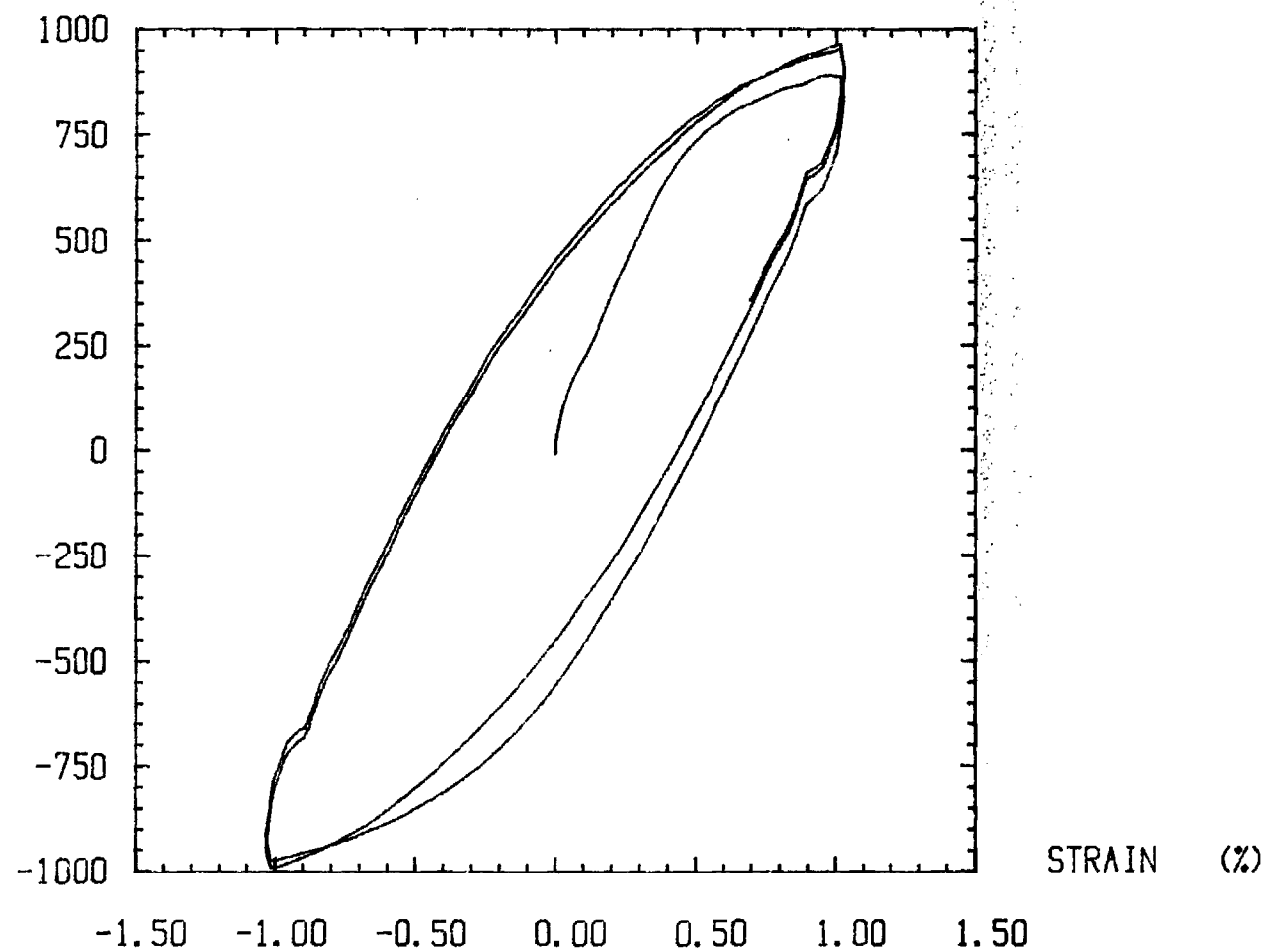CYCLE #1-2   SPECIMEN F5   RATE = .001 /SEC

CYCLE #10936   SPECIMEN F5   RATE = .001 /SEC

STRESS   (MPa)

CYCLE #1-3   SPECIMEN F6C   RATE =   .01 /SEC

STRESS   (MPa)

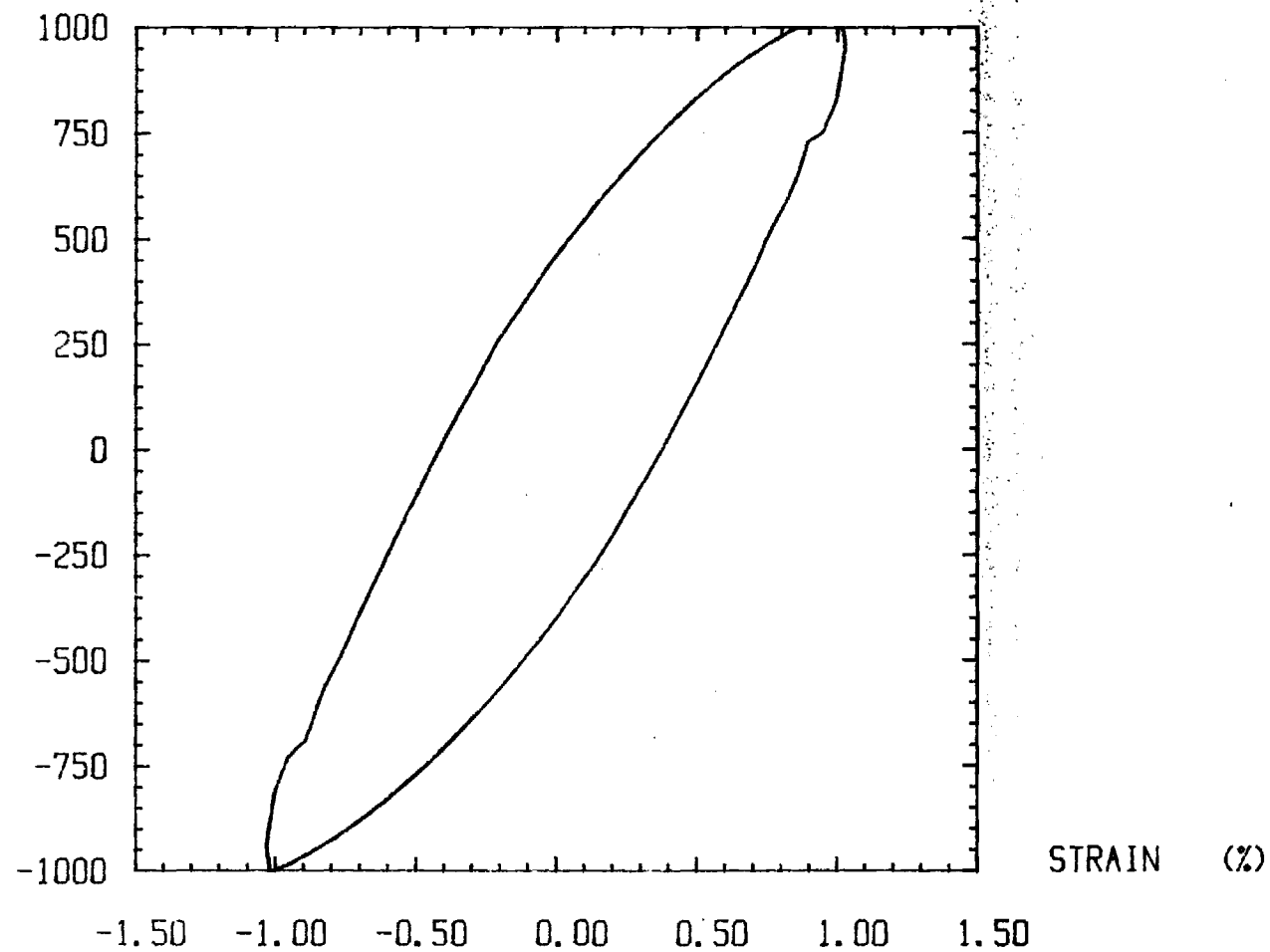
STRAIN   (%)

CYCLE #19-21 SPECIMEN F6C RATE = .01 /SEC

STRESS (MPa)

STRAIN (%)

CYCLE #1-4   SPECIMEN F8   RATE =   .01 /SEC

STRESS   (MPa)

CYCLE #16-19 SPECIMEN F8 RATE = .01 /SEC

STRESS   (MPa)

STRAIN   (%)

CYCLE #100-107 SPECIMEN F8 RATE = .01 /SEC

STRESS   (MPa)

STRAIN   (%)
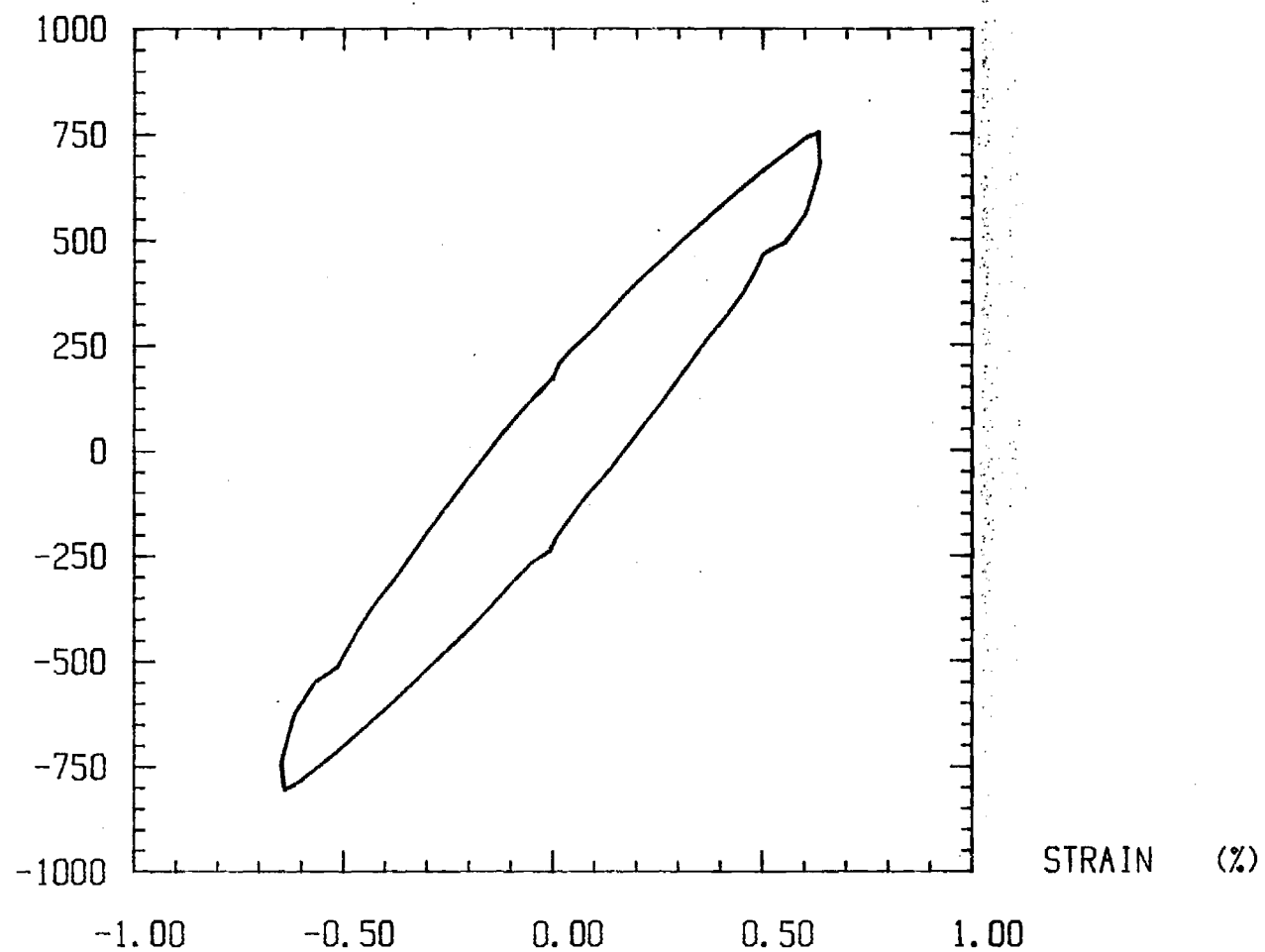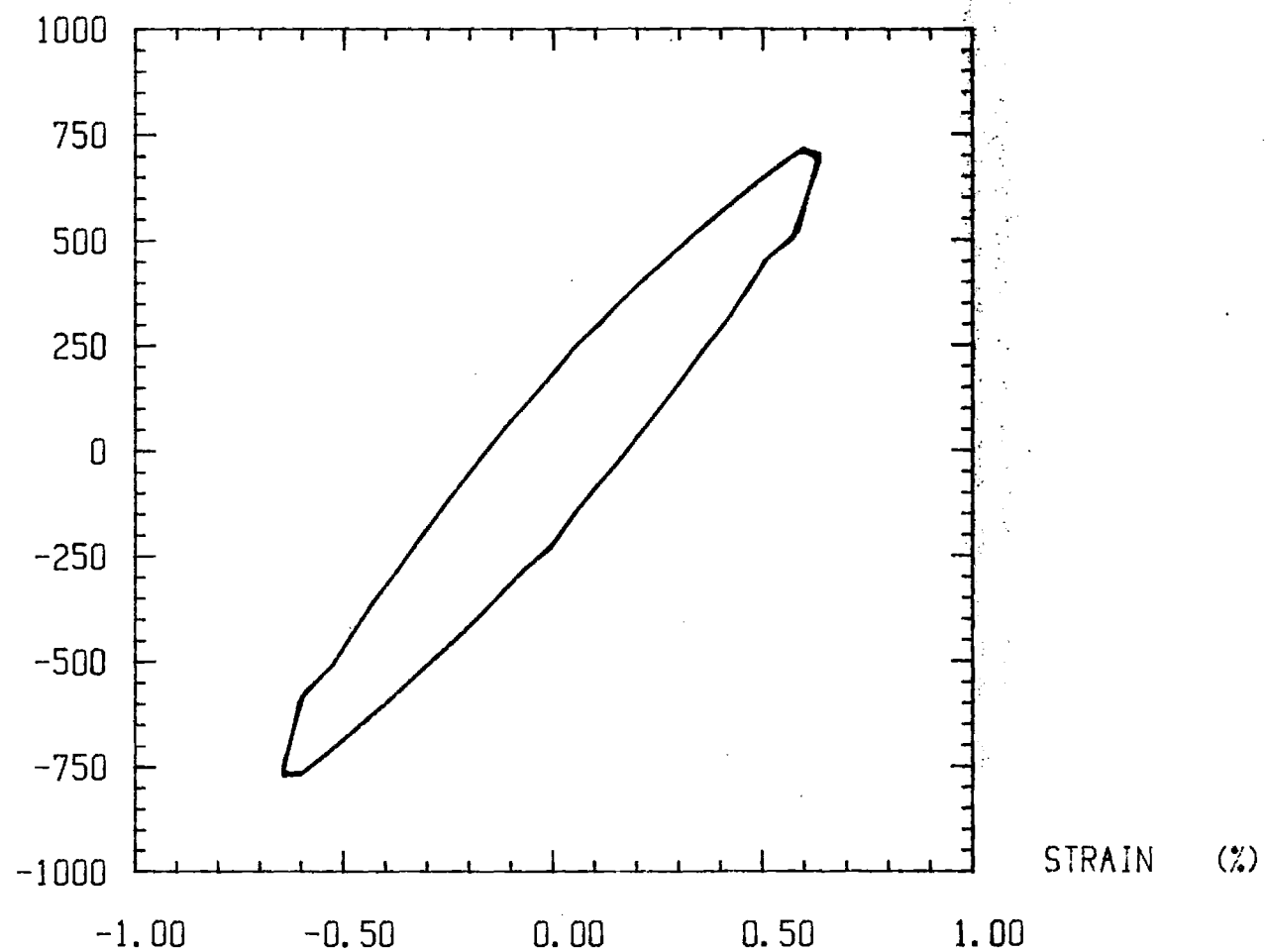
CYCLE #1 SPECIMEN F11 RATE = .0001 /SEC

STRESS (MPa)

STRAIN (%)
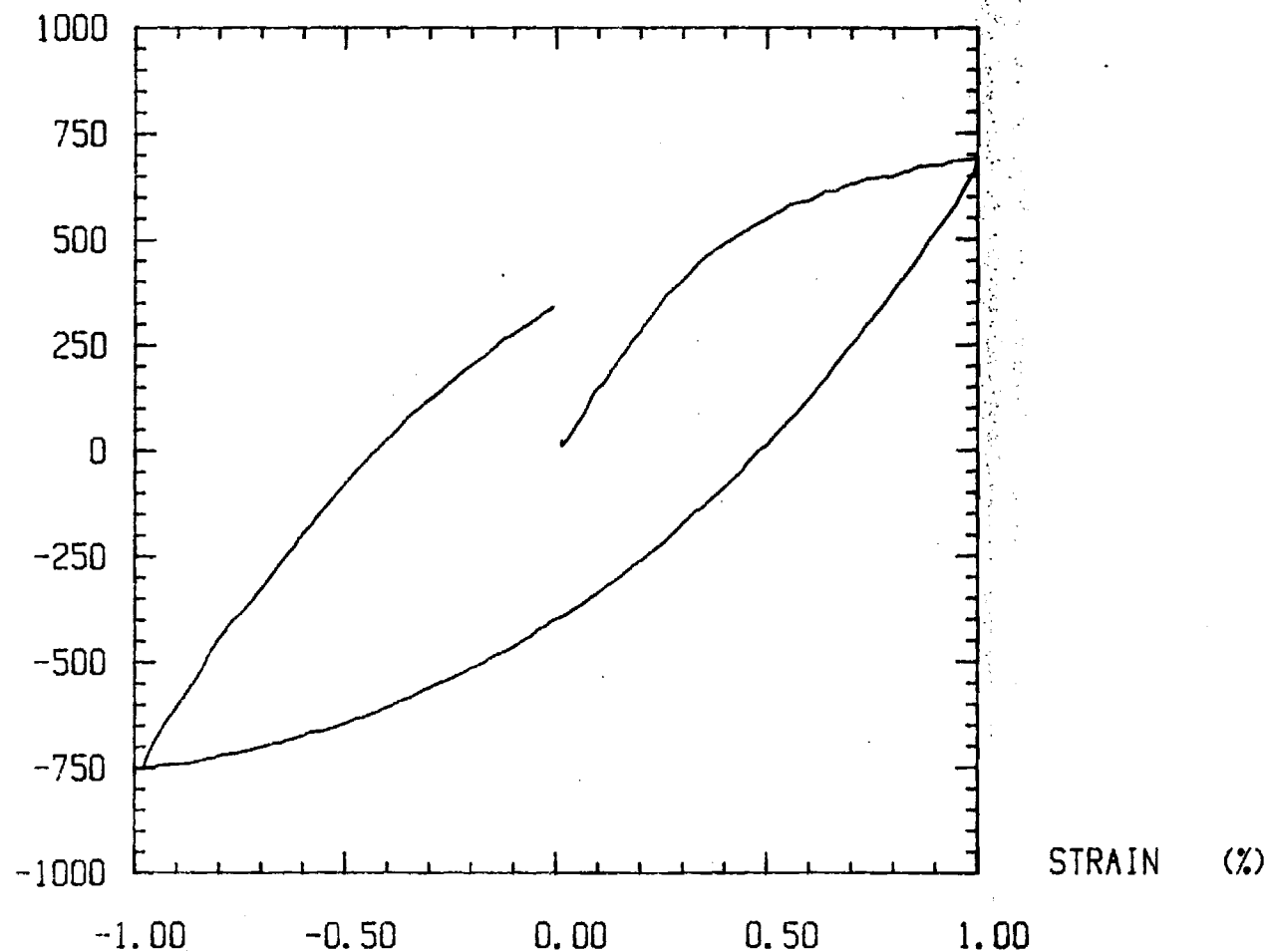
CYCLE #4   SPECIMEN F11   RATE = .0001 /SEC
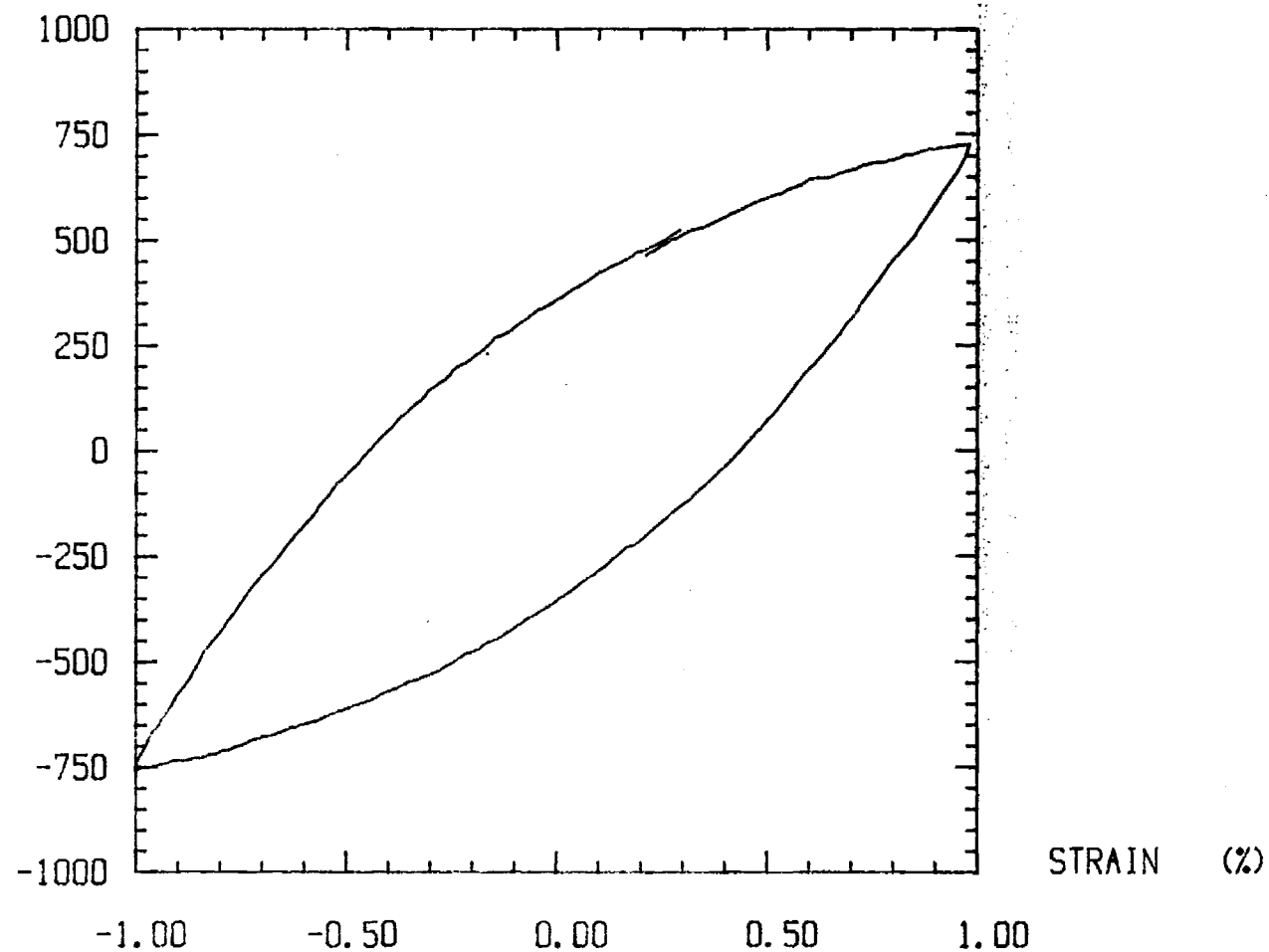
STRESS   (MPa)

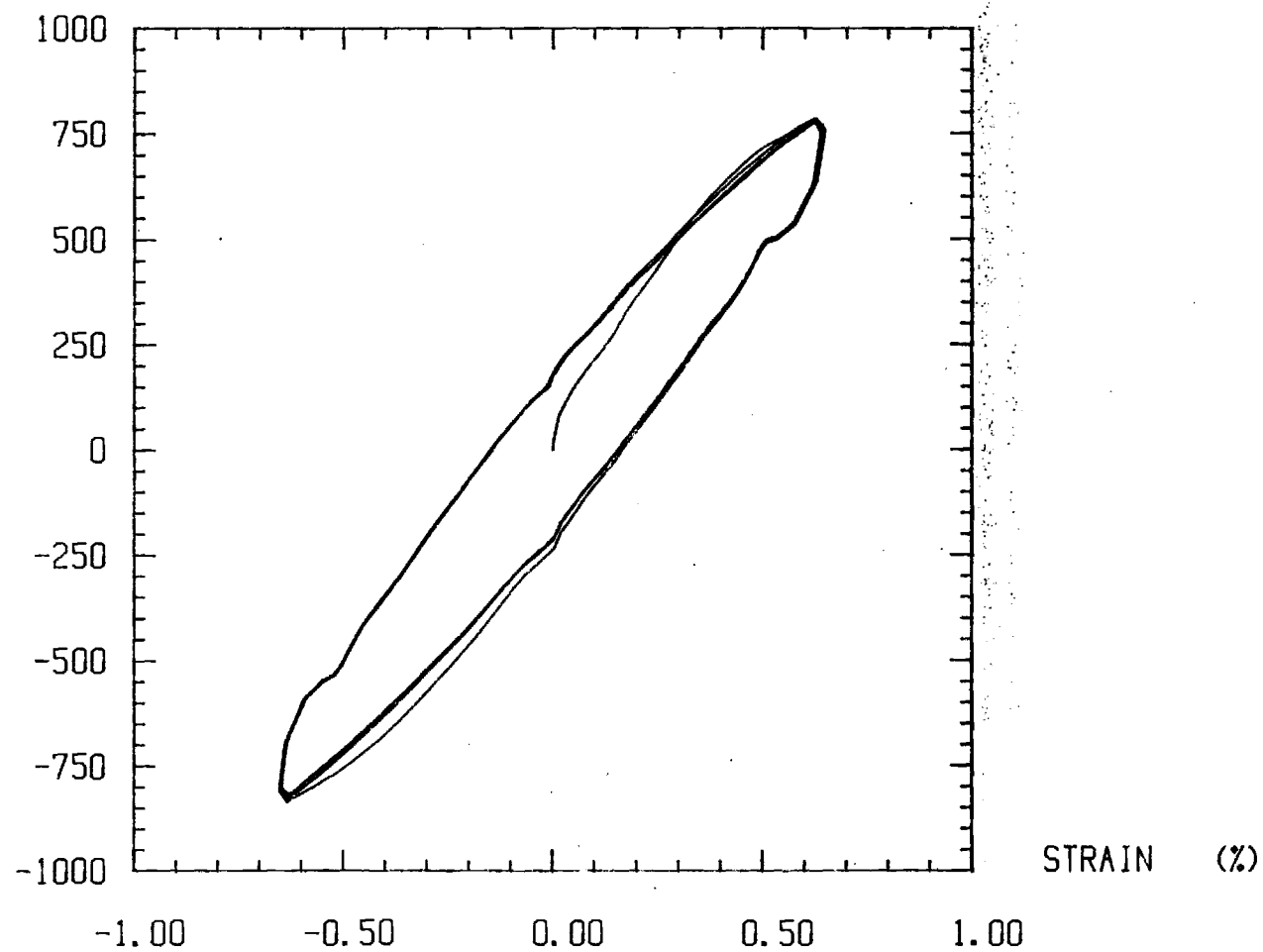CYCLE #8   SPECIMEN F11   RATE = .0001 /SEC

STRESS   (MPa)

STRAIN   (%)
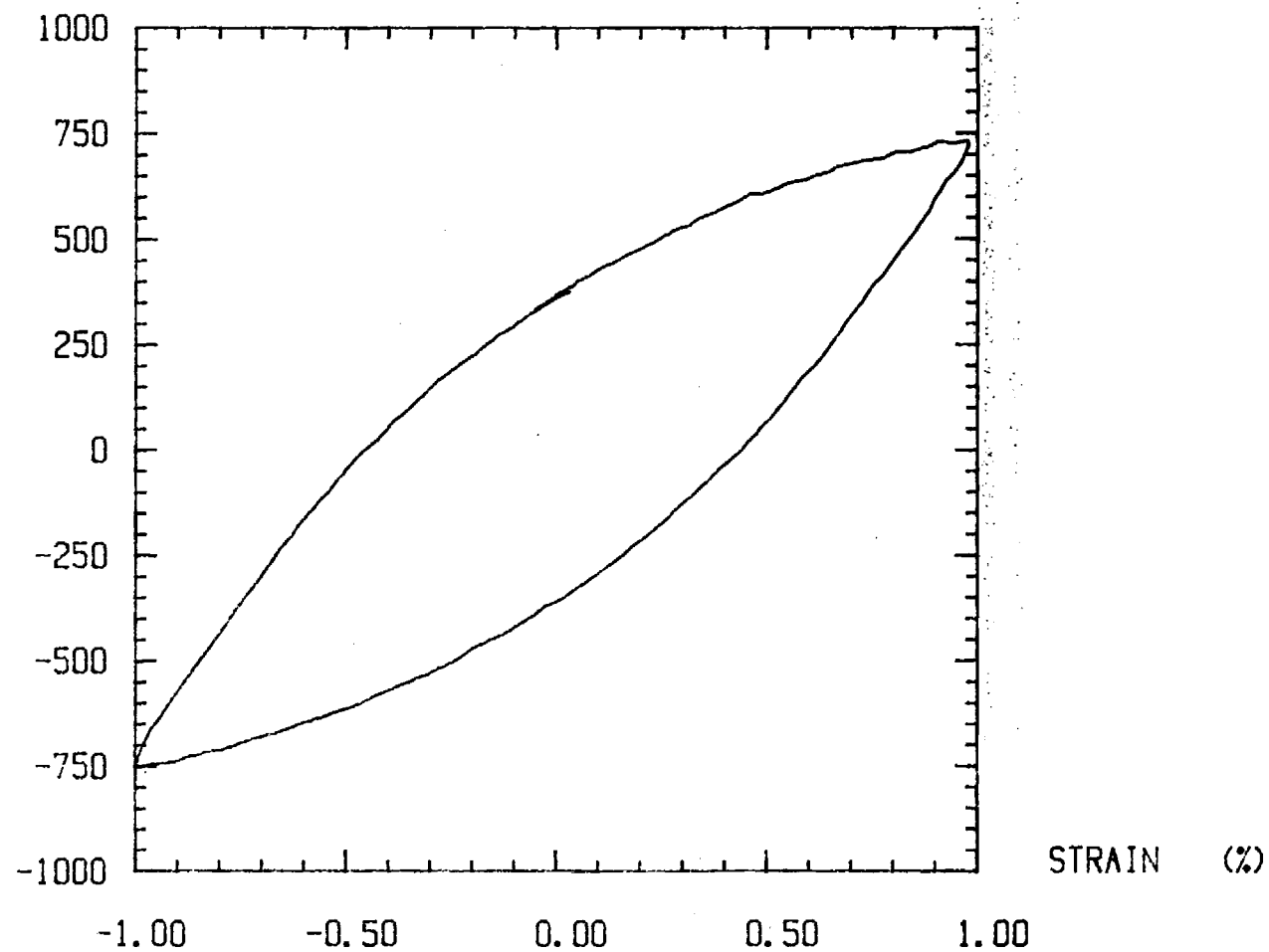
CYCLE #1   SPECIMEN f12B   RATE =   .0001 /SEC
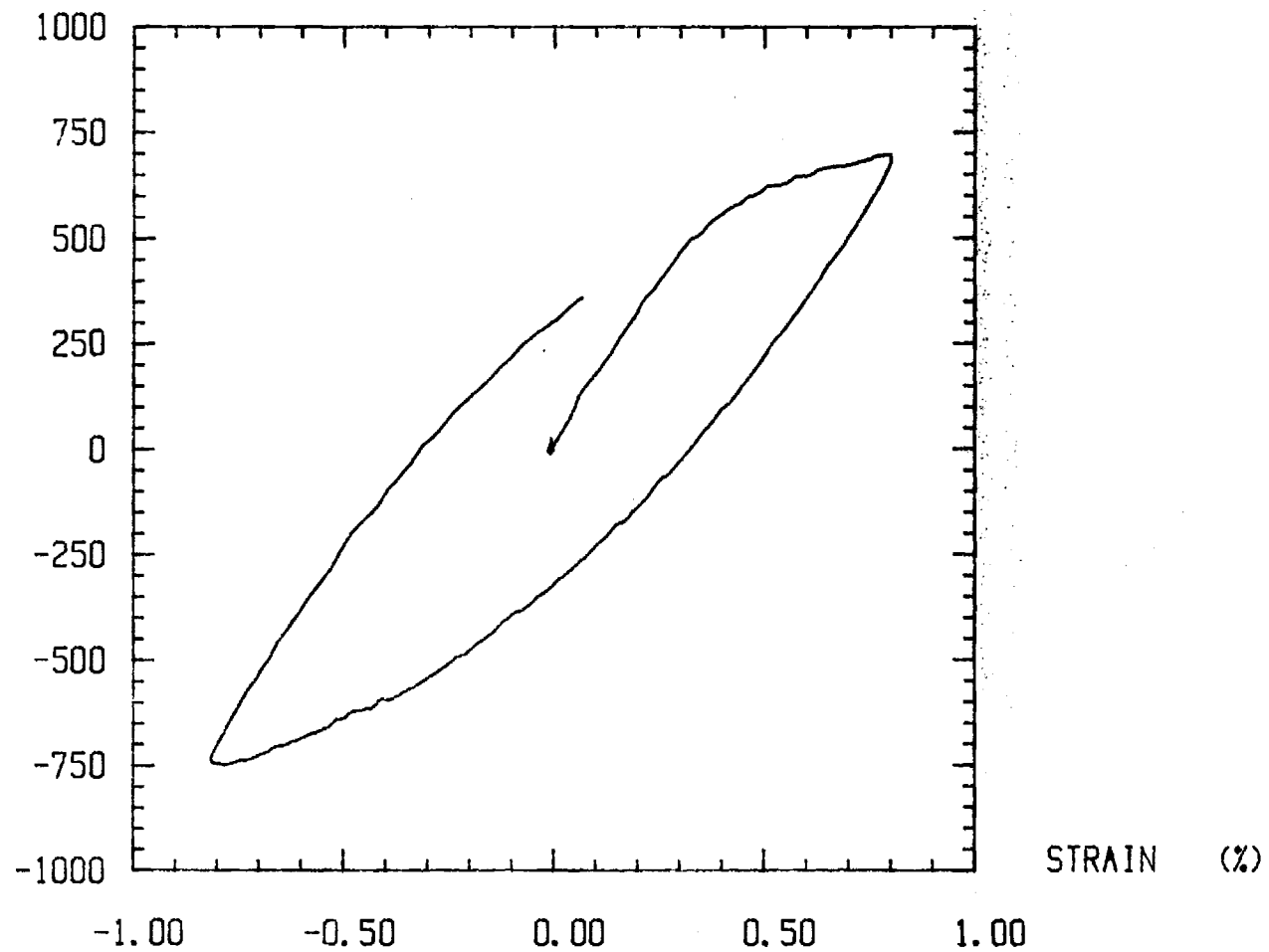
CYCLE #4-5   SPECIMEN F12B   RATE =   .0001 /SEC

STRESS   (MPa)

STRAIN   (%)
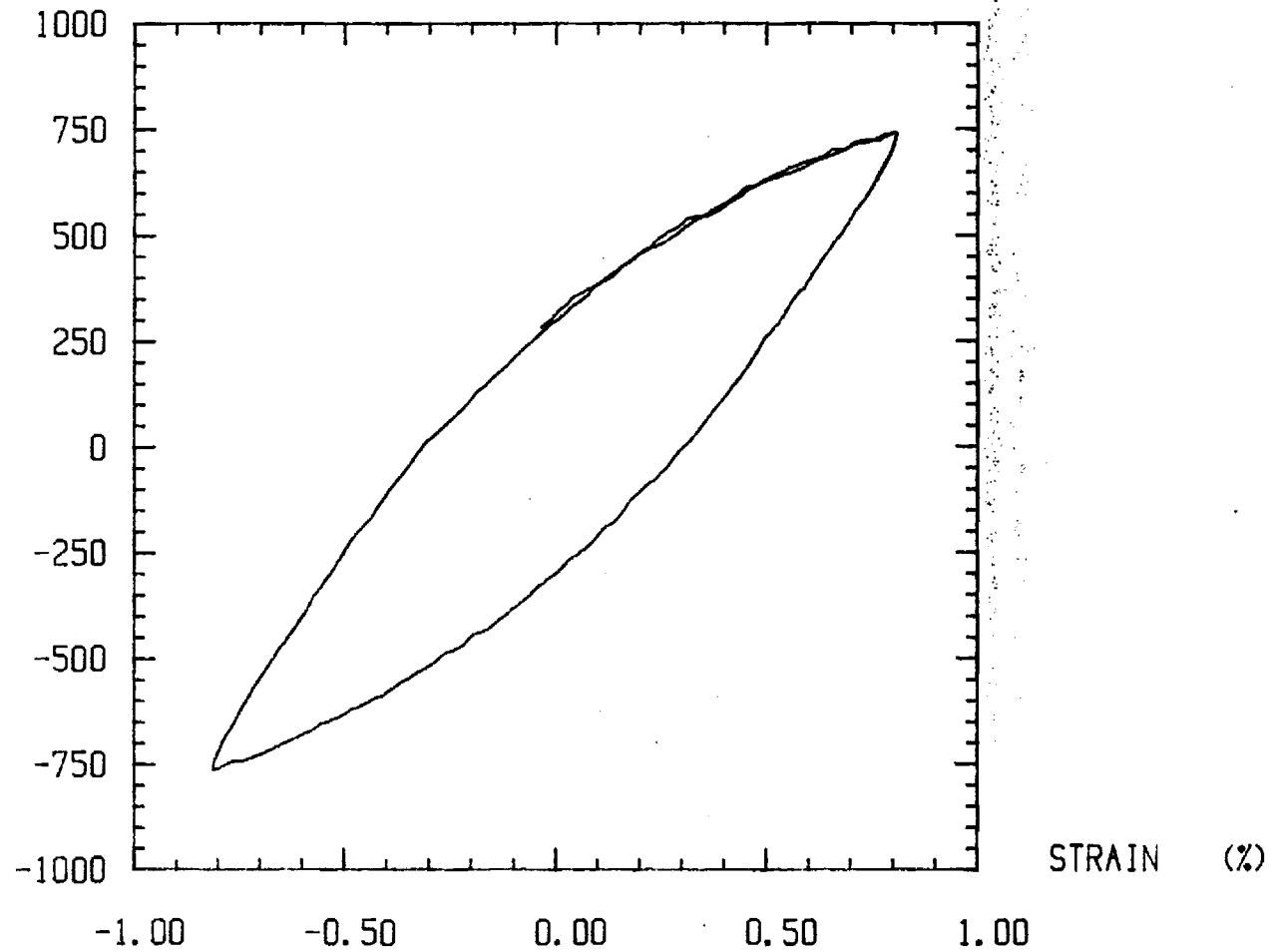
CYCLE #24-25   SPECIMEN F12B   RATE = .0001 /SEC
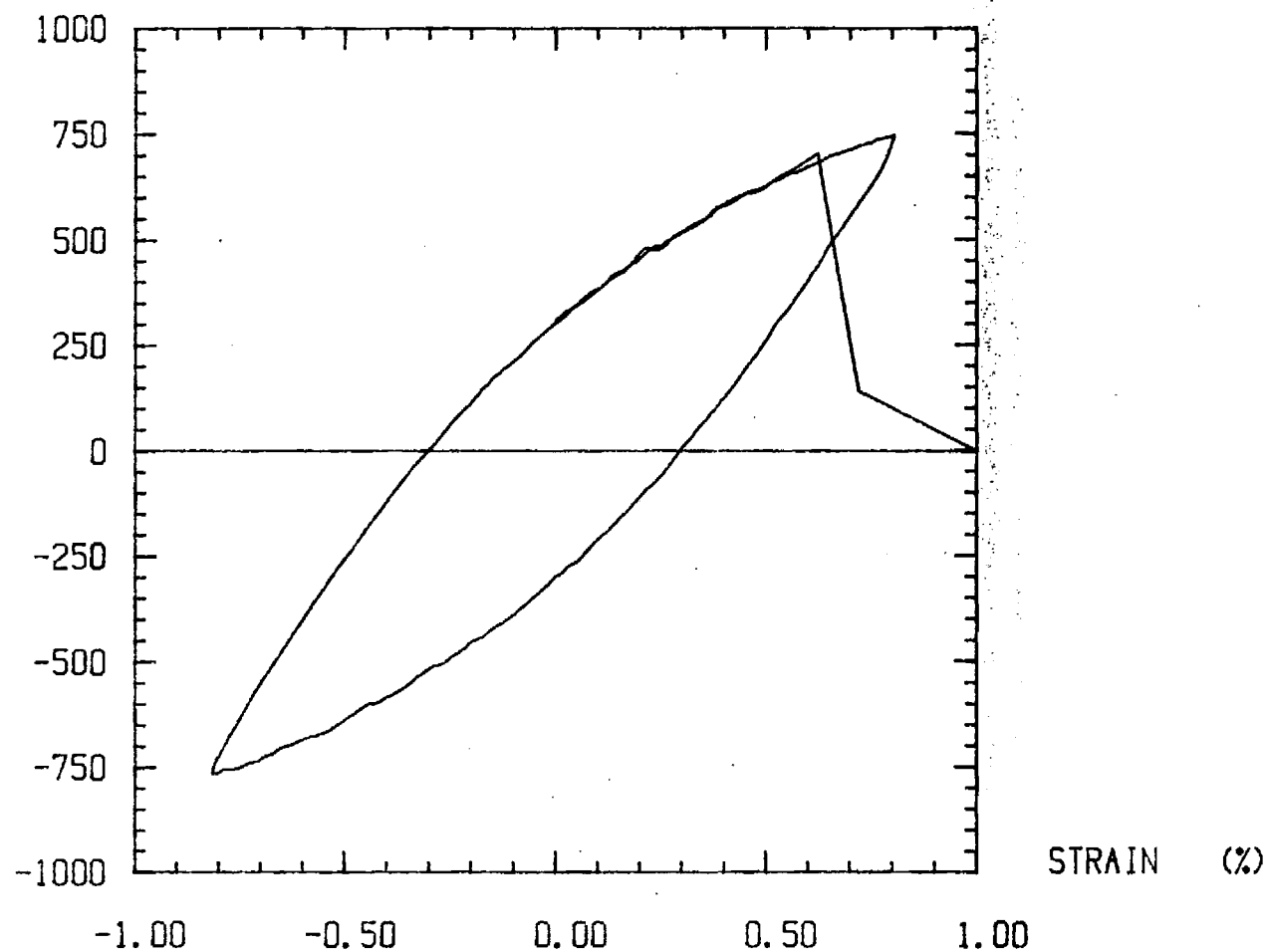
CYCLE #1-3   SPECIMEN F13   RATE =   .0001 /SEC

STRESS   (MPa)

STRAIN   (%)
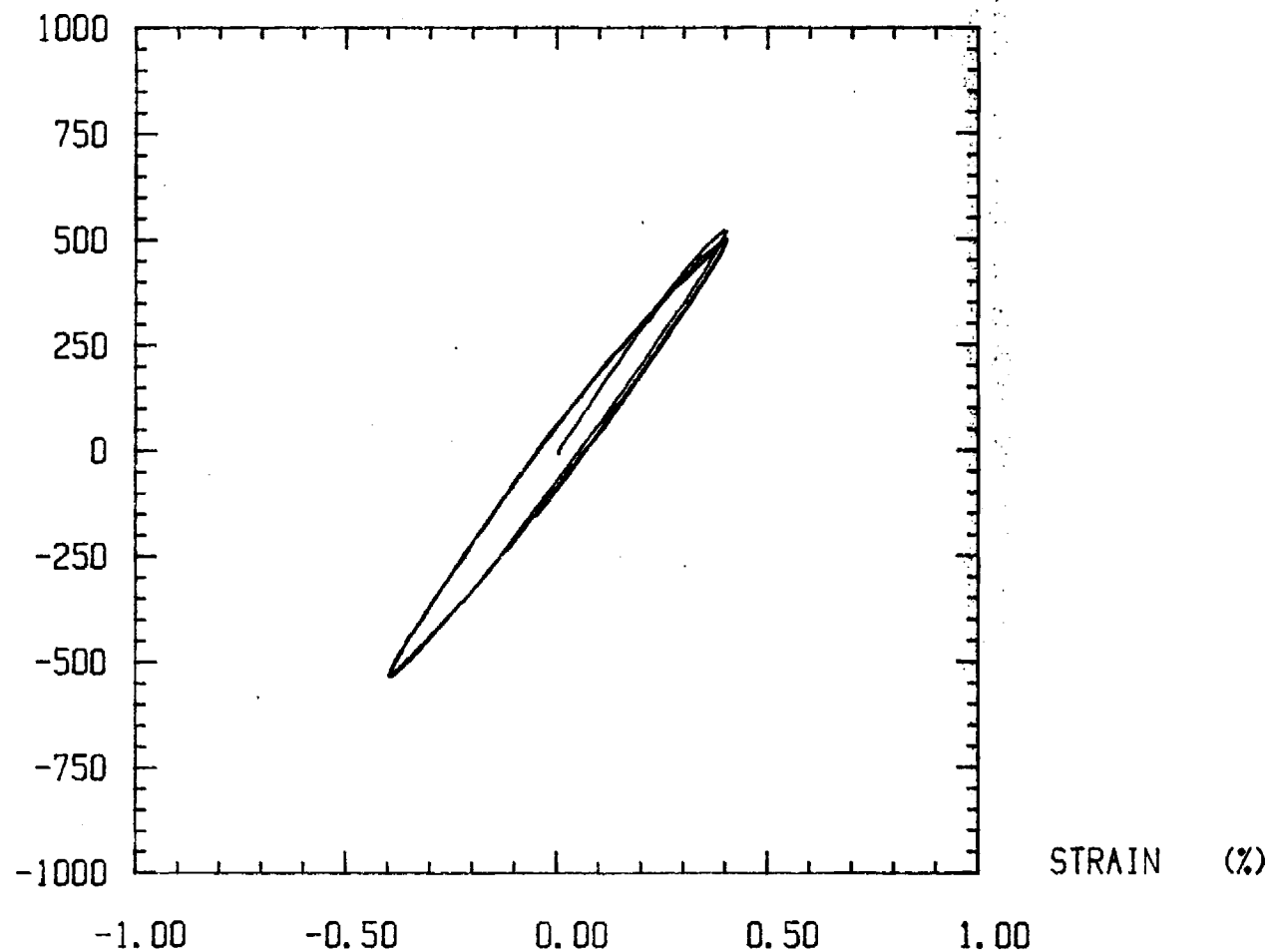
CYCLE #16-18   SPECIMEN F13   RATE = .0001 /SEC
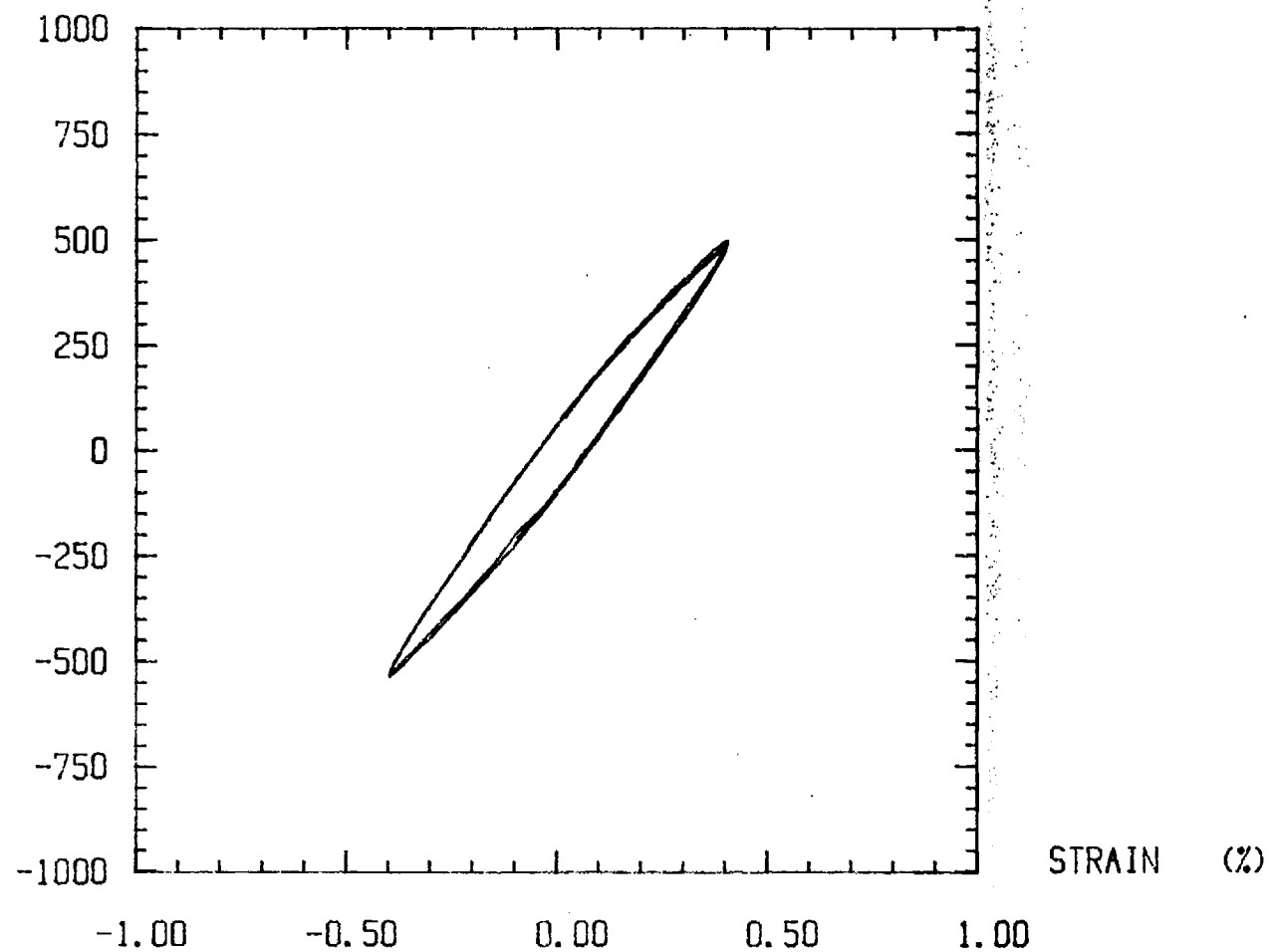
STRESS   (MPa)

CYCLE #64-66   SPECIMEN F13   RATE = .0001 /SEC

STRESS   (MPa)

STRAIN   (%)
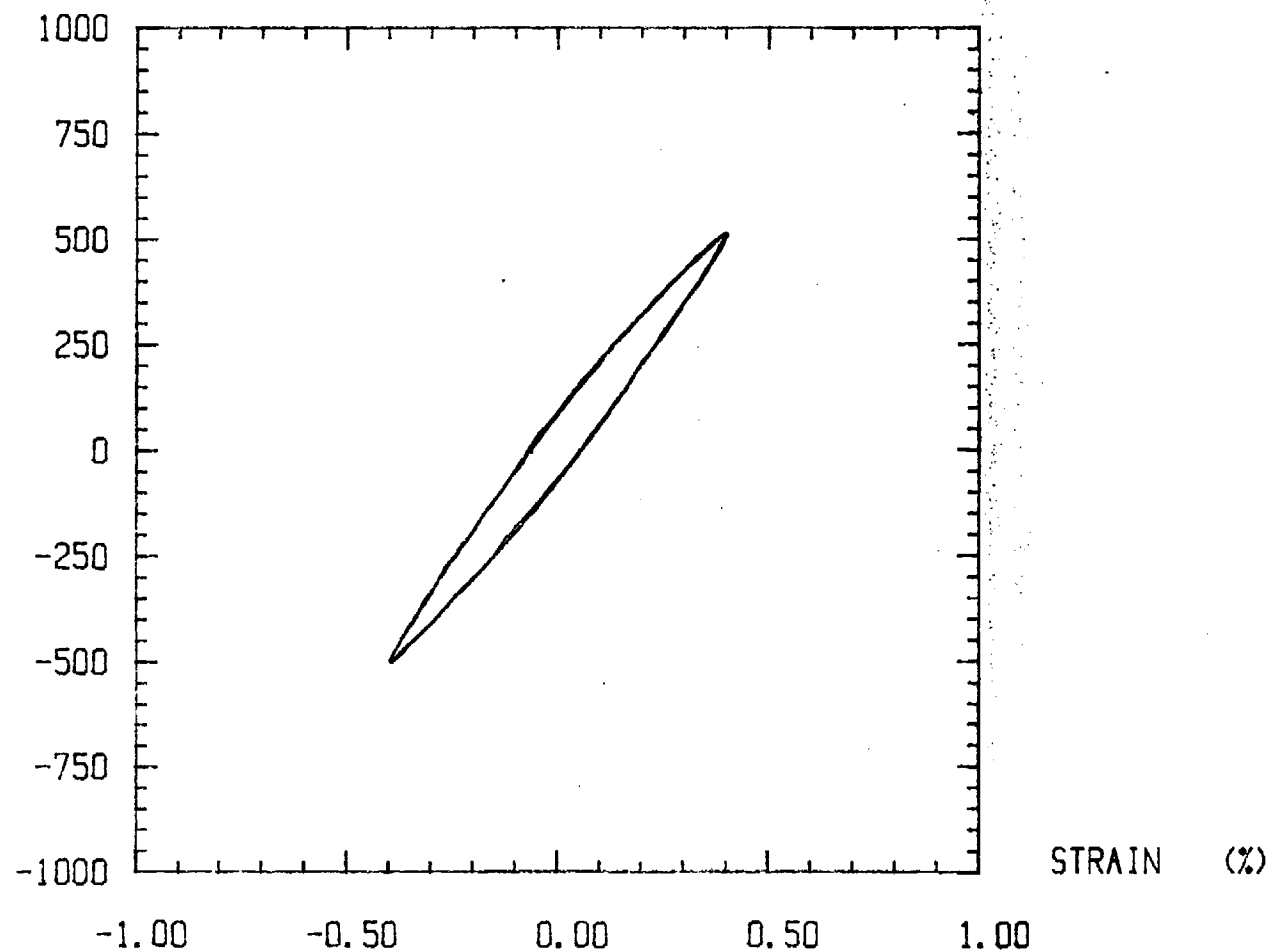
CYCLE #350-352 SPECIMEN F13 RATE = .0001 /SEC
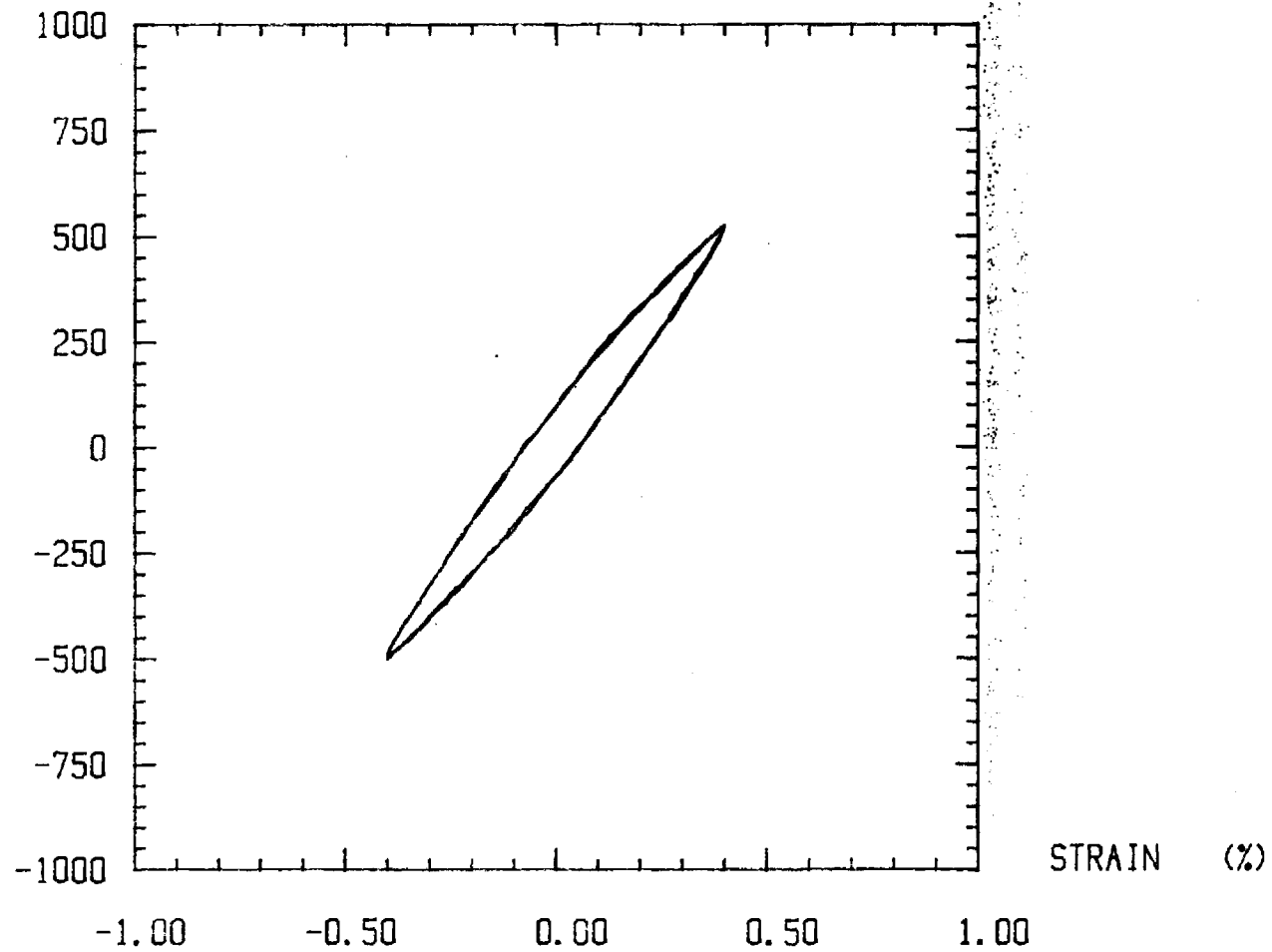
STRESS (MPa)

STRAIN (%)

LETTER REPORT

"DAMAGE RATE APPROACHES FOR THERMOMECHANICAL FATIGUE
OF SUPERALLOYS"

By David L. McDowell
Principal Investigator

R.L.T. Oehmke
Research Engineer

Gary Reynolds
Graduate Research Assistant

Project # E-25-M13
General Motors PO# H636356

August 10, 1987

Submitted to Allison Gas Turbine Operations, General Motors
Corporation

Sponsor Technical Contact:

Dr. W.E. Schneider/T-10
Allison Gas Turbine Operations
General Motors Corporation
2001 South Tibbs Ave.
Indianapolis, IN 46241
(317) 242-7703

Sponsor Administration and Contractual Matters:

Darrell L. Mackey/U02
Allison Gas Turbine Operations
General Motors Corporation
P.O. Box 420
Indianapolis, IN 46206-0420
(317) 242-6954

Georgia Tech

August 10, 1987

Dr. W.E. Schneider/T-10
Allison Gas Turbine Operations
General Motors Corp.
2001 South Tibbs Avenue
Indianapolis, IN 46241

Dear Dr. Schneider:

This report summarizes the activities of our effort on GM PO#H636356, "Damage Rate Approaches for Thermomechanical Fatigue of Superalloys" for the period June 1, 1987 to July 31, 1987.

In an attached informal report, we present further reduction of the existing data in the program to-date, including strain rate-dependent cyclic and monotonic properties of MAR-M 246 at 900°C.

A second lot of specimens was received the week of May 10-17. The specimens have been sent to a machine shop for further preparation necessary to meet the tolerance specifications on the button-end surfaces and the button-end fillet radii, as discussed in the last progress report. Cyclic testing will resume as soon as the specimen preparation is completed. We are currently proceeding in the long term creep testing program.

Sincerely,

David L. McDowell
Principal Investigator

DLM

* UPDATE OF ANALYSIS OF RESULTS *
MAR M 246 TESTING PROGRAM

MONOTONIC & LCF TESTS

July 20, 1987
Revised and Corrected August 8, 1987

Gary J. Reynolds
Graduate Research Assistant
School of Mechanical Engineering
Georgia Institue of Technology

TABLE OF CONTENTS

Determination of Young's Modulus

MONOTONIC TEST	STRAIN RATE	YOUNG'S MODULUS
M-01	10^{-3} sec^{-1}	140396.0 MPa
M-02	10^{-2} sec^{-1}	161001.0 MPa
M-03	10^{-5} sec^{-1}	123141.9 MPa
M-04	10^{-4} sec^{-1}	146615.8 MPa
M-05	10^{-1} sec^{-1}	156413.3 MPa

Average value of E (Young's Modulus)... = 145513.6 MPa
Standard Deviation......................= 14887.6 MPa

Monotonic Test : M5

STRESS (MPa)

GJR 28-JUN-87

E = 156413. 3 MPa

20 Data Pts.

STRAIN (%)

2.
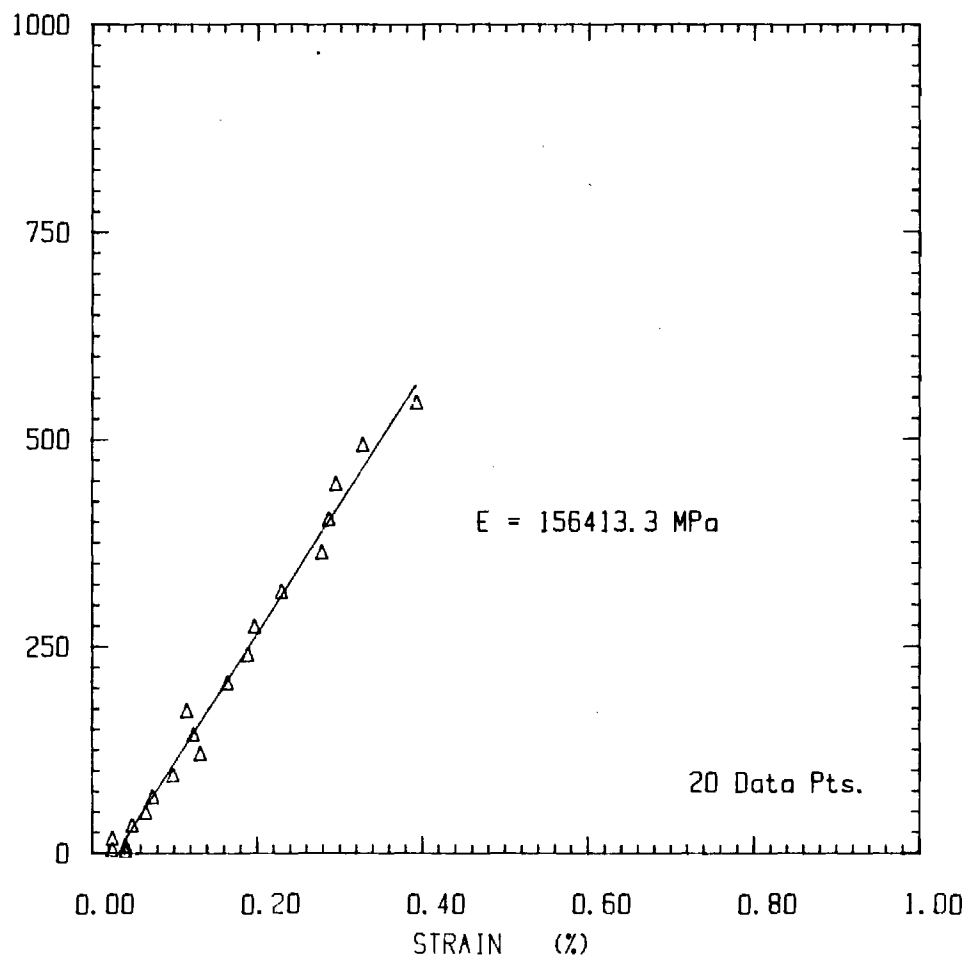
Monotonic Test : M4

STRESS   (MPa)

GJR   28-JUN-87

E = 146615.8 MPa

73 Data Pts.
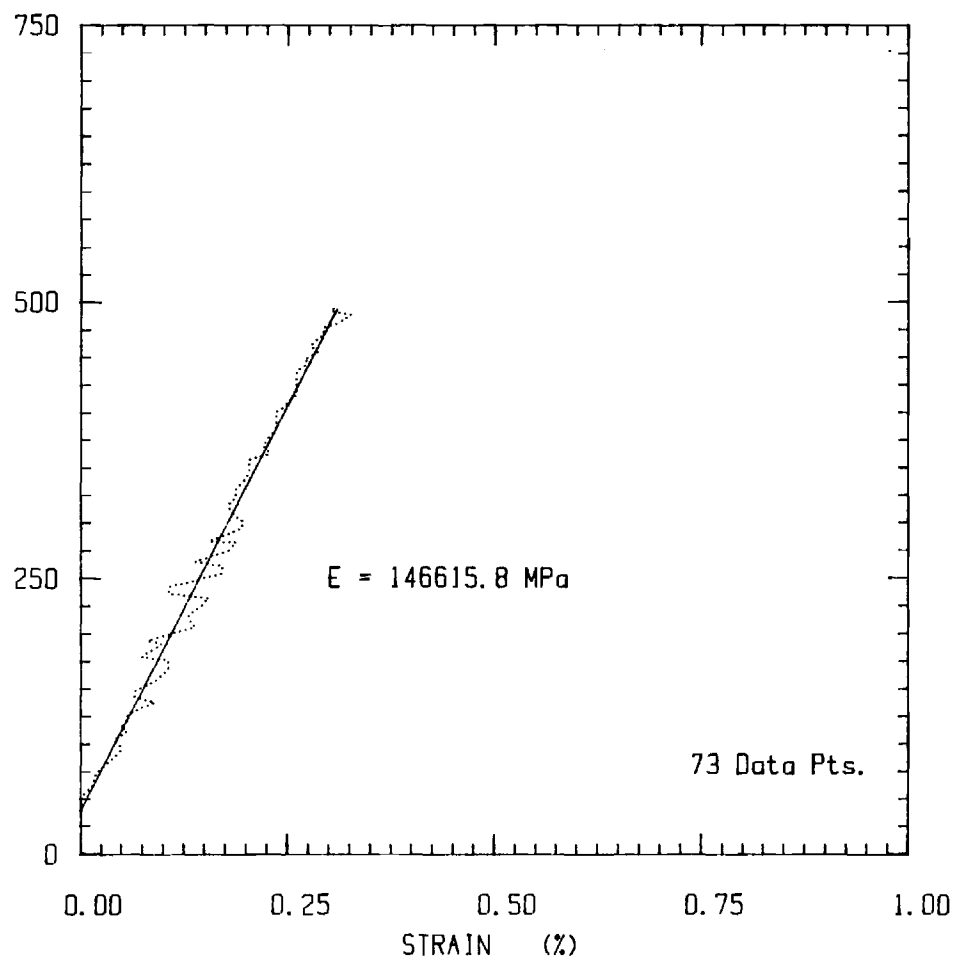
STRAIN   (%)

Monotonic Test : M3

STRESS   (MPa)

E = 123141.9 MPa

47 Data Points

0.00   0.25   0.50   0.75   1.00

STRAIN   (%)

4.
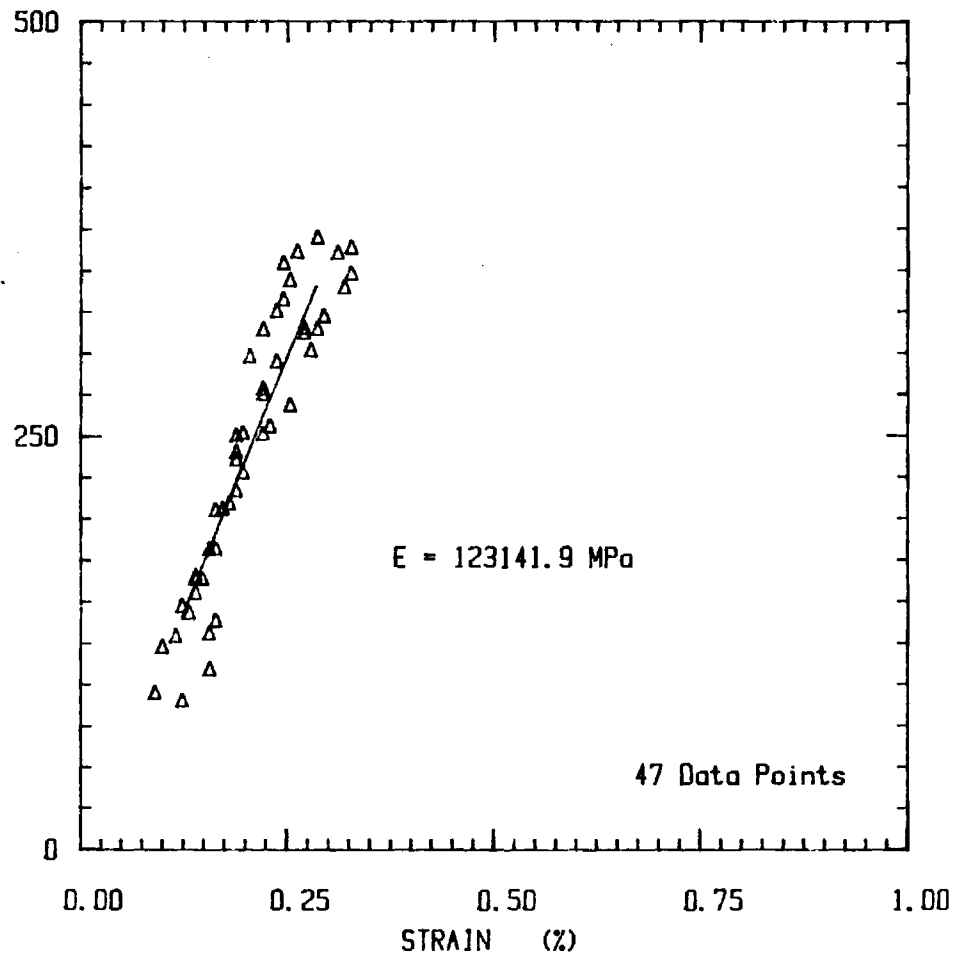
Monotonic Test : M2

STRESS   (MPa)

GJR   27-JUN-87

750

500

E = 161001.0 MPa

250

0

0.00   0.50   1.00   1.50   2.00   2.50
STRAIN   (%)

5.
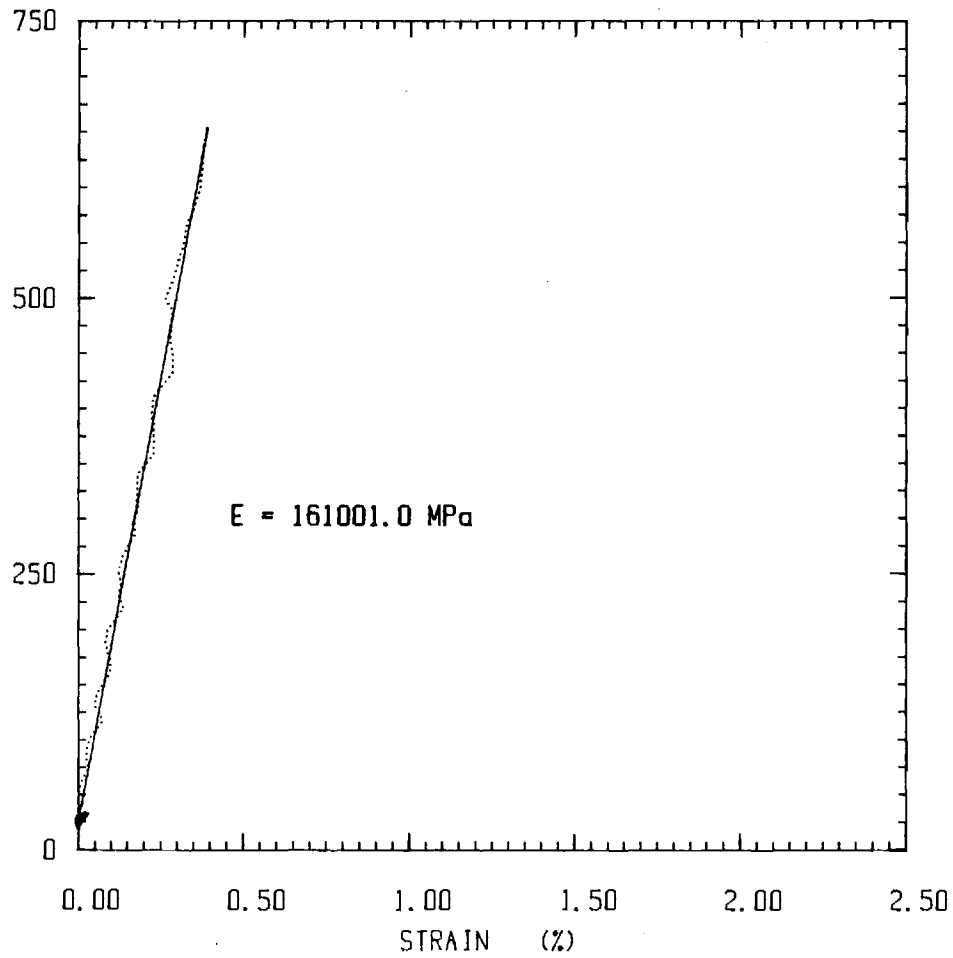
Monotonic Test : M1

STRESS   (MPa)

GJR   27-JUN-87
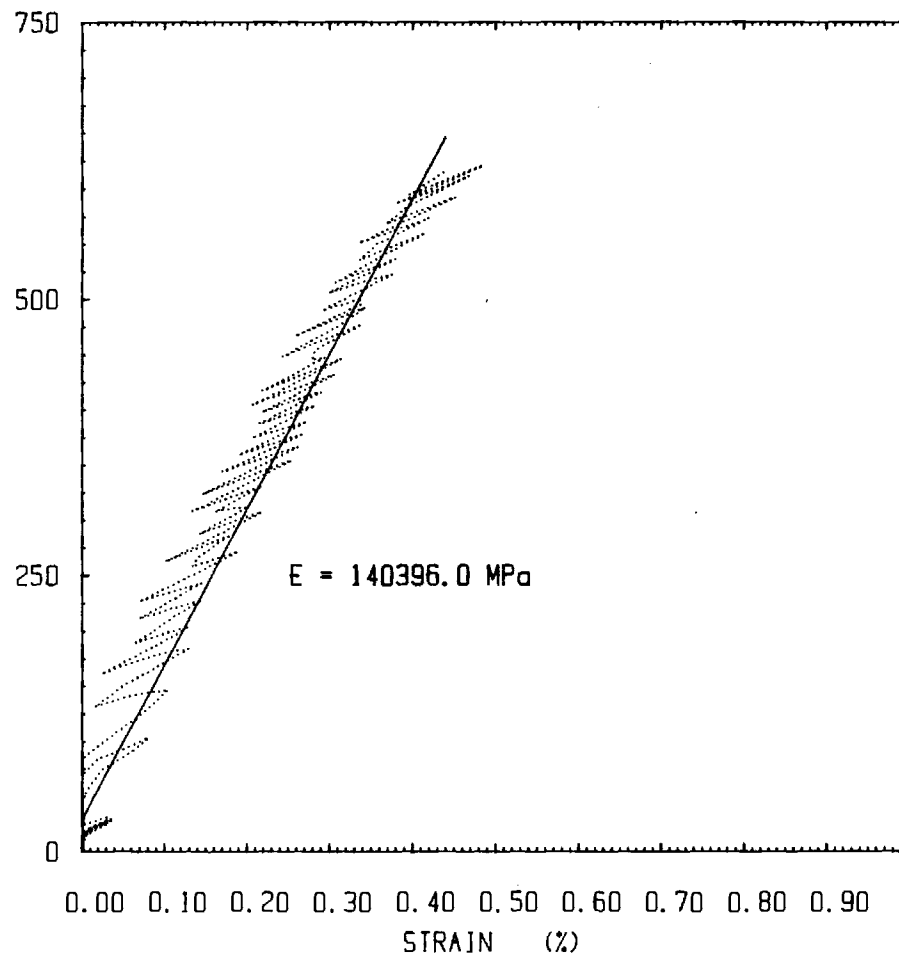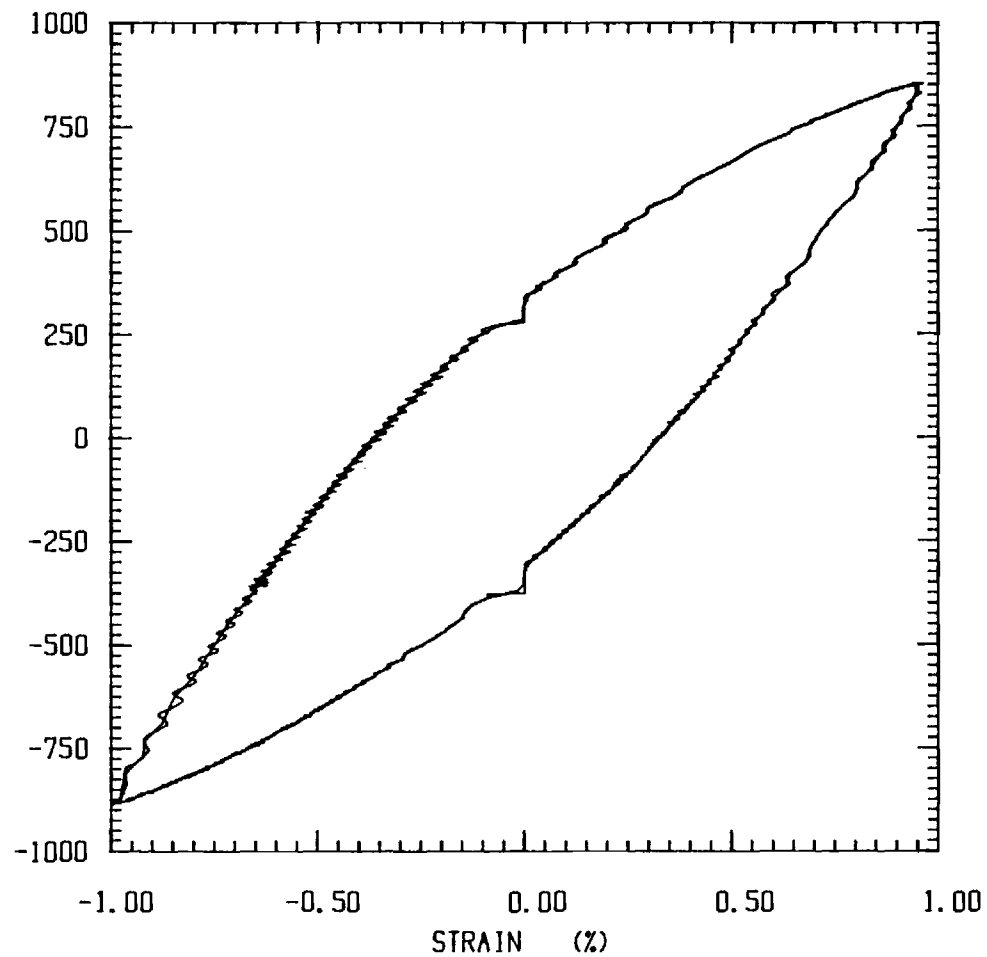
E = 140396.0 MPa

STRAIN   (%)

TEST F01   CYCLE #8   STRAIN RATE = .001 /SEC

STRESS   (MPa)

_ = 5 Point Averaging of Data

_ = Complete Data Set

STRAIN   (%)

TEST F11 CYCLE #8 STRAIN RATE = .0001 /SEC

STRESS (MPa)

_ = 5 Point Averaging of Data

.... = Complete Data Set

STRAIN (%)

∞
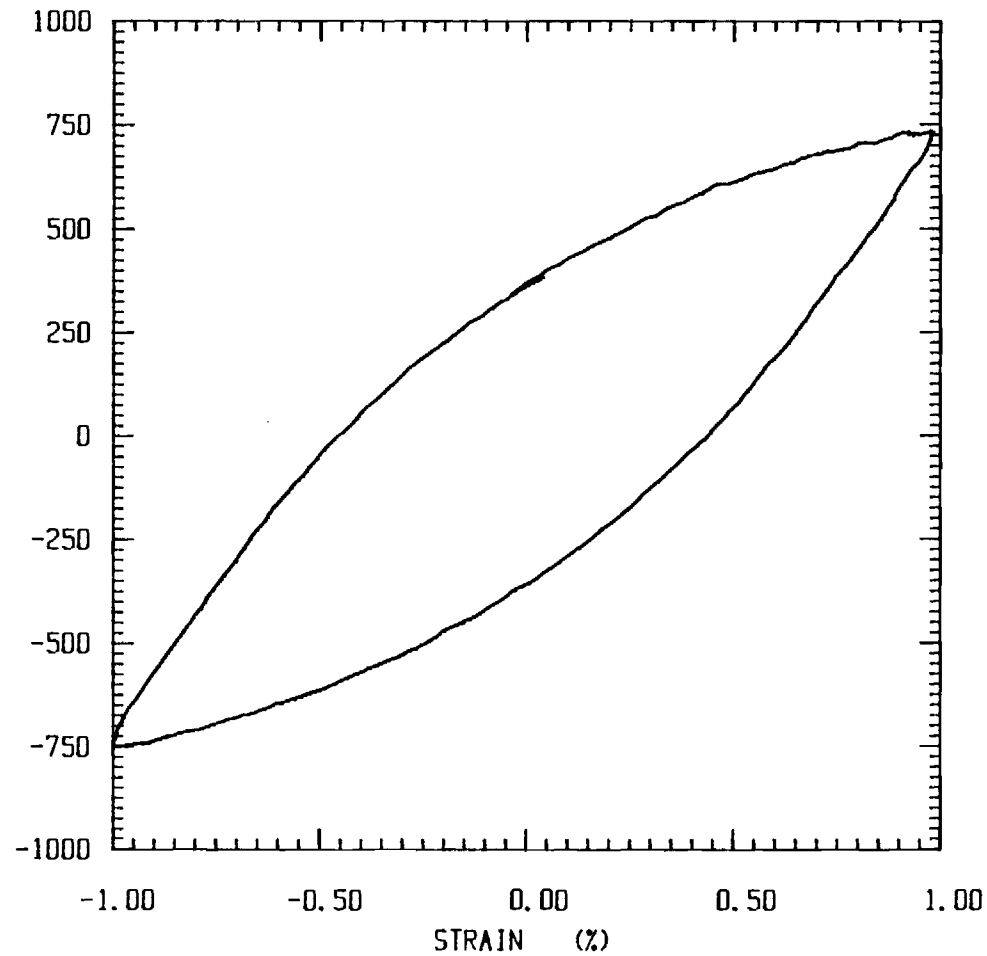
LOOP DATA

Strain Rate = 10^{-4} sec^{-1}

ST I.D.	2N$_f$	CYCLE ANAL.	$\Delta\sigma/2$	$\Delta\epsilon/2$	$\Delta\epsilon^p/2$
F-11	28	8	746.94 MPa	0.9967 %	0.4537 %
F-12B	50	8	763.79 MPa	0.8121 %	0.2872 %
F-13	748	128	510.83 MPa	0.4024 %	0.0514 %

Strain Rate = 10^{-3} sec^{-1}

ST I.D.	2N$_f$	CYCLE ANAL.	$\Delta\sigma/2$	$\Delta\epsilon/2$	$\Delta\epsilon^p/2$	
F-01	36	8	871.60 MPa	0.9824 %	0.3834 %	
F-02	90	16	717.51 MPa	0.7158 %	0.2227 %	
F-03	192	32	723.34 MPa	0.6058 %	0.1087 %	
F-04	1166	200	556.69 MPa	0.3968 %	0.0142 %	*

Strain Rate = 10^{-2} sec^{-1}

ST I.D.	2N$_f$	CYCLE ANAL.	$\Delta\sigma/2$	$\Delta\epsilon/2$	$\Delta\epsilon^p/2$
F-06C	48	16	1015.25 MPa	1.0143 %	0.3163 %
F-08	236	64	775.52 MPa	0.6387 %	0.1057 %

$\Delta\sigma/2$ and $\Delta\epsilon/2$ were determined from the complete hysteresis loop data files — using the points of maximum and minimum σ and ϵ and taking the average of the two values to determine the respective amplitudes.

$\Delta\epsilon^p/2$ was determined from : $\Delta\epsilon^p/2 = \Delta\epsilon/2 - \Delta\sigma/2E_{ave}$

Where E_{ave} is the average computed Young's Modulus (145513.6 MPa).

* This use of this small strain amplitude data point resulted in unreasonable values for the fatigue life constants. Therefore, it was not used in the determination of those values. (See pages 22 - 24.)

TEST F11 CYCLE #8 STRAIN RATE = .0001 /SEC
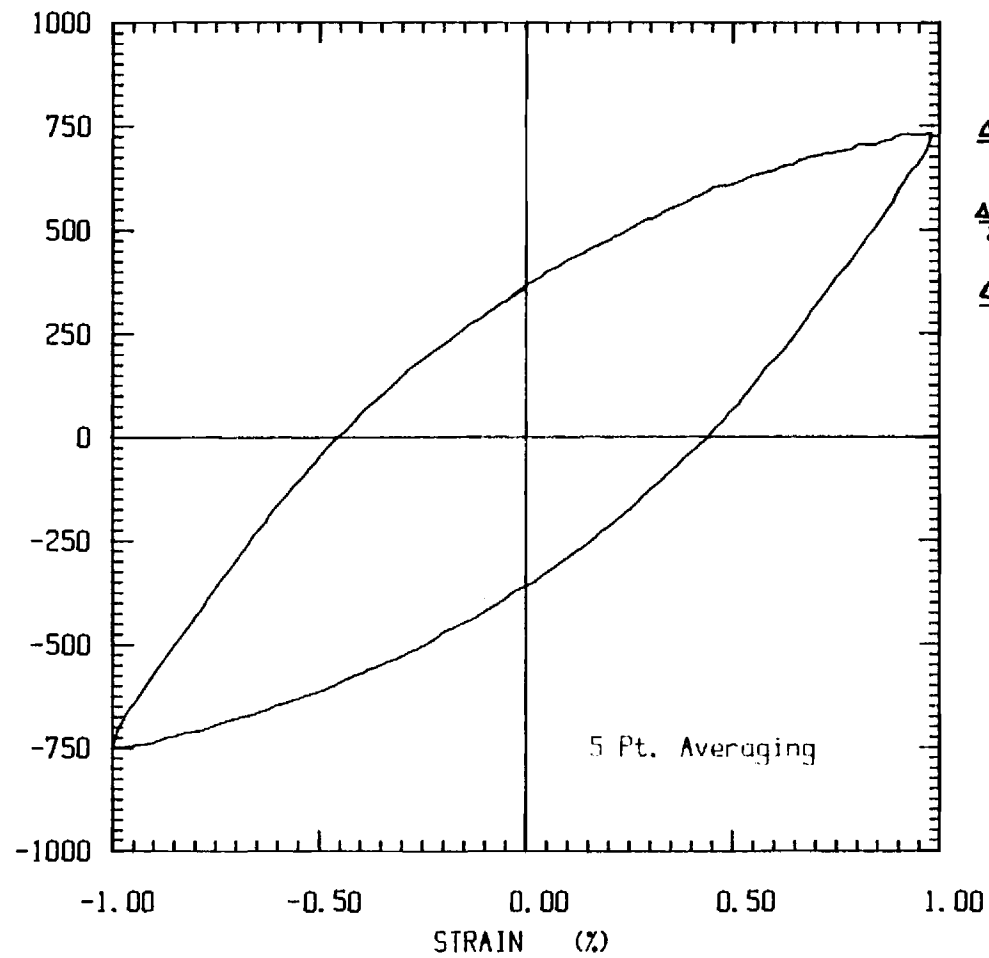
STRESS   (MPa)

$\dfrac{\Delta\sigma}{2}$ = 746.94 MPa

$\dfrac{\Delta\varepsilon}{2}$ = 0.9967 %

$\dfrac{\Delta\varepsilon^{P}}{2}$ = 0.4587 %

5 Pt. Averaging

STRAIN   (%)

TEST F12B   CYCLE #8   STRAIN RATE =   .0001 /SEC
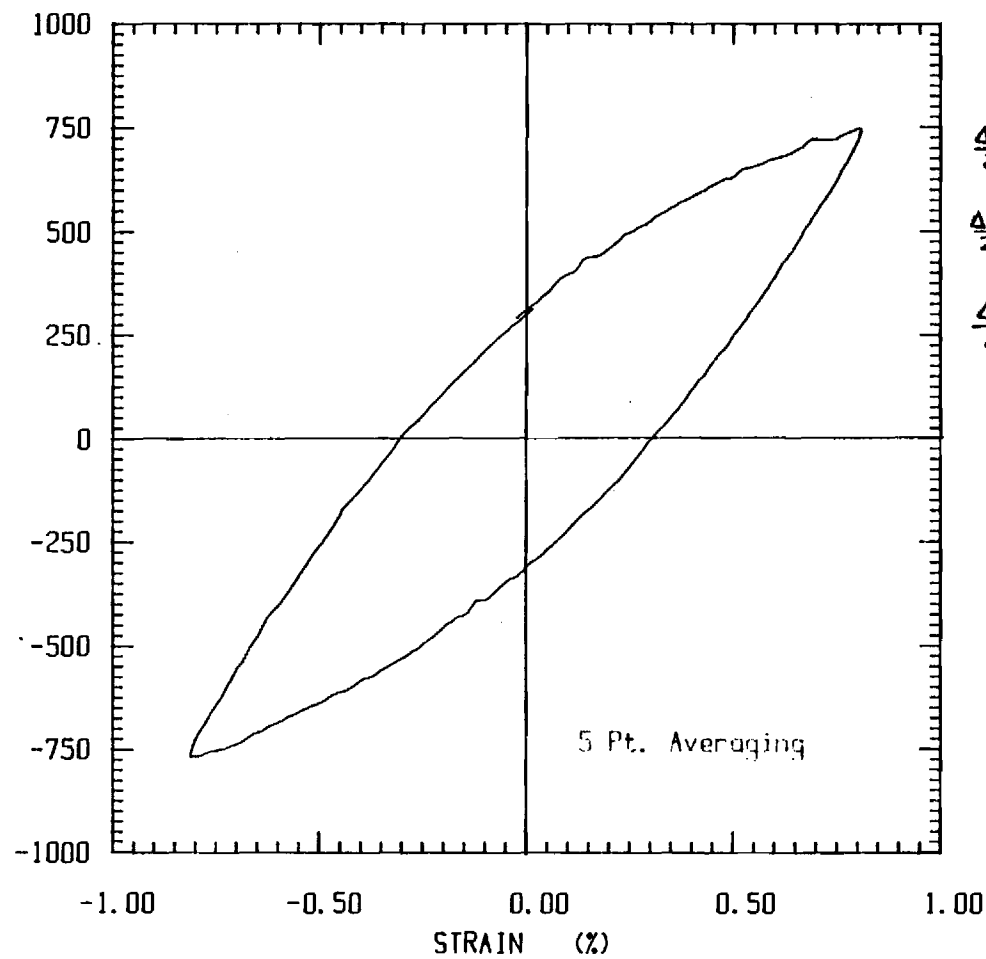
STRESS   (MPa)

$\frac{\Delta\sigma}{2}$ = 763.79 MPa

$\frac{\Delta\epsilon}{2}$ = 0.8121 %

$\frac{\Delta\epsilon^p}{2}$ = 0.2972 %

5 Pt. Averaging

STRAIN   (%)

TEST F13   CYCLE #128   STRAIN RATE = .0001 /SEC

STRESS   (MPa)
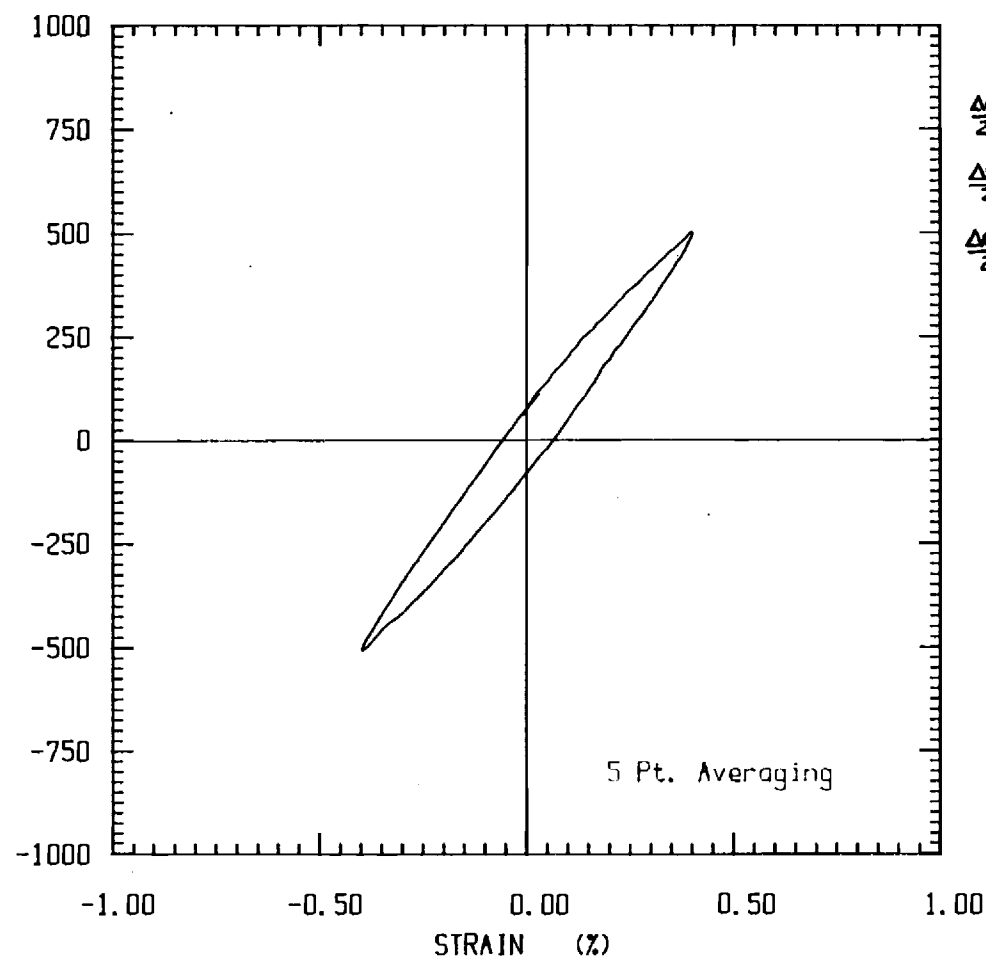
$\frac{\Delta\sigma}{2}$ = 510.83 MPa

$\frac{\Delta\epsilon}{2}$ = 0.4024 %

$\frac{\Delta\epsilon^{P}}{2}$ = 0.0514 %

5 Pt. Averaging

STRAIN   (%)

Mar M 246 at 900 deg C ; Rate = .0001/sec.

Stress Amplitude (MPa)

$\sigma_f' = 1186.53$ MPa

$b = -0.12596$

$$\frac{\Delta\sigma}{2} = 1186.53 \left[2N_f\right]^{-0.12596}$$

Number of Reversals
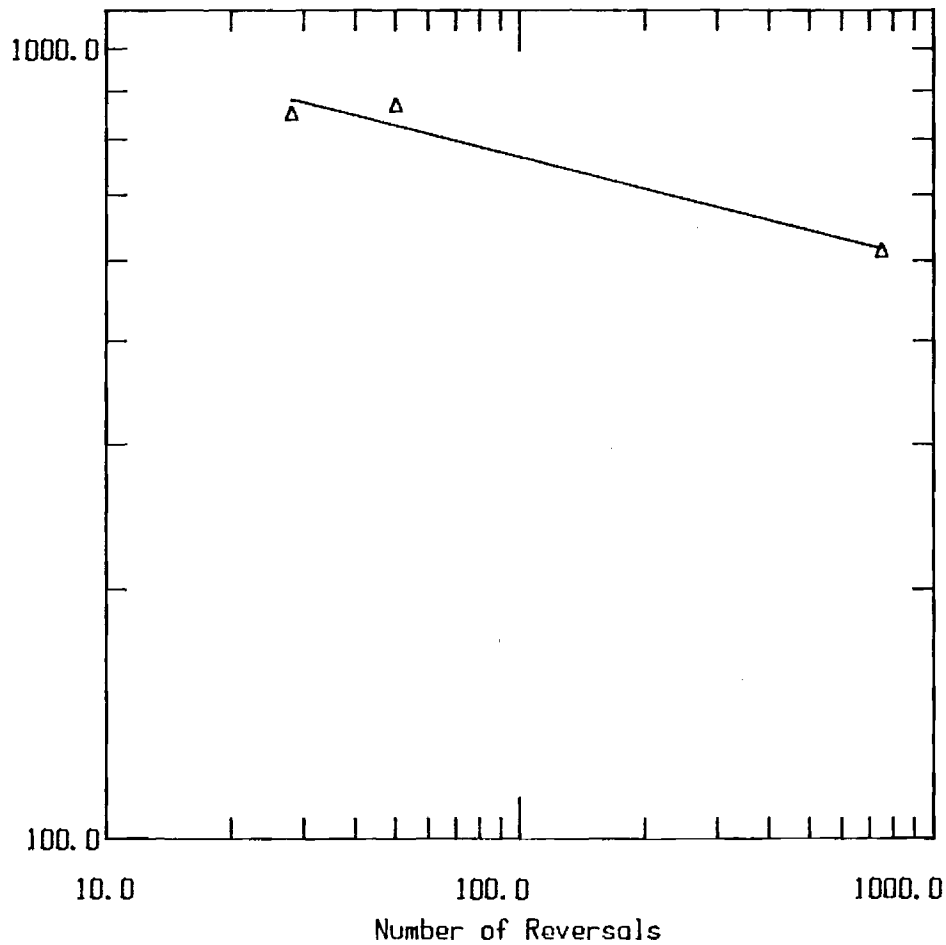
Mar M 246 at 900 deg C : Rate = .0001/sec.

Plastic Strain Amplitude (in/in)
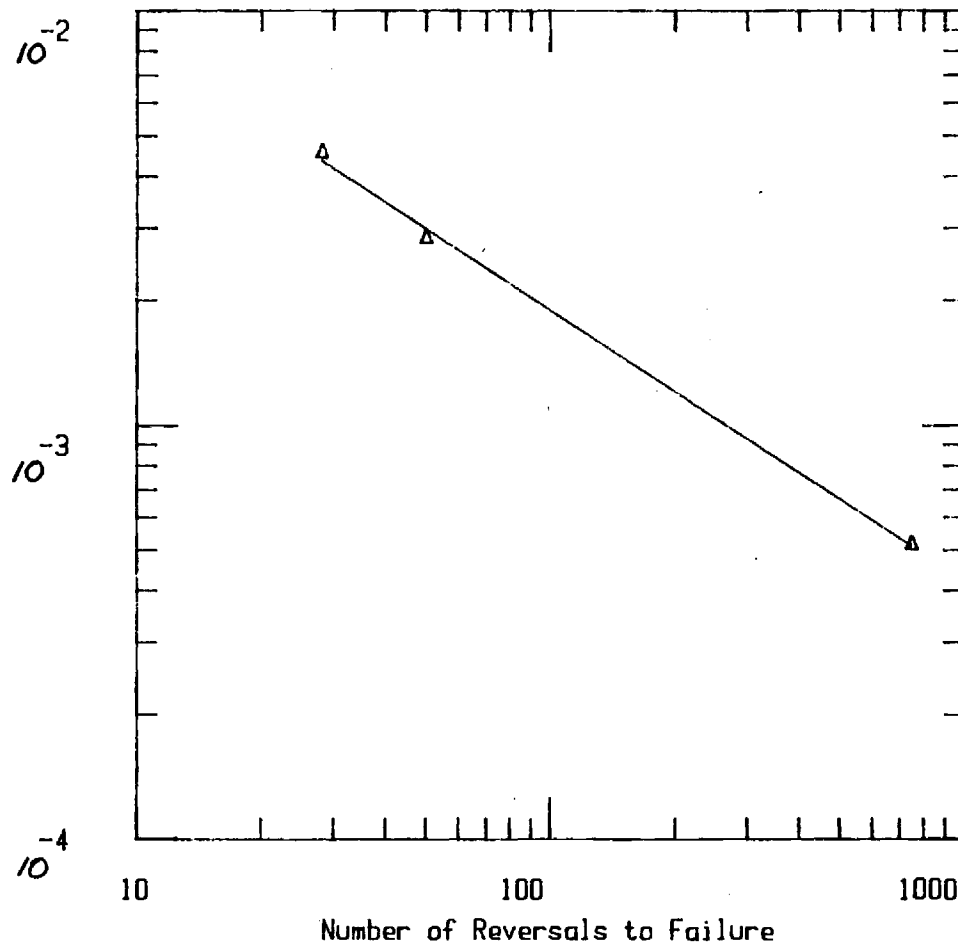
$$\frac{\Delta \epsilon^p}{2} = \epsilon_f' \left[2N_f \right]^c$$

$\epsilon_f' = 0.03879$ in/in

$c = -0.6545$

Number of Reversals to Failure

Mar M 246 at 900 deg C : Rate = .0001/sec.

Total Strain Amplitude (in/in)
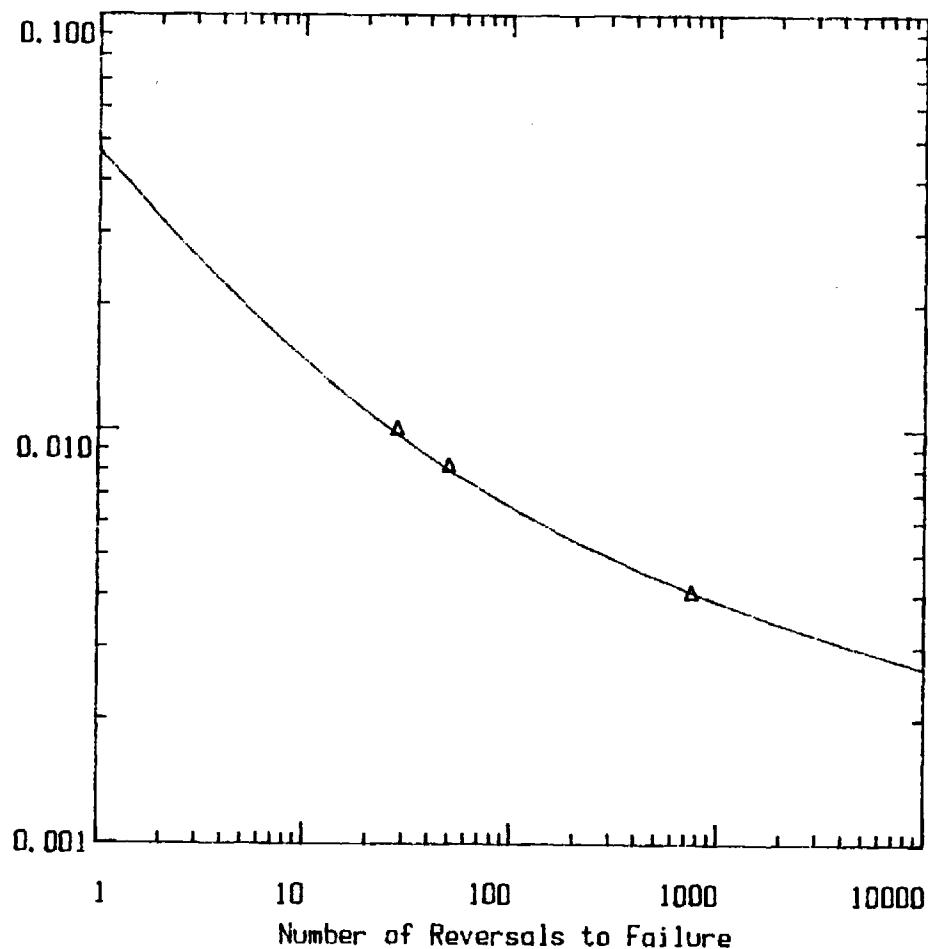
$$\frac{\Delta \epsilon^{T}}{2} = \frac{\sigma_{f}'}{E}\left[2N_{f}\right]^{b} + \epsilon_{f}'\left[2N_{f}\right]^{c}$$

E = 145513.6 MPa

σ_{f}' = 1186.53 MPa

b = -0.12596

ϵ_{f}' = 0.03879 in/in

c = -0.6545

— = POINTS GENERATED BY ABOVE $\frac{\Delta \epsilon}{2}$ EQUATION

$\triangle$ = STRAIN AMPLITUDE AS CALCULATED FROM THE CHOSEN HYSTERESIS LOOPS.

Number of Reversals to Failure

TEST F01   CYCLE #8   STRAIN RATE = .001 /SEC
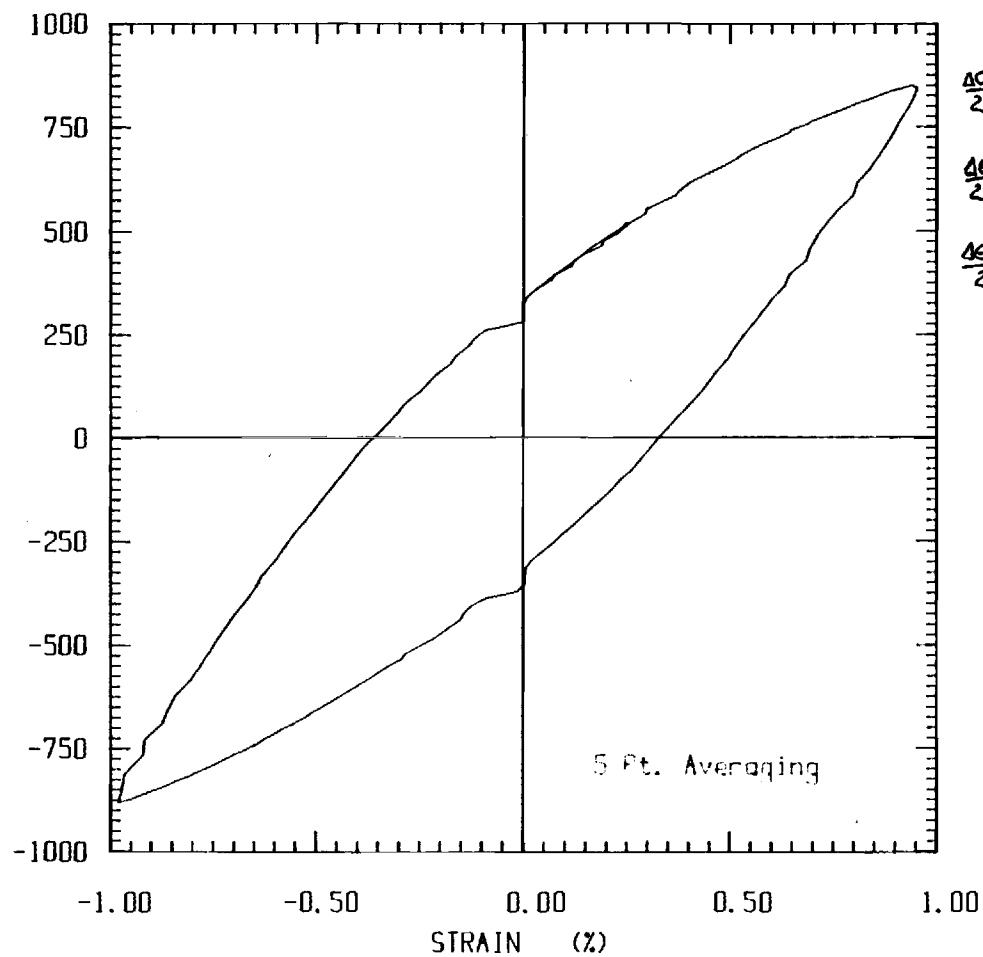
STRESS   (MPa)

$\frac{\Delta \sigma}{2}$ = 871.596 MPa

$\frac{\Delta \epsilon}{2}$ = .9824 %

$\frac{\Delta \epsilon^P}{2}$ = 0.3834 %

5 Pt. Averaging

STRAIN   (%)

TEST F02   CYCLE #16   STRAIN RATE = .001 /SEC

STRESS   (MPa)

$\frac{\Delta\sigma}{2}$ = 717.51 MPa

$\frac{\Delta\epsilon}{2}$ = 0.7158 %

$\frac{\Delta\epsilon^P}{2}$ = 0.2227 %

5 Pt. Averaging
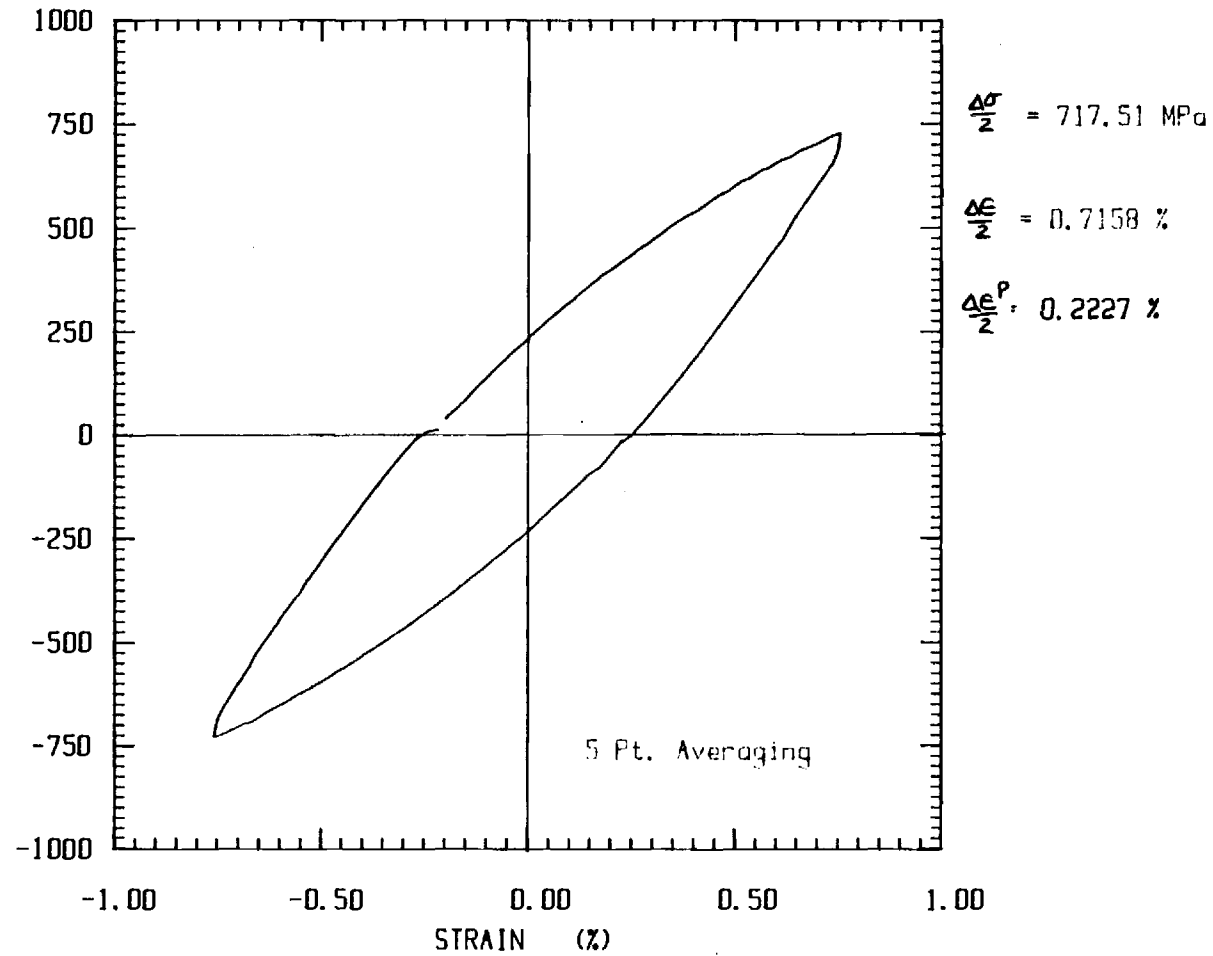
TEST F03   CYCLE #32   STRAIN RATE =   .001 /SEC

STRESS   (MPa)

$\frac{\Delta\sigma}{2}$ = 723. 34 MPa

$\frac{\Delta\epsilon}{2}$ = 0. 6058 %

$\frac{\Delta\epsilon^P}{2}$ = 0. 1087 %

5 Pt. Averaging
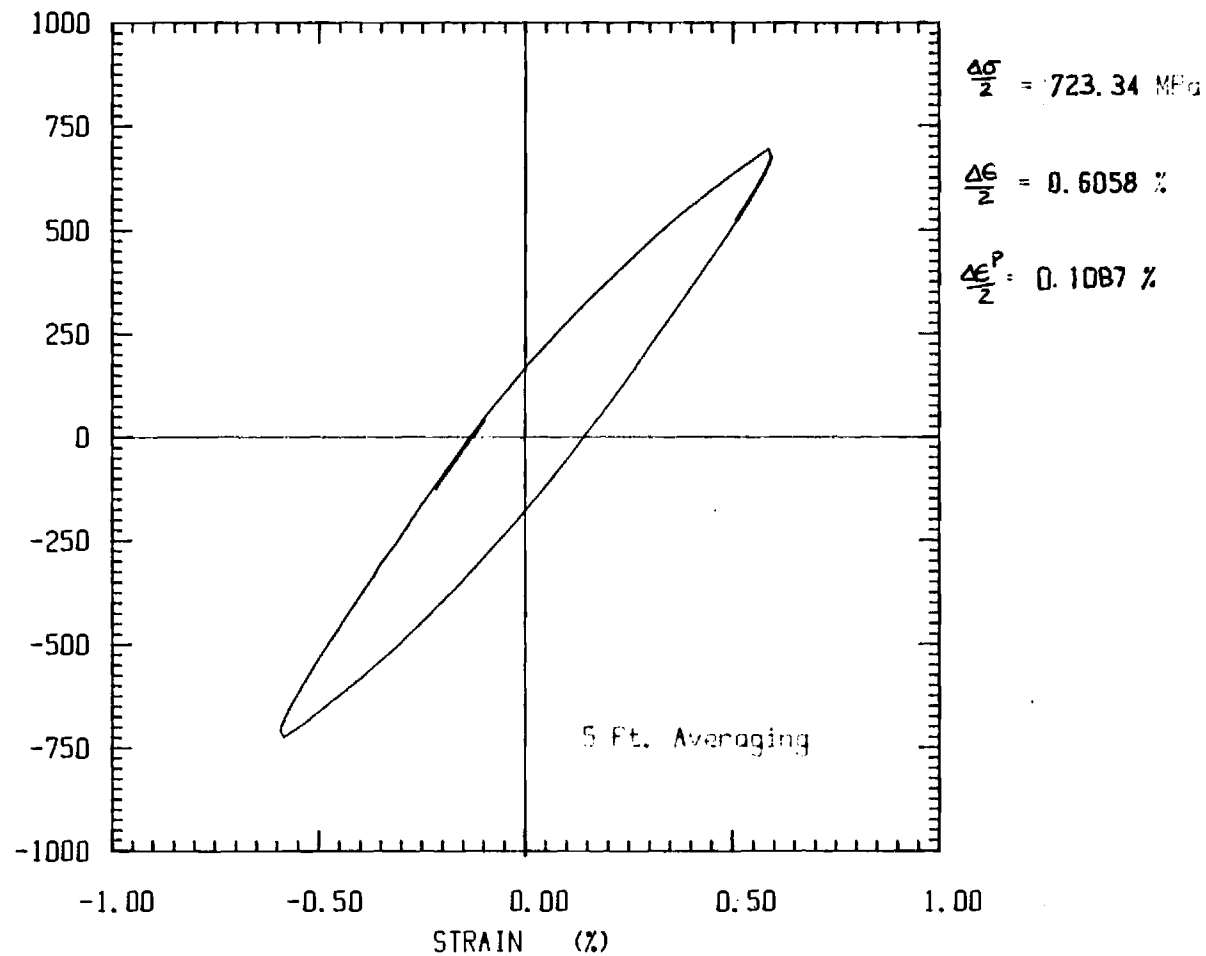
STRAIN   (%)

TEST F04   CYCLE #200   STRAIN RATE =   .001 /SEC

STRESS   (MPa)
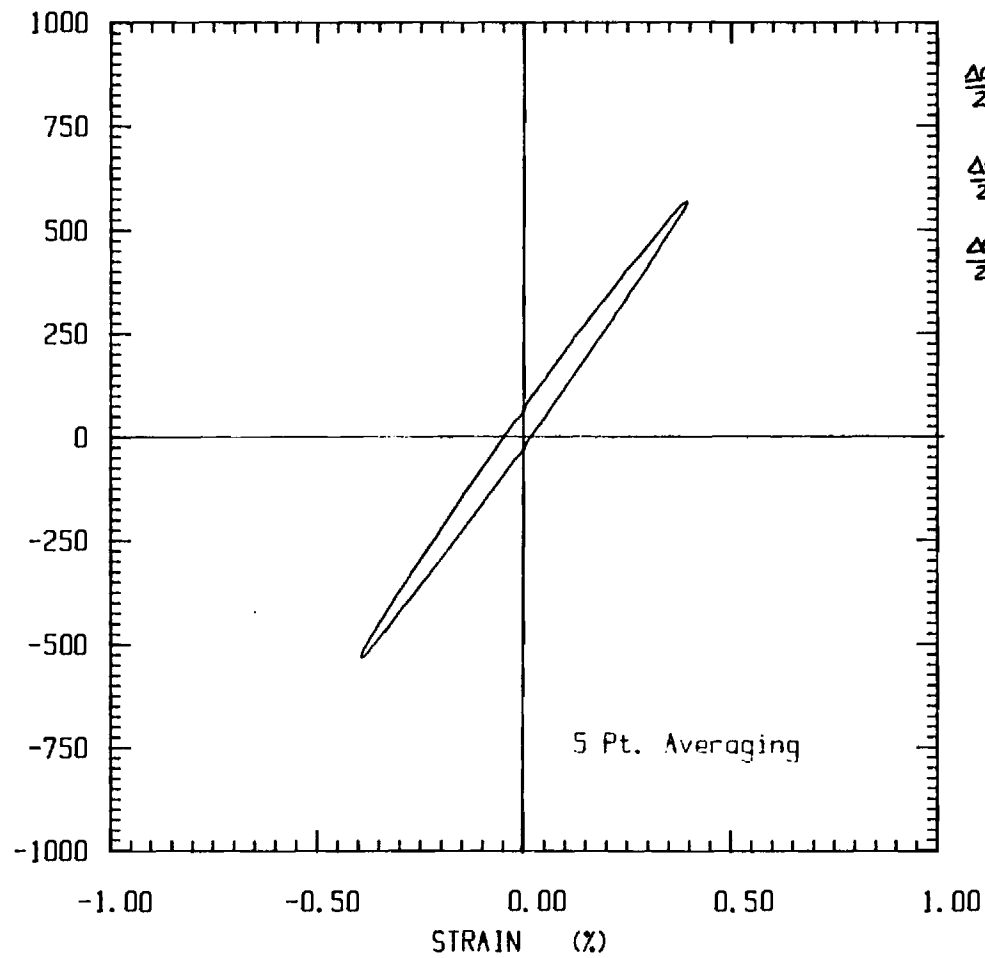
$\frac{\Delta\sigma}{2}$ = 556.69 MPa

$\frac{\Delta\epsilon}{2}$ = 0.3968 %

$\frac{\Delta\epsilon^P}{2}$: 0.0142 %

5 Pt. Averaging

STRAIN   (%)

Mar M 246 at 900 deg C ; rate = .001/sec.

Stress Amplitude (MPa)
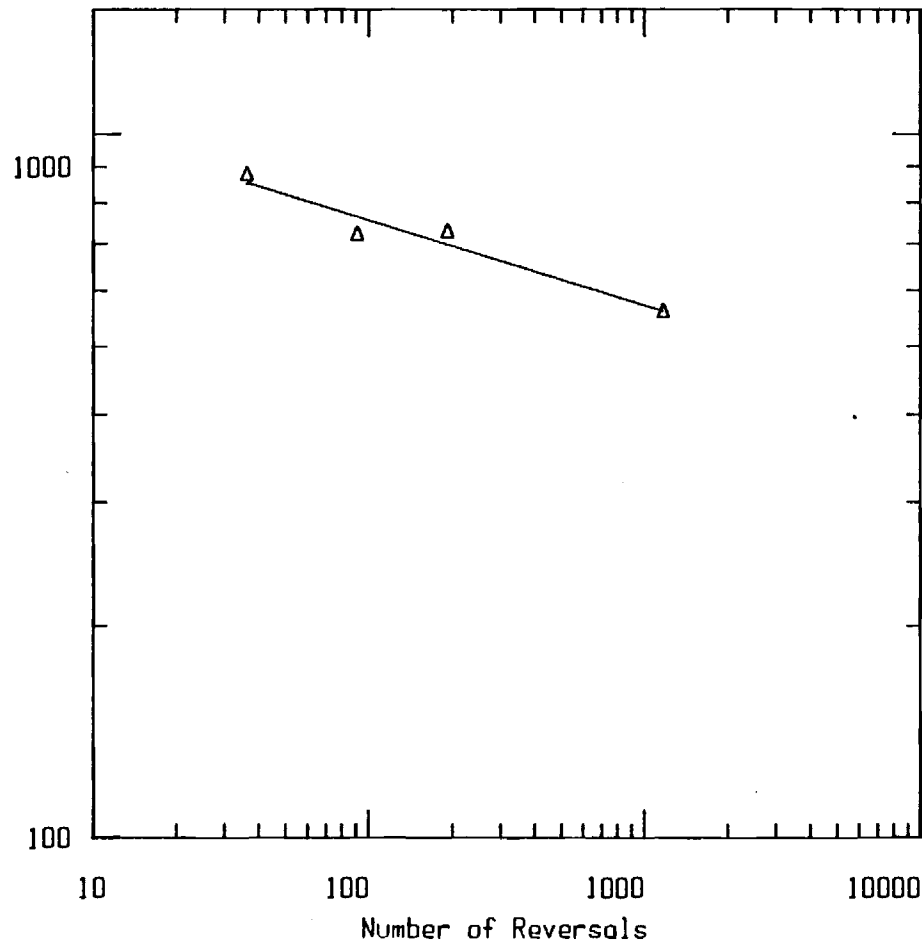
Slope = -0.12117

Stress Intercept = 1314.17 MPa

$$\frac{\Delta \sigma}{2} = 1314.17 \left[2N_f \right]^{-0.12117}$$

1000

100

10   100   1000   10000

Number of Reversals

Mar M 246 at 900 deg C ; rate = .001/sec.

Log of Stress Amplitude (MPa)
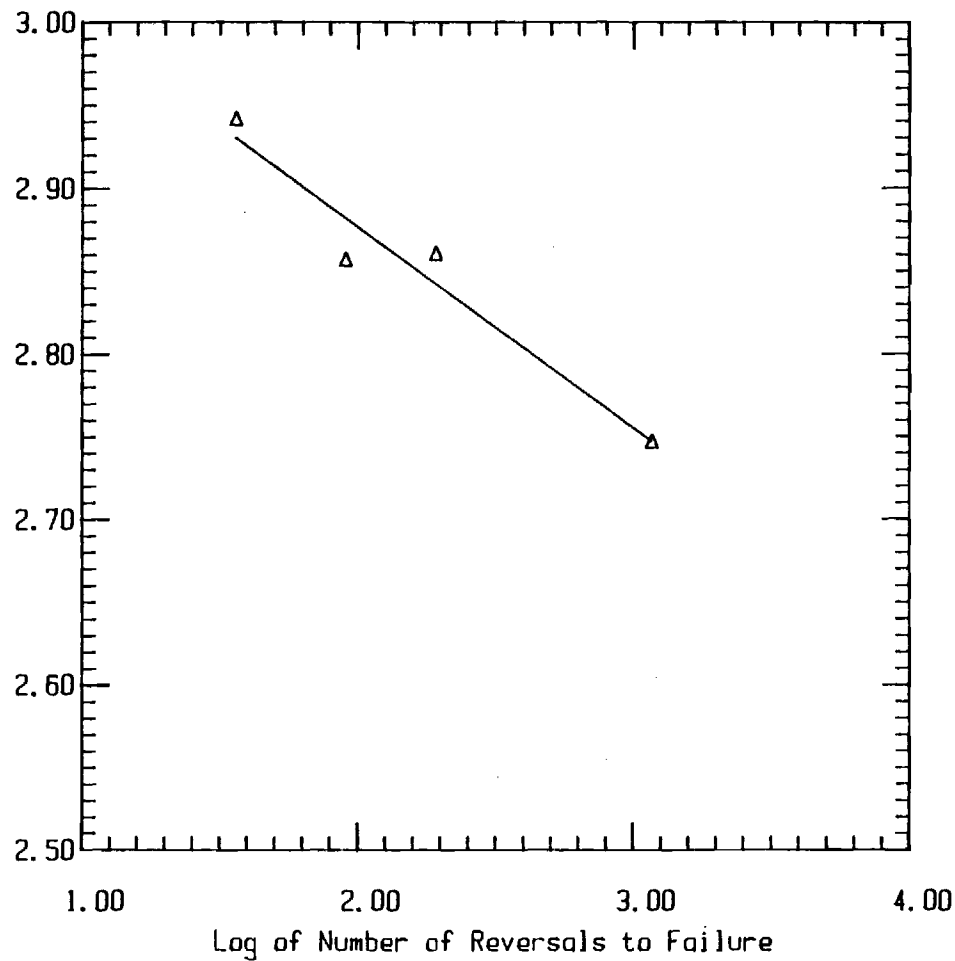
Slope = -0.12117

Stress Intercept = 3.11865
- or - inverse log yields : 1314.17 MPa

$$\frac{\Delta\sigma}{2} = 1314.17 \left[2N_f \right]^{-0.12117}$$

Log of Number of Reversals to Failure

Mar M 246 at 900 deg C : Rate = .001/sec.

Log Plastic Strain Amplitude
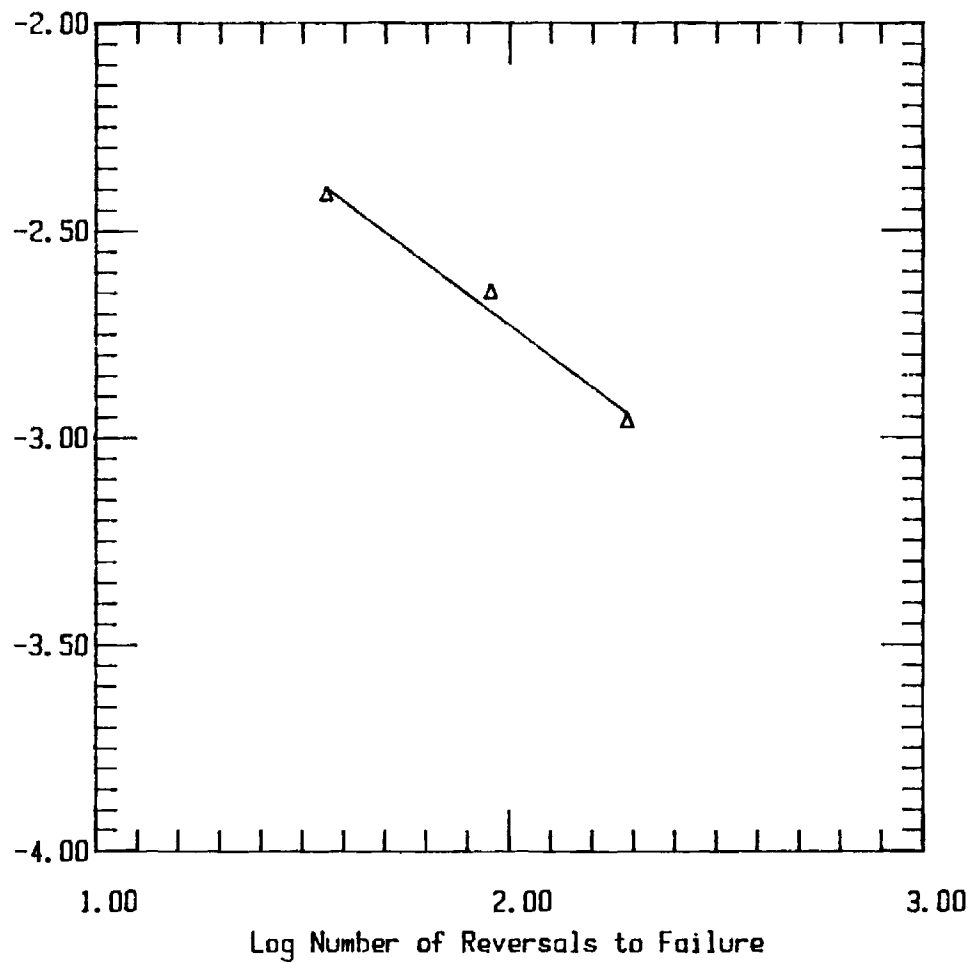
$$\frac{\Delta \epsilon^{P}}{2} = \epsilon_{f}{}' \left[2N_{f} \right]^{c}$$

Slope = -0.7475

Intercept = 0.05836 in/in

Log Number of Reversals to Failure

Mar M 246 at 900 deg C : Rate = .001/sec.

Plastic Strain Amplitude (in/in)
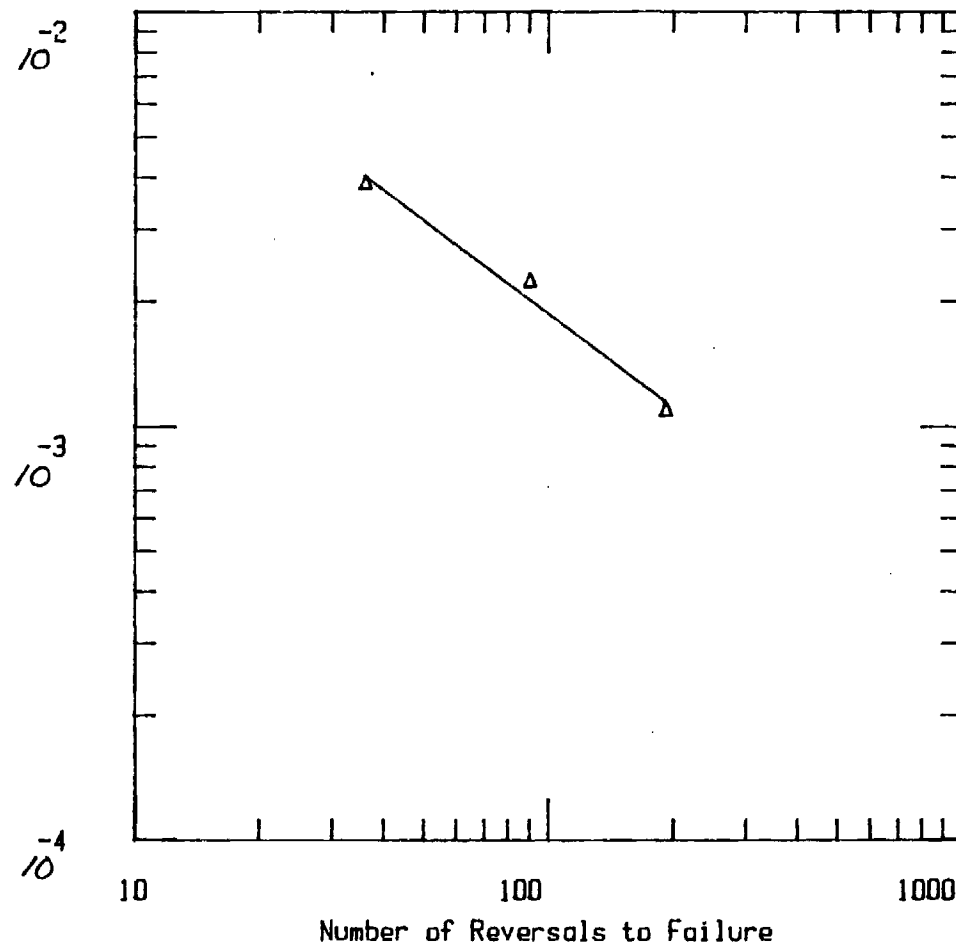
$$\frac{\Delta \epsilon^p}{2} = \epsilon_f{}' \left[2N_f \right]^c$$

$\epsilon_f{}' = 0.05836$ in/in

$c = -0.7475$

Number of Reversals to Failure

Mar M 246 at 900 deg C : Rate = .001/sec.

Total Strain Amplitude (in/in)
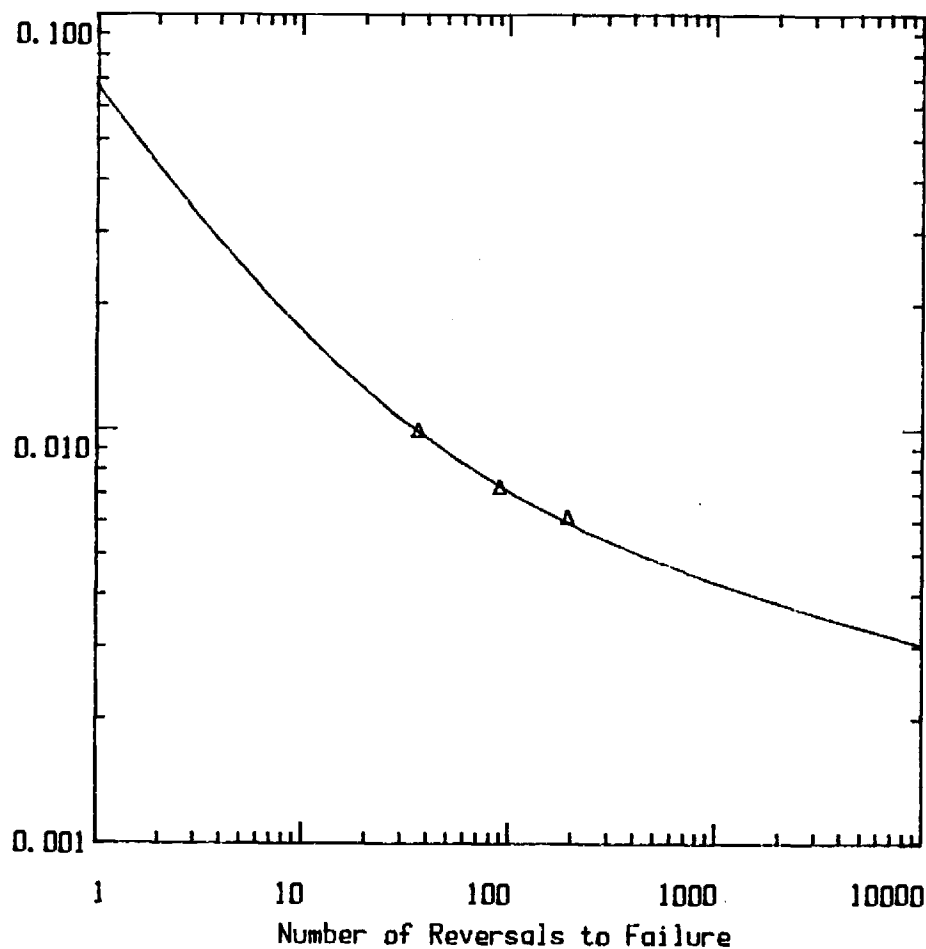
$$\frac{\Delta \epsilon^T}{2} = \frac{\sigma_f'}{E} \left[2N_f\right]^b + \epsilon_f' \left[2N_f\right]^c$$

$E = 145513.6$ MPa

$\sigma_f' = 1314.17$ MPa

$b = -0.1212$

$\epsilon_f' = 0.05836$ in/in

$c = -0.7475$

— = POINTS GENERATED BY ABOVE $\frac{\Delta \epsilon}{2}$ EQUATION

Δ = STRAIN AMPLITUDE AS CALCULATED FROM THE CHOSEN HYSTERESIS LOOPS

Number of Reversals to Failure

TEST F06C   CYCLE #16   STRAIN RATE = .01 /SEC
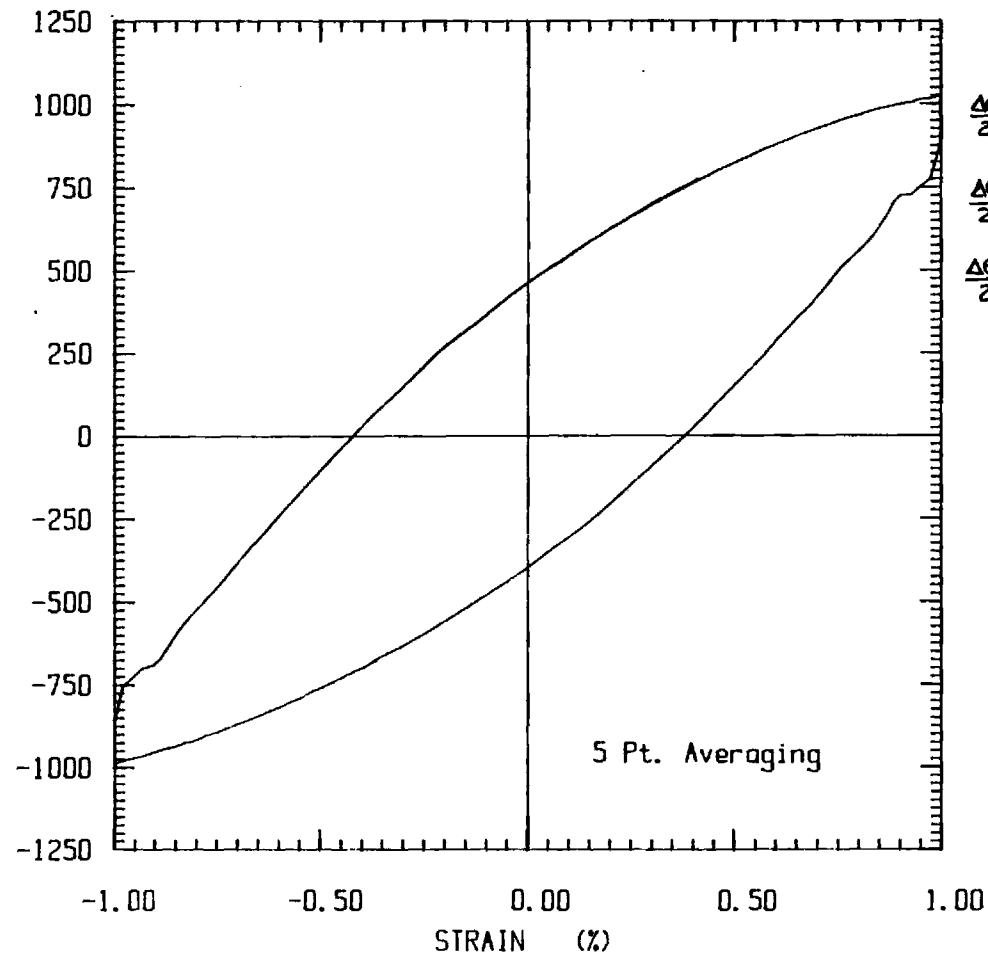
STRESS   (MPa)

$\frac{\Delta\sigma}{2}$ = 1015.25 MPa

$\frac{\Delta\epsilon}{2}$ = 1.014 %

$\frac{\Delta\epsilon^{p}}{2}$ = 0.3163 %

5 Pt. Averaging

STRAIN   (%)

CYCLE #64   TEST F08   STRAIN RATE = .01 /SEC

STRESS   (MPa)
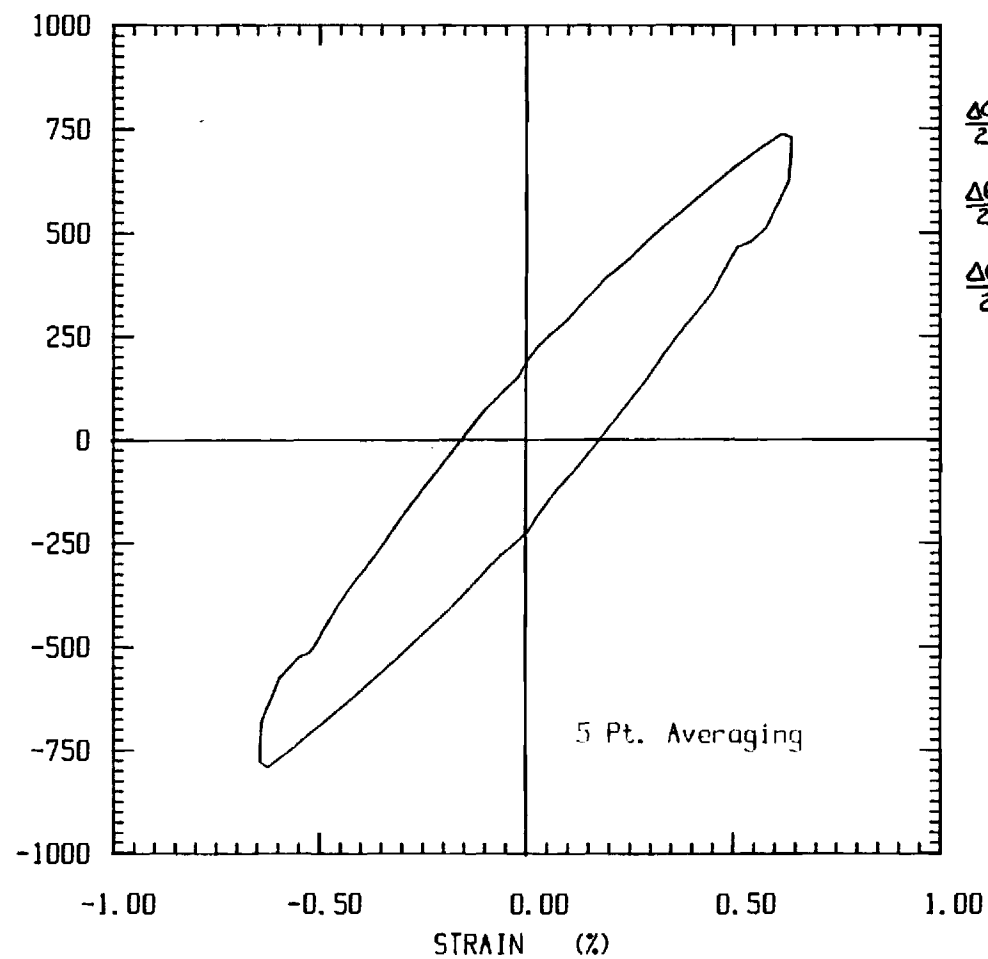
$\frac{\Delta\sigma}{2}$ = 775.52 MPa

$\frac{\Delta\epsilon}{2}$ = 0.6387 %

$\frac{\Delta\epsilon^P}{2}$ = 0.1057 %

5 Pt. Averaging

Mar M 246 at 900 deg C : Rate = .01/sec.

Plastic Strain Amplitude (in/in)

$$\frac{\Delta \epsilon'}{2} = \epsilon_f' \left[2N_f \right]^c$$

$\epsilon_f' = 0.04537$ in/in

$c = -0.6881$

Number of Reversals to Failure
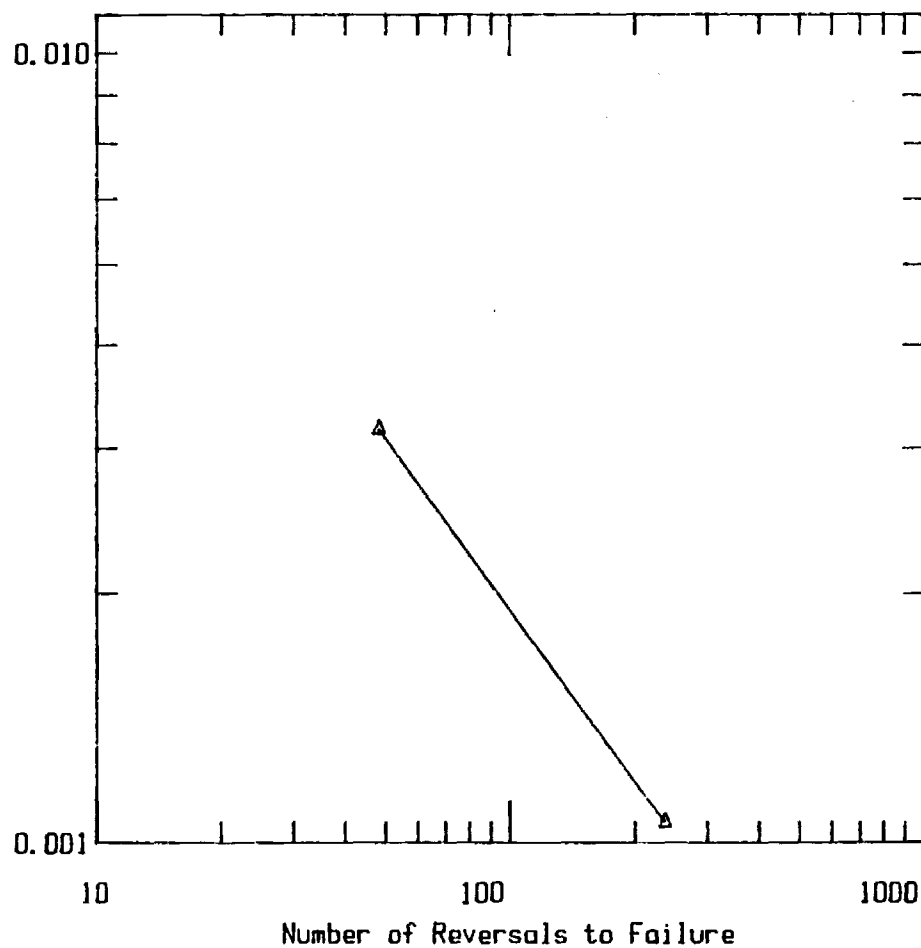
Mar M 246 at 900 deg C : Rate = .01/sec.

Stress Amplitude (MPa)
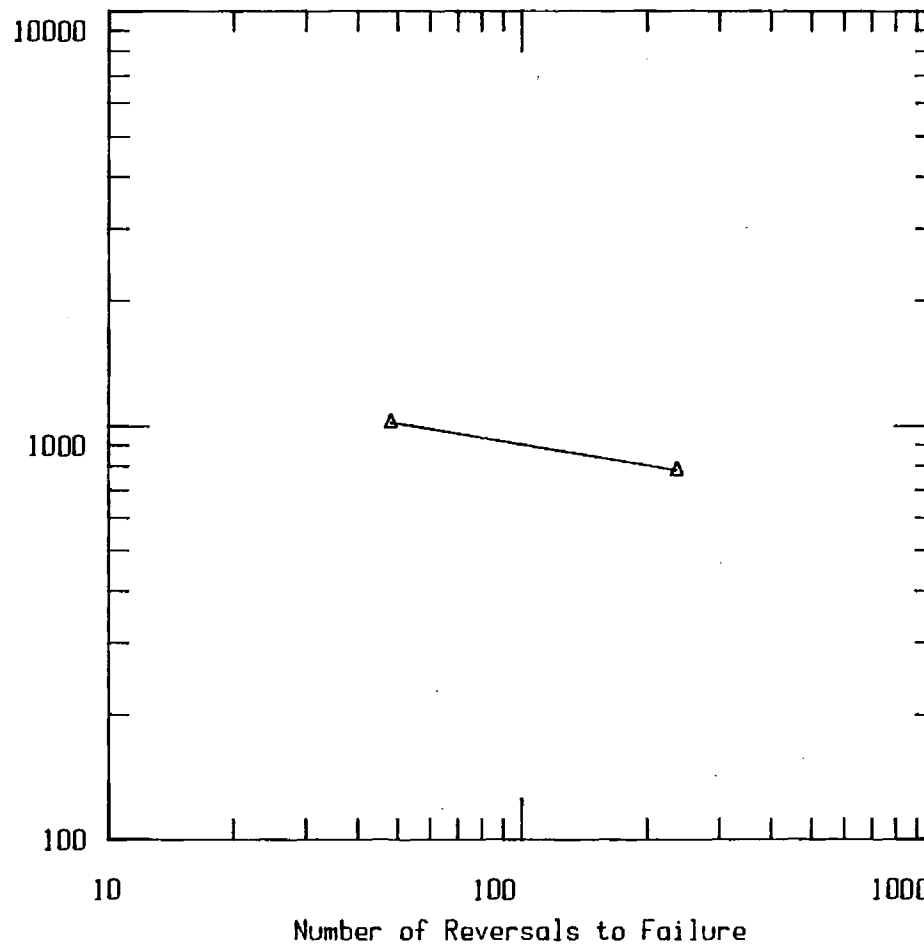
$\sigma_f' = 1953.98$ MPa

$b = -0.1691$

$$\frac{\Delta\sigma}{2} = 1953.98 \left[2N_f\right]^{-0.1691}$$

Number of Reversals to Failure

Mar M 246 at 900 deg C : Rate = .01/sec.

Total Strain Amplitude (in/in)
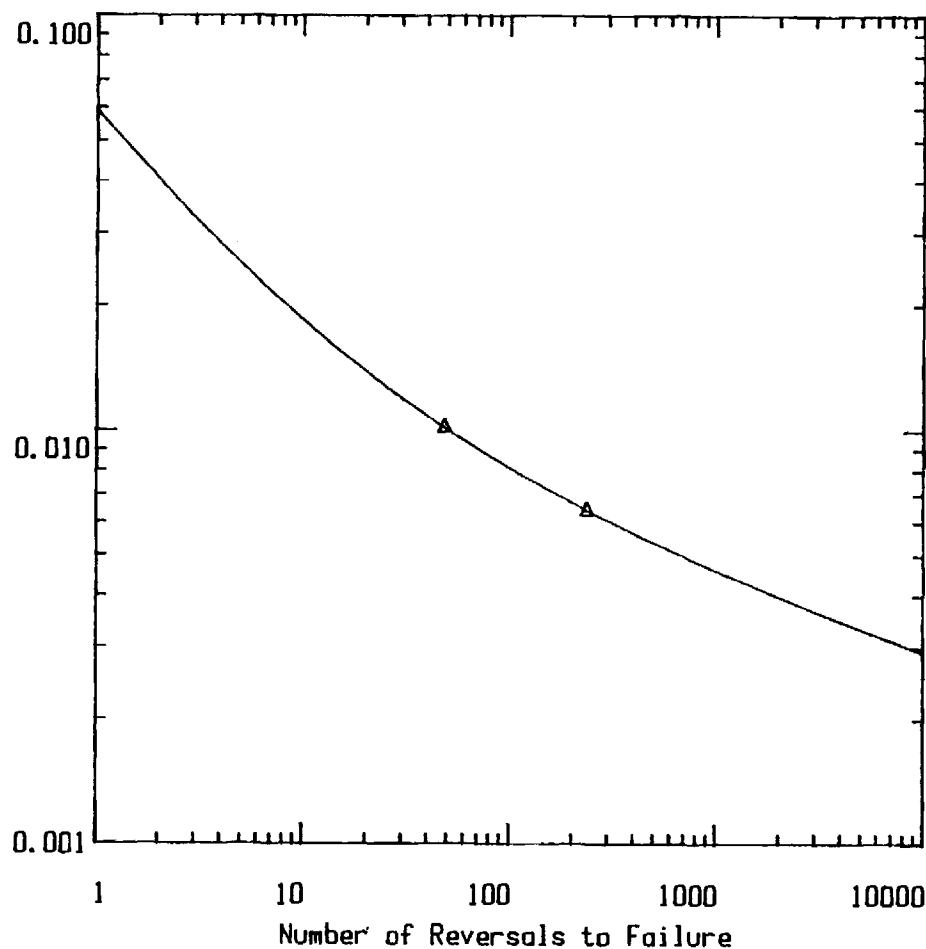
$$\frac{\Delta \epsilon^T}{2} = \frac{\sigma_f'}{E}\left[2N_f\right]^b + \epsilon_f'\left[2N_f\right]^c$$

E = 145513.6 MPa

σ_f' = 1953.98 MPa

b = -0.1691

ϵ_f' = 0.04537 in/in

c = -0.6881

— = POINTS GENERATED BY ABOVE $\frac{\Delta \epsilon}{2}$ EQUATION

Δ = STRAIN AMPLITUDE AS CALCULATED FROM THE CHOSEN HYSTERESIS LOOPS.

0.100
0.010
0.001

1   10   100   1000   10000

Number of Reversals to Failure

SUMMARY OF FATIGUE LIFE CONSTANTS

Strain Rate	σ_f'	b	ϵ_f'	c
10^{-4} sec^{-1}	1186.53 MPa	-0.1260	0.03879 in/in	-0.6029
10^{-3} sec^{-1}	1314.17 MPa	-0.1212	0.05836 in/in	-0.7475
10^{-2} sec^{-1}	1953.98 MPa	-0.1691	0.04537 in/in	-0.4837

$$\frac{\Delta\epsilon^T}{2} = \frac{\sigma_f'}{E}\left[2N_f\right]^b + \epsilon_f'\left[2N_f\right]^c$$

$\sigma_f' \equiv$ Fatigue strength coefficient.

$b \equiv$ Fatigue strength exponent.

$\epsilon_f' \equiv$ Fatigue ductility coefficient.

$c \equiv$ Fatigue ductility exponent.

Mar M 246 at 900 deg C

Stress Amplitude (MPa)

Calculations based on loop tips. *
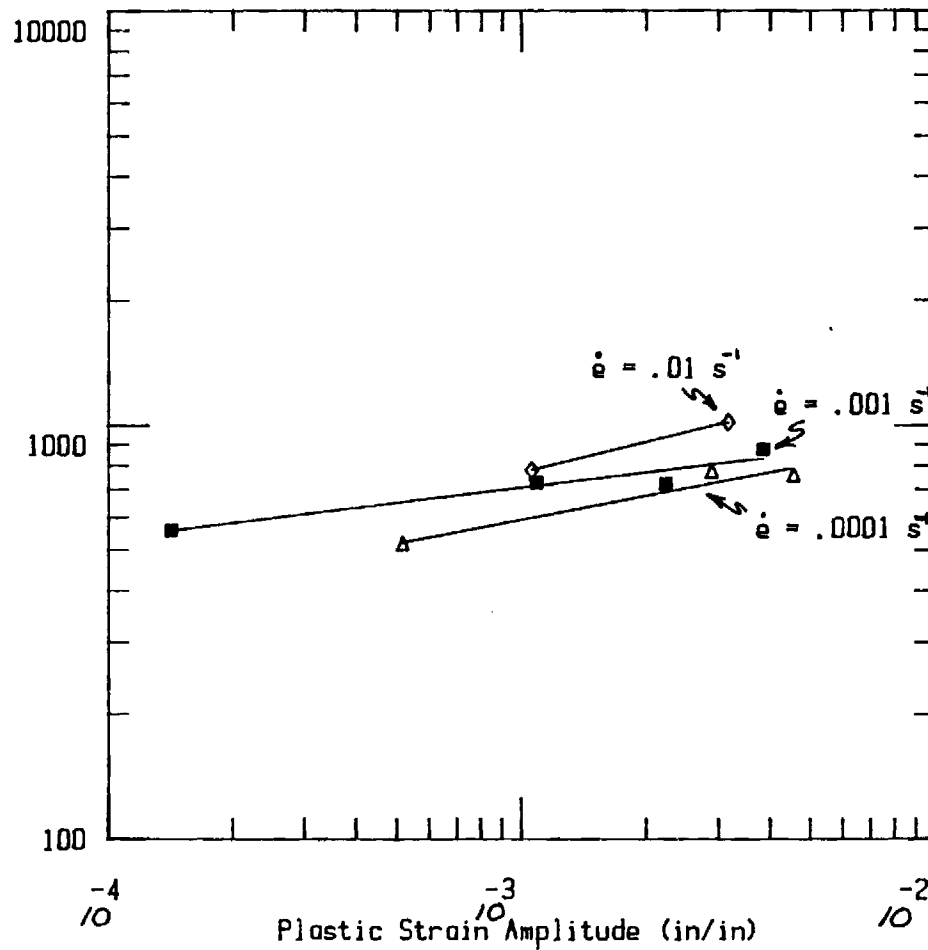
For $\dot{e} = .01\ s^{-1}$:

$$\frac{\Delta\sigma}{2} = K'\left[\frac{\Delta\epsilon^{P}}{2}\right]^{n'}$$

$K' = 4178.30$ MPa

$n' = 0.2458$

For $\dot{e} = .001\ s^{-1}$:

$$\frac{\Delta\sigma}{2} = K'\left[\frac{\Delta\epsilon^{P}}{2}\right]^{n'}$$

$K' = 1630.01$ MPa

$n' = 0.1219$

For $\dot{e} = .0001\ s^{-1}$:

$$\frac{\Delta\sigma}{2} = K'\left[\frac{\Delta\epsilon^{P}}{2}\right]^{n'}$$

$K' = 2194.27$ MPa

$n' = 0.1908$

$$* \quad \frac{\Delta\epsilon^{P}}{2} = \frac{\Delta\epsilon}{2} - \frac{\Delta\sigma}{2E}$$

Plastic Strain Amplitude (in/in)

Mar M 246 at 900 deg C

Stress Amplitude (MPa)

Calculations based on <u>loop shape.</u>

$\dot{e} = .01\ s^{-1}$

$\dot{e} = .001\ s^{-1}$

$\dot{e} = .0001\ s^{-1}$

10000.

1000.

100.

10^{-4} 10^{-3} 10^{-2}

Plastic   Strain Amplitude (in/in)
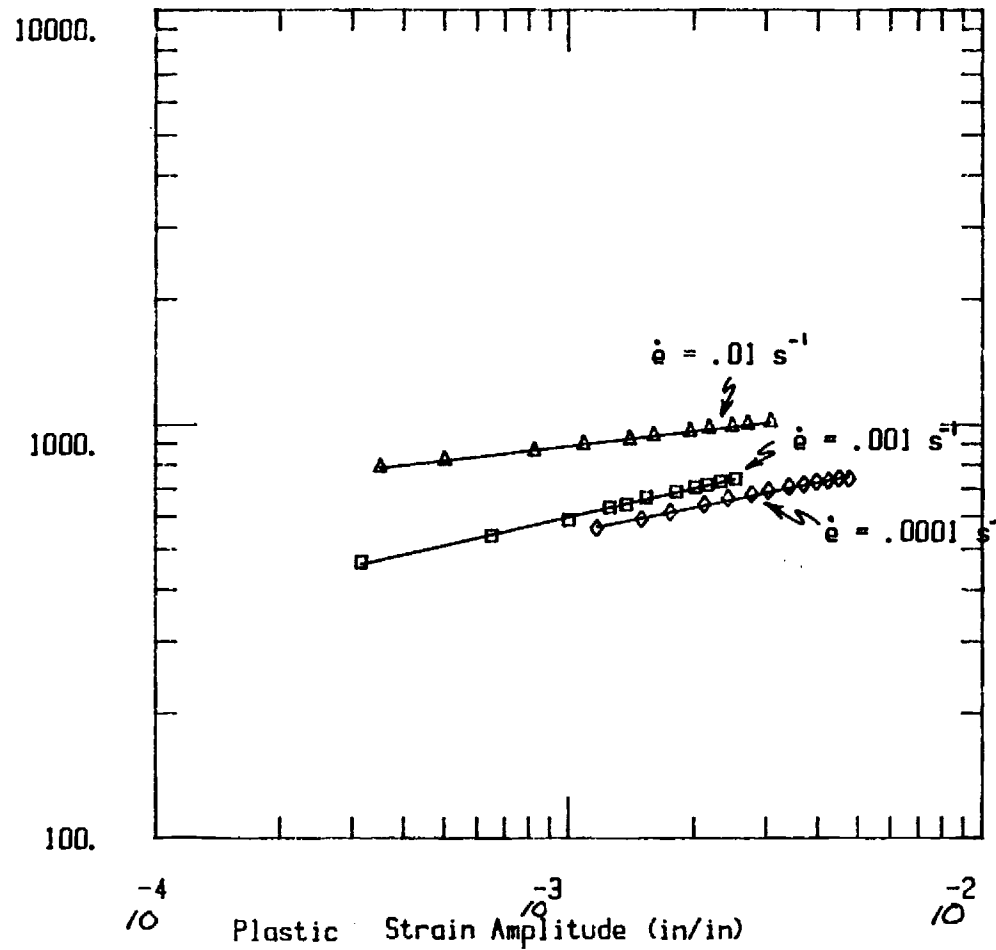
For $\dot{e} = .01\ s^{-1}$:

$$\frac{\Delta\sigma}{2} = K' \left[\frac{\Delta\epsilon^{p}}{2}\right]^{n'}$$

$K' = 2016.04$ MPa

$n' = 0.1187$

For $\dot{e} = .001\ s^{-1}$:

$$\frac{\Delta\sigma}{2} = K' \left[\frac{\Delta\epsilon^{p}}{2}\right]^{n'}$$

$K' = 2906.50$ MPa

$n' = .2290$

For $\dot{e} = .0001\ s^{-1}$:

$$\frac{\Delta\sigma}{2} = K' \left[\frac{\Delta\epsilon^{p}}{2}\right]^{n'}$$

$K' = 2231.98$ MPa

$n' = .2037$

32.

SUMMARY OF CYCLIC CONSTANTS

I. Using Hysteresis Loop Shape

STRAIN RATE	K'	n'
10^{-4} sec^{-1}	2231.98 MPa	0.2037
10^{-3} sec^{-1}	2906.50 MPa	0.2290
10^{-2} sec^{-1}	2016.04 MPa	0.1187

II. Using Hysteresis Loop Tips

STRAIN RATE	K'	n'	
10^{-4} sec^{-1}	2194.27 MPa	0.1908	
10^{-3} sec^{-1}	1630.01 MPa	0.1219	*
10^{-2} sec^{-1}	4178.30 MPa	0.2458	

$$\frac{\Delta\sigma}{2} = K' \left[\frac{\Delta\epsilon^p}{2}\right]^{n'}$$

K' ≡ Cyclic strength coefficient.

n' ≡ Cyclic hardening exponent.

* It should be noted that these calculations are based on a relatively small number of hysteresis loop tips and, hence, this procedure has a much lower confidence level than using the hysteresis loop shape.

MONOTONIC TEST #M-03 STRAIN RATE = .00001 /SEC

STRESS (MPa)
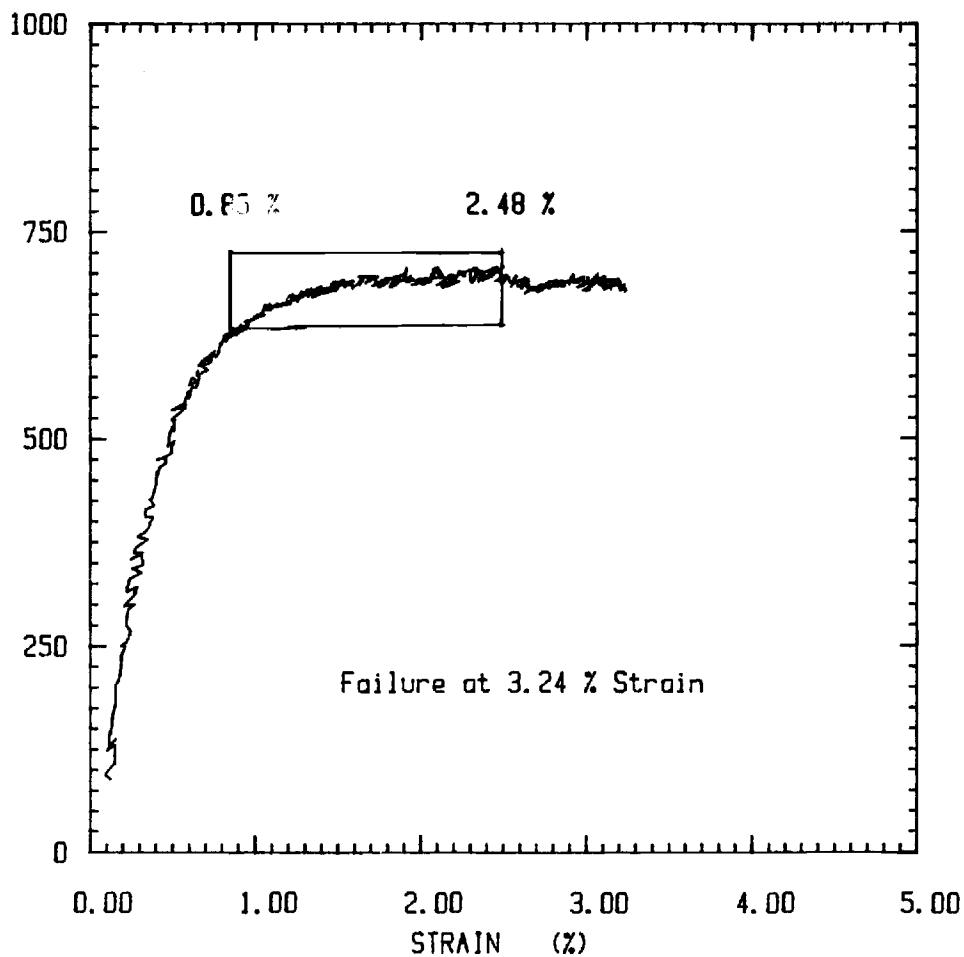
Box defines data used to determine the strength coefficient, K, and the strain hardening exponent, n.

0.85 %   2.48 %

Failure at 3.24 % Strain

STRAIN (%)

MONOTONIC TEST #M-03 STRAIN RATE = .00001 /SEC

LOG STRESS
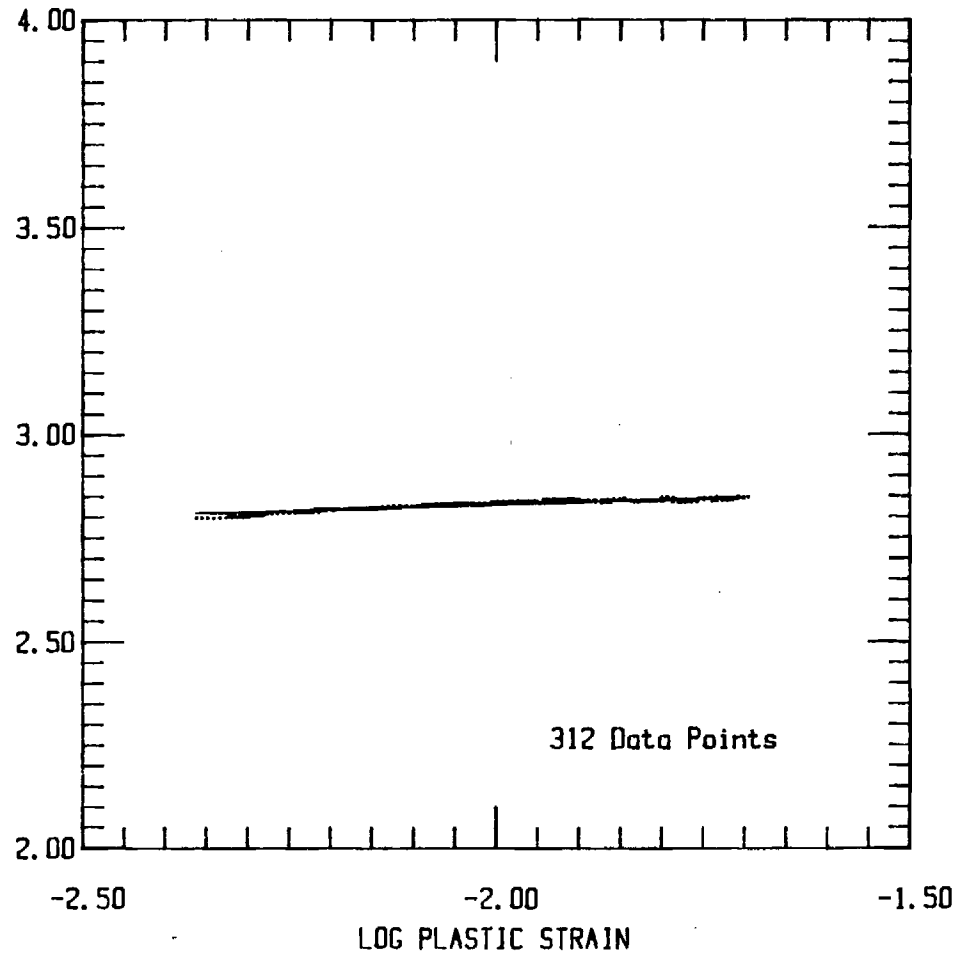
K = 899.27 MPa   n = 0.06186
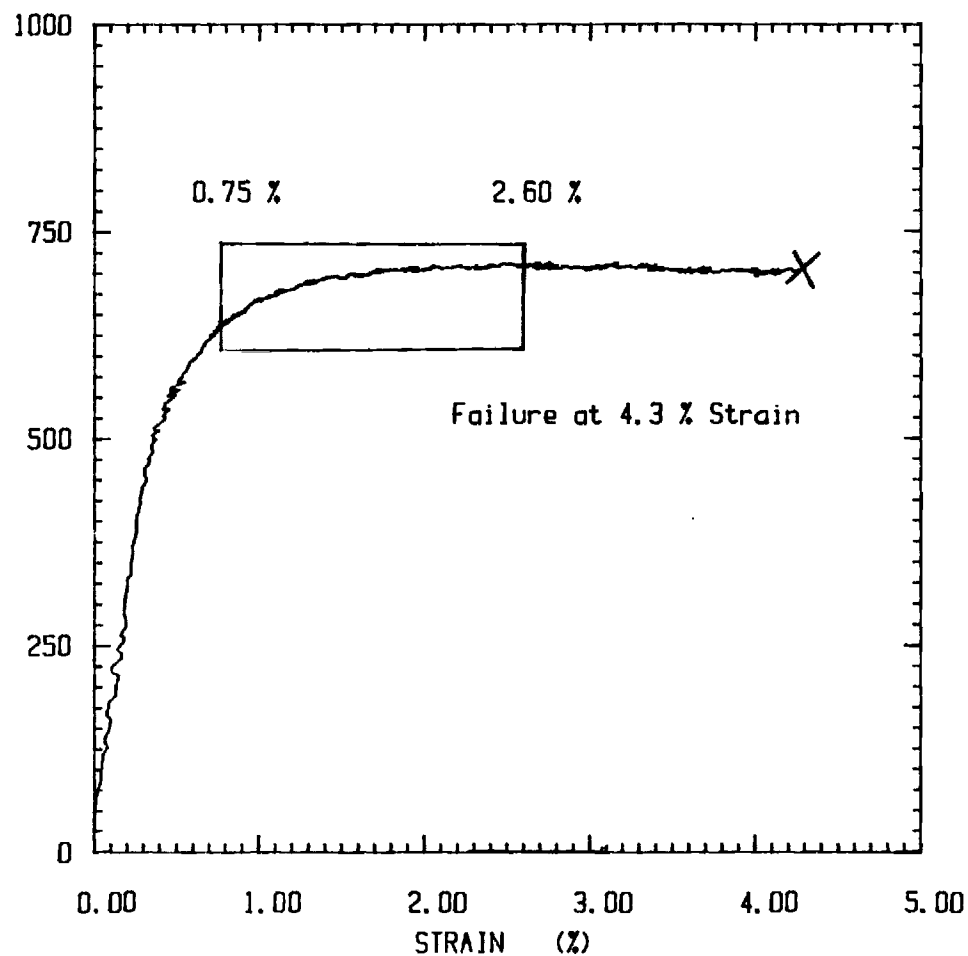
312 Data Points

LOG PLASTIC STRAIN

MONOTONIC TEST #M-04 STRAIN RATE = .0001 /SEC

STRESS   (MPa)

Box defines data used to determine strength coefficient, K, and the strain hardening exponent, n.

0.75 %   2.60 %

Failure at 4.3 % Strain

STRAIN   (%)

MONOTONIC TEST #M-04 STRAIN RATE = .0001 /SEC

LOG STRESS
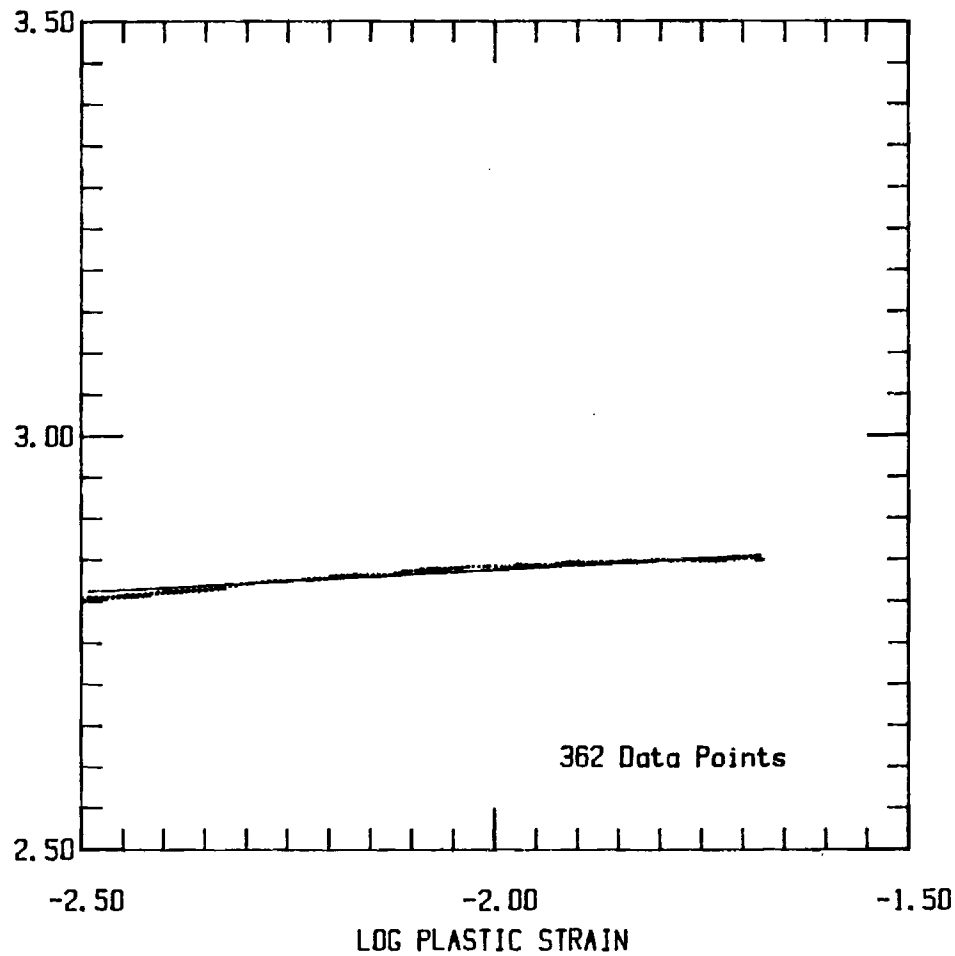
K = 885.83 MPa   n = 0.05446
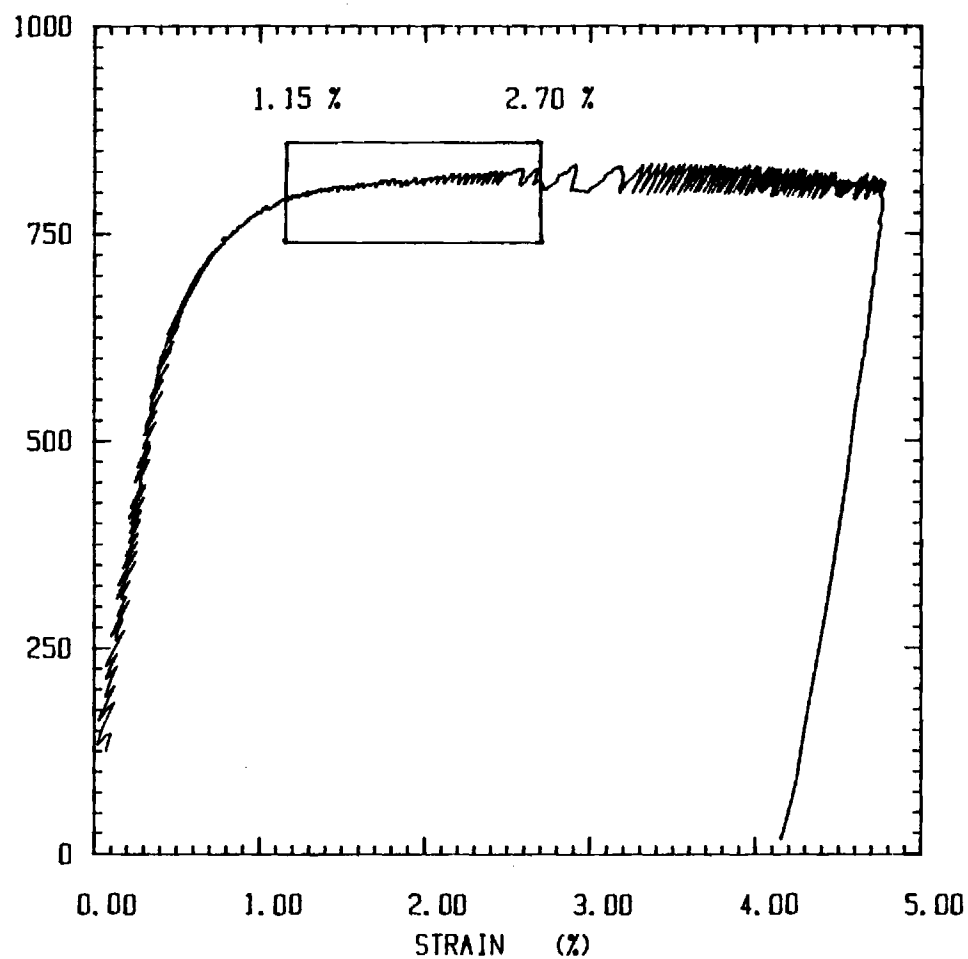
362 Data Points

LOG PLASTIC STRAIN

MONOTONIC TEST #M-01 STRAIN RATE = .001 /SEC

STRESS   (MPa)

Box defines data used to determine

the strength coefficient, K, and the

strain hardening exponent, n.

MONOTONIC TEST #M-01 STRAIN RATE = .001 /SEC

LOG STRESS

K = 907.21 MPa   n = 0.02589
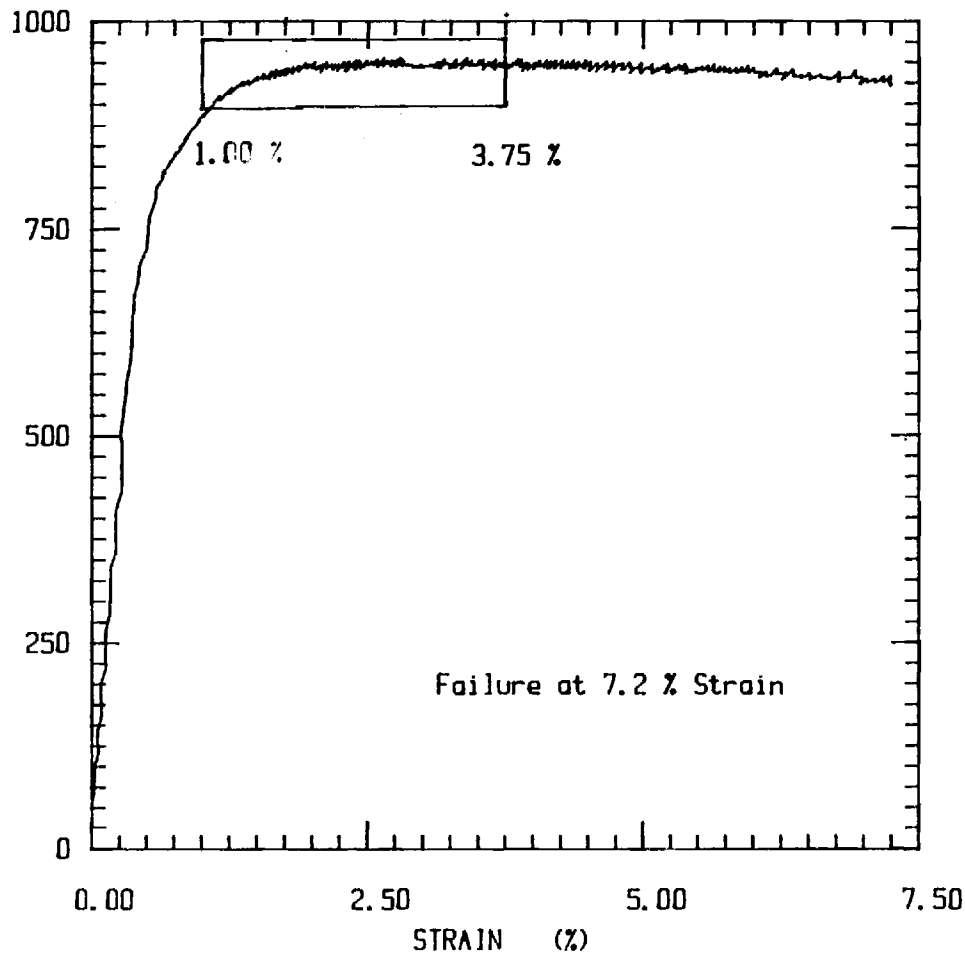
313 Data Points

LOG PLASTIC STRAIN

MONOTONIC TEST #M-02 STRAIN RATE = .01 /SEC

STRESS   (MPa)

Box defines data used to determine
the strength coefficient, K, and the
strain hardening exponent, n.

MONOTONIC TEST #M-02 STRAIN RATE = .01 /SEC

LOG STRESS

K = 1049.93 MPa   n = 0.02666

270 Data Points

LOG PLASTIC STRAIN
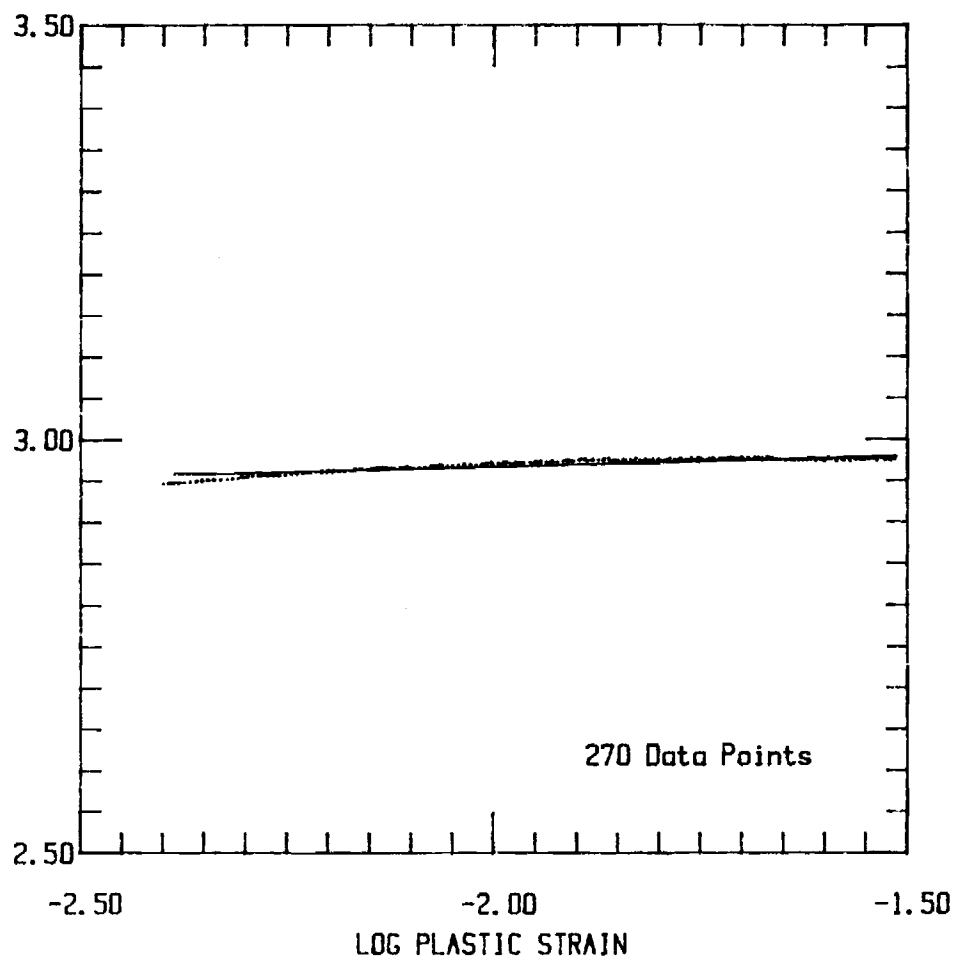
MONOTONIC TEST #M-05 STRAIN RATE = .1 /SEC

STRESS   (MPa)
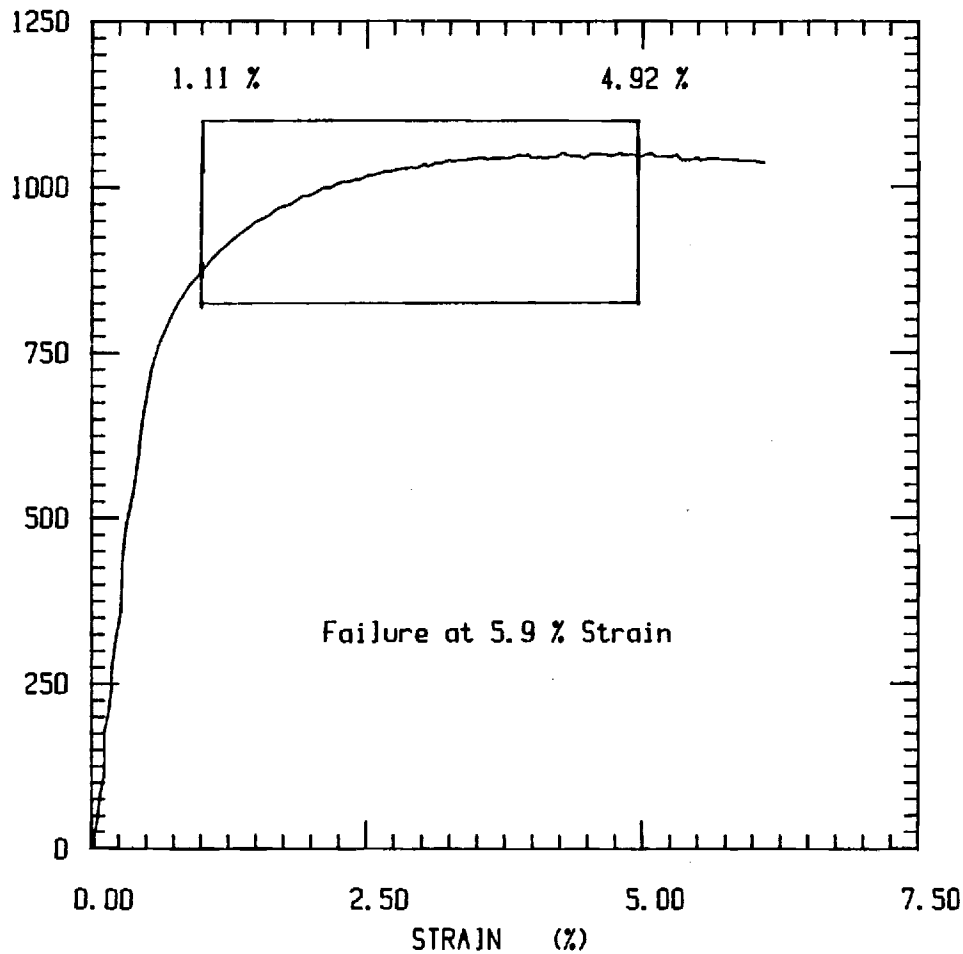
Box defines data used to determine

strength coefficient, K, and the strain

hardening exponent, n.

MONOTONIC TEST #M-05 STRAIN RATE = .1 /SEC

LOG STRESS

K = 1332.97 MPa   n = 0.06991

66 Data Points

LOG PLASTIC STRAIN

44.
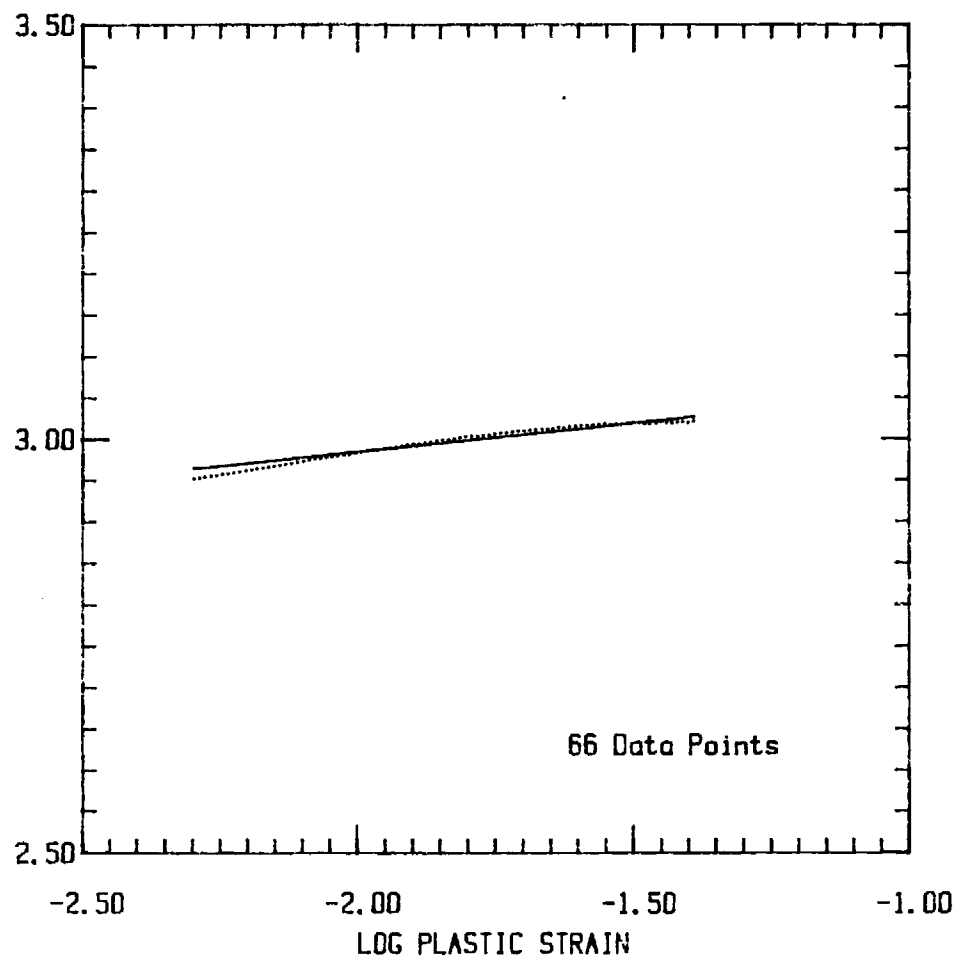
MONOTONIC ANALYSIS

STRAIN RATE	MONOTONIC TEST	K	n
10^{-5} sec^{-1}	M-03	899.72 MPa	0.06186
10^{-4} sec^{-1}	M-04	885.83 MPa	0.05446
10^{-3} sec^{-1}	M-01	907.21 MPa	0.02589
10^{-2} sec^{-1}	M-02	1049.93 MPa	0.02666
10^{-1} sec^{-1}	M-05	1332.97 MPa	0.06991

K $\equiv$ Strength Coefficient
n $\equiv$ Strain-hardening Exponent

$$\sigma = K \left[\epsilon^p \right]^n$$

LETTER REPORT

"DAMAGE RATE APPROACHES FOR THERMOMECHANICAL FATIGUE
OF SUPERALLOYS"

By David L. McDowell
Principal Investigator

R.L.T. Oehmke
Research Engineer

Gary Reynolds
Graduate Research Assistant

Project # E-25-M13
General Motors PO# H636356

September 10, 1987

Submitted to Allison Gas Turbine Operations, General Motors
Corporation

Sponsor Technical Contact:

Dr. W.E. Schneider/T-10
Allison Gas Turbine Operations
General Motors Corporation
2001 South Tibbs Ave.
Indianapolis, IN 46241
(317) 242-7703

Sponsor Administration and Contractual Matters:

Darrell L. Mackey/U02
Allison Gas Turbine Operations
General Motors Corporation
P.O. Box 420
Indianapolis, IN 46206-0420
(317) 242-6954

September 10, 1987

Dr. W.E. Schneider/T-10
Allison Gas Turbine Operations
General Motors Corp.
2001 South Tibbs Avenue
Indianapolis, IN 46241

Dear Dr. Schneider:

This report summarizes the activities of our effort on GM PO#H636356, "Damage Rate Approaches for Thermomechanical Fatigue of Superalloys" for the period August 1, 1987 to August 31, 1987.

In summary, our first year effort on this program has resulted in rather significant characterization of the deformation and fatigue response of MAR-M 246 at 900°C as detailed in the July period letter report and in the proposal for second year funding which was submitted June 20, 1987.

Work in-progress during the month of August has addressed the creep behavior of MAR-M 246 at 900°C, further cyclic testing, and characterization of oxidation penetration.

We look forward to receiving continued funding on the project, as per the aforementioned June 20 proposal, as soon as possible.

Sincerely,

David L. McDowell
Principal Investigator

DLM

LETTER REPORT

"DAMAGE RATE APPROACHES FOR THERMOMECHANICAL FATIGUE
OF SUPERALLOYS"

By David L. McDowell
Principal Investigator

R.L.T. Oehmke
Research Engineer

Gary Reynolds
Graduate Research Assistant

Project # E-25-M13
General Motors PO# H636356

February 1, 1988

Submitted to Allison Gas Turbine Operations, General Motors
Corporation

Sponsor Technical Contact:

Dr. W.E. Schneider/T-10
Allison Gas Turbine Operations
General Motors Corporation
2001 South Tibbs Ave.
Indianapolis, IN 46241
(317) 242-7703

Sponsor Administration and Contractual Matters:

Darrell L. Mackey/U02
Allison Gas Turbine Operations
General Motors Corporation
P.O. Box 420
Indianapolis, IN 46206-0420
(317) 242-6954

February 2, 1988

Dr. W.E. Schneider/T-10
Allison Gas Turbine Operations
General Motors Corp.
2001 South Tibbs Avenue
Indianapolis, IN 46241

Dear Dr. Schneider:

This report summarizes the activities of our effort on GM PO#H636356, "Damage Rate Approaches for Thermomechanical Fatigue of Superalloys" for the period September 1987 to January 31, 1988.

Enclosed please find a report which describes several creep tests run on MAR-M 246 at 900°C. Also included is a discussion of creep constants pertaining to both a simple power law secondary creep description and to a more sophisticated continuum damage formulation which is part of the overall effort in development of damage rate equations. We are currently in the process of repeating these creep tests to estimate scatter.

We have sectioned some of the 900°C fatigue specimens and examined the fracture surfaces and specimen surfaces at the outside diameters to determine (a) the extent of intergranular fracture and (b) the distribution of microcracks as a function of strain range and total environmental exposure time. The results are very interesting in that crack initiation appears to predominate at slip band intersections with the free surface at high $\Delta\epsilon^p$ and short test times, while grain boundary cracking predominates at longer test durations and small $\Delta\epsilon^p$.

Development of the fatigue damage rate equation is ongoing. We expect to begin a series of 900°C vacuum tests in February or March.

Sincerely,

David L. McDowell
Principal Investigator

DLM

CREEP TEST ANALYSIS
OF MAR-M 246 IN AIR AT 900°C

RESULTS AND DISCUSSION

Experimental Procedures

Three creep tests were completed for this study; a high stress level (413 MPa) and a low stress level (300 MPa) test, as well as a high-low step stress sequence (415/299 MPa) test. The tests were performed using a SATEC C-Type creep frame consisting of a 20:1 lever arm with a twelve-thousand pound pulling capacity, an automatic control load elevator, and a furnace shutoff interlock.

Temperature control was accomplished with an OMEGA Model 115 controller fed with an input signal from the interior of a rebuilt SATEC C-Type resistance furnace via a chromel-alumel thermocouple. The maximum operating temperature of the furnace was 2000°F (1143°C). A temperature gradient of only 1°C over the gage section of a test specimen, affixed with five beaded chromel-alumel thermocouples, was achieved with this setup.

Engineering creep strain was measured with a ATS capacitance gauge attached to a four arm high temperature extensometer. An output signal was sent to an amplifier and recorded with a strip chart recorder. The capacitance gauge

used had a resolution of 1×10^{-5} inches (0.01%) for a maximum
amplified output of ten volts.

A set of MAR-M 246 adapters were specially made to adapt
the button-head LCF-type specimens to the 0.75" pull rods. The
pull rods attached to these adapters were also fabricated out
of MAR-M 246 to ensure proper perfomance of the mechanical
system at the operating temperature of 900°C.

Fundamental Results

Engineering strain versus time data for secondary and
tertiary creep is presented in Figure 1. The corresponding
basic characteristics of the trio of creep tests are outlined
in Table 1.

To begin to characterize creep life with a continuum
damage model, the steady state (stage II) creep strain rate
was assumed to behave as dictated by a Norton power law creep

$$\dot{e}_{ss}^{\,c} = A(\sigma)^n \qquad (1)$$

where $\dot{e}_{ss}^{\,c}$ = steady state creep strain rate

σ = applied nominal stress

A,n = constants

As calculated from the two constant nominal stress creep
tests, the exponent n was determined to be 6.65, and the

constant $A = 3.18 \times 10^{-21}$ hr^{-1} MPa$^{-6.65}$. This formulation provides a simple, although incomplete, description of the dependence of creep strain rate on stress. As the continuum damage model is developed, the creep strain rate will be predicted not only for steady state creep, but for tertiary creep coupled with the damage parameter D_c discussed in the program proposal.

Application of the Continuum Damage Approach

The scalar creep damage parameter can be interpreted as the normalized loss of area of the specimen cross section due to the formation of voids or cracks [22]. In other words, a high value of D_c would correspond to a high ratio of void area to grain boundary area in a specimen undergoing creep damage. With no damage, D_c is set equal to zero; and at failure, the parameter is normalized to unity.

A generalization of the damage rate method and a specific form of the continuum damage approach was suggested by Chaboche et. al. [25] as a creep damage model :

$$\dot{D}_c = \left[\frac{\sigma}{A(1-D_c)} \right]^r (1-D_c)^{r-k(\sigma)} \qquad (2)$$

where A, r = temperature dependent constants

$k(\sigma)$ = stress dependent constant

By factoring out the quantity $(1-D_c)^r$ and combining constants, a more compact form of this equation may be introduced, i.e.

$$\dot{D}_c = \frac{B\sigma^r}{(1-D_c)^{k(\sigma)}} \tag{3}$$

It is important to note that the purpose of the stress dependence on the parameter k, as defined by Chaboche, is to account for nonlinear damage cumulation for stress amplitude step tests.

This form of the differential equation is solved by separation of variables for a constant nominal stress creep test. The damage parameter limits of integration are $D_c = 0$ to $D_c = 1$ and the time limits are $t = 0$ to $t = t_R = $ time to rupture). The following expression results:

$$t_R = \frac{1}{B\sigma^r[k(\sigma) + 1]} \tag{4}$$

By taking the logarithm of both sides, the material constant r is readily determined.

$$\log t_R = -\log B[k(\sigma) + 1] - r \log \sigma \tag{5}$$

The quantity -r is the slope of the time to rupture versus stress plot on a log scale. This calculation is shown in Figure 2; i.e. r = 5.76.

It is important to note, however, that there is an appreciable amount of scatter in creep rupture time data, typically as much as a factor of two at a given stress level. The preliminary analysis herein is somewhat incomplete since there were only two constant stress creep tests performed, and hence, only two data points for the determination of r. In a worst case consideration, r could change from its present value by as much as ±50% given sufficient data to characterize it with some measure of statistical support. In an attempt to study the question of scatter in rupture time, the two constant nominal stress creep tests will be repeated under identical conditions.

In further characterization of the creep damage of MAR-M 246 using expression (3), the constants B and $k(\sigma)$ were estimated. This was accomplished using data from the step-stress sequence creep test. As with the above determination of r, the solution to the continuum creep damage model was utilized. Dividing the limits on integration into two parts - one for the high stress level initial segment of the step stress test, and the other for the low stress level completion - the following integrals may be written :

$$\int_0^{D_{INT}} (1 - D_C)^{k(\sigma_{HI})} \, dD_C = \int_0^{t_{INT}} B(\sigma_{HI})^r \, dt \qquad (6a)$$

$$\int_{D_{INT}}^{1} (1 - D_C)^{k(\sigma_{LOW})} \, dD_C = \int_{t_{INT}}^{t_R} B(\sigma_{LOW})^r \, dt \qquad (6b)$$

where $\sigma_{LOW}, \sigma_{HI}$ = low and high stress levels, respectively, of the sequence creep test

D_C = scalar creep damage parameter

D_{INT} = value of D_C at time at which stress level was decreased

t_{INT} = time at which stress level was decreased

t_R = time to rupture

$k(\sigma_{LOW}), k(\sigma_{HI})$ = constants depending on low and high stress levels respectively

B, r = temperature dependent constants

The solution of these integrals is :

$$\frac{1 - [1 - D_{INT}]^{(k(\sigma_{HI}) + 1)}}{k(\sigma_{HI}) + 1} = B(\sigma_{HI})^r (t_{INT}) \qquad (7a)$$

$$\frac{(1 - D_{INT})^{(k(\sigma_{LOW}) + 1)}}{k(\sigma_{LOW}) + 1} = B(\sigma_{LOW})^r (t_R - t_{INT}) \qquad (7b)$$

Thus, two equations were formulated containing four unknown quantities, D_{INT}, $k(\sigma_{HI})$, $k(\sigma_{LOW})$, and B. To complete a system of four equations, two additional expressions were required. By using the constant-stress-to-failure creep tests, two equations in the form of (5) were incorporated without adding any additional unknown variables. For the high stress level test,

$$(t_{RH})^{-1} = B\sigma^r [k(\sigma_{HI}) + 1] \qquad (8)$$

and for the low stress level creep test,

$$(t_{RL})^{-1} = B\sigma^r [k(\sigma_{LOW}) + 1] \qquad (9)$$

where t_{RH} and t_{RL} are the rupture times of the respective tests in the absense of loading sequence effects.

An iterative approach was developed to solve this set of four nonlinear equations. First, the creep damage parameter at the time of stress interruption was selected and held fixed. An arbitrary value for the constant B was then used in expressions (8) and (9) to obtain a first estimate of $k(\sigma_{HI})$

and $k(\sigma_{LOW})$ respectively. Constant B and these values of $k(\sigma)$ were subsequently used in a Gauss-Seidel iteration routine of equations (7) to get a further calculation of $k(\sigma_{HI})$ and $k(\sigma_{LOW})$ based on the scalar creep damage parameter. This process of altering the value of B and iterating was repeated until convergence was reached with the value of $k(\sigma_{HI})$ being slightly greater, but reasonably close to the value of $k(\sigma_{LOW})$. This procedure was carried out for fixed values of D_{INT} ranging from .05 to .20. The results of this iteration procedure are presented in Table 6.

Based on the application of a similar creep analysis performed on IN 100 (also a Ni-base superalloy) by Chaboche and workers [25], reasonable values for $k(\sigma)$ would be in the range of 4 or 5. The values of $k(\sigma_{HI})$ settled upon were greater than $k(\sigma_{LOW})$ to produce a greater damage rate for the more highly stressed case. It should be noted that the estimates of $k(\sigma)$ for each stress level calculation using the equations based on constant stress are also included in the tabulated results. With these calculations, the values of $k(\sigma_{HI})$ are slightly less than the calculations for $k(\sigma_{LOW})$ – and are both higher than the "anticipated" values. Consideration of strain to failure in the coupled strain – damage equation will result in some further iteration of $k(\sigma)$ values as discussed later.

It is encouraging that the measures for the creep damage

parameter are within reason, based on the work of Chaboche, since $k(\sigma)$ values are in the proximity of 4 to 5. More specifically, using the iterated formulations of (7), $k(\sigma)$ ranged from 3.75 to 5.97 for D_{INT} between .07 and .10. Using the equations based on the constant stress tests (8 and 9), $k(\sigma)$ was estimated between 4.03 and 5.27 for the damage parameter valued in the range .10 to .12.

Much of the previous analysis was based on a rough estimate of the value of the interrupted creep damage parameter. It is possible; however, to determine D_{INT} based entirely on metallurgical study, and therefore determine the values of the other constants of the continuum damage equation more readily. This would require another creep test at the same stress level as one of the previously completed constant stress tests. At a predetermined time, the creep test would be halted and the MAR-M 246 specimen removed and sectioned. From a study of void growth as a function of grain boundary area, the damage parameter could be determined directly.

If this test were conducted at the higher stress level ($\sigma = \sigma_{HI}$) then the expression involving σ_{LOW} would be eliminated and only two equations with two unknown quantities ($k(\sigma_{HI})$ and B) would remain. These parameters could be solved explicitly and the resulting value of B could be used in conjunction with the test data for the low stress level test to determine $k(\sigma_{LOW})$ explicitly.

It is therefore felt that at least one additional creep test be run at either a stress level of 300 MPa or 413 MPa and halted before rupture. A study of D_{INT} based on the physical condition of the MAR-M 246 specimen and the resulting calculations of the remaining continuum damage equation constants, as outlined, would yield invaluable information on the accuracy of the creep characterization performed in this study.

Creep Strain Rate Analysis

Using the effective stress concept for uniaxial loading, as defined by Lemaitre [27],

$$\tilde{\sigma} = \frac{\sigma}{1 - D} \quad \text{where } D = D_c \quad (10)$$

where $\tilde{\sigma}$ = effective stress
Then the creep strain rate equation (1) may be re-written as,

$$\dot{e}^c = A \left[\frac{\sigma}{1 - D_c} \right]^n \quad (11)$$

Which, by considering a separate exponent on the damage accumulation term as proposed by Rabotnov [21], may be re-formulated as,

$$\dot{e}^c = A\sigma^n \left[\frac{1}{1 - D_c}\right]^\nu \tag{12}$$

The creep strain rate $\dot{e}^c$ is used here since both secondary and tertiary creep are included.

The main purpose of this dual exponent approach is to better model the tertiary creep regime and rupture time. Using the values of B and $k(\sigma_{HI})$ deemed most likely to represent the true physical situation, the set of coupled non-linear differential equations (3 and 11) were solved using a fourth order Runge-Kutta method. Constant B was again slightly altered until the value of the creep damage parameter reached unity at the time of rupture of the high stress level test. The value of ν was then altered until the numerical solution of engineering creep strain at the time of specimen failure best fit the experimental rupture strain for this test. This numerical approximation was plotted against the experimental data as shown in Figure 3. The quality of the approximation was improved by slight adjustments made to the values of constants A and n from the original Norton power law creep calculations. Special consideration was given to the secondary creep regime, due to its engineering importance.

A similar procedure was followed in an attempt to fit the data from the low stress level creep test. Ideally, the values

of B, r, A, n, and ν should remain unchanged since they are stress-independent and this test was performed at the same temperature as the first. Using the same value of B, $k(\sigma_{LOW})$ was reduced until the continuum damage equation produced a damage parameter of unity at the experimental time to rupture of this test. The resulting value of $k(\sigma_{LOW})$ was then less than that of $k(\sigma_{HI})$; which is a more physically sound condition than the estimates in Table 2. The value of ν used to produce identical numerical/experimental strain-to-failures for the high stress level test was incorporated into this fitting procedure. The result was a predicted strain-to-failure of 8.5% greater than that experimentally observed, a small difference considering the possible scatter associated with rupture data.

The numerical approximation to the creep data is plotted in comparison to the experimental data in Figure 4. The only additional change from the values in the high stress level fit is that the constant A was reduced slightly to provide improved numerical/experimental agreement for the secondary creep stage. Since secondary creep rates exhibit scatter, it may be desirable to view A as an average for the two tests.

The values of all constants used in these fitting procedures are given in Table 3. Note that the best fit, determined by graphic comparison between experimental and numerical data, resulted in $k(\sigma_{HI})$ = 5.11 , $k(\sigma_{LOW})$ = 4.72.

These results correspond to an interrupted scalar damage value D_{INT} of approximately .10 to .11, within a reasonable range, although somewhat arbitrary in the absence of metallurgical damage quantification.

Due to potential confusion of the reader in following the numerical procedures outlined, a simplified step by step guide to the creep characterization process is included in Appendix A. The procedures are broken into two segments; one for the estimation of constants of the continuum damage equation, and the other for the numerical solution to the coupled striain/damage equations.

A plot of the scalar creep damage parameter D_c versus normalized time for both constant stress creep tests is presented in Figure 5. This data graphically demonstrates the more damaging effects of low-high stress level sequences compared to high-low stress sequences for the same time fraction, t/t_R. These effects are in agreement with the work of Woodford [23].

APPENDIX A

Guide to Creep Analysis Numerical Procedures

PROCEDURE I : Estimation of constants D_{INT}, B, $k(\sigma_{HI})$, and $k(\sigma_{LOW})$

STEP 1: Choose a value of D_{INT}. Based on studies of IN 100, the value of D_{INT} should be in the proximity of .10.

STEP 2: Choose a value for B.

STEP 3: With solutions to the creep continuum damage equation based on the constant stress 413 MPa test and the 300 MPa test, determine $k(\sigma_{HI})$ and $k(\sigma_{LOW})$ respectively, using equations (8) and (9).

STEP 4: Use the values of D_{INT}, B, $k(\sigma_{HI})$, and $k(\sigma_{LOW})$ determined in steps 1-3 in an iterative solution to the continuum damage equation based on the step stress sequence test. Use equations (7a) and (7b).

STEP 5: If the solution to STEP 4 converges for $k(\sigma_{HI})$ slightly greater than $k(\sigma_{LOW})$, go to STEP 6; else, return to STEP 2 and alter the value of B.

STEP 6: The values of B, $k(\sigma_{HI})$, and $k(\sigma_{LOW})$ are determined for the value of D_{INT} chosen in STEP 1. These results are recorded in Table 2. Use these results of D_{INT} and B a final time in equations (8) and (9) to determine a further estimation of $k(\sigma_{HI})$ and $k(\sigma_{LOW})$ - also recorded (in parentheses) in Table 2.

STEP 7: Return to STEP 1 and repeat the process for another value of D_{INT}.

PROCEDURE II : Numerical solution to the coupled strain/damage equations for two constant stress creep tests.

STEP 1: Numerically solve the set of two, nonlinear, coupled differential equations (3) and (11) for the higher stressed creep test. Use the most reasonable

value for $k(\sigma_{HI})$, and the corresponding value of B from Table 2. Choose a value for ν.

STEP 2: Alter the value of B until the value of the creep damage parameter, D, is equal to unity at the experimental rupture time of the high stress level test.

STEP 3: Without changing the parameter B, alter the value of ν until the numerical solution to nominal strain at rupture equals the experimental result.

STEP 4: Adjust the values of A and/or n from the results of equation (1) to improve the closeness of the numerical/experimental nominal creep strain data. This is done graphically; i.e. refer to Figure 3.

STEP 5: Using the values of B, A, n, and ν determined in steps 1-4, numerically solve equations (3) and (11) for the lower stressed creep test. Initially, use the value of $k(\sigma_{HI})$ as a first approximation to $k(\sigma_{LOW})$.

STEP 6: Do not change the value of B, but instead alter the value of $k(\sigma_{LOW})$ until D = 1 at the experimental time to rupture of the low stress level test.

STEP 7: Do not alter ν, but attempt to improve numerical and experimental correlation by changing the value of A.

   * Results to these numerical solutions are shown in Figures 3 and 4 and in Table 3.

Table 1 : Creep Test Data for MAR-M 246 in Air at 900°C

Specimen I.D.	Nominal Stress	Nominal Strain to Rupture	Time to Rupture, t_R	Steady-state Creep Strain Rate $(\dot{e}_{ss}^c)$
G23	413 MPa	0.0635 in/in	27.35 hr	81.11×10^{-5} hr^{-1}
G21	300	0.0446	174.70	9.53×10^{-5}
G19 a.	415		13.80	54.60×10^{-5}
G19 b.	299	0.0420	140.00	6.97×10^{-5}

Notes : a. Test G19 was a step-stress sequence test; loaded to 415 MPa for one half of the time to rupture of test G23 and then,
b. loaded until failure at the stress level of test G21

Table 2 : Estimated Values of Constants for
Creep Damage Rate Equation

D_{INT}	B	$k(\sigma_{HI})$	$k(\sigma_{LOW})$
.05	2.43×10^{-18}	8.76 (11.53)*	8.74 (11.86)*
.07	3.43×10^{-18}	5.97 (7.87)	5.89 (8.11)
.10	4.98×10^{-18}	3.80 (5.11)	3.75 (5.27)
.12	6.05×10^{-18}	2.93 (4.03)	2.91 (4.16)
.15	7.70×10^{-18}	2.08 (2.95)	2.07 (3.06)
.17	8.82×10^{-18}	1.70 (2.45)	1.68 (2.54)
.20	10.55×10^{-18}	1.26 (1.89)	1.24 (1.96)

D_{INT} : Creep damage parameter.

B : Temperature dependent constant.

$k(\sigma_{HI})$: Stress-dependent constant for high stress level
creep test.

$k(\sigma_{LOW})$: Stress-dependent constant for low stress level
creep test.

NOTE: Values in parentheses are determined from the
solution of the continuum damage equations for constant
stress creep (equations 8 and 9) with the B values
given in the table. Values beside the $k(\sigma_{HI})$ estimates
are based on the 413 MPa creep test, and those next to the
$k(\sigma_{LOW})$ estimates are based on the 300 MPa test.

Table 3 : Creep Characterization Constants

Constant		413 MPa Test	300 MPa Test	
$k(\sigma)$	:	5.11	4.72	
A	:	2.8×10^{-21}	2.4×10^{-21}	a.
n	:	6.66	6.66	
r	:	5.76	5.76	
B	:	5.51×10^{-18}	5.51×10^{-18}	b.
ν	:	3.9	3.9	

NOTES: a). Original calculation of A, based on
n = 6.66 and equation (1), was 3.0×10^{-21}.
b). Original estimate of B was 4.98×10^{-18}.

Nominal Creep Strain (in/in)
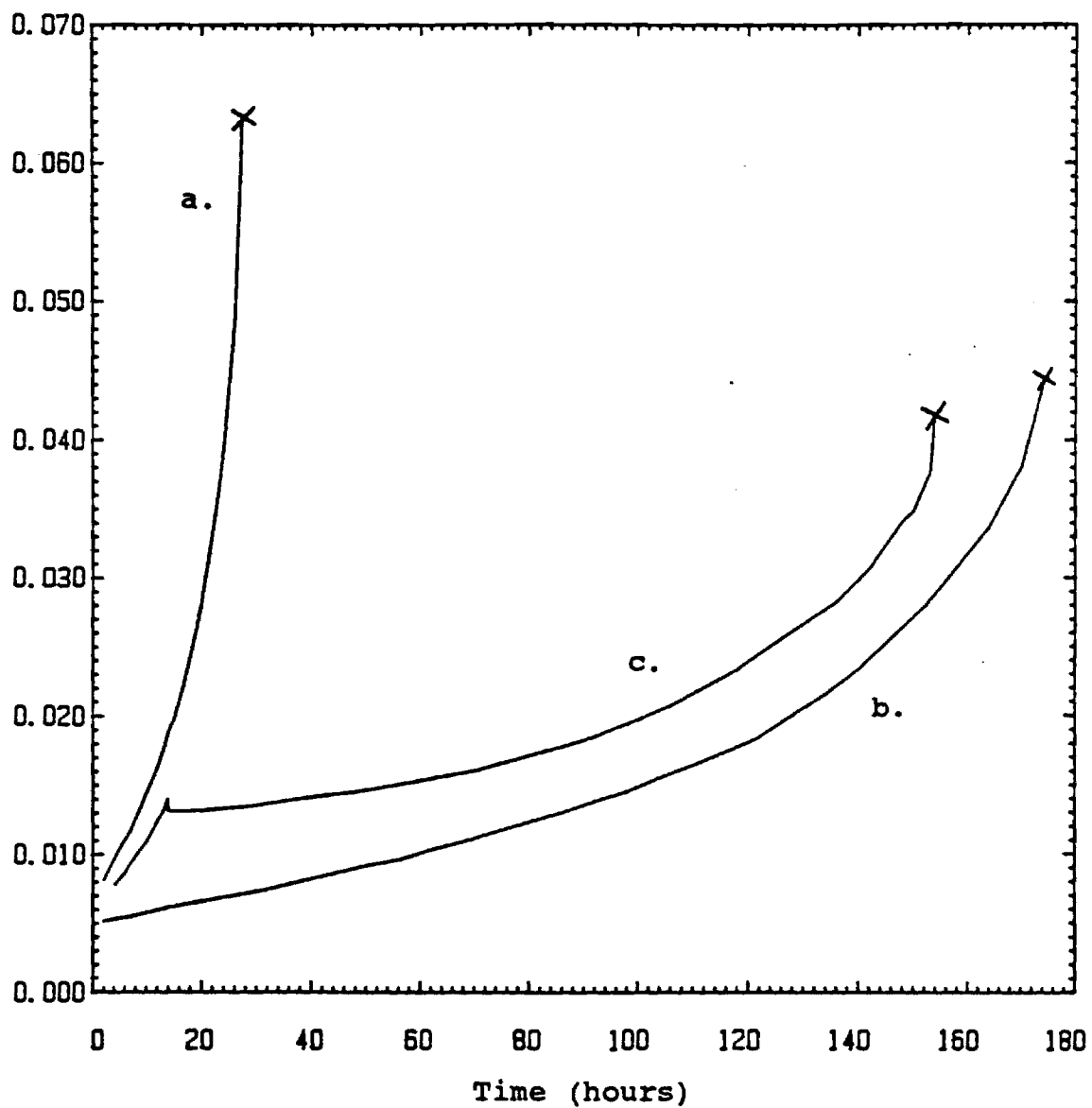
Figure 1. Nominal creep data for MAR-M 246 tested in
air at 900°C.
a). $\sigma = 413$ MPa   b). $\sigma = 300$ MPa
c). $\sigma = 415 / 299$ MPa step

Time to rupture (hours)
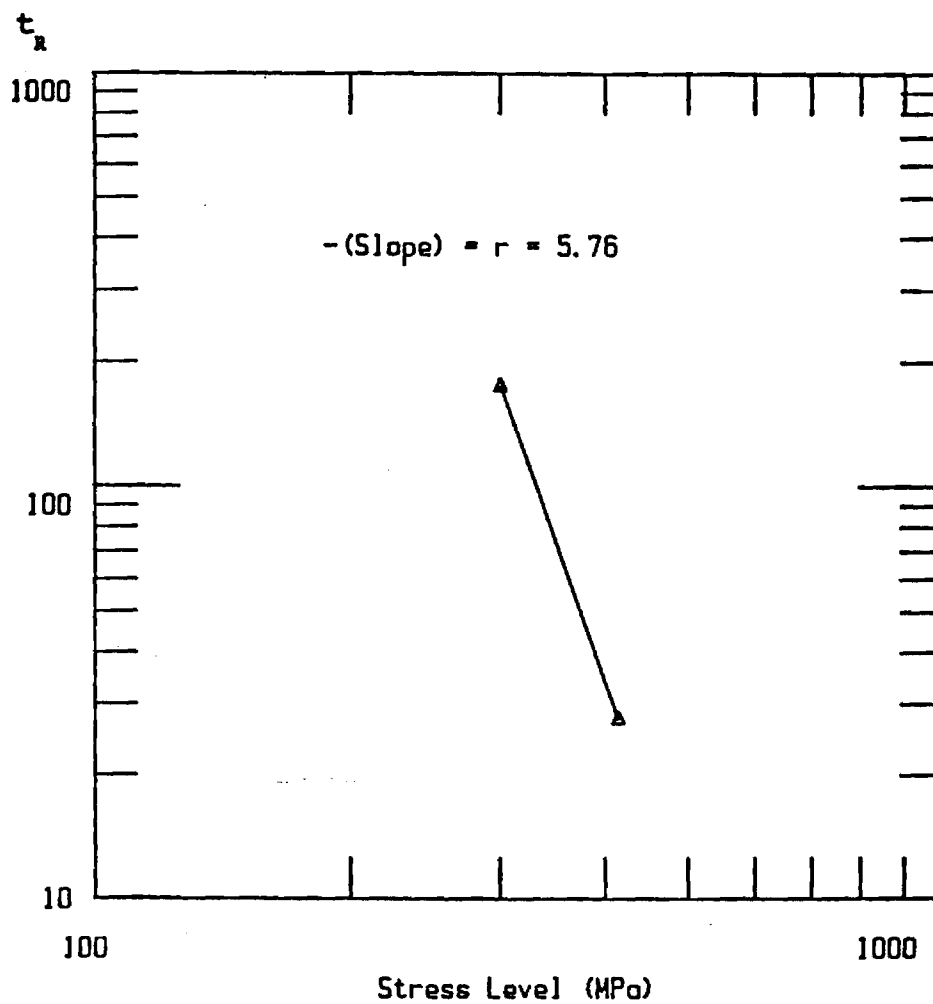
Figure 2. Determination of the creep damage constant r.

Nominal Creep Strain (in/in)
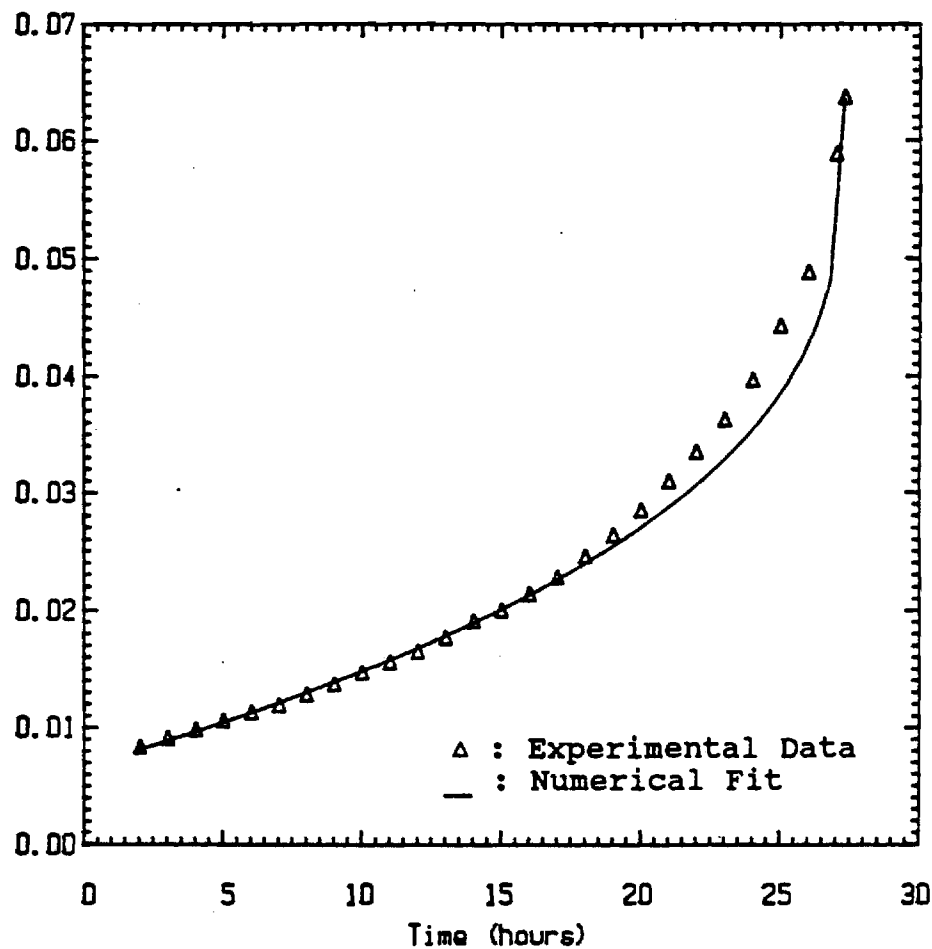
Figure 3. Numerical analysis of creep strain rate equation
        versus experimental creep strain data for MAR-M 246
        tested in air at 900°C under a stress of 413 MPa.

Nominal
Creep Strain (in/in)
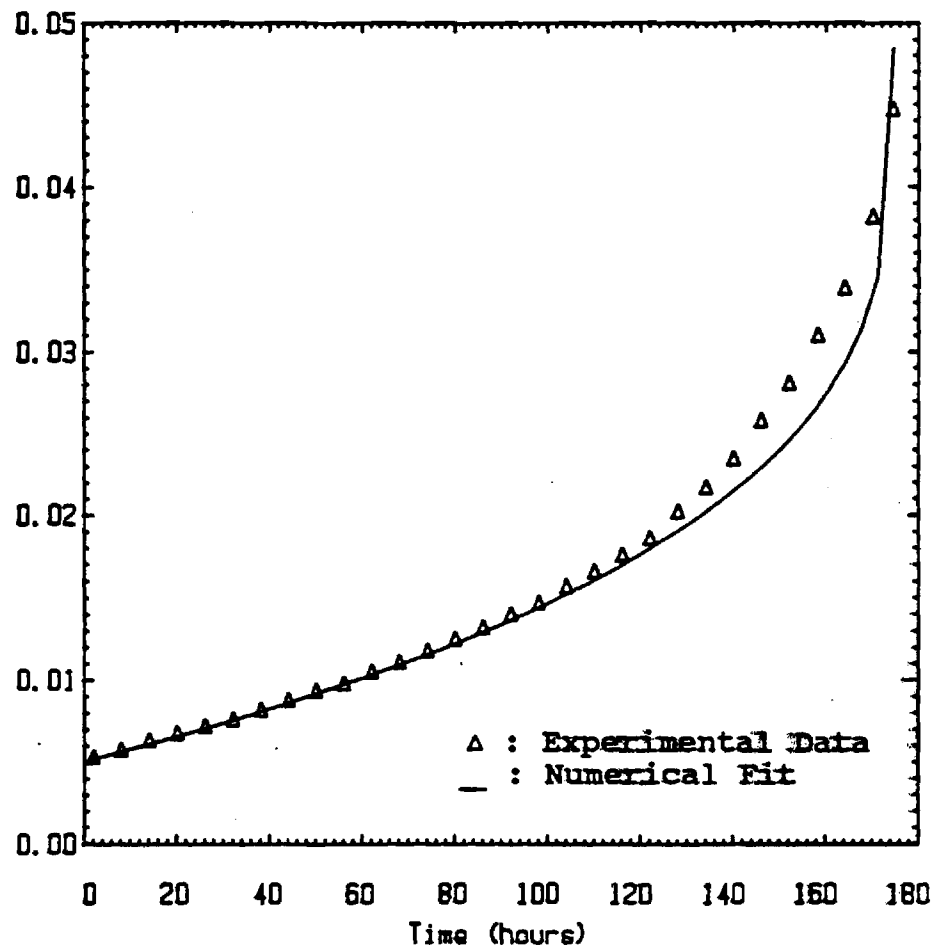
Figure 4. Numerical analysis of creep strain rate equation versus experimental creep strain data for MAR-M 246 tested in air at 900°C under a stress of 300 MPa.
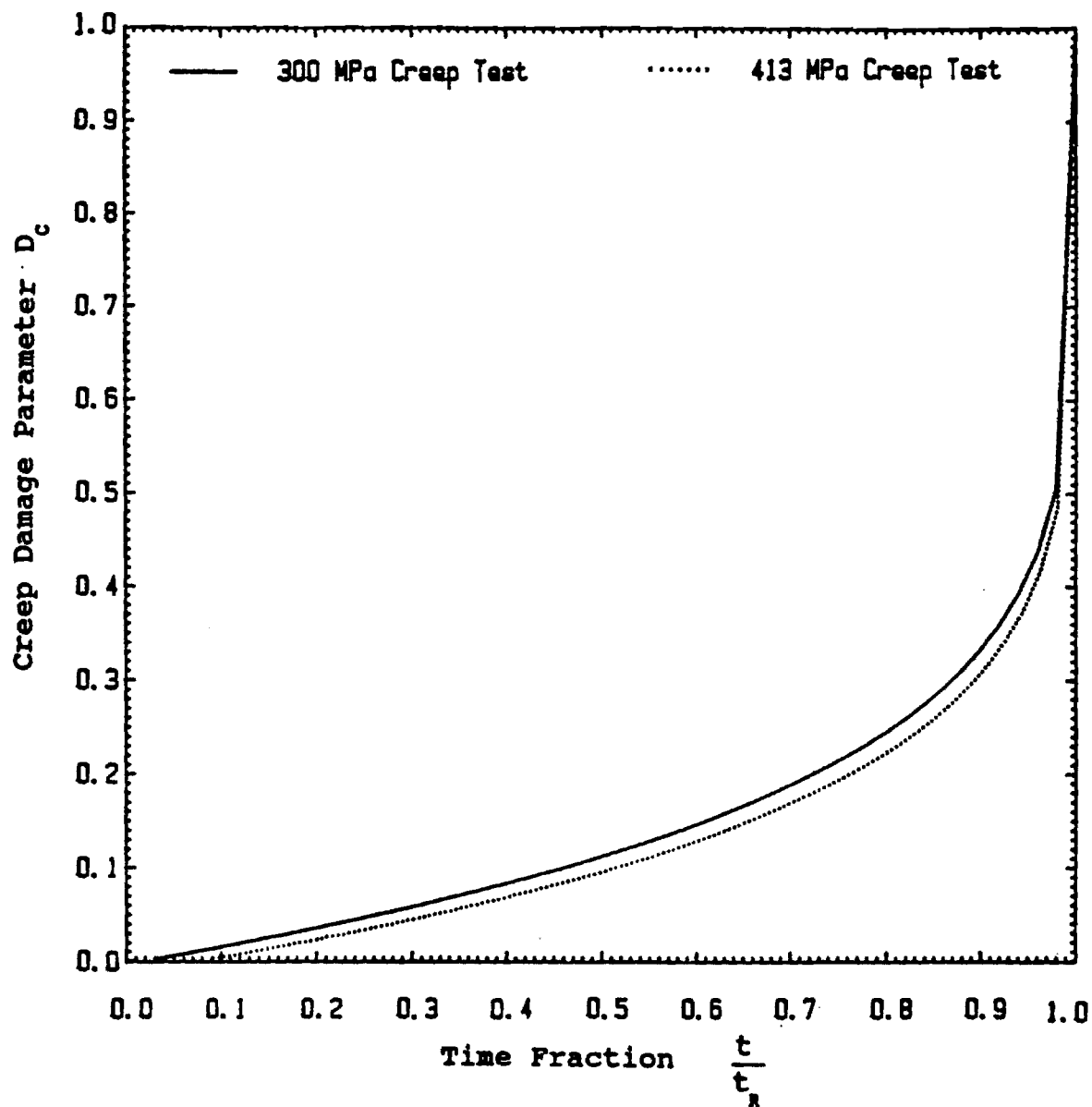
Figure 5. Creep damage parameter versus normalized time for
two constant-stress creep tests of MAR-M 246 in
air at 900°C.

LETTER REPORT

"DAMAGE RATE APPROACHES FOR THERMOMECHANICAL FATIGUE
OF SUPERALLOYS"

By David L. McDowell
Principal Investigator

R.L.T. Oehmke
Research Engineer

Gary Reynolds
Graduate Research Assistant

Project # E-25-M13
General Motors PO# H636356

March 1, 1988

Submitted to Allison Gas Turbine Operations, General Motors
Corporation

Sponsor Technical Contact:

Dr. W.E. Schneider/T-10
Allison Gas Turbine Operations
General Motors Corporation
2001 South Tibbs Ave.
Indianapolis, IN 46241
(317) 242-7703

Sponsor Administration and Contractual Matters:

Darrell L. Mackey/U02
Allison Gas Turbine Operations
General Motors Corporation
P.O. Box 420
Indianapolis, IN   46206-0420
(317) 242-6954

March 2, 1988

Dr. W.E. Schneider/T-10
Allison Gas Turbine Operations
General Motors Corp.
2001 South Tibbs Avenue
Indianapolis, IN 46241

Dear Dr. Schneider:

This report summarizes the activities of our effort on GM
PO#H636356, "Damage Rate Approaches for Thermomechanical Fatigue
of Superalloys" for the period February 1, 1988 to February 29,
1988.

Enclosed please find a brief report which describes several
repeated creep tests on MAR-M 246 at 900°C. These data give some
indication of scatter; differences in steady state creep rate are
maximally 25%, while variation of rupture time is within a usual
scatter of a factor of two.   Note that the Monkman-Grant strain,
the product of the secondary creep rate and rupture time, is very
nearly constant as is commonly observed for much more ductile
materials. In short, the creep behavior at 900°C is very similar
to that of wrought, ductile materials apart from lower secondary
creep rates.

As mentioned previously, we have sectioned some of the 900°C
fatigue specimens and examined the fracture surfaces and specimen
surfaces at the outside diameters to determine (a) the extent of
intergranular fracture and (b) the distribution of microcracks as
a function of strain range and total environmental exposure time.
The results are very interesting in that crack initiation appears
to predominate at slip band intersections with the free surface
at high $\Delta\epsilon^p$ and short test times, while grain boundary cracking
predominates at longer test durations and small $\Delta\epsilon^p$. We are in
the process of sorting out the implications of the secondary
crack distributions and sizes and environmental influence. The
vacuum tests will provide much information related to how
environmental effects should be treated in the damage rate
equation.

Sincerely,

David L. McDowell
Principal Investigator

DLM

Table 3 : Creep Test Data for MAR-M 246 in Air at 900°C

Specimen I.D.	Nominal Stress (MPa)	Nominal Strain to Failure (in/in)	Time to Failure (hours)	Steady-state Nominal Creep Strain Rate ($\dot{e}_{ss}^c$)	Monkmann-Grant Strain ($\dot{e}_{ss}^c \cdot t_R$)
G23	413	0.0635	27.35	81.1×10^{-5} hr^{-1}	0.0222
S999-5 c.	413	0.0416	31.80	61.4×10^{-5}	0.0195
G21	300	0.0446	174.70	9.53×10^{-5}	0.0166
S999-4 c.	299	0.0492	300.30	7.25×10^{-5}	0.0218
G19 a.	415		13.80	54.6×10^{-5}	
G19 b.	299	0.0420	140.00	6.97×10^{-5}	

Notes : a. Test G19 was a step-stress sequence test; loaded to 415 MPa for one half of the time to rupture of test G23 and then,
   b. loaded until failure at the stress level of test G21
   c. After the initial creep analysis was completed, tests were performed to aquire an indication of the scatter in the constant stress creep test data.

Mar M 246 at 900 deg C   Stress = 413 MPa

Nominal Creep Strain (in/in)

Time (hours)
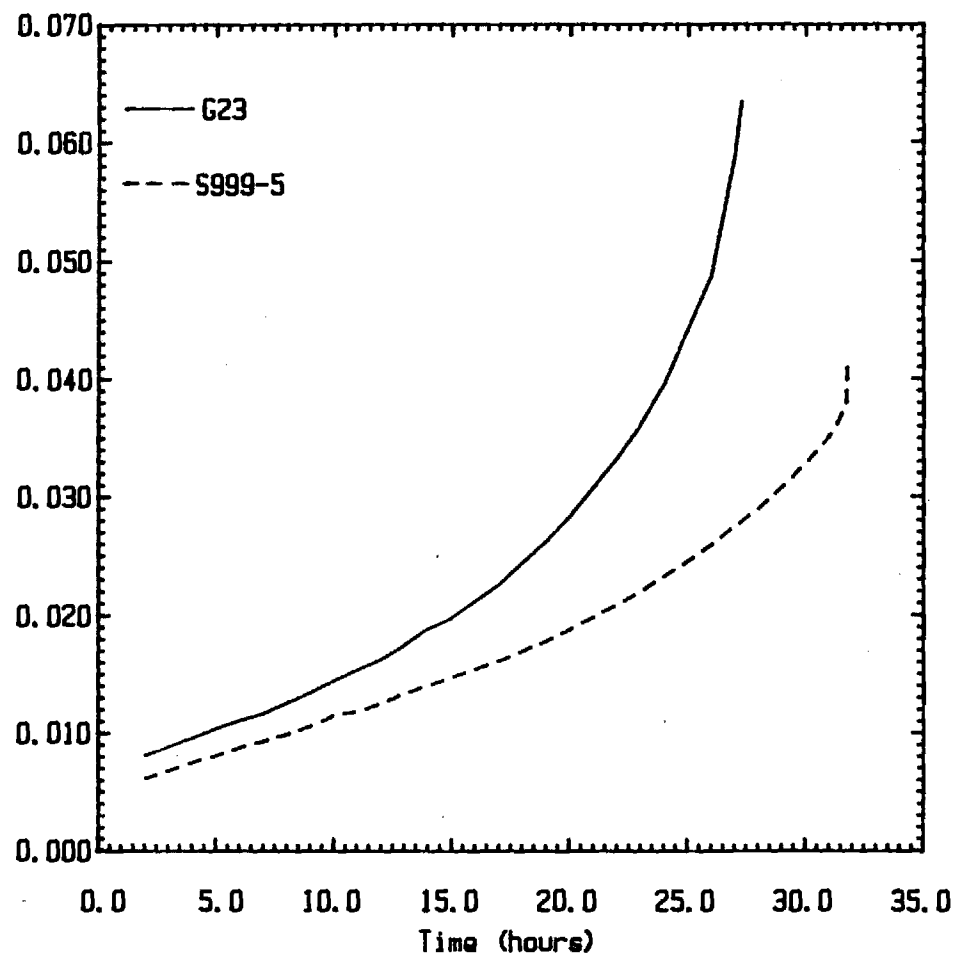
Mar M 246 at 900 deg C   Stress = 300 MPa

Nomial Creep Strain (in/in)
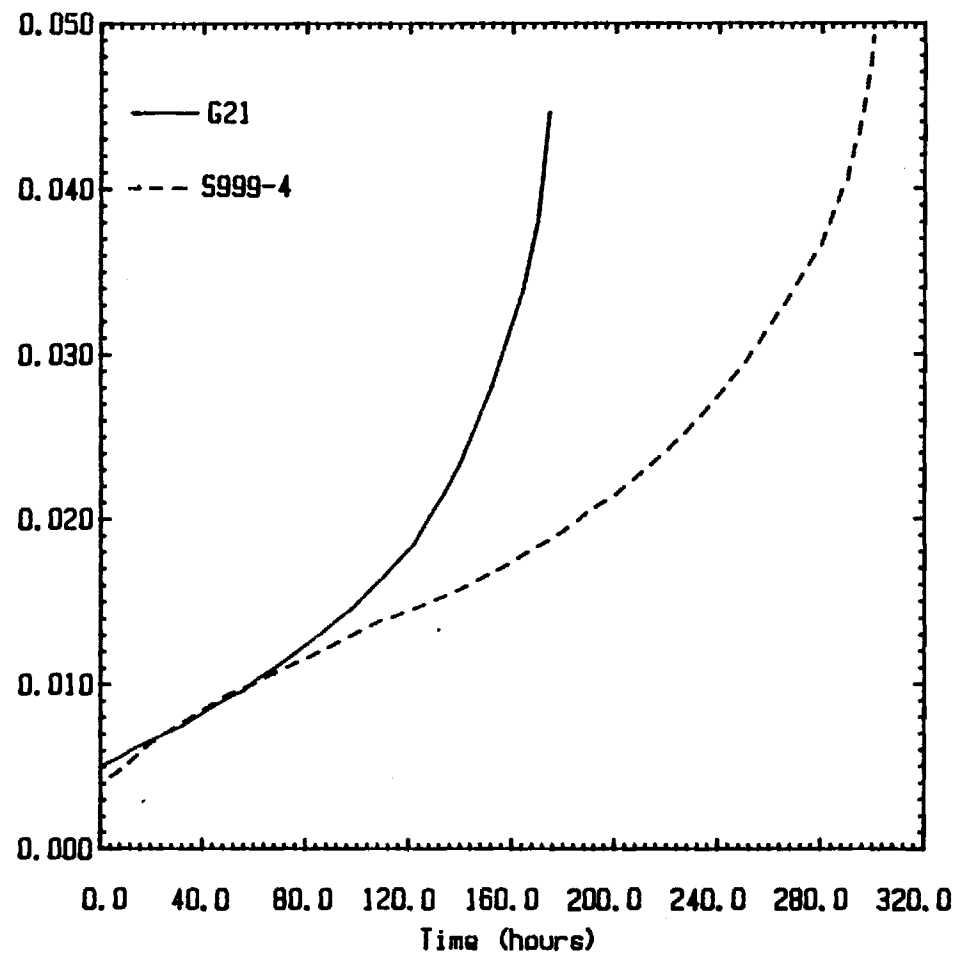
LETTER REPORT

"DAMAGE RATE APPROACHES FOR THERMOMECHANICAL FATIGUE
OF SUPERALLOYS"

By David L. McDowell
Principal Investigator

R.L.T. Oehmke
Research Engineer

Project # E-25-M13
General Motors PO# H636356

June 1, 1988

Submitted to Allison Gas Turbine Operations, General Motors
Corporation

Sponsor Technical Contact:

Dr. W.E. Schneider/T-10
Allison Gas Turbine Operations
General Motors Corporation
2001 South Tibbs Ave.
Indianapolis, IN 46241
(317) 242-7703

Sponsor Administration and Contractual Matters:

Darrell L. Mackey/U02
Allison Gas Turbine Operations
General Motors Corporation
P.O. Box 420
Indianapolis, IN 46206-0420
(317) 242-6954

June 6, 1988

Dr. W.E. Schneider/T-10
Allison Gas Turbine Operations
General Motors Corp.
2001 South Tibbs Avenue
Indianapolis, IN 46241

Dear Dr. Schneider:

This report summarizes the activities of our effort on GM PO#H636356, "Damage Rate Approaches for Thermomechanical Fatigue of Superalloys" for the period March 1, 1988 to May 31, 1988.

As we discussed during my recent visit to Indianapolis, we are proceeding to essentially replicate the matrix of fatigue tests at 900°C. We are doing so by "filling in" the original matrix, testing at strain amplitudes in-between those originally conducted. We expect that this more complete test matrix, while somewhat time-consuming, will give us a much more accurate idea of material scatter and behavior in the slightly longer life regime in several cases. Upon completion of this replicate set this summer, we intend to continue with vacuum tests at 900°C.
We will send you a complete set of fatigue test results when we have finished and compiled them.

Sincerely,

David L. McDowell
Principal Investigator

DLM

LETTER REPORT

"DAMAGE RATE APPROACHES FOR THERMOMECHANICAL FATIGUE
OF SUPERALLOYS"

By David L. McDowell
Principal Investigator

R.L.T. Oehmke
Research Engineer

Project # E-25-M13
General Motors PO# H636356

July 1, 1988

Submitted to Allison Gas Turbine Operations, General Motors
Corporation

Sponsor Technical Contact:

Dr. W.E. Schneider/T-10
Allison Gas Turbine Operations
General Motors Corporation
2001 South Tibbs Ave.
Indianapolis, IN 46241
(317) 242-7703

Sponsor Administration and Contractual Matters:

Darrell L. Mackey/U02
Allison Gas Turbine Operations
General Motors Corporation
P.O. Box 420
Indianapolis, IN 46206-0420
(317) 242-6954

July 1, 1988

Dr. W.E. Schneider/T-10
Allison Gas Turbine Operations
General Motors Corp.
2001 South Tibbs Avenue
Indianapolis, IN 46241

Dear Dr. Schneider:

This report summarizes the activities of our effort on GM PO#H636356, "Damage Rate Approaches for Thermomechanical Fatigue of Superalloys" for the period May 1, 1988 to June 31, 1988.

We are in the process of filling in the matrix of fatigue tests at 900°C and are progressing nicely in this endeavor. We will be able to estimate the degree of scatter more precisely with these additional tests.

We received your latest shipment of specimens last month and, in preliminary dimensional checks, found that a key shoulder dimension is consistently undersize by 40 mils. This dimension is denoted in the working drawing as .499"/.500"; the tolerance is tight because it is this part of the specimen that serves to align the specimen within the grips. Please find enclosed the memorandum from Roger Oehmke which details the inaccuracies. We will proceed with testing this set of specimens after sending them out for corrective work to ensure uniformity of the critical dimension and machining a set of associated grip adaptors. The money in the supplies budget should be adequate for these purposes.

I suggest that to obviate these specimen fabrication problems, which also occurred last year, GM ship us bar stock material in the future and permit us to contract with a machinist experienced in maintaining test specimen tolerances. I suggest that we include these costs in the supplies category in the next fiscal year contract period. Please let me know what you think since this will affect my cost estimate for next year's program.

Sincerely,

David L. McDowell
Principal Investigator

DLM

Georgia Tech

THE GEORGE W. WOODRUFF SCHOOL OF
MECHANICAL ENGINEERING

Georgia Institute of Technology
Atlanta, Georgia 30332-0405

June 17, 1988

MEMORANDUM

TO: Dave McDowell

FROM: Roger Oehmke

SUBJECT: GM Specimens, Series T132, T133, T138, T139

The specimens we recently received from GM are not properly machined and cannot
be used for testing. Specifically, the legs on all of the specimens are consistently .040"
undersize. The drawings for this specimen clearly show that the dimension should be
.499/.500". This tight spec is needed since the specimen is located laterally using the
leg surface. Any deviation from the specification prevents accurate alignment and
contributes to bending. In their present condition, none of the specimens can be
tested without significant bending errors.

RO:cc

MAR. M 246

Gongrnl Motors specimens

I.D.	① A	B	② A	B	③ A	B	④ (A+B)/2	
T132-1	.5055	.5067	.750	.7492	.461	.459	.2505	
T132-3	.500	.4995	.750	.7499	.4565	.4572	.2501	
T132-2	.491	.4881	.750	.7481	.4606	.4610	.2492	
T132-4	.5012	.4995	.7995	.7490	.4605	.4605	.2491	
T132-5	.4971	.5012	.748	.7485	.4601	.4599	.2501	
T133-1	.503	.4989	.7496	.7488	.4600	.4600	.2496	
T133-2	.4968	.5000	.7481	.7492	.4610	.4600	.2476	
T133-3	.4878	.5035	.7481	.7490	.4601	.4606	.2490	
T133-4	.5005	.5000	.7487	.7497	.4604	.4591	.2508	
T133-5	.5032	.4988	.7492	.7495	.4602	.4602	.2470	
T138-1	.502	.4821	.7492	.7498	.4603	.4604	~~.2486~~	.2490
T138-2	.4989	.502	.750	.750	.4591	.4595	.2506	
T138-3	.4912	.4993	.7502	.7497	.4611	.4596	.2500	
T138-4	.4990	.501	.7499	.7506	.4610	.4611	.2496	
T138-5	.5032	.5003	.7505	.7506	.4622	.4609	.2510	
T139-1	.5010	.5048	.7500	.7500	.4610	.4550	.250	
T139-2	.5000	.5011	.7500	.7500	.4600	.4595	.2511	
T139-3	.5021	.5018	.7511	.7489	.4620	.4611	.2495	
T139-4	.5000	.4998	.7497	.7498	.4610	.4632	.2482	
T139-5	.501	.509	.7493	.7360	.4615	.4613	.2496	

Surfaces A, B, C and D Must Be Parallel Within .001
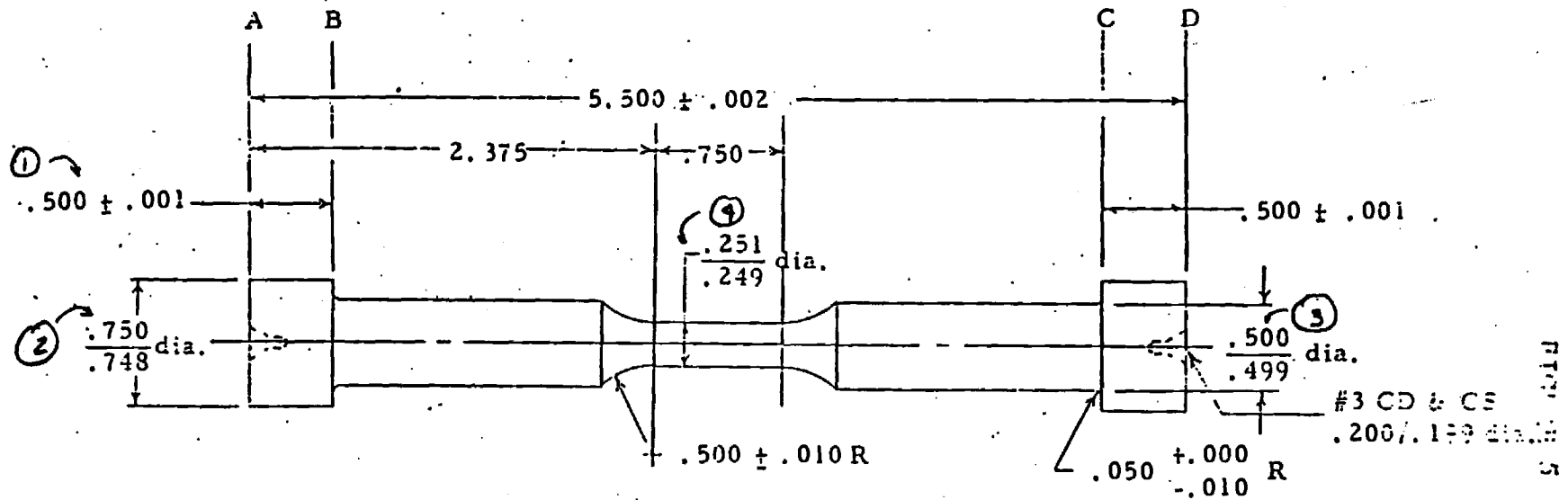
5.500 ± .002

2.375 .750

① .500 ± .001

④ .251/.249 dia.

② .750/.748 dia.

.500 ± .001

⑤ .500/.499 dia.

#3 CD & CS
.200/.199 dia.

.500 ± .010 R

.050 +.000 -.010 R

LOW CYCLE FATIGUE SPECIMEN	METCUT RESEARCH ASSOCIATES INC.
	CINCINNATI, OHIO 45209
	DWG. NO. 720303-1

MONTHLY LETTER REPORT
Project No. E-25-M13

"DAMAGE RATE APPROACHES FOR THERMOMECHANICAL
FATIGUE OF SUPERALLOYS"

Prepared by:
David L. McDowell, Principal Investigator
R.L.T. Oehmke, Research Engineer

Submitted to:
Allison Gas Turbine Operations
General Motors Corporation

Sponsor Technical Contact:
Dr. W.E. Schneider/T-10
Allison Gas Turbine Operations
General Motors Corporation
Indianapolis, IN   46241

Sponsor Administration and Contractual Matters:
Darrell L. Mackey/U02
Allison Gas Turbine Operations
General Motors Corporation
Indianapolis, IN   46206-0420

September 1988

GEORGIA INSTITUTE OF TECHNOLOGY
A UNIT OF THE UNIVERSITY SYSTEM OF GEORGIA
SCHOOL OF MECHANICAL ENGINEERING
ATLANTA, GEORGIA 30332

LETTER REPORT

"DAMAGE RATE APPROACHES FOR THERMOMECHANICAL FATIGUE
OF SUPERALLOYS"

By David L. McDowell
Principal Investigator

R.L.T. Oehmke
Research Engineer

Project # E-25-M13

September 1988

Submitted to Allison Gas Turbine Operations, General Motors
Corporation

Sponsor Technical Contact:

Dr. W.E. Schneider/T-10
Allison Gas Turbine Operations
General Motors Corporation
2001 South Tibbs Ave.
Indianapolis, IN 46241
(317) 242-7703

Sponsor Administration and Contractual Matters:

Darrell L. Mackey/U02
Allison Gas Turbine Operations
General Motors Corporation
P.O. Box 420
Indianapolis, IN 46206-0420
(317) 242-6954

September 10, 1988

Dr. W.E. Schneider/T-10
Allison Gas Turbine Operations
General Motors Corp.
2001 South Tibbs Avenue
Indianapolis, IN 46241

Dear Dr. Schneider:

This report summarizes the activities of our effort on GM PO#H723543, "Damage Rate Approaches for Thermomechanical Fatigue of Superalloys" for the period July 1, 1988 to September 30, 1988.

We have completed all baseline fatigue tests in laboratory air at 900°C and have not seen a significant increase in scatter. Please find a summary of tests completed and presentation of data in APPENDIX A. The M.S. Thesis of Gary J. Reynolds may be found in APPENDIX B. His thesis develops many of the key ideas behind the damage rate approach; vacuum tests will help clarify the role of environment.

As we discussed recently on the telephone, I have formally submitted a proposal to you for third year funding in the amount of $45,000.00. Although I have relayed the information you gave me regarding overdue payments to our office of contract administration, you may want to talk to them directly if problems continue with the billing or payments. Mr. Ron Bell (404-894-3870) of GTRC is a useful contact.

Sincerely,

David L. McDowell
Principal Investigator

DLM

APPENDIX A

Summary of Experiments Completed

Surfaces A,B,C, and D must be parallel within .001
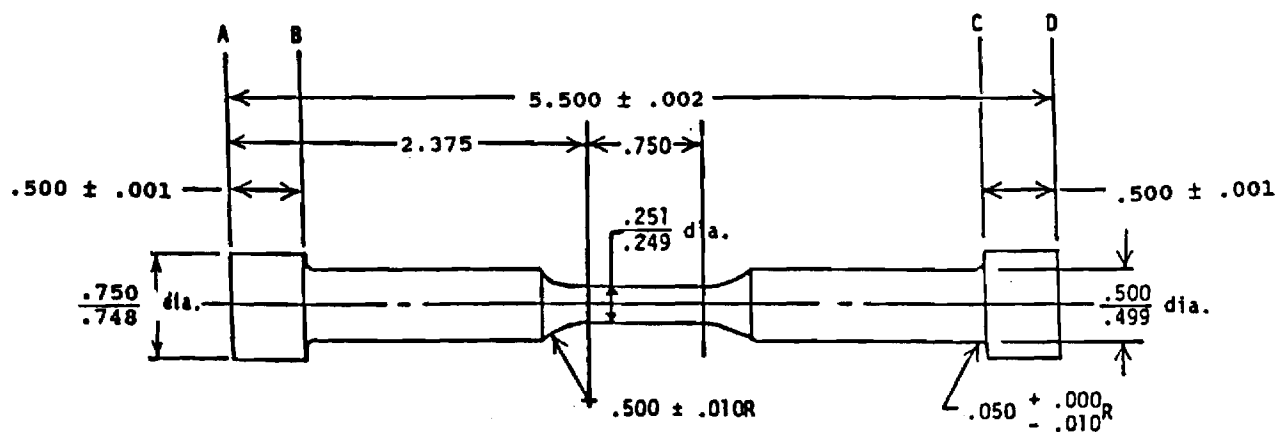
All dimensions are in inches.

Figure 1. Tensile and low cycle fatigue specimen dimensions.
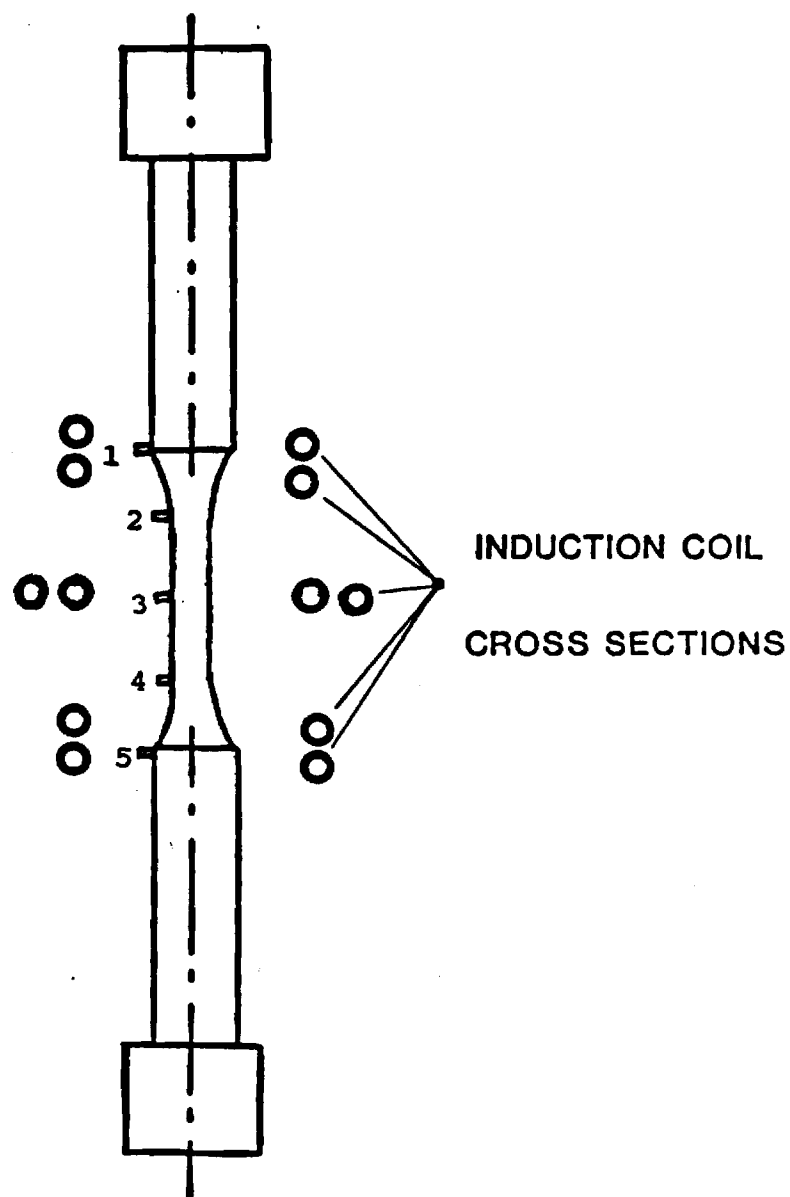
Figure 2. Schematic of the calibration specimen for tensile and LCF testing in air at 900°C. Thermocouple #1 was used for control.

APPENDIX

Table 1 : Strain-Controlled Fatigue Tests
Temperature: 900°C
Environment: Laboratory Air

ϵ rate (sec^{-1})	$\Delta\epsilon/2$	$\Delta\sigma/2$ (MPa)	$2N_f$
10^{-3}	.0098	872	36
	.009	797	60
	.008	737	76
	.0072	718	90
	.0061	723	192
	.005	649	504
	.004	557	1166
	.003	346	14842
	Sequence:0.002 for 284 143644 reversals followed by 0.004 to failure	144724	
10^{-2}	.01	1015	48
	.009	725	70
	.007	795	156
	.0064	776	236
	.005	642	748
	.0038	529	2576
	.003	424	8000
10^{-4}	.01	747	28
	.009	775	56
	.0081	764	50
	.007	679	64
	.005	594	550
	.004	511	748
	.003	423	3008

Table 2 : Creep Test Data for MAR-M 246
in Air at 900°C

Specimen I.D.	Nominal Stress (MPa)	Nominal Strain to Failure (in/in)	Time to Failure (hours)	Steady-state Nominal Creep Strain Rate ($\dot{e}_{ss}$)	Monkman-Grant Strain ($\dot{e}_{ss} \cdot t_R$)
G23	413	0.0635	27.35	81.1×10^{-5} hr^{-1}	0.0222
S999-5 c.	413	0.0416	31.80	61.4×10^{-5}	0.0195
G21	300	0.0446	174.70	9.53×10^{-5}	0.0166
S999-4 c.	299	0.0492	300.30	7.25×10^{-5}	0.0218
G19 a.	415		13.80	54.6×10^{-5}	
G19 b.	299	0.0420	140.00	6.97×10^{-5}	

Notes : a. Test G19 was a step-stress sequence test; loaded to 415 MPa for
one half of the time to rupture of test G23 and then,
b. loaded until failure at the stress level of test G21
c. After the initial creep analysis was completed, tests were performed
to aquire an indication of the scatter in the constant stress creep
test data.

Table 3 : Tensile Test Data for MAR-M 246 in Air at 900°C

Specimen I.D.	Strain Rate (sec^{-1})	Strain to Failure (%)	Young's Modulus (GPa) b.	0.2% Yield Strength (MPa)	U.T.S. (MPa) c.	K (MPa) d.	n e.
G13	10^{-1}	5.9	156.41	814	1051	1332.97	0.06991
G11	10^{-2}	7.2	161.00	851	950	1049.93	0.02666
G15	10^{-3}	a.	140.40	729	821	907.21	0.02589
G3	10^{-4}	4.3	146.62	611	706	885.83	0.05446
G1	10^{-5}	3.2	123.14	570	695	899.72	0.06186

NOTES : a. Specimen strained to 5% strain and then unloaded.
b. Average Young's modulus = 145.51 GPa.
c. Ultimate Tensile Strength
d. K = Strength coefficient
e. n = Strain hardening exponent

FIGURES: EXPERIMENTAL DATA

COFFIN-MANSON CONSTANTS
MAR-M-246, AIR, 900°C

$\dot{\epsilon}$	σ_f'	b	ϵ_f'	c
.01	1606.7	-.144	.074989	-.76
.001	1244.5	-.11	.085	-.81
.0001	1142.9	-.133	.036	-.615

Constants determined from regression analysis on experimentally determined data points. Points with mean stresses excluded from analysis.

FIGURE 1. Stress amplitude versus reversals to failure of MAR-M-246 at a strain rate of .01 sec^{-1} and at 900°C. Open circles are experimentally determined data points. All points are used in a linear regression routine to determine the characteristics of the dashed line through the data points.

FIGURE 2. Stress amplitude versus reversals to failure of MAR-M-246 at a strain rate of .001 sec⁻¹ and at 900°C. Open circles are experimentally determined data points. All points, except the $2N_f$ = 14,842 and $2N_f$ = 1166, are used in a regression routine to determine the

FIGURE 3. Stress amplitude versus reversals to failure of MAR-M-246 at a strain rate of .0001 sec⁻¹ and at 900°C. Open circles are experimentally determined data points. All points, except $2N_f = 3008$, are used in a regression routine to determine the characteristics of the dashed line.

FIGURE 4. Composite graph of stress amplitude versus reversals to failure of MAR-M-246
at all 3 strain rates, .01, .001, and .0001 sec^{-1}, at 900°C. Open symbols are
experimentally determined data points. Data points with mean stresses are not
included in regression.
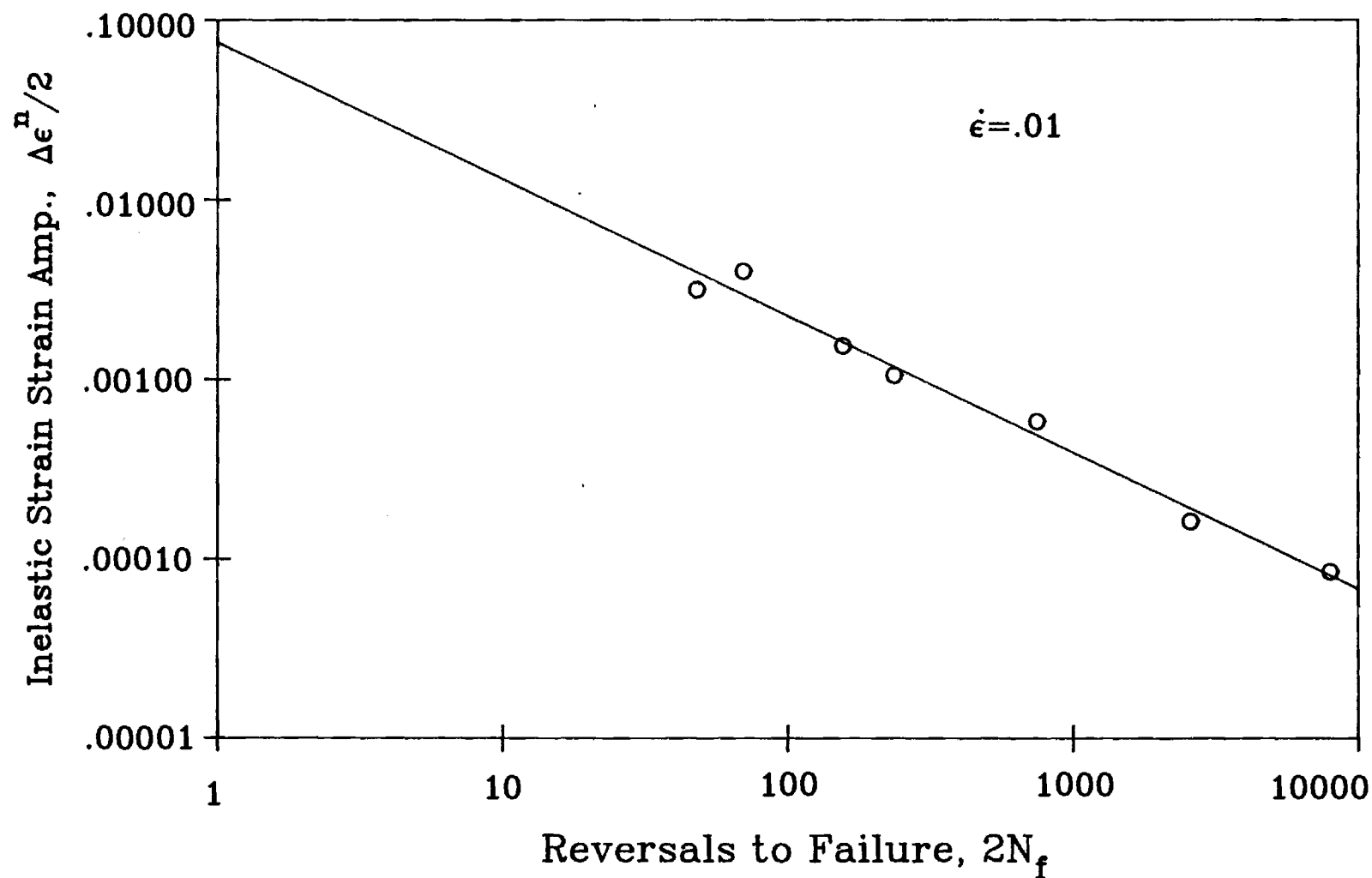
FIGURE 5. Inelastic Strain Amplitude versus Reversals to failure of MAR-M-246 at a strain rate of .01 sec⁻¹ and at 900°C. Open circles are experimentally determined points. All points included in regression analysis.
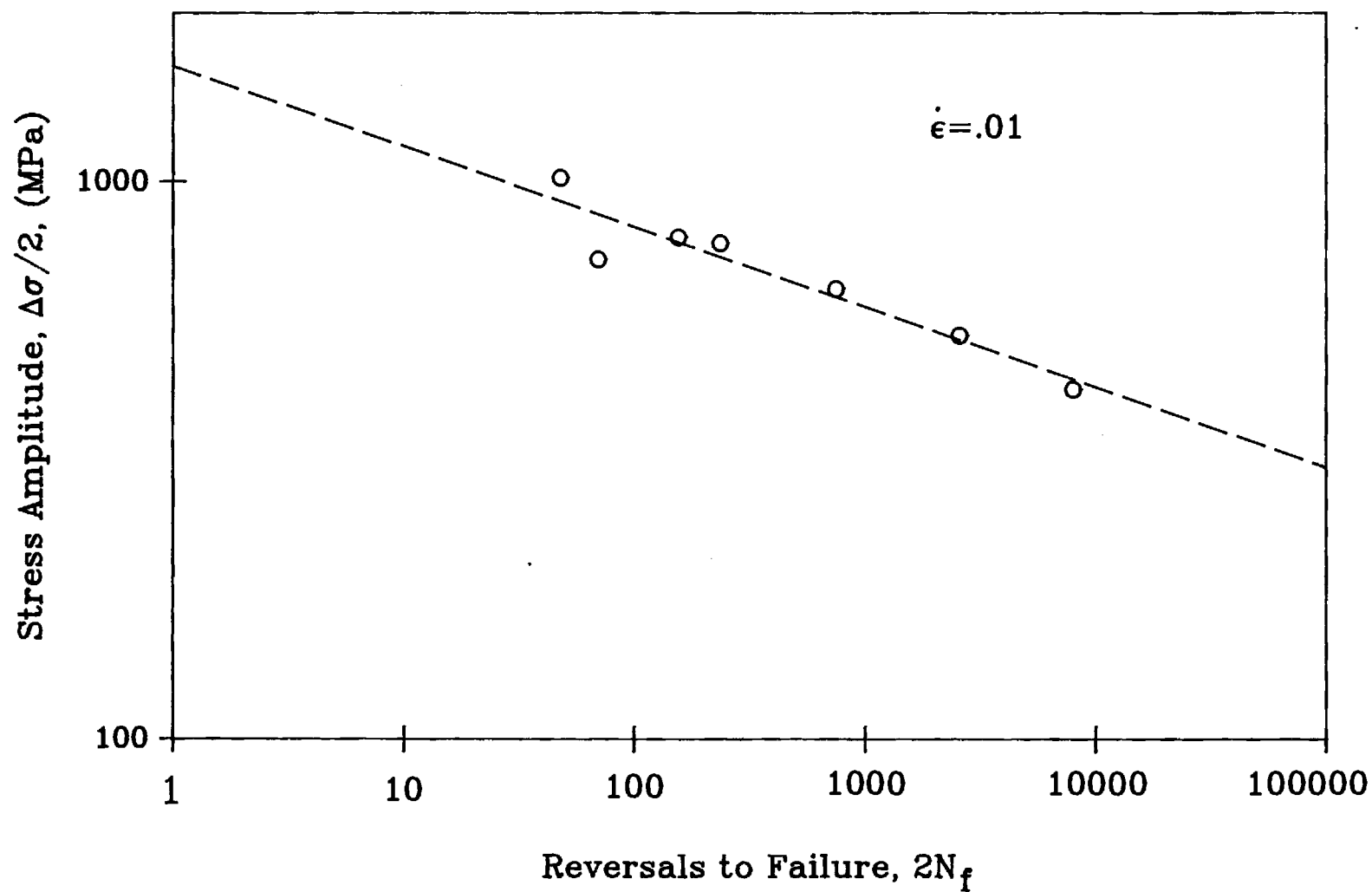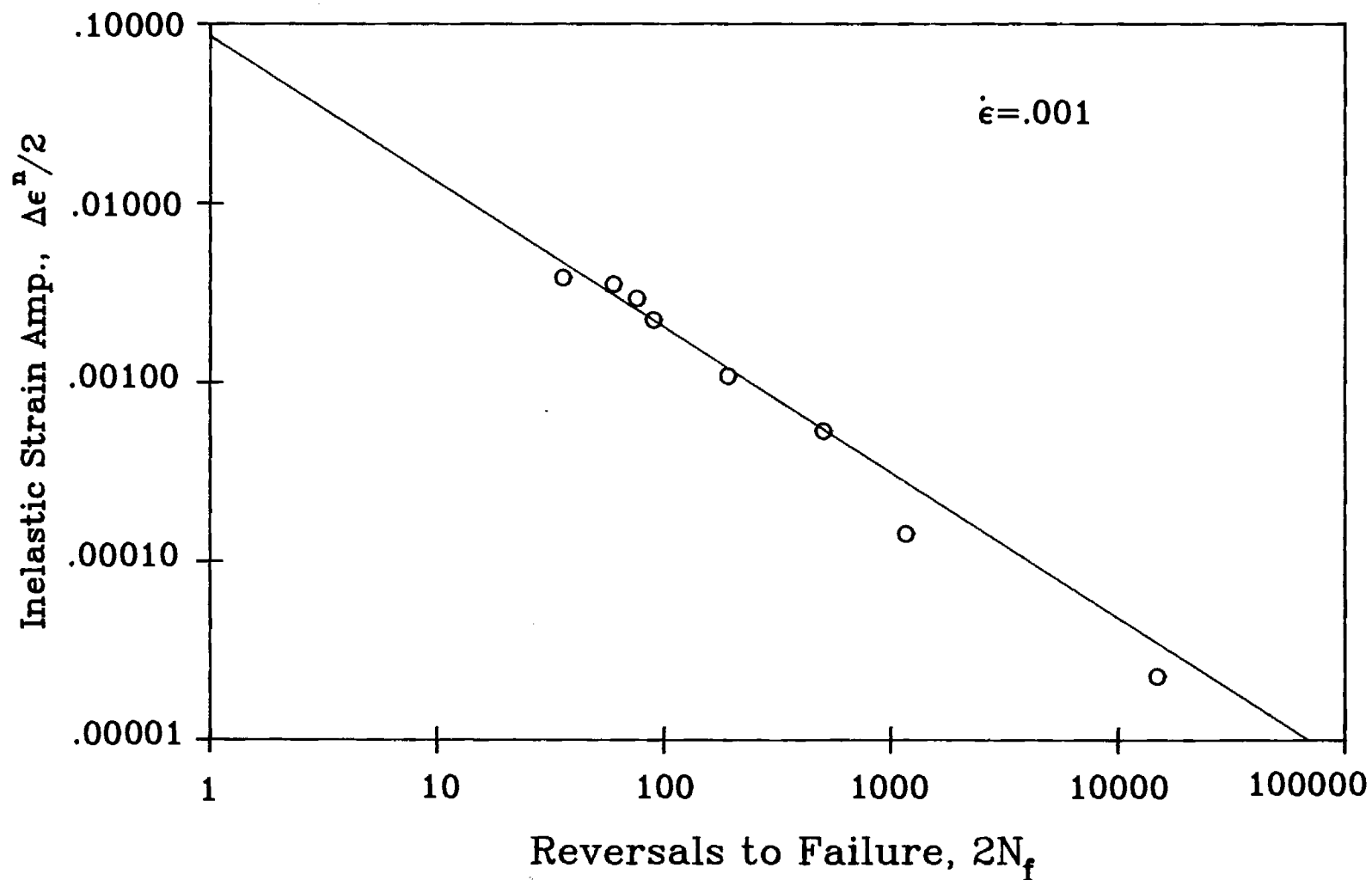
FIGURE 6. Inelastic Strain Amplitude versus Reversals to failure of MAR-M-246 at a strain rate of .001 sec^{-1} and at 900°C. Open circles are experimentally determined points. The data points at $2N_f$ = 14842 and $2N_f$ = 1166 contained mean stresses and are not included in the regression analysis.
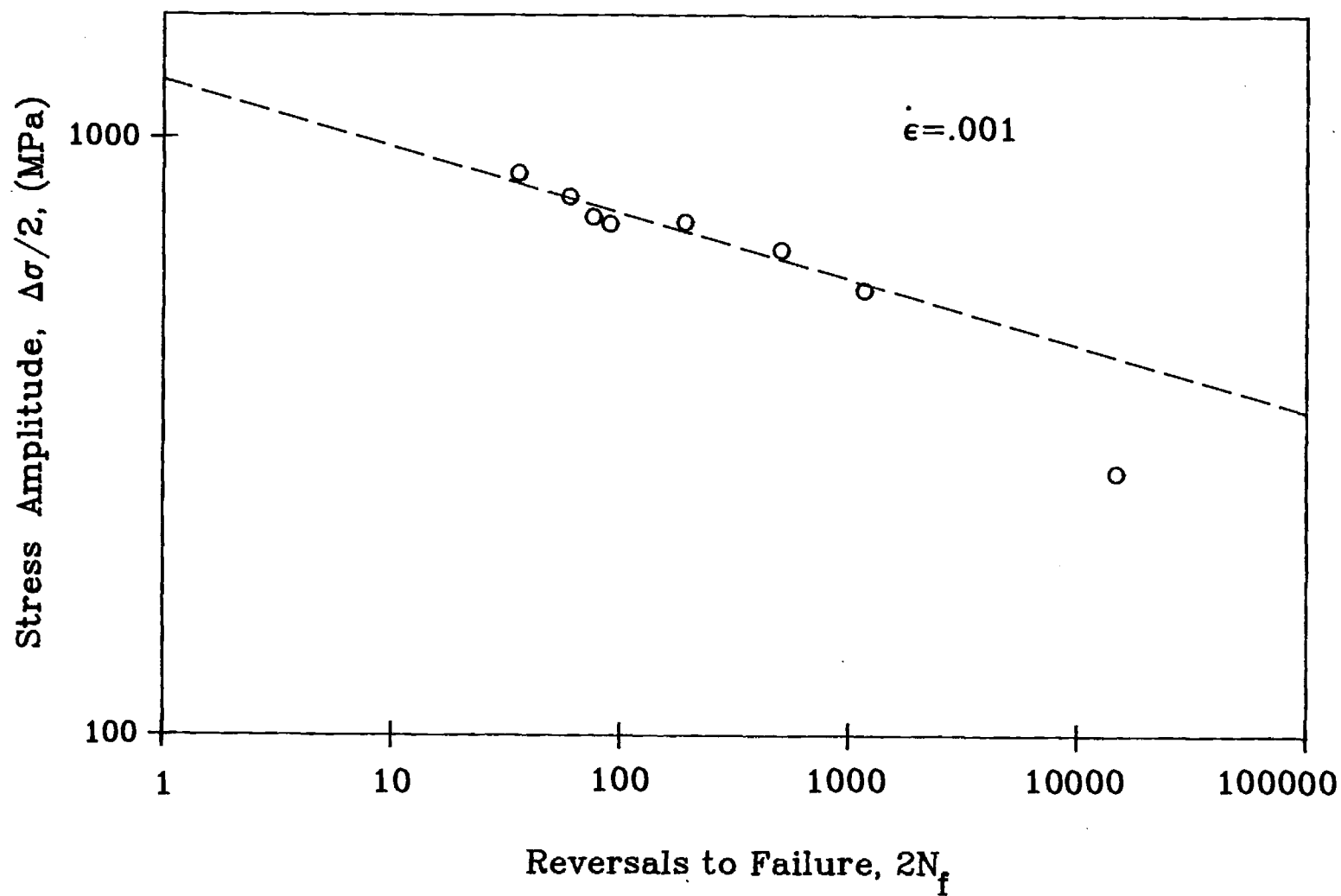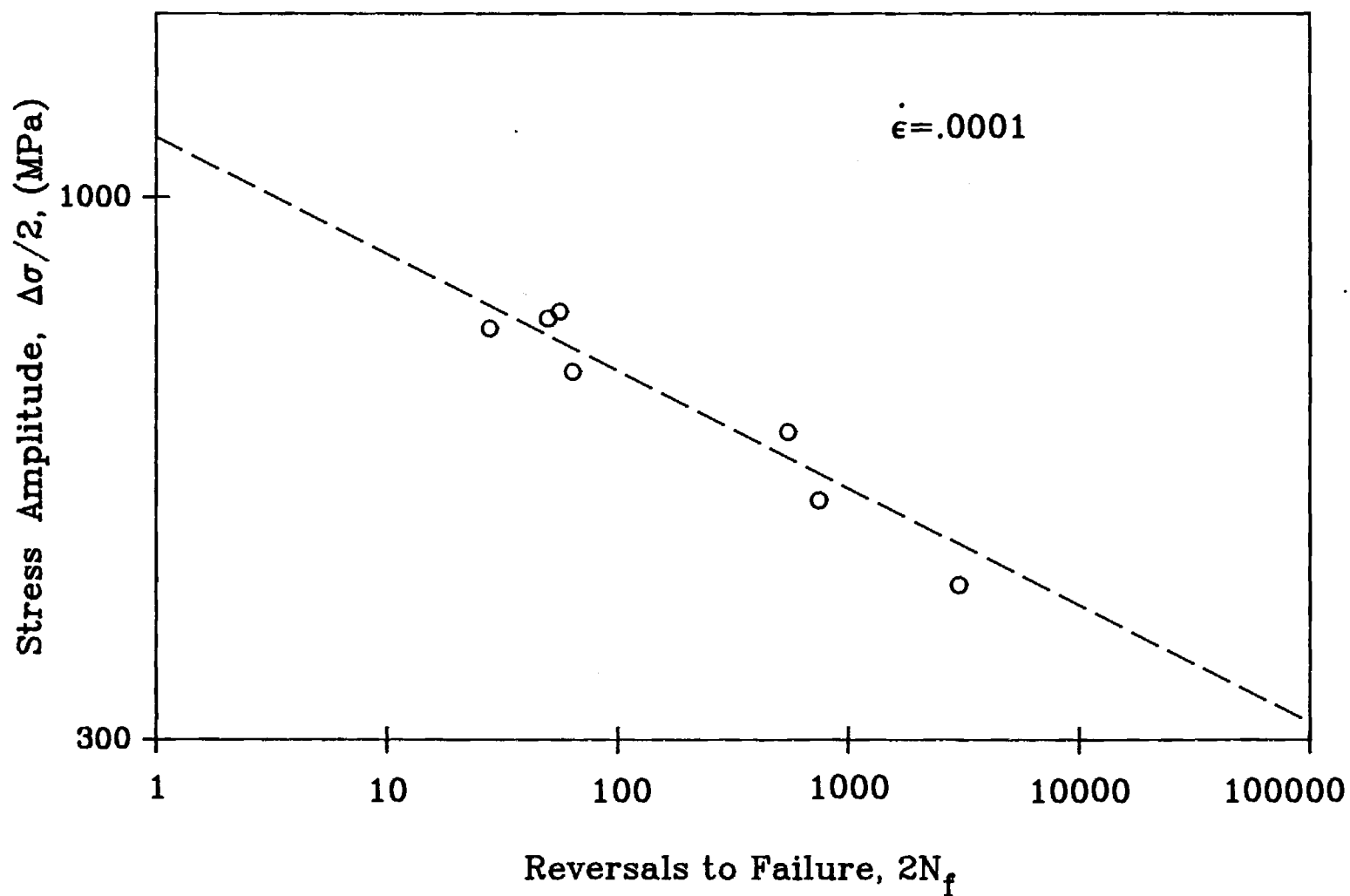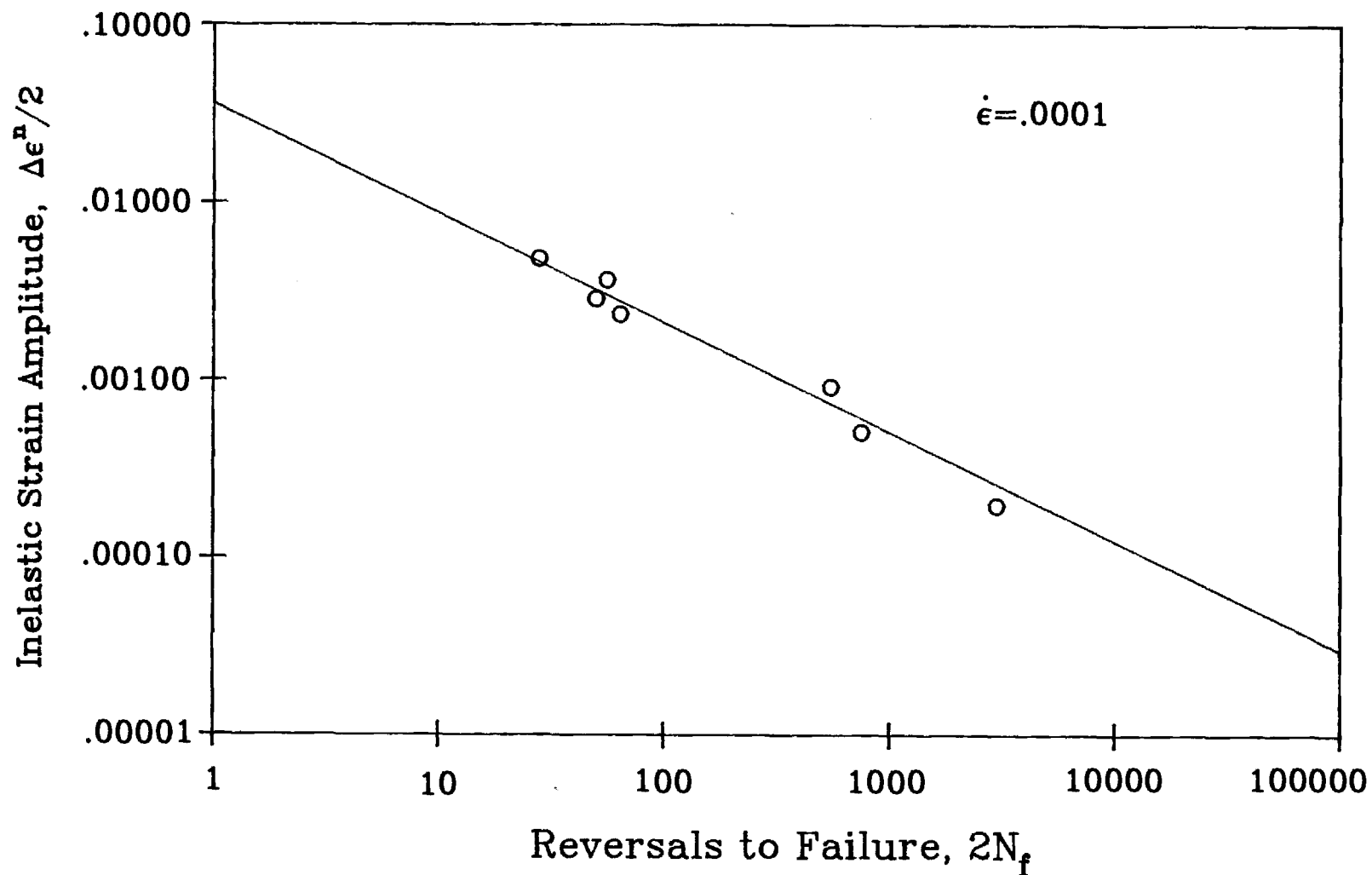
FIGURE 7. Inelastic Strain Amplitude versus Reversals to failure of MAR-M-246 at a strain rate of .0001 sec^{-1} and at 900°C. Open circles are experimentally determined points. The data point at $2N_f$ = 3008 contained a mean stress and is not included in the regression analysis.
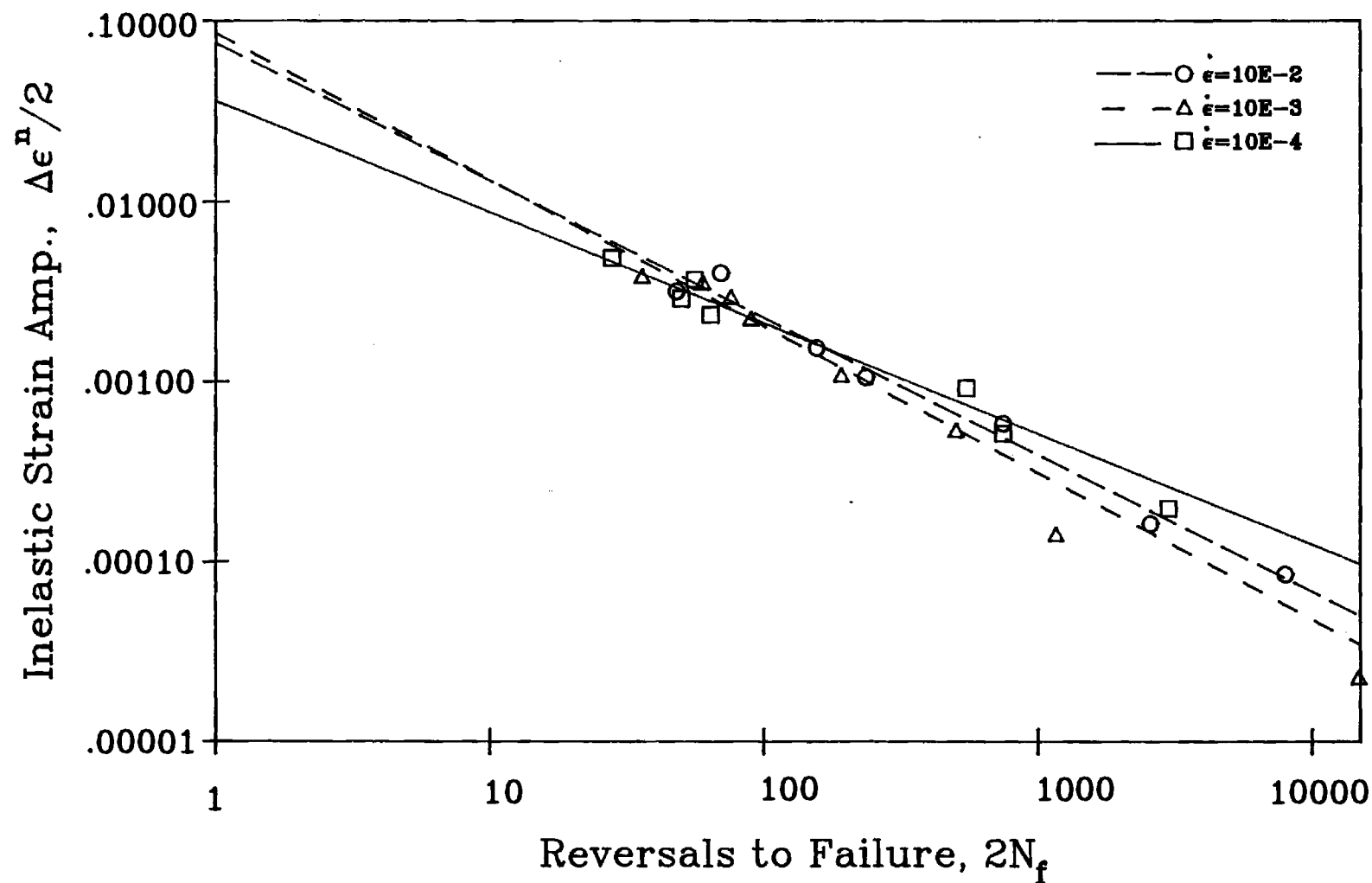
FIGURE 8. Composite graph of inelastic strain amplitude versus reversals to failure of MAR-M-246 at all 3 strain rates, .01, .001, and .0001 sec⁻¹, at 900°C. Open symbols are experimentally determined data points. Data points with mean stresses are not included in regression.
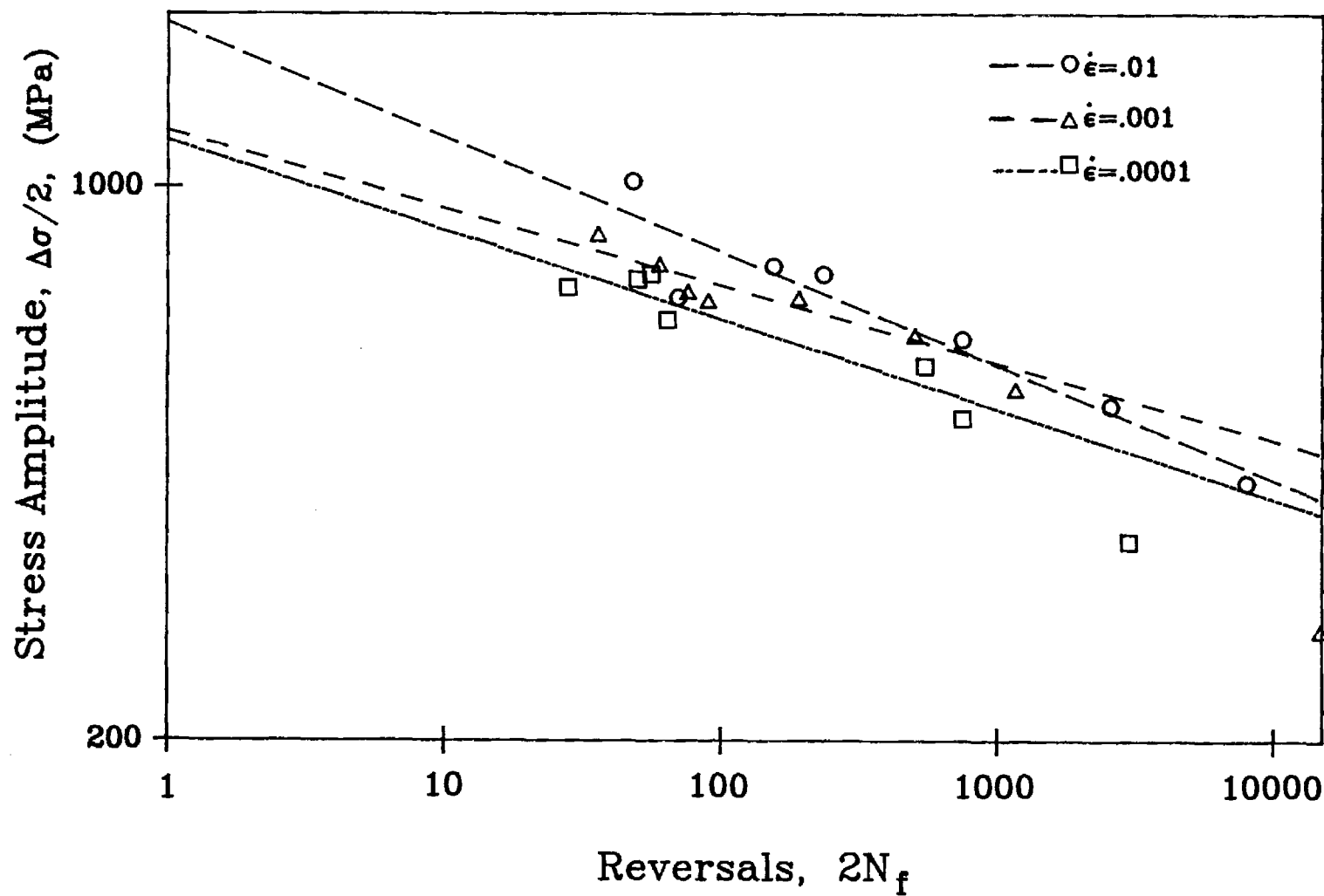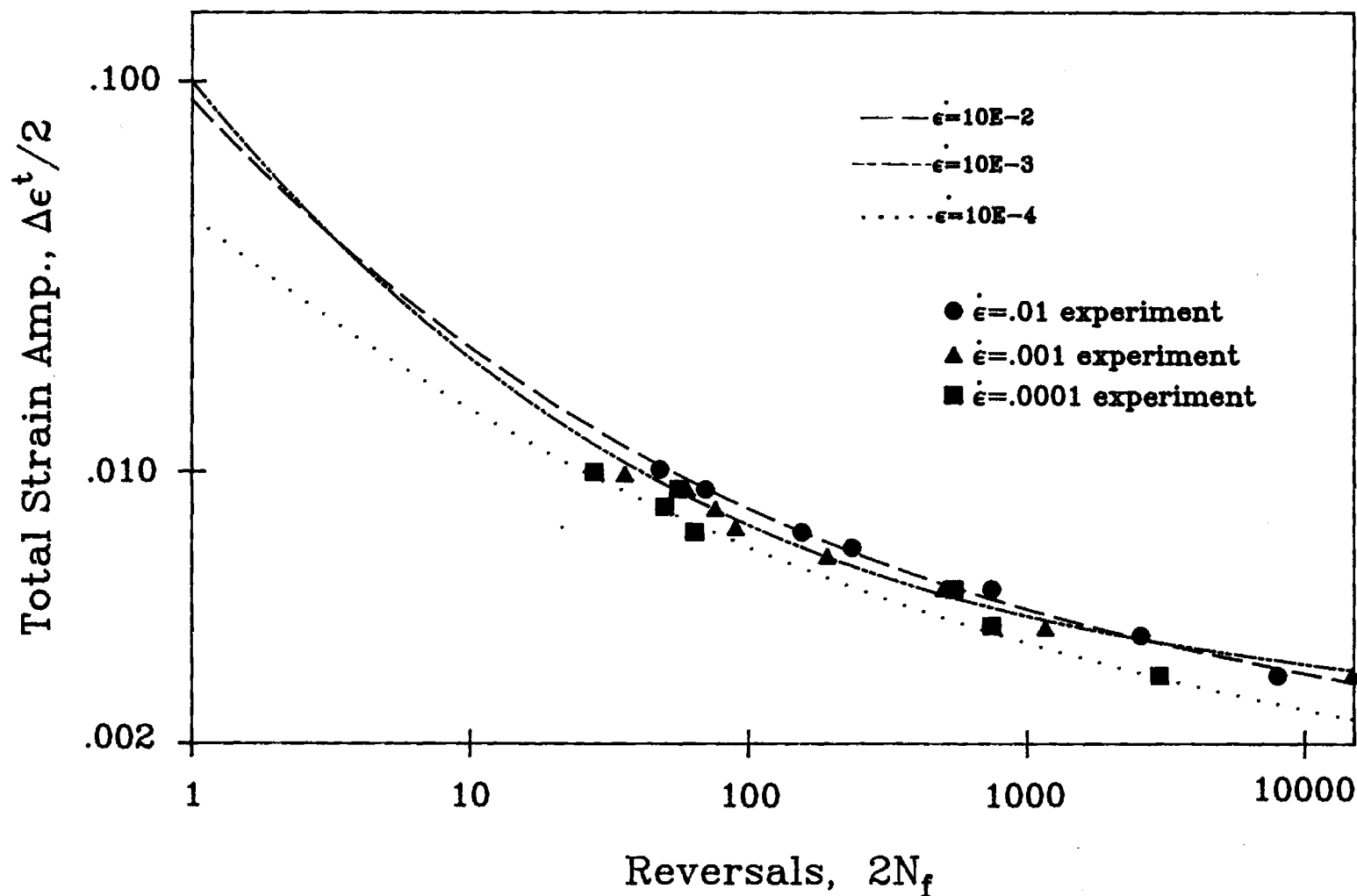
FIGURE 9. Graph of total strain amplitude versus reversals to failure of MAR-M-246 at all 3 strain rates, .01, .001, and .0001 sec⁻¹, at 900°C. Filled in symbols represent experimentally determined data points. The curves are calculated using Coffin-Manson constants determined from the experimental values.
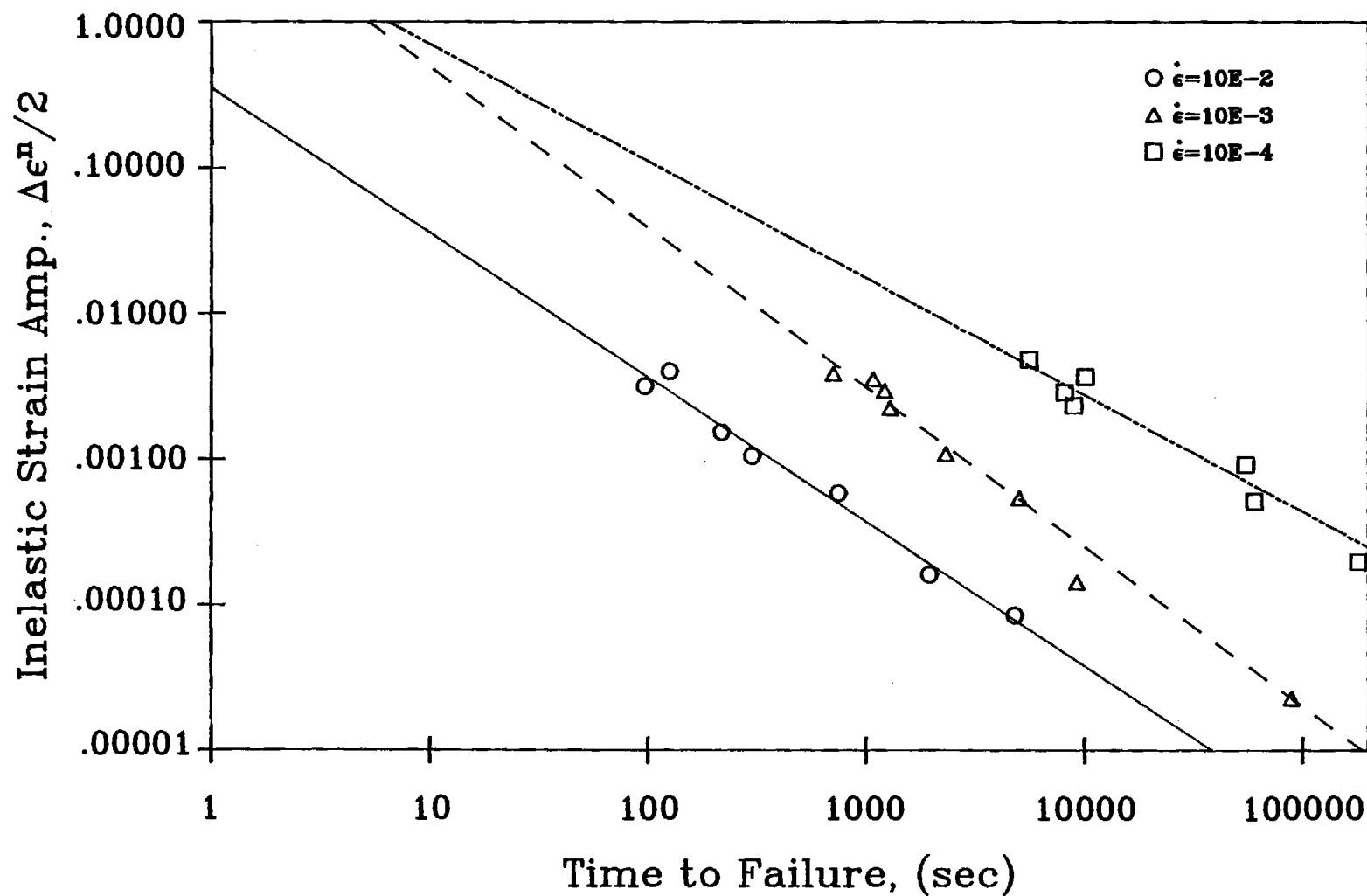
FIGURE 10. Inelastic strain amplitude versus time to failure of MAR-M-246 at 900°C for all three strain rates, .01, .001, and .0001 sec⁻¹.
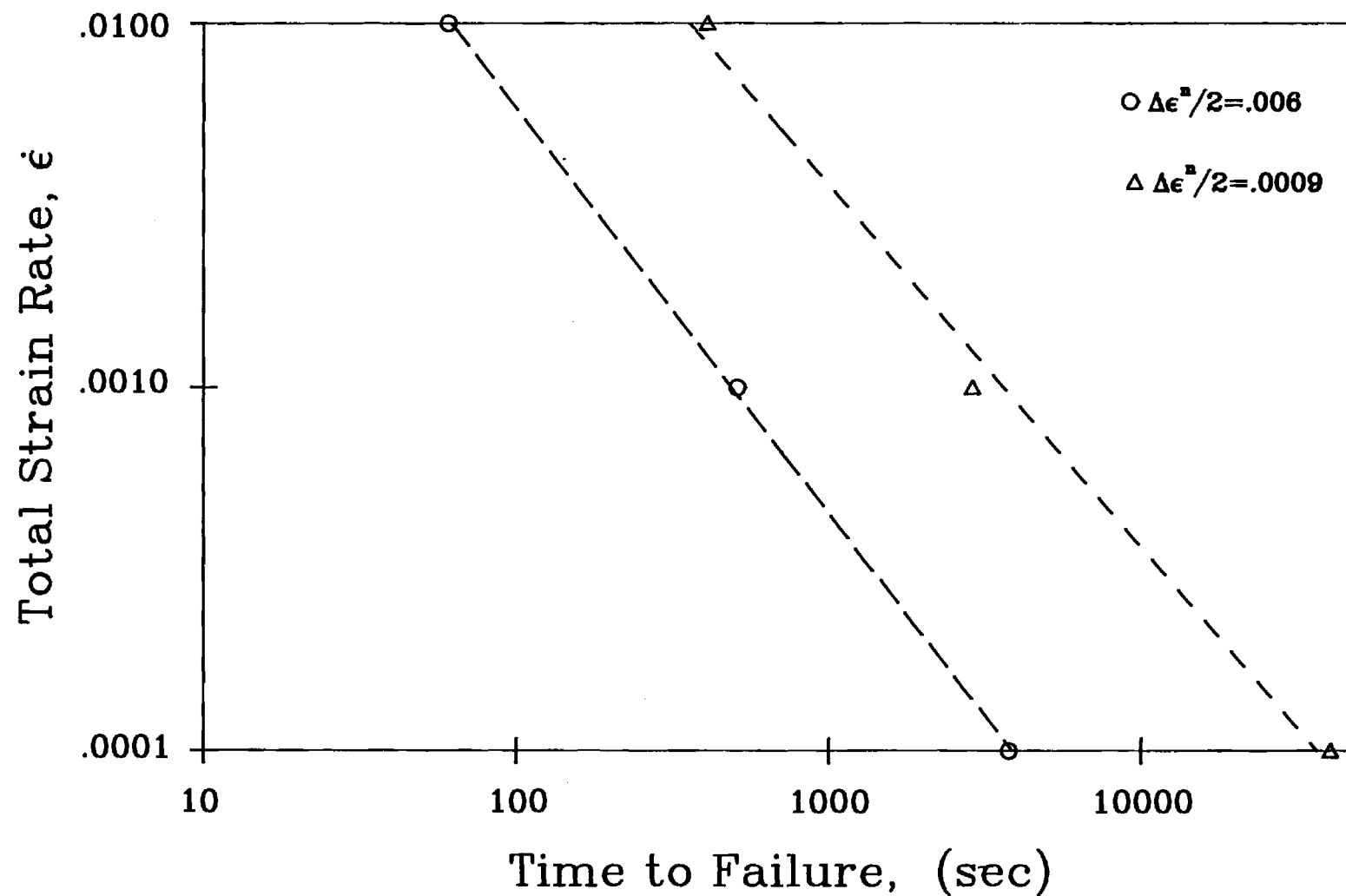
FIGURE 11. Total strain rate versus time to failure of MAR-M-246 at 900°C for the 2 inelastic strain amplitudes, .006 and .0009.

APPENDIX B

M.S. Thesis of Gary J. Reynolds

DAMAGE RATE APPROACHES FOR NICKEL-BASE SUPERALLOYS

A THESIS
Presented to
The Faculty of the Division of Graduate Studies

by

Gary James Reynolds

In Partial Fulfillment
of the Requirements for the Degree
Master of Science in Mechanical Engineering

Georgia Institute of Technology
September, 1988

ACKNOWLEDGEMENTS

TABLE OF CONTENTS

LIST OF TABLES

LIST OF ILLUSTRATIONS

SUMMARY

Attempts at experimentally approximating the thermo-
mechanical fatigue (TMF) of nickel-base superalloys (used in
turbine engine hot section components) have been extended,
for the most part, from earlier work with the more ductile
alloys. Aspects of two promising approaches for modeling TMF
of superalloys, the Damage Rate Method and the Continuum
Damage Approach, were combined to form a hybrid micro-crack
growth model which considers creep, fatigue, and
environmental damage as well as interactions. The overall
goal of the experimental program was aimed at predicting
crack initiation life; however, only the initial
investigation and development of the model for an isothermal
environment was undertaken in this study.

Parameters for the model were determined via tensile,
low cycle fatigue, and creep tests performed on MAR-M 246 (a
cast Ni-base superalloy) in air at 900°C. A form of the
Continuum Damage Approach was used to model the creep
behavior of the material. Methods for determining the creep
parameters were established although the statistical
significance of these quantities has not been fully
established may be suspect due to the limited amount of data
obtained. Fatigue-environment behavior was characterized
with a damage rate equation. Modifications were made to the

initally proposed model based on short crack considerations
and arguments for micro-crack/macro-crack continuity and
parabolic oxidation kinetics. The fatigue parameters were
estimated from the available data set and methods for
improving those calculations through future testing programs
were outlined. A brief study of specimen fracture surfaces,
concentrating on the influence of oxygen penetration, was
performed to confirm the above mentioned arguments.

Indications for future improvements of the micro-crack
growth model presented in this report stress the importance
of conducting tests in vacuum for the quantification of
environmental effects on damage. In addition, the
correlative capability of the damage equations must be
assessed via experiments which combine cycling with hold
times.

CHAPTER I

INTRODUCTION

Nickel-base alloys are amoung the most complex and the most widely used for elevated temperature applications of all the superalloys. For example, nickel-base superalloys make up for over 50% of the weight of today's advanced aircraft engines [1]. As the quest to maximize the overall service life and to increase the thrust-to-weight ratio of gas turbine engines progresses, the need to accurately predict the working life of engine components is becoming increasingly more important.

The science of experimentally approximating the thermo-mechanical fatigue (TMF) of turbine engine hot section components is relatively young; the attempts which have been made are, for the most part, extensions of earlier work with the more ductile alloys. Classical approaches were adopted, such as the frequency modified relationships [2] and Strain Range Partitioning [3], which use parametric expressions to relate the number of cycles to crack initiation to different parameters describing cyclic loading. More recently, continuous damage growth equations have been applied to predict crack initiation and creep-fatigue interaction in terms of physical measures of damage, e.g. crack length and

cavity growth. Examples of these methods, which are described in the next chapter of this thesis, are the Continuum Damage and Damage Rate approaches [4].

In an attempt to further understand and characterize the TMF behavior of Ni-base superalloys, a comprehensive program to study the fatigue, creep, and environmental properties, as well as interactions, of a representative nickel-base superalloy (cast MAR-M 246) was undertaken. The initial phase of this investigation is reported in this thesis. The overall program was aimed at developing a hybrid form of the Damage Rate Method and the Continuum Damage Approach with constants and parameters determined from isothermal, uniaxial low cycle fatigue and creep test data. The program concentrates on initiation rather than propagation due to the findings of numerous experimental studies which have shown that linear elastic fracture mechanics concepts can be successfully applied to the growth of dominant macro-cracks.

Although the overall goal of the project was to develop a TMF model for Ni-base superalloys, the present study is concerned with the isothermal characterization of MAR-M 246 tested in laboratory air at atmospheric pressure at a single temperature of 900°C. Through the analysis of creep, tensile, and low cycle fatigue (LCF) data, the groundwork for crack growth prediction on the substructural scale was

performed. The results of this study will only begin to formulate the background for the TMF model, indicating future directions.

This thesis is organized into four major divisions. First, a detailed yet brief description of presently used models for creep-fatigue damage prediction is presented for background purposes. The basis for the Ni-base TMF model is formed from this information. Secondly, a description of the types of tests performed and the procedures and equipment used in the acquisition of the physical data is outlined. Thirdly, the test results are used to formulate an initial creep-fatigue-environment model for the prediction of crack initiation life. The creep analysis is detailed first, followed by the fatigue-environment characterization. These analyses are separate from one another and may be studied exclusively. Lastly, indications for future testing and analysis are proposed.

CHAPTER II

BACKGROUND

Review of Applicable Approaches for Isothermal Loading

Although a general procedure for initiation life under thermomechanical loading conditions has not yet been established, several current isothermal approaches for combined creep-fatigue-environmental damage will be briefly reviewed. The applicability of these approaches to life prediction of Nickel-base superalloys will then be studied.

Linear Time and Cycle Fraction Summation

This simplistic approach, first proposed by Robinson [5] in 1938, assumes that the time and cycle fractions are summed to unity, i.e.

$$\sum_{K} \frac{N_K}{(N_I)_K} + \sum_{j} \frac{t_j}{(t_R)_j} = 1 \qquad (2.1)$$

where N_I = crack initiation life for pure cycling at the kth amplitude level

t_R = rupture time at the jth stress and temperature

Unfortunately, experiments have shown that life fractions at failure have been found to range from 0.36 to 2.08 for superalloys and steels [6]. This would tend to invalidate the linear summation rule. This is not only true for creep-

fatigue interaction, but for multi-step histories of creep or fatigue loading measured separately. It is, however, possible to obtain conservative results by limiting the damage to a specified level other than unity; D^* for example,

$$\sum_K \frac{N_K}{(N_I)_K} + \sum_J \frac{t_J}{(t_R)_J} \leq D^* \qquad (2.2)$$

as is done in the ASME Boiler and Pressure Vessel Code [7]. This modification does not greatly increase lifetime estimation accuracy. Furthermore, if D^* is chosen to be "small", it may occasionally be non-conservative, which in turn, introduces possible large over-conservatism for less damaging loading histories.

There is no good mechanistic interpretation of this damage summation technique – in fact it is in conflict with knowledge of physical damage accumulation processes. For example, it is well known that prior cycling affects subsequent creep rupture behavior of materials through cyclic hardening or softening mechanisms. Yet the rupture times used in the linear summation rule are based on monotonic creep rupture tests. Obviously the linear model is not valid in this circumstance.

Microcrack Propagation Models

Some workers [8-10] have devised microcrack propagation models for fatigue and fatigue dominated creep-fatigue interaction. Skelton [8] has proposed the plastic strain range-based growth law,

$$\frac{da}{dN} = d\left[\frac{\Delta\epsilon^{P}}{K}\left(\frac{4a^{1-n}}{G}\right)^{1/\gamma+\beta}\right]^{1/\alpha} \qquad (2.3)$$

where d = initiation depth of an engineering size crack

(on the order of 0.2 mm)

a = crack length

$\Delta\epsilon^{P}$ = plastic strain range

G,n = constants defining the crack tip radius

K,α = Coffin-Manson constants

β = cyclic strain hardening exponent

γ = plastic-to-total strain proportionality factor

This equation is valid for high plastic strain ranges and/or continuous cycling, i.e. conditions which promote fatigue dominated failure. It is essentially a modification of the Coffin-Manson Law which accounts for different definitions of initiation crack size based on the crack tip ductility.

Wareing [9] has proposed the following equation for fatigue crack growth through cavitated material:

$$\frac{da}{dN} = \Delta\epsilon^{P}W \qquad (2.4)$$

where W is the specimen width.

The creep damage rules depend on whether void growth occurs by constrained or unconstrained grain boundary diffusion. In the case of unconstrained grain boundary diffusion, the cavity growth rate per cycle is given by [10],

$$\frac{dr}{dN} = \frac{(t_h + t_c)\Lambda D_{gb}\delta(\sigma - 2\gamma/r)}{2kTr^2} \tag{2.5}$$

where   r = cavity radius

t_h, t_c = hold time and cycle time, respectively

Λ = atomic volume

D_{gb} = grain boudary diffusion coefficient

σ = relaxed stress at the end of a hold period

γ = grain boundary diameter

δ = grain boundary surface energy

k = Boltzmann's constant

T = absolute temperature

For a constrained condition (uneven cavity distribution or the presence of grain boundary precipitates) the cavity growth rate is simplified as,

$$\frac{dr}{dN} = \frac{\lambda^2 s \dot{\epsilon}}{4\pi r^2}(t_h + t_c) \tag{2.6}$$

where λ = cavity spacing

s = grain size

$\dot{\epsilon}$ = strain rate

Assuming failure to be defined as the impingment of adjacent cavities, the solution to (2.5) may be written as,

$$N_f = \frac{2kT}{\delta\Lambda\sigma D_{gb}} \frac{1}{(t_h + t_c)} \frac{r^3}{3} \qquad (2.7)$$

and the solution for constrained grain boundary diffusion void growth, equation (2.6), may be written as,

$$N_f = \frac{4\pi r^3}{3} \frac{1}{\lambda^2 s\epsilon (t_h + t_c)} \qquad (2.8)$$

As pointed out by Miller, Hamm, and Phillips [11], unconstrained and constrained diffusive cavity growth occurs at low stresses. At higher stresses, the deformation of the matrix governs cavity growth and the growth rate is again proportional to the strain rate, i.e.

$$\frac{dr}{dt} = C\dot{\epsilon} \qquad (2.9)$$

Miller et al. [10] have also carried out the numerical integration for N_f including stress relaxation,

$$N_f = \frac{r^3}{3D_{gb}} 2kT \left[\int_{t_1}^{t_h} \sigma dt \right]^{-1} \qquad (2.10)$$

for the case of unconstrained growth; and

$$N_f = \frac{4\pi r^3}{3\mu^2 s} \cdot \frac{E}{(\sigma_1 - \sigma_h)} \qquad (2.11)$$

for constrained grain boundary diffusion. Note that t_1 and σ_1 are the time and stress, respectively, at one minute into the hold period, and t_h and σ_h are the hold time and stress, respectively, at the end of the hold period. It should be noted that the operative mechanism for cavity growth during the hold time is primarily unconstrained or constrained cavity growth for stainless steels and Cr-Mo-V steels reported by Ellison, Hamm, etc.

The usual approach taken by those who utilize these microcrack growth models is to distinguish creep dominated situations from fatigue dominated ones and to apply the proper damage growth law. The interaction between creep and fatigue damage is not explicitly taken into account. The values of the Coffin-Manson constants in equation (2.3), K and α, are chosen to reflect the detrimental effect of hold times under tensile stress.

Strain Range Partitioning

The Strain Range Partioning (SRP) method relates cyclic inelastic strain to fatigue life without explicit consideration of environmental contributions.

According to Manson et al. [12-14], time-dependent hysteresis loops can be identified as having four distinct components of inelastic strain. It is argued that these four components of the overall cyclic inelastic strain range have different mechanistic bases for creep-fatigue interaction and damage accumulation.

Compressive-going inelastic strains are differentiated from tensile-going inelastic strains. Furthermore, "time-dependent" plastic strains are differentiated from creep strains. Hence, loops are composed of the following four types of inelastic strain ranges:

$\Delta\epsilon^{cp}$ = creep reversed by compressive plasticity

$\Delta\epsilon^{pc}$ = tensile plasticity reversed by compressive creep

$\Delta\epsilon^{pp}$ = completely reversed plasticity

$\Delta\epsilon^{cc}$ = completely reversed creep

Then, finding the relationships,

$$\Delta\epsilon^{pp} = A_1 N_{pp}^{B_1} \qquad (2.11)$$

$$\Delta\epsilon^{pc} = A_2 N_{pc}^{B_2} \qquad (2.12)$$

$$\Delta\epsilon^{cp} = A_3 N_{cp}^{B_3} \qquad (2.13)$$

$$\Delta\epsilon^{cc} = A_4 N_{cc}^{B_4} \qquad (2.14)$$

from experimental data, the damage summation is performed according to

$$\frac{1}{N_I} = \frac{F_{pp}}{N_{pp}} + \left(\frac{F_{cp}}{N_{cp}} \text{ or } \frac{F_{pc}}{N_{pc}}\right) + \frac{F_{cc}}{N_{cc}} \qquad (2.15)$$

where the inelastic strain fractions are given by

$$F_{pp} = \Delta\epsilon^{pp}/\Delta\epsilon^N \qquad (2.16)$$

$$F_{cp} = \Delta\epsilon^{cp}/\Delta\epsilon^N \qquad (2.17)$$

$$F_{pc} = \Delta\epsilon^{pc}/\Delta\epsilon^N \qquad (2.18)$$

$$F_{cc} = \Delta\epsilon^{cc}/\Delta\epsilon^N \qquad (2.19)$$

Here, $\Delta\epsilon^N$ is the combined inelastic strain range. A maximum of three types of inelastic strain ranges can exist for a given loop. In general, good correlation can be obtained for isothermal fatigue with and without hold times. Some good correlations have been obtained for austenitic stainless steel for thermomechanical loading by applying this method using isothermally determined constants [3]. Variations on the SRP method have been offered by Saltsman and Halford [15] to account for differences in transgranular or intergranular propagation of creep-fatigue cracks in the N_{pc} or N_{cp} equations.

One obvious advantage of this approach is that tensile and compressive loading are treated differently. This flexibility is desirable to encompass all experimental results.

Frequency Modified Approaches

The basis of this type of approach is that the Coffin-Manson relationship is modified by the frequency of the strain cycle since time-dependent effects, whether creep or environmentally related, exert influence in the low frequency domain [16-17].

According to Coffin's [2] early approach, the frequency ν modifies the Coffin-Manson law, i.e.

$$(N_{I}\nu^{K-1})^{\beta} \Delta\epsilon^{p} = M \qquad (2.20)$$

where β, K, and M are material constants at a given temperature, and N_{I} is the number of cycles to initiate a crack. In this approach, a hold period is considered as a change in test frequency. The effects of unbalanced tensile and compressive going frequencies (and loop shapes) were later incorporated by Coffin in the expression,

$$N_{I} = \left(\frac{A}{\Delta\epsilon^{p}}\right)^{1/\beta} \left(\frac{\nu_{t}}{2}\right)^{1-K} \left(\frac{\nu_{c}}{\nu_{t}}\right)^{d} \qquad (2.21)$$

where ν_{t} and ν_{c} are tensile-going and compressive-going frequencies, respectively. The values of the constants A, β, and K are determined from balanced loop data, and d is obtained from unbalanced data.

Ostergren's damage function [18] uses the net tensile hysteretic energy in the fatigue equation to reflect mean stress effects. In some superalloys, it is thought that

tensile mean stresses introduced by compressive strain hold times are responsible for compressive hold times being more damaging than tensile hold times [17]. Ostergren's damage function is expressed as,

$$\sigma_t \ \Delta\epsilon^p \ N_I^{\beta} \ \nu^{\beta(\kappa-1)} = C \qquad (2.22)$$

where β, κ, and C are material constants, ν is the test frequency (CPM), and σ_t is the peak tensile stress in the hysteresis loop. This approach has resulted in agreement to within a factor of two for isothermal fatigue of Hastelloy-X (with and without tensile and compressive hold times). This frequency modified approach did not, however, produce good correlations after long aging periods. This may be attributed to the fact that environmental effects (i.e. oxidation processes) are not rigorously accounted for.

To bring into consideration waveshape dependence, ν is defined differently. For waveshape _independent_ materials,

$$\nu = (\frac{1}{t_o + t_t + t_c}) \qquad (2.23)$$

where t_o, t_t, and t_c represent time per cycle of continuous cycling, tensile hold time, and compressive hold time, respectively. To account for waveshape _dependence_,

$$\nu = (\frac{1}{t_o + t_t - t_c}) \qquad \text{for } t_t > t_c \qquad (2.24)$$

or, in a simplified form $\nu = 1/t_o$ for $t_t < t_c$.

These corrections on frequency imply that the time-dependent damage is recovered during compressive loading. This seems reasonable for creep cavity growth or triple point cracking induced by grain boundary sliding, but environmental attack (oxidation along grain boundaries) would appear to differ mechanistically.

Continuum Damage Approach

Sometimes called a damage parameter approach, this method was first proposed by Kachanov [19]. Early formulations of this idea were intended to model the accumulation of creep damage either uncoupled [20] or coupled with creep strain.

The continuum damage approach is a local approach in the same sense as the local strain approach to fatigue design and analysis. In practice, it is applied within the framework of finite element analysis.

Development of the method for creep, fatigue, and creep-fatigue interaction has been undertaken primarily by SNECMA and ONERA in France. Chaboche, Lemaitre [21,22], Plumtree [23] and others [3] in France have applied the technique to isothermal and non-isothermal creep-fatigue interaction. They claim to have achieved accuracy in life prediction of actual components to within a factor of two based on this type of approach. For simplicity, the uniaxial

case will be discussed here.

The effective stress is defined as,

$$\tilde{\sigma} = \frac{\sigma}{1 - D} \qquad (2.25)$$

where D is defined as the scalar damage parameter. For undamaged material, $D = 0$; at failure, $D = D_{critical}$. Early writings interpreted D as the normalized loss of area of the cross section by virtue of void or crack formation [21]. Usually, $D_{critical} = 1$.

This approach has the advantage that damage at any point in life can be interpreted as a change in stiffness. For example, for load-controlled pure fatigue cycling, the steady state stress-strain relation is given by,

$$\Delta\epsilon_{ss}{}^{p} = \left(\frac{\Delta\sigma}{K} \right)^{1/m} \qquad (2.26)$$

As damage accumulates,

$$\Delta\epsilon^{p} = \left[\frac{\Delta\sigma}{K(1-D)} \right]^{1/m} \qquad (2.27)$$

which, when combining the above equations, results in,

$$D = 1 - \left[\frac{\Delta\epsilon_{ss}{}^{p}}{\Delta\epsilon^{p}} \right]^{m} \qquad (2.28)$$

Hence, the damage parameter may be identified directly with the increase in plastic strain range due to the accumulation

of damage in fatigue (e.g. the growth of micro-cracks).
Likewise, D may be associated with a change in elastic
unloading stiffness in general. A similar reasoning may be
followed for creep damage. Assuming a Norton creep law with
strain hardening; i.e.,

$$\sigma = A(\dot{\epsilon}_{ss}^{c})^{1/n} \qquad (2.29)$$

where $\dot{\epsilon}_{ss}^{c}$ = steady state (secondary) creep strain rate

  A,n = constants

The change in stiffness is prompted by an increase in the
creep rate primarily during tertiary creep, therefore,

$$\frac{\sigma}{1-D} = A(\dot{\epsilon}^{c})^{1/n} \qquad (2.30)$$

which leads to, as with the cyclic behavior, a directly
measurable damage parameter,

$$D = 1 - \left(\frac{\dot{\epsilon}_{ss}^{c}}{\dot{\epsilon}^{c}}\right)^{m} \qquad (2.31)$$

Note that for both creep and fatigue, the damage essentially
accumulates after steady state conditions have been reached.
Two important points must be made. The first is that
deformation processes and microstructural events occurring
early in life are not considered explicitly as damage. This
is similar to the assumptions of crack growth governed by

fracture mechanics. The second point is that the damage is no longer identified with cycle or time fractions, as is the case in essentially all other phenomenological approaches.

Chaboche [21] suggests that when several processes are operative, coupled equations can be written to introduce the effects of interactions, i.e.

$$dD_p = f_p(\phi, \alpha, D_p, D_t, D_F, T) d\sigma \qquad (2.32)$$

$$dD_t = f_t(\phi, \alpha, D_t, D_p, D_F, T) dt \qquad (2.33)$$

$$dD_F = f_F(\phi, \alpha, D_F, D_p, D_t, T) dN \qquad (2.34)$$

Where ϕ denotes the forcing variables, α represents internal variables, and T is the absolute temperature. In this format, D_p represents "static" plastic damage (e.g. ductile hole growth during plastic flow), D_t represents time-dependent damage, and D_F represents cycle-dependent fatigue damage. A step which is often made for purposes of simplification is to assume that the damage variables are additive, implying equivalence of the damage processes. For creep-fatigue interaction, for example, setting $D_c = D_t$ produces,

$$D = D_c + D_F \qquad (2.35)$$

and

$$dD_c = f_c(\phi, \alpha, D, T) dt \qquad (2.36)$$

$$dD_F = f_F(\phi, \alpha, D, T) dN \qquad (2.37)$$

where D_c reflects the creep damage accumulation. It should be noted that D_t can also include environmental corrosive effects, a phenomenon of special interest in the following study. Separate study of environmental effects has not previously been pursued in the context of continuum damage, probably due to the inability to separate time-dependent cavity growth from environmental attack without vacuum or inert environment testing.

After studying the damage accumulation curves for carbon steels, stainless steels, copper, and Ni-base alloy IN 100, Chaboche and workers [24] have suggested the following forms of the Continuum Damage Approach for uniaxial loading:

$$\frac{dD_F}{dN} = [1 - [1 - D]^{\beta+1}]^{\alpha(\sigma_M, \sigma_m)} \left[\frac{\sigma_M - \sigma_m}{M(\sigma_m)(1-D)} \right]^{\beta} \qquad (2.38)$$

$$\frac{dD_c}{dt} = \left(\frac{\sigma}{A(1-D)\sigma_u} \right)^r [1-D]^{r-k(\sigma)} \qquad (2.39)$$

where σ_M and σ_m are the maximum and mean stresses in the cycle, repectively, and A, r, and β are temperature dependent constants. The rupture strength in a monotonic test, σ_u, is temperature-dependent as well. Specific forms for α and M are given by,

$$\alpha(\sigma_M, \sigma_m) = 1 - a \left\{ \frac{\sigma_M - \sigma_\ell^*(\sigma_m)}{\sigma_u - \sigma_M} \right\} \qquad (2.40)$$

$$\sigma_\ell^*(\sigma_m) = \sigma_\ell + (1 - b \frac{\sigma_\ell}{\sigma_u}) \; \sigma_m \qquad (2.41)$$

$$M(\sigma_m) = M_o(1 - b \frac{\sigma_m}{\sigma_u}) \qquad (2.42)$$

where M_o and a are temperature-dependent coefficients, σ_ℓ is the fatigue limit under completely reversed loading, and b is a temperature-independent coefficient. The exponent $k(\sigma)$ is determined from creep tests at several stress levels. The purpose of the stress dependence of the exponents k and α is to introduce nonlinear damage accumulation for variable loading histories. As pointed out by Chaboche, the results of the continuous fatigue damage analysis for two level cycling tests are similar to that predicted by the Double Linear Damage Rule of Manson and associates [25]. Of course, the continuous damage approach automatically generalizes to any number of loading levels.

Integrating equation (2.38) results in life under pure fatigue loading described by,

$$N_f = \frac{1}{(\beta+1)[1 - \alpha(\sigma_M, \sigma_m)]} \left[\frac{\sigma_M - \sigma_m}{M(\sigma_m)} \right]^{-\beta} \qquad (2.43)$$

with the evolution of damage given by,

$$D_F = D = [1 - (N/N_f)^{1/(1-\alpha)}]^{1/(\beta+1)} \qquad (2.44)$$

Hence, α can be determined with β known by examining the change in stiffness versus cycle fraction for several stress amplitude levels, with and without mean stress. The values of M and β can be determined from completely reversed fatigue tests.

Integrating the creep equation for pure creep loading yields a rupture time of,

$$t_R(\sigma) = \frac{1}{k(\sigma)+1} \left(\frac{\sigma}{A\sigma_u} \right)^{-r} \qquad (2.45)$$

with the damage evolution given by,

$$D_C = D = 1 - [1 - \frac{t}{t_R(\sigma)}]^{1/(k(\sigma)+1)} \qquad (2.46)$$

As before, damage is not a unique function of time fraction, but depends on stress level. From a plot of stiffness change (see equation 2.31) versus time fraction for several stress levels, $k(\sigma)$ can be determined. The constants A and r can be evaluated from isochronous curves of stress versus rupture time for each temperature at which tests are conducted.

Chaboche et al. [3,21-24] have obtained good correlation for IN 100 at 1000°C for two level creep tests, two level fatigue tests, fatigue tests at various frequencies with tensile and compressive hold times, creep after prior fatigue cycling, and fatigue after prior creep.

Lemaitre and associates have also written the continuum damage equations in terms of strain [23], the more usual condition at notches. This may be accomplished using stress-strain relationships. For constant strain rate tests with triangular waveforms, assuming that the Norton creep law holds such that $\dot{\epsilon} = \dot{\epsilon}^c$ (total strain rate equals creep strain rate), the number of cycles, N_c, under creep-dominated cycling is related to the cycle frequency and the strain range in a manner very similar to Coffin's frequency modified approach for balanced loops discussed earlier. For both creep- and fatigue-dominated cycling, the damage can be expressed as,

$$D = 1 - \frac{\Delta\sigma}{\Delta\sigma^*} \qquad (2.47)$$

where $\Delta\sigma^*$ is the cyclically stabilized stress range under strain control.

The damage evolution equations then become,

$$\frac{dD_c}{dN} = \frac{(1 - D)^{-q}}{(q + 1)N_c(\Delta\epsilon)} \qquad (2.48)$$

for constant strain rate cycling, and,

$$\frac{dD_F}{dN} = \frac{(1 - D)^{-p}}{(p + 1)N_F(\Delta\epsilon)} \qquad (2.49)$$

for fatigue cycling at high frequency. These strain-based equations are not directly amenable to strain hold periods of stress relaxation. Here N_c and N_F are functions of the strain range.

The concept of continuous damage does not require auxiliary rules for stress relaxation or creep during hold times. The constitutive equations for deformation and damage are integrated simultaneously.

Damage Rate Approach

This approach is mechanistic in the sense that creep damage is viewed as cavity or wedge crack growth and fatigue damage as intergranular or transgranular cracks. The damage is not expressed in terms of creep-fatigue failure prediction methodologies.

According to this strain-based approach [26,27], the growth of fatigue cracks is coupled with cavity growth through the equation,

$$\frac{1}{a}\frac{da}{dt} = \left\{ \begin{matrix} T \\ C \end{matrix} \right\} (1 + \alpha \ln c/c_0) \left|\dot{\epsilon}^N\right|^m \left|\epsilon^N\right|^k \qquad (2.50)$$

where   c = cavity size, including "r" and "w" type

        a = current crack length

        $|\epsilon^N|$ = absolute value of current rate and time

            -dependent and time-independent inelastic

            strain accumulated from the last reversal of

            inelastic strain

        $|\dot{\epsilon}^N|$ = absolute value of inelastic strain rate

        T,C = coefficients for tensile and compressive

            stress, respectively

        T,C,m,k,α = temperature, environment, and

            microstructural dependent material parameters

Hence, the rate of growth of a fatigue crack is influenced by the inelastic strain rate, inelastic strain amplitude, current crack length, whether the loading is predominately tensile or compressive, and the extent of cavity growth. Therefore, there is a coupling of the fatigue damage with creep damage. If the cavity size $c \leq c_o$, it is assumed that the crack does not interact with cavities.

Cavity growth is governed by the equation,

$$\frac{1}{c}\frac{dc}{dt} = \{ {}_{-G}^{G} \} \; |\dot{\epsilon}^N|^m \; |\epsilon^N|^{k_c} \qquad (2.51)$$

where   G,-G = coefficients to be used in the presence of

            tensile and compressive stress, respectively

        m, k_c = temperature, environment, and micro-

structural dependent material parameters

This formulation permits both growth and shrinkage of creep cavities. Failure is defined as the time required to reach a fatigue crack of length a_f or a cavity size of c_f, whichever occurs first. Note that fatigue damage does not influence the creep damage rate.

Parameters m, k, and $(C + T)/2 \ln (a_f/a_o)$ can be determined from fast-slow fatigue data, k_c can be found from monotonic creep rupture tests, and the product αG can be determined from slow-fast cycling.

The damage rate approach has been successfully applied to creep-fatigue lifetime prediction of the austenitic stainless steels [27] and Cr - Mo - V steels [26].

Brief Critique of Predictive Approches for Isothermal and Non-Isothermal Creep/Fatigue/Environment Interaction for Nickel-base Alloys

When evaluating the previously discussed creep-fatigue approaches for nickel-base superalloys, there are several factors which immediately become apparent. First of all, comparisons of the methods based on predicting the creep-fatigue life of more ductile metals (e.g. 1% Cr - Mo - V) do not necessarily extend to the less ductile superalloys. The inelastic strain range is small for the superalloys as compared to the stainless or pressure vessel steels.

Secondly, the effect of tensile and compressive hold times in superalloys are generally opposite that observed for more ductile metals [17,28]. Compressive hold periods under strain control are more damaging than tensile hold periods. Coffin attributes this to the observed development of compressive mean stresses for tensile hold periods due to stress relaxation, and vice-versa for compressive hold periods. In contrast, the effect of tensile hold periods on load-controlled fatigue crack propagation tests is quite detrimental. Coffin reasons that this is due to a delay in the initiation life for smooth specimens.

A third factor, explicitly addressed in this study, is the fact that creep-fatigue interaction for superalloys is very different from the interaction of cavities and fatigue cracks noted for ductile metals. The role of environment is much more pronounced for the superalloys. Antolovich [28] found that prior exposure to environment at low stress levels drastically reduced life; machining away the surface removed this effect. Furthermore, Antolovich was able to correlate the oxygen penetration depth at crack initiation, ℓ_i, with the maximum stress at initiation, σ_i^{max},

$$\sigma_i^{max}(\ell_i)^p = C_o \qquad (2.52)$$

where p and C_o are material constants. The exponent p was approximately 0.23 for Rene 80, Rene 77, and Nimonic 90 at

elevated temperatures.

With these general differences between heavily studied ductile metals and superalloys established, the various damage accumulation techniques can be critiqued.

Linear Time and Cycle Fraction Summation

Since this approach is not mechanistically sound and since damage accumulation is understood to be highly nonlinear, this approach warrants no further discussion.

Microcrack Propagation Models

The microcrack propagation approaches developed by the British imply that a microcrack is present essentially from the begining of the loading history, which does not conform to experimental observation in many cases. These models apply well to crack growth for cavitated ductile materials; however, the applicability to superalloys has not yet been demonstrated in the isothermal or nonisothermal case. The form of the equations for nonisothermal loading is questionable.

Frequency Modified Approaches

The frequency modified approaches as suggested by Coffin [2] and Ostergren [18] include frequency effects in a relatively crude manner. Effects of hold times, for example, are incorporated by defining a lower effective cycle frequency. Since these approaches do not provide a mechanistically accurate way to include hold time effects,

extensions to more complex histories and nonisothermal conditions would be extremely tenuous and difficult.

A more mechanistically based frequency modified approach has been suggested by Antolovich [29]. Assuming a metallurgically stable structure and out-of-phase TMF cycling, crack initiation is defined as the point where the diffusion length along a grain boundary equals the slip band spacing. Damage accumulates via slip at low temperature and by oxidation and carbide formation at high temperature. The resulting initiation life is given by,

$$N_i = \frac{A^2 \nu}{D_o} \exp \left(\frac{Q}{RT_{eff}} \right) \left(\Delta \epsilon^p \right)^{-2\delta} \tag{2.53}$$

where D_o is a diffusion coefficient, ν is temperature cycle frequency, Q is the activation energy, R is the universal gas constant, and A and δ are constants. T_{eff} is the effective temperature formed from,

$$\exp \left(- \frac{Q}{RT_{eff}} \right) = \frac{1}{\Delta T} \int_{T_\ell}^{T_h} \exp \left(-\frac{Q}{RT} \right) dT \tag{2.54}$$

where $\Delta T = T_h - T_\ell$

Antolovich similarly introduced an accelerated void growth TMF model, assuming a tension-tension out-of-phase cycle. Defining failure as the point when the effective grain boundary stress exceeds the cohesive strength,

$$N_f = \frac{1}{6.6} \; [\frac{\nu}{N_A D_o}]^{1/2} \; [\frac{\sigma_c - k'(\Delta\epsilon^P)^{N'}}{(\Delta\epsilon^P)^2}]^{3/2} \; \exp(\frac{Q}{2RT_{eff}}) \tag{2.55}$$

where $\Delta\sigma = k'(\Delta\epsilon^P)^{N'}$, N_A = voids/unit area

σ_c = cohesive strength, given by

$$\sigma_c = \frac{1}{1 - A_{gb} N_A \pi R_v^2} \tag{2.56}$$

where A_{gb} = 3/L = total grain boundary area

R_v = void radius at failure

While no data has been analyzed to support or refute this model, its usefulness appears to lie in its ability to reflect effects of varying grain size, frequency, effective temperature, etc. on N_f. Such a model, of course, presents difficulties in terms of the extensive level of metallographic examination required to determine N_A, R_v, and whether the assumed rupture criterion is correct. Furthermore, the concept of effective temperature is fundamentally uncertain. Other workers [30,31] have shown that the creep rupture criterion is more aptly described by the product of applied stress and volume fraction of voids. In their final forms, these equations appear to be frequency and temperature modified approaches. There are no explicit provisions for temperature hold times or for more general

loading conditions.

Strain Range Partitioning

In principle, this method is very desirable insofar as it is relatively easy to apply. Several very significant deficiencies exist regarding thermomechanical fatigue life prediction of superalloys.

One deficiency is that this method requires the determination of the foward and reverse plastic and creep strains within a cycle. This implies that a classical decomposition of inelastic strain into time- and rate-dependent plastic and creep strains be made. Such a decomposition has been shown to be undesirable.

A second point to be made is that the cyclic plastic strains for superalloys in typical engine applications are quite small. Inaccuracy in their determination can lead to substantial error in the relatively sensitive plastic strain-life equation in the SRP method.

Finally, for nonisothermal loading, Halford and co-workers [15] have proposed a modification to the coefficients and exponents in equations (2.11) through (2.14) to account for thermal history effects on the plastic strain-life relationships. In other words, the isothermally determined relationships are inadequate, since superalloys can exhibit significant thermomechanical history effect [32]. However, this method, as in frequency

modified approaches, is not of incremental form. A rational extension to nonisothermal loading is not readily possible.

Continuum Damage Approach

There are significant advantages obtained by applying this method to the superalloys. The technique requires stresses and not plastic strains, which are difficult to accurately predict; and life correlations to within a factor of two for nonisothermal loading have already been accomplished.

In general, stresses are less sensitive than plastic strains to thermomechanical history effects. This fact, coupled with small cyclic plastic strains for superalloys, may lead to stress as the the most viable basis for TMF life prediction for this class of materials.

There are, however, disadvantages in the particular form of the continuum damage approach used by Chaboche and associates. One such disadvantage is that the creep damage evolution is based on monotonic creep tests without prior cycling, although the creep response is highly dependent on cyclic plasticity. Also, a significant crack contribution may be included in the fatigue damage law derived from solid specimen uniaxial tests. Thirdly, stiffness changes do not reflect grain boundary creep damage very well [33]. The most important disadvantages in this approach are that the environmental damage is completely neglected and there is

no distinction between tensile and compressive hold times, contrary to experimental results.

From the work of Krempl and Ostergren [34], it can be shown that frequency modified approaches can be derived as a particular form of continuum damage mechanics. This is also true of the Coffin-Manson low cycle fatigue law. These results indicate that a continuum damage growth law can be a useful tool in cumulative damage summation since the damage is progressive; time or cycle fractions are not required.

Damage Rate Approach

This approach appears to very accurately reflect the interaction of a growing fatigue crack with voids due to compressive loading, and coupling of the crack growth rate with void fraction, but not vice-versa. The failure criteria for fatigue and creep are not related in this method, which is mechanistically appealing. This approach, however, appears to be difficult to generalize and requires a considerable amount of testing for characterization. Furthermore, the capability to model time-dependent environmental interaction with crack growth does not exist in the present form. There is no provision or methodology suggested for extending this method to nonisothermal loading.

For materials which do exhibit a creep-fatigue interaction, with little influence of environment, this method works quite well for isothermal loading. It should be stressed that the incremental form of these equations provides the framework for time- and temperature-dependent loading.

CHAPTER III

MATERIALS AND PROCEDURE

Material

The material chosen for this investigation was MAR-M 246. The composition of this nickel-base superalloy is given in Table 1. The high temperature strength of this alloy is due, in part, to a precipitation of finely dispersed gamma prime $Ni_3(Ti,Al)$; in addition, its superiority over wrought alloys can be attributed to improved solid solution strengthening obtained with the presence of a significant amount of tungsten [35].

The material was supplied by Allison Gas Turbine Engine Division of General Motors Corporation in the form of conventionally cast 0.75" cylindrical ingots. Smooth bar tensile and low cycle fatigue specimens, with button-head ends, were machined from these castings by the supplier. Specimen dimensions are given in Figure 1.

Cooling rates for the material were not available, but the effects of the cooling of the castings are discussed in Chapter IV of this report.

Experimental Procedure

Test Matrices

As mentioned in the introduction, the present study is the beginning of an overall program to investigate life prediction (defined by crack initiation) as applied to both isothermal and non-isothermal loading histories of nickel-based superalloys . Although variables chosen for the study include environment and temperature, this portion of the program will be concerned with tests run in air at atmospheric pressure and a single temperature of 900°C.

Both tensile and LCF tests were conducted with strain rates, in decade increments, between 10^{-1} and 10^{-4} sec^{-1}. In addition, a tensile test was conducted at 10^{-5} sec^{-1}. Strain amplitudes for low cycle fatigue tests were chosen (in 0.2% increments) between 0.2% strain and 1.0% strain. Three creep tests were completed for this study: a high stress-level and a low stress-level test, as well as a high-low stress sequence test. Test matrices for each of the above mentioned testing procedures are shown in Table 2.

Specimen Preparation

All specimens were polished in the gage section using a sequence of 320, 400, 600 grit wet/dry sandpaper and finished with 6 micron diamond paste. This procedure produced a smooth, mirror-like surface. The polished specimens were then cleansed with acetone and stored until

testing in sealed test tubes.

Mechanical Testing : Creep Tests

The creep tests included in this study were performed using a SATEC C-Type creep frame. This apparatus consisted of a 20:1 lever arm with a twelve-thousand pound tension capacity, an automatic control load elevator, and a furnace shutoff interlock.

In order to perform the elevated temperature tests, the existing SATEC C-Type resistance furnace had to be redesigned and rebuilt. The original three inch bore of the furnace was increased to five inches to accommodate the extensometer (described below) by replacing the resistance heating elements. In addition to increased size, the new elements had a greater power capacity that, when coupled with additional KAOWOOL ceramic insulation, increased the maximum operating temperature from 1250°F (726°C) to 2000°F (1143°C).

Furnace temperature was controlled with an OMEGA Model 115 controller. This consisted of four 40 amp. solid state relays fed with an input signal through a chromel-alumel thermocouple. A temperature gradient of only 1°C over the gage section of a test specimen was achieved with this set-up.

Creep strain was measured via an ATS capacitance gauge attached to a four arm high temperature extensometer. An

output signal was sent to an amplifier and recorded with a strip chart recorder. A complete description of the extensometer is included in Appendix A.

Mechanical Testing : Tensile and Low Cycle Fatigue

All tensile and LCF tests were performed using an MTS 10000 Kg capacity closed-loop servo hydraulic testing system in total axial strain control mode. Feedback was monitored by an LVDT. A ramp waveform was used. The desired strain rates were derived by choosing a frequency based on the total strain amplitude as follows:

$$\nu \; (Hz) \; = \; \frac{1 \; cycle}{4(\Delta \epsilon^t/2)} \; x \; \dot{\epsilon} \qquad (3.1)$$

where $\Delta \epsilon^t/2$ = total strain amplitude

$\dot{\epsilon}$ = strain rate

Low cycle fatigue tests were performed over the same strain rates as the tensile tests using a fully reversed triangular wave (i.e. a dual-ramp waveform). Specimens were held in place by mechanically locking, water cooled, wedge grips - also with a load capacity of 10000 Kg.

The extensometer used for the tensile and LCF program was based on a modification of an MTS Model 632.11 clip gauge. A complete description of this equipment is found in Appendix A.

Specimens were heated using a 1.5 kilowatt CYCLE-DYNE induction unit controlled by a EUROTHERM Model C96.1 controller. The induction heater was connected to 0.125" diameter copper tubing. This tubing was wrapped around the specimen approximately one-half inch from the gage section surface. The copper coil consisted of two turns at both the top and bottom shoulder areas of the sample and two concentric turns at the center of the gage section. Water was circulated through the coil during operation for cooling purposes.

To produce the proper temperature gradient, a specimen was affixed with five beaded chromel-alumel thermocouples and placed in the MTS load frame grips. This is shown schematically in Figure 2. Adjustments were made to the coil shape and orientation until a temperature gradient in the specimen gage section was no greater than ±2.5°C. During testing, thermocouples were attached to the top and bottom shoulders - one was used for control as dictated by the calibration; the other, as a backup in the event the first should fail.

Data was aquired with a NICOLET Model 2090:2B digital recording oscilloscope. Strain gage and load cell output voltages were recorded on floppy disks for conversion and reduction to stress versus strain ASCII data files via an IBM AT computer. A complete description of the data

aquisition and manipulation procedures are described in Appendix A.

Sample Sectioning and Examination

Several specimens were selected for metallographic analysis and were sectioned and mounted as shown in Figure 3. All optical metallography specimens were prepared using standard techniques. Longitudinal sections cut through one fracture surface and transverse sections cut below and parallel to the other fracture surface of a specimen were mounted in diallyl phthalate, rough polished on silicon carbide papers (in a 320, 400, 600 grit sequence), and finely polished using a sequence of 1 micron, 0.5 micron, 0.05 micron alumina slurry. Optical samples were etched using a solution of 33% nitric acid, 33% acetic acid, 33% water, and 1% hydrflouric acid. Immersion times were approximately four to five seconds. A LEITZ metallograph was used to examine grain size and secondary crack penetration depths.

Complete fracture surfaces were mounted with silver paste on aluminum posts for SEM analysis. A CWIKSCAN 100 field emmission scanning electron microscope was used for fracture surface analysis. Initiation sites were examined where possible, in addition to a study of secondary cracking and inclusions.

CHAPTER IV

RESULTS AND DISCUSSION

Creep Characterization

Fundamental Results

Engineering strain versus time data for secondary and tertiary creep is presented in Figure 4. The corresponding basic characteristics of the creep tests are outlined in Table 3.

To begin to characterize creep life with a continuum damage model, the steady state (stage II) creep strain rate was assumed to behave as dictated by   Norton power law creep,

$$\dot{e}_{ss}^{c} = A(\sigma)^{n} \qquad (4.1)$$

where $\dot{e}_{ss}^{c}$ = steady state nominal creep strain rate

σ = applied nominal stress

A, n = constants

As calculated from the two constant nominal stress creep tests, the exponent n was determined to be 6.65, and the constant $A = 3.18 \times 10^{-21}$ hr^{-1} $MPa^{-6.65}$. This formulation provides a simple, although incomplete, description of the dependence of creep strain rate on stress. As the continuum

damage model is developed, the creep strain rate will be predicted not only for steady state creep, but for tertiary creep coupled with the creep damage parameter D_c, as discussed in Chapter II.

Application of the Continuum Damage Approach

The scalar creep damage parameter can be interpreted as the normalized loss of area of the specimen cross section due to the formation of voids or cracks [21]. In other words, a high value of D_c would correspond to a high ratio of void area to grain boundary area in a specimen undergoing creep damage. With no damage, D_c is set equal to zero; and at failure, the parameter is normalized to unity.

A generalization of the damage rate method and a specific form of the continuum damage approach was suggested by Chaboche et al. [24] as a creep damage model:

$$\dot{D}_c = \left[\frac{\sigma}{A(1-D_c)} \right]^r (1-D_c)^{r-k(\sigma)} \qquad (4.2)$$

where A, r = temperature dependent constants

$\qquad k(\sigma)$ = stress dependent constant

By factoring out the quantity $(1-D_c)^r$ and combining constants, a more compact form of this equation may be introduced, i.e.

$$\dot{D}_c = \frac{B\sigma^r}{(1-D_c)^{k(\sigma)}} \qquad (4.3)$$

It is important to note that the purpose of the stress dependence on the parameter k, as defined by Chaboche, is to account for nonlinear damage cumulation for stress amplitude step tests.

This form of the differential equation is solved by separation of variables for a constant nominal stress creep test. The damage parameter limits of integration are $D_c = 0$ to $D_c = 1$ and the time limits are $t = 0$ to $t = t_R$ (= time to rupture). The following expression results:

$$t_R = \frac{1}{B\sigma^r[k(\sigma) + 1]} \qquad (4.4)$$

By taking the logarithm of both sides, the material constant r is readily determined.

$$\log t_R = -\log B[k(\sigma) + 1] - r \log \sigma \qquad (4.5)$$

The quantity -r is the slope of the time to rupture versus stress plot on a log scale. This calculation is shown in Figure 5; i.e. r = 5.76.

It is important to note, however, that there is an appreciable amount of scatter in creep rupture time data, typically as much as a factor of two at a given stress

level. The preliminary analysis herein is somewhat incomplete since there were only two constant stress creep tests performed, and hence, only two data points for the determination of r. In a worst case consideration, r could change from its present value by as much as ±50% given sufficient data to characterize it with some measure of statistical support.

In an attempt to study the question of scatter in rupture time, the two constant nominal stress creep tests were repeated (specimens S999-4 and S999-5) under identical conditions. These tests produced rupture times and strain-to-failure data as presented in Table 3. Although the creep test analysis, as conducted in this study, was completed before these additional tests were performed it is important to note that with all four constant nominal stress tests considered, the value of r is changed from r = 5.76 to r = 6.61.

In further characterization of the creep damage of MAR-M 246 using expression (4.3), the constants B and k(σ) were estimated. This was accomplished using data from the step-stress sequence creep test. As with the above determination of r, the solution to the continuum creep damage model was utilized. Dividing the limits on integration into two parts - one for the high stress level initial segment of the step stress test, and the other for the low stress level

completion - the following integrals may be written :

$$\int_{0}^{D_{INT}} (1 - D_c)^{k(\sigma_{HI})} \, dD_c \;=\; \int_{0}^{t_{INT}} B(\sigma_{HI})^r \, dt \qquad (4.6a)$$

$$\int_{D_{INT}}^{1} (1 - D_c)^{k(\sigma_{LOW})} \, dD_c \;=\; \int_{t_{INT}}^{t_R} B(\sigma_{LOW})^r \, dt \qquad (4.6b)$$

where $\sigma_{LOW}, \sigma_{HI}$ = low and high stress levels, respectively, of the sequence creep test

D_c = scalar creep damage parameter

D_{INT} = value of D_c at time at which stress level was decreased

t_{INT} = time at which stress level was decreased

t_R = time to rupture

$k(\sigma_{LOW}), k(\sigma_{HI})$ = parameter values depending on low and high stress levels respectively

B, r = temperature dependent constants

The solution of these integrals is :

$$\frac{1 - [1 - D_{INT}]^{(k(\sigma_{HI}) + 1)}}{k(\sigma_{HI}) + 1} \;=\; B(\sigma_{HI})^r (t_{INT}) \qquad (4.7a)$$

$$\frac{(1 - D_{INT})^{(k(\sigma_{LOW}) + 1)}}{k(\sigma_{LOW}) + 1} = B(\sigma_{LOW})^r(t_R - t_{INT}) \quad (4.7b)$$

Thus, two equations were formulated containing four unknown quantities, D_{INT}, $k(\sigma_{HI})$, $k(\sigma_{LOW})$, and B. To complete a system of four equations, two additional expressions were required. By using the constant-stress-to-failure creep tests, two equations in the form of (4.5) were incorporated without adding any additional unknown variables. For the high stress level test,

$$(t_{RH})^{-1} = B\sigma^r[k(\sigma_{HI}) + 1] \quad (4.8)$$

and for the low stress level creep test,

$$(t_{RL})^{-1} = B\sigma^r[k(\sigma_{LOW}) + 1] \quad (4.9)$$

where t_{RH} and t_{RL} are the rupture times of the respective tests in the absense of loading sequence effects.

An iterative approach was developed to solve this set of four nonlinear equations. First, the creep damage parameter at the time of stress interruption was selected and held fixed. An arbitrary value for the constant B was then used in expressions (4.8) and (4.9) to obtain a first estimate of $k(\sigma_{HI})$ and $k(\sigma_{LOW})$ respectively. Constant B and

these values of $k(\sigma)$ were subsequently used in a Gauss-Seidel iteration routine of equations (4.7) to get a further calculation of $k(\sigma_{HI})$ and $k(\sigma_{LOW})$ based on the scalar creep damage parameter. This process of altering the value of B and iterating was repeated until convergence was reached with the value of $k(\sigma_{HI})$ being slightly greater, but reasonably close to the value of $k(\sigma_{LOW})$. This procedure was carried out for fixed values of D_{INT} ranging from .05 to .20. The results of this iteration procedure are presented in Table 6.

Based on the application of a similar creep analysis performed on IN 100 (also a Ni-base superalloy) by Chaboche and co-workers [24], reasonable values for $k(\sigma)$ would be in the range of 4 or 5. The values of $k(\sigma_{HI})$ settled upon were greater than $k(\sigma_{LOW})$ to produce a greater damage rate for the more highly stressed case. It should be noted that the estimates of $k(\sigma)$ for each stress level calculation using the equations based on constant stress are also included in the tabulated results. With these calculations, the values of $k(\sigma_{HI})$ are slightly less than the calculations for $k(\sigma_{LOW})$ - and are both higher than the "anticipated" values. Consideration of strain to failure in the coupled strain - damage equation will result in some further iteration of $k(\sigma)$ values as discussed later.

It is encouraging that the measures for the creep damage parameter are within reason, based on the work of Chaboche, since $k(\sigma)$ values are in the proximity of 4 to 5. More specifically, using the iterated formulations of (4.7), $k(\sigma)$ ranged from 3.75 to 5.97 for D_{INT} between .07 and .10. Using the equations based on the constant stress tests (4.8 and 4.9), $k(\sigma)$ was estimated between 4.03 and 5.27 for the damage parameter valued in the range .10 to .12.

Much of the previous analysis was based on a rough estimate of the value of the interrupted creep damage parameter. It is possible; however, to determine D_{INT} based entirely on metallurgical study, and therefore determine the values of the other constants of the continuum damage equation more readily. This would require another creep test at the same stress level as one of the previously completed constant stress tests. At a predetermined time, the creep test would be halted and the MAR-M 246 specimen removed and sectioned. From a study of void growth as a function of grain boundary area, the damage parameter could be determined directly.

If this test were conducted at the higher stress level ($\sigma = \sigma_{HI}$) then the expression involving σ_{LOW} would be eliminated and only two equations with two unknown quantities ($k(\sigma_{HI})$ and B) would remain. These parameters could be solved explicitly and the resulting value of B

could be used in conjunction with the test data for the low stress level test to determine $k(\sigma_{LOW})$ explicitly.

It is therefore felt that at least one additional creep test should be run at either a stress level of 300 MPa or 413 MPa and halted before rupture. A study of D_{INT} based on the physical condition of the MAR-M 246 specimen and the resulting calculations of the remaining continuum damage equation constants, as outlined, would yield invaluable information on the accuracy of the creep characterization performed in this study.

Creep Strain Rate Analysis

Using the effective stress concept for uniaxial loading, as defined by Lemaitre [36],

$$\tilde{\sigma} = \frac{\sigma}{1 - D} \quad \text{where } D = D_c \qquad (4.10)$$

where $\tilde{\sigma}$ = effective stress

Then the creep strain rate equation (4.1) may be re-written as,

$$\dot{e}^c = A \left[\frac{\sigma}{1 - D_c} \right]^n \qquad (4.11)$$

Which, by considering a separate exponent on the damage accumulation term as proposed by Rabotnov [20], may be re-formulated as,

$$\dot{e}^c = A\sigma^n \left[\frac{1}{1 - D_c}\right]^\nu \qquad (4.12)$$

The creep strain rate $\dot{e}^c$ is used here since both secondary and tertiary creep are included.

The main purpose of this dual exponent approach is to better model the tertiary creep regime and rupture time. Using the values of B and $k(\sigma_{HI})$ deemed most likely to represent the true physical situation, the set of coupled non-linear differential equations (4.3 and 4.11) were solved using a fourth order Runge-Kutta method. Constant B was again slightly altered until the value of the creep damage parameter reached unity at the time of rupture of the high stress level test. The value of ν was then altered until the numerical solution of engineering creep strain at the time of specimen failure best fit the experimental rupture strain for this test. This numerical approximation was plotted against the experimental data as shown in Figure 6. The quality of the approximation was improved by slight adjustments made to the values of constants A and n from the original Norton power law creep calculations. Special consideration was given to the secondary creep regime, due to its engineering importance.

A similar procedure was followed in an attempt to fit the data from the low stress level creep test. Ideally, the values of B, r, A, n, and ν should remain unchanged since

they are stress-independent and this test was performed at
the same temperature as the first. Using the same value of
B, $k(\sigma_{LOW})$ was reduced until the continuum damage equation
produced a damage parameter of unity at the experimental
time to rupture of this test. The resulting value of $k(\sigma_{LOW})$
was then less than that of $k(\sigma_{HI})$; which is a more
physically sound condition than the estimates in Table 6.
The value of ν used to produce identical
numerical/experimental strain-to-failures for the high
stress level test was incorporated into this fitting
procedure. The result was a predicted strain-to-failure
8.5% greater than that experimentally observed, a small
difference considering the possible scatter associated with
rupture data.

The numerical approximation to the creep data is
plotted in comparison to the experimental data in Figure 7.
The only additional change from the values in the high
stress level fit is that the constant A was reduced from
2.8×10^{-21} to 2.4×10^{-21} to provide improved numerical/ex-
perimental agreement for the secondary creep stage. Since
secondary creep rates exhibit scatter, it may be desirable
to view A as an average for the two tests.

The values of all constants used in these fitting
procedures are given in Table 7. Note that the best fit,
determined by graphic comparison between experimental and

numerical data, resulted in $k(\sigma_{HI}) = 5.11$, $k(\sigma_{LOW}) = 4.72$.
These results correspond to an interrupted scalar damage
value D_{INT} of approximately .10 to .11, within a reasonable
range, although somewhat arbitrary in the absence of
metallurgical damage quantification.

Due to potential confusion of the reader in following
the numerical procedures outlined, a simplified step by step
guide to the creep characterization process is included in
Appendix B. The procedures are broken into two segments; one
for the estimation of constants of the continuum damage
equation, and the other for the numerical solution to the
coupled strain/damage equations.

A plot of the scalar creep damage parameter D_c versus
normalized time for both constant stress creep tests is
presented in Figure 8. This data graphically demonstrates
the more damaging effects of low-high stress level sequences
compared to high-low stress sequences for the same time
fraction, t/t_R. These effects are in agreement with the work
of Woodford [30].

Fatigue Characterization

Fatigue Damage Model

As discussed in the literature review of this study,
Majumdar and Maiya [27] present a strain-based damage rate
model which couples the cyclic extension of fatigue cracks
with creep cavitation growth. The appeal of this approach

lies in the fact that the formulation has the potential to predict pure fatigue damage, pure creep damage, and creep-fatigue interactions accurately. This damage rate model has been successfully applied to creep-fatigue life prediction of Type 304 stainless steel in the range of 480°C to 600°C. At the various temperatures used in the study, predicted lives deviated from experimental determinations well within a factor of two. A second class of material, 2-1/4 Cr - 1 Mo steel, was also analyzed in the same temperature regime with similar results to those of the stainless steel. Hence, it can be stated that this damage rate model works well for materials which exhibit creep-fatigue interaction under isothermal loading.

There are certain aspects of the damage rate model which present uncertainties in its application to life prediction of Ni-base alloys, i.e. the material of concern to this study. First and foremost, there is no provision to calculate time-dependent environmental interaction with crack growth in the model's form as shown in equation (2.50). In addition to creep damage, environmental damage can influence the fatigue damage rate since embrittlement of grain boundaries ahead of the fatigue crack enhances growth. This is especially important when considering superalloys due to the greatly pronounced effect of environment on damage as shown, for example, by Pedron and Pineau [37] and

Cook and Skelton [38].

A second important shortcoming of this damage rate approach is that there is no methodology suggested for extending the model to nonisothermal loading. Although this initial study is concerned with life prediction of a Ni-base superalloy at a single temperature, it is the intention of the overall experimental program to approximate thermomechanical fatigue of Ni-base superalloys.

It is important to note two further uncertainties in the approach suggested by Majumdar and Maiya. The application of this model to more ductile materials does not necessarily extend to the less ductile superalloys. The plastic strain range is relatively small for Ni-base alloys as compared to those for stainless or pressure vessel steels; this can lead to significant relative errors in applying the life prediction method to actual components where the plastic strain ranges must be estimated. A final uncertainty concerns the approximation of the initial crack length, which is assumed to nucleate at some time early in the fatigue life. Estimations used by Majumdar [27] were on the order of the initial roughness of tested specimens. Unfortunately, due to a lack of well-developed striations on the fracture surface of many of his tested specimens, crack length measurements were not possible,and hence, the value of the initial micro-crack length was somewhat arbitrary.

Of course, this is a classical problem of "initiation mechanics". In this presentation, a more detailed treatment of micro-crack initiation will be undertaken.

Based on these uncertainties of the fatigue damage rate model derived by Majumdar and Maiya, a variant of this approach and the continuum damage approach may be proposed :

$$\frac{1}{D_F} \dot{D}_F = A(\sigma) \left[1 + \alpha \ln \frac{D_C}{D_{CO}} + \beta \ln \frac{D_E}{D_{EO}} \right] |\dot{\epsilon}^N|^m \left(\frac{\Delta \epsilon^N}{2} \right)^n \qquad (4.13)$$

where, D_F = fatigue damage (crack length)

D_E = environmental damage (oxygen penetration depth)

D_{CO}, D_{EO} = thresholds below which fatigue damage does not interact with creep or environmemtal damage, respectively

$|\dot{\epsilon}^N|$ = absolute value of inelastic strain rate

$(\Delta \epsilon^N)/2$ = inelastic strain amplitude

$A(\sigma)$ = coefficient to account for mean stress effects

α, β, m, n = material parameters ; temperature-dependent

Although this formulation is written in terms of continuum damage parameters to follow the representation of the creep damage model, a direct analogy can be made between D_F and "a" (crack length) in the Majumdar and Maiya representation in equation (2.50). Unlike the continuum creep damage parameter D_C, D_F and D_E do not range in value

from 0 to 1 as a fractional representation of material damage. Instead, they have an absolute physical value of crack length and oxygen penetration depth, respectively.

The major difference between this hybrid continuum damage rate equation and that of the original damage rate approach lies in the fact that there is an explicit environmental damage consideration. Parabolic oxygen penetration [39] is assumed and can be represented generically by the equation,

$$D_E = h(t) \ exp \left(\frac{-Q(\sigma)}{RT} \right) \qquad (4.14)$$

where, $Q(\sigma)$ = activation energy for oxidation

R = universal gas constant

T = absolute temperature

$h(t)$ = time-dependent coefficient = $D_o t^{-1/2}$ for parabolic oxygen penetration

It is not possible to ascertain exact environmental effects of damage on fatigue life without conducting material tests in a vacuum environment. Since this is not yet done in this study, environmental effects on the low cycle fatigue life of MAR-M 246 will be estimated through metallographic analysis of specimen fracture surfaces and secondary cracking. Results will be compared with recent studies of environmental damage of nickel-base superalloys

at elevated temperatures in a later section.

Classification of Fatigue Damage

Fatigue damage is defined in terms of crack length. The
first difficulty encountered in the development of fatigue
damage initiation is found in its definition. There are three
stages of crack initiation as outlined by Chaboche [4]. The
first is crack nucleation, which is often associated with
slip band spacing at the specimen surface or along grain
boundaries which intersect slip bands. This definition
will be studied in detail later.

The second level of fatigue damage is micro-crack
initiation and propagation, the "substructural scale". One
definition of initiation at this stage is the transition
between crystallographic and principal stress cracking, i.e.
extension through or along a few grains [4]. Of primary
concern in this study is micro-crack propagation. It is in
this regime that the continuum damage rate equation for
fatigue will be applied.

The third stage of initiation is macro-crack
initiation. At this level, a crack has to show a definite
"geometrical dominance" in order to apply fracture mechanics
concepts. In engineering structures, this level of damage is
initiated when a crack is on the order of 1 mm, typically
encompassing at least several grains. A large number of
studies have been conducted on Ni-base superalloys at elevated

temperatures which model macro-crack propagation through the use of the Paris Growth Law :

$$\frac{da}{dN} = C(\Delta K)^M \qquad\qquad (4.15)$$

where,   a = current crack length

N = current cycle number

ΔK = stress intensity factor range

C,M = constants

For example, Shahinian [40] has studied macro-crack propagation of several nickel-base alloys between 24°C and 704°C, where ΔK is normalized by the elastic modulus in an attempt to account for temperature (i.e, environmental) effects. Resultant values for C and M were approximately 2.8×10^6 and 3.5, respectively, at room temperature and 1.7×10^6 and 3.5, respectively, at 704°C.

Due to the progress of researchers [see 40-42] in modelling macro-crack propagation of Ni-base superalloys, the application of the methodologies of this stage of cracking in this work is not deemed necessary.

Short Crack Considerations

Although this study is concerned with crack nucleation and propagation on the substructural scale, the relationship between the proposed damage rate model and macro-crack propagation correlated by the Paris Law must be studied. On

the macro scale, the Paris Growth Law may be written in rate form ,

$$\frac{da}{dt} = \nu C (\Delta K)^M \qquad (4.16)$$

where ν = cycling frequency

The limits of integration on the crack length parameter range from macro-crack initiation, $a = a_i$, to a critical crack length resulting in failure, $a = a_f$.

It is important to note that in Majumdar and Maiya's damage rate model for fatigue [27] (see 2.50), the crack growth rate is proportional to some power of the inelastic strain amplitude with explicit crack length dependence, i.e.

$$\dot{a} \propto a \left(\frac{\Delta \epsilon^N}{2} \right)^m \qquad (4.17)$$

In other crack propagation models, for example [9] and [43], there is no "a" dependence proposed. For micro-crack propagation, the question then arises, is crack length dependence necessary in a fatigue damage model?

In the case of dependence only on $(\Delta \epsilon^N / 2)$, i.e. no "a" dependence, the assumption is made that far field inelastic strain amplitude (or stress amplitude) relates uniquely to the crack tip inelastic strain amplitude through a Neuber's Rule type of argument. However, for the case of even a short

crack, it is established that linear elastic fracture mechanics (LEFM) can apply, limited in accuracy, of course, by the anisotropic effects inherent to the case of crack length on the order of microstructural periodicities. However, the complete William's Series expansion for stress (and stress range) at a crack tip, as discussed by Carlson and Saxena [44], includes terms of higher order which become important for short cracks, i.e.

$$\sigma_{yy}(x,0) = K_I/\sqrt{2\pi x} + c\sqrt{x/a} + O(x^{3/2}) + \ldots \quad (4.18)$$

where, $\sigma_{yy}(x,0)$ = stress ahead of crack tip

K_I = stress intensity factor for Mode I (opening) fracture = $Y\sigma\sqrt{\pi a}$

x = distance from crack tip

c = constant

It is evident from this argument of crack length dependence of cyclic crack tip stress amplitude, and hence, inelastic strain amplitude, that a need is established for "a" dependence in a fatigue micro-crack growth law.

From equation (4.18), for x ≅ a and a ≅ D (where D is defined as the process zone size), the first two terms of the expansion can be of the same order of magnitude. Therefore, the stress field at a crack tip excluding the higher order terms of the William's Series expansion may be smaller in magnitude than if the complete series (i.e. higher

order terms included) was utilized. Furthermore, using the higher order terms in (4.18) results in an "a" dependence different from that if only the first term were used. If only the first term was considered, the crack length dependence would be defined by K_I. Since $K_I = Y\sigma\sqrt{\pi a}$, the dependence of crack length in the fatigue damage model would be,

$$\dot{a} \propto G(a^{1/2}) \qquad (4.19)$$

where G is some function of $a^{1/2}$.

If an erroneous attempt was made to use ΔK to correlate fatigue crack growth for constant amplitude and constant strain rate cycling, then,

$$\dot{a} \propto (\Delta K)^{2q} \propto a^q \qquad (4.20)$$

where q is a constant.

With the complete solution, the _influence_ of the higher order terms may be instantaneously thought of as contributing to a fictitious crack length in a ΔK expression such as (4.16),

$$\dot{a} \propto (\Delta K_h)^M \qquad (4.21)$$

where, $\Delta K_h = Y\Delta\sigma\sqrt{\pi(a+a_h)}$

a_h = correction for higher order terms

M = Paris Growth Law exponent

Equating expressions (4.20) and (4.21) for a constant stress range, $\Delta\sigma$,

$$(\Delta K_h)^M = (\Delta K)^{2q} \qquad (4.22)$$

which may be rewritten,

$$q = \frac{M}{2} \, (\log\Delta K_h / \log\Delta K) \qquad (4.23)$$

Since $\Delta K \leq \Delta K_h$ for $a_h \geq 0$, the bound results that $q \geq (M/2)$. Hence, this argument establishes not only a need for crack length dependence in the fatigue damage rate equation, but a nonlinear dependence governed by the exponent q (as shown in 4.20) for substructural crack propagation. It must also be noted that q can be variable; i.e. its value could depend on other state variables or indeed crack length itself. In fact, Carlson and Saxena have shown that the nature of the higher order terms is geometry dependent, so that a_h and ultimately q would also depend on geometry. However, this level of complexity will not be introduced in the present work, but we merely recognize that micro-crack length dependence differs from the dominant micro-crack case.

The preceding discussion was based upon the differences between the treatment of long and short cracks. Long cracks exhibit a "threshold" ΔK_{th} effect. This means that when a crack length is reached where influencing effects of the inelastic strain amplitude and stress amplitude at the crack

tip on the crack propagation rate (da/dN) reach a threshold level, propagation may successfully be correlated via LEFM techniques.

For short cracks, the crack tip $\Delta\sigma$-$\Delta\epsilon^N$ fields include higher order terms than the $x^{-1/2}$ singular solution; the dependence on crack length with $q \geq M/2$ reflects this. If the transition from micro-crack propagation to the Paris Growth Law regime were truely made, the nonlinear crack length exponent, q, would yield a simplistic "continuity" condition of $q = M/2$. However, threshold effects associated with the crack tip plastic strain range are incorporated via the relation $(\Delta\epsilon^N/2)^n$, where n may implicitly include micro-structural effects such as crack closure.

For the micro-crack regime of damage, a modification to the damage rate model discussed above is now presented :

$$\frac{1}{a^q} \frac{da}{dt} = A(\sigma)\left[1 + \alpha\ln\frac{D_C}{D_{CO}} + \beta\ln\frac{D_E}{D_{EO}}\right]|\dot{\epsilon}^N|^m\left(\frac{\Delta\epsilon^N}{2}\right)^n \qquad (4.24)$$

To prevent confusion on later integration of this model, the limits of integration on crack length in (4.24) range from crack nucleation length at the substructural level, $a = a_0$, to macro-crack initiation, $a = a_i$. The limits on time range from $t = 0$ (assuming immediate nucleation) to $t = t_i$.

Development of Fatigue-Environment Interaction Theory

Proposed in the fatigue continuum/damage rate model is an explicit coupling of environmental damage with a parabolic oxygen penetration equation. However, it is not known at this point whether such a coupling, as expressed in the $\beta \ln(D_E/D_{EO})$ term, will predict the environmental aspect of fatigue damage with the success of the $\alpha \ln(D_C/D_{CO})$ term for creep-fatigue interaction as demonstrated by Majumdar [27].

The pertinent question to be discussed is how can fatigue-environment interaction be characterized? Two aspects of environmental damage, as defined in terms of oxygen penetration, may be considered. The first is a discontinuous effect of oxygen penetration on damage. By this, it is meant that as a crack propagates, oxidation ahead of the crack tip reaches a threshold level where the crack instantaneously jumps along this environmentally attacked path. The second is a continuous effect of oxygen penetration on damage. This simply means that the micro-crack propagates in a continuous manner with a continuous buildup of an oxygen damaged path ahead of the crack tip. This study will focus on these two physical characterizations of fatigue-environmental damage interaction.

Discontinuous Environmental Effects on Fatigue

When considering the discontinuous effect of oxygen penetration on damage as described above, an attempt to model the discontinuity (i.e. crack "jumping" along an environmentally penetrated path) can be made through the use of a Dirac delta function as follows:

$$\frac{1}{a^q} \frac{da}{dt} = A(\sigma) \left[1 + \alpha \ln \frac{D_c}{D_{co}} \right] |\dot{\epsilon}^N|^m \left(\frac{\Delta \epsilon^N}{2} \right)^n + a^{-q} \sum_j \delta(t-t_{ox_j}) \, \beta(t)$$

(4.25)

where, β = function governing time-dependent diffusion of oxygen at the micro-crack tip

t_{ox_j} = time for oxidation penetration for j^{th} discrete crack growth event

Note that t_{ox_j} must be related to the satisfaction of some crack tip rupture criterion based on a combination of stress and oxidation penetration depth. With this expression the rate of fatigue damage is continuous until a time is reached when $t = t_{ox}$ and a critical depth of oxygen penetration causes an instantaneous jump in the crack length governed by the time-dependent function β.

Unfortunately, a discontinuous description of this nature contains inconsistencies. After each "jump" is encountered, the limits of integration of the rate equation must be altered to account for the instantaneous increase in

micro-crack length. This formulation would also lead to incorrect sequence effects (i.e. a low-high stress sequence would appear more damaging than a high-low stress sequence effect). This feature runs counter to observed physical observations of fatigue damage. It is therefore felt that a continuous damage growth mode dependent on environmental penetration is more mechanistically appealing. Even if cracks grow intermittently at the substructural level, as is sometimes observed, the assumption of a continuous growth law is consistent with the analogous treatment of intermittent macro-crack propagation at the structural or continuum level.

Continuous Environmental Effects on Fatigue

Rate-Type Effects Incorporated in $|\dot{\varepsilon}|^m$ Term.

A continuous effect of oxygen penetration on fatigue micro-crack propagation would allow for the environmental interaction initially considered explicitly in the $\beta \ln(D_E/D_{EO})$ term to be incorporated in the strain rate dependence of the damage rate model. In other words, the strain rate dependence can be considered as a combined description of strain rate and oxygen penetration damage. This could be viewed, for example, as a frequency modified approach [2]. At the outset, it should be noted that such an approach does not include explicit dependence on environmental penetration and, as such, is on somewhat weak

physical grounds.

For constant strain rate (here we do distinguish between inelastic and total strain rate), completely reversed cyclic deformation (no mean stress effects), integration of the damage rate model on the micro-crack scale yields the following :

$$\frac{1}{a_0^{q-1}} - \frac{1}{a^{q-1}} = A'(q-1)\,|\dot{\varepsilon}|^m\left(\frac{\Delta\varepsilon^N}{2}\right)^n \cdot t \qquad (4.26)$$

where, a_0, a = micro-crack nucleation length and current
micro-crack length, respectively

t = current time

A' = current value of $A(\sigma)$ for zero mean stress

Note that for symmetric cycling, the assumption is made that creep cavity growth does not occur. Therefore, the constant α in equation (4.13) has been set equal to zero.

In order to agree with the physics of the problem, the current crack length must be greater than the crack nucleation length. This means that the right side of the above equation must be positive - resulting in a lower bound for the exponent q of unity.

There are several ways to approximate values for the left side of the equality (4.26). First consider both a_0 and a_i to be constants. Considering the limits of integration of

equation (4.13) for crack length to be between $a = a_0$ and

$a = a_i$ (= macro-crack initiation length), and for time between

$t = 0$ and $t = t_i$, the resulting integration gives,

$$\frac{1}{a_0^{q-1}} - \frac{1}{a_i^{q-1}} = A'(q-1)\left|\dot{\epsilon}\right|^m\left(\frac{\Delta\epsilon^N}{2}\right)^n t_i \qquad (4.27)$$

Combining constants and taking the logarithm of both sides, the following equation results :

$$P = m \log\left|\dot{\epsilon}\right| + n \log\frac{\Delta\epsilon^N}{2} + \log t_i \qquad (4.28)$$

where P is a constant.

From this expression, the exponent n is readily determined for <u>constant values</u> of a_0, a_i, and strain rate. The quantity n is the negative inverse of the slope of the inelastic strain amplitude versus time to failure on a log scale. It was assumed that the propagation life was negligible compared to the total fatigue life, hence, $t_i = t_f$. The calculations for the strain rates used in the MAR-M 246 low cycle fatigue tests are shown in Figure 20; i.e. for $\dot{\epsilon} = 10^{-2}$ sec^{-1}, n = 1.04; for $\dot{\epsilon} = 10^{-3}$ sec^{-1}, n = 0.91; for $\dot{\epsilon} = 10^{-4}$ sec^{-1}, n = 1.13. The resulting average value of n is 1.03.

The resulting linearity of the data in Figure 20 lends credibility to the idea that the environmental effect on

fatigue damage is not, as originally proposed, based on a $\beta \ln(D_E/D_{EO})$ term in the damage rate equation (4.24). The form of equation (4.24) implies a nonlinear $\log(\Delta \epsilon^N/2)$ versus $\log t_f$ plot. Although the values of n are close, which means the $\log(\Delta \epsilon^N/2)$ versus $\log t_f$ curves are very nearly parallel, this observation is based on a small data set. Also note that the assumption of constant a_0 and a_i is indeed suspect. Further analysis of the oxygen penetration effect must be undertaken.

Maintaining the idea that a_0 is constant, a further classification of the left side of the equality in (4.26) concerns the value of the fatigue damage at the onset of macro-cracking; i.e. $a = a_i$. Initiation at this level may be expressed in terms of oxidation penetration depth,

$$\left(\frac{\Delta \sigma}{2}\right) l_i^{\ell} = C_1 \qquad (4.29)$$

Here ℓ and C_1 are constants and l_i is associated with the oxygen penetration depth resulting in crack formation at a critical stress amplitude level. Hence, this is a psuedo-fracture criterion. Values for the exponent ℓ of apporoximately 0.23 have been observed by Antolovich and Jayaraman [28] for several Ni-base alloys at elevated temperatures. For example, Rene 80 at 982°C and 871°C had values of ℓ of 0.21 and 0.23, respectively. Studies with

Rene 77 at 927°C and Nimonic 90 at 810°C resulted in values of 0.25 and 0.23 for ℓ, respectively.

Applying this result for macro-crack initiation in expression (4.27), assuming $l_i = a_i$, and using the cyclic stress-strain power law relation (see equation C.6) to rewrite the stress amplitude in terms of strain amplitude, the formulation becomes (assuming constant $|\dot{\epsilon}|$):

$$a_0^{(1-q)} - \left[\frac{C_1}{K'\left(\frac{\Delta\epsilon^N}{2}\right)^{n'}} \right]^{(1-q)/\ell} = (q-1)A' \, |\dot{\epsilon}|^m \left(\frac{\Delta\epsilon^N}{2}\right)^n t_i \quad (4.30)$$

where, K' = cyclic strength coefficient

n' = cyclic strain hardening exponent, and again,

a_0 is considered constant.

This characterization, no matter what values were chosen for the exponents q, ℓ, n', would not produce linear curves for the $\log(\Delta\epsilon^N/2)$ versus $\log t_f$ data at constant strain rates. Although a mechanical argument was enabled, this formulation does not reproduce aforementioned trends.

A third classification of the left side of equation (4.26) maintains the ideas developed above for macro-crack initiation and, in addition, presents a refinement to the assumption that crack nucleation is defined in terms of slip band spacing. This observation, as reported by Antolovich, Lerch, and others [46,47] is based on a relationship between

slip band spacing and plastic strain amplitude,

$$i = C_2 \left(\frac{\Delta \epsilon^P}{2} \right)^{-k} \qquad (4.31)$$

where, i = slip band spacing (stress-dependent)

C_2, k = constants

This formulation models the observed phenomenon of decreased slip band spacing for increased plastic strain amplitude. For Waspaloy (a wrought Ni-base superalloy) tested at room temperature in an air environment, values for C_3 and k were found to be 0.846 and 0.518 respectively [45].

Following the assumption that $i = a_0$ [46], the substitution of (4.31) into (4.30) using the inelastic strain amplitude, results in

$$C_2^{(1-q)} \left(\frac{\Delta \epsilon^N}{2} \right)^{-k(1-q)} - \left[\frac{C_1}{K' \left(\frac{\Delta \epsilon^N}{2} \right) n'} \right]^{(1-q)/\ell} = (q-1)A' \left| \dot{\epsilon} \right|^m \left(\frac{\Delta \epsilon^N}{2} \right)^n t_i \qquad (4.32)$$

and after rearranging constants and exponents,

$$C_2^{(1-q)} \left(\frac{\Delta \epsilon^N}{2} \right)^{-k(1-q)} - \frac{C_1}{K'}^{(1-q)/\ell} \left(\frac{\Delta \epsilon^N}{2} \right)^{-n'(1-q)/\ell} = (q-1)A' \left| \dot{\epsilon} \right|^m \left(\frac{\Delta \epsilon^N}{2} \right)^n t_i \qquad (4.33)$$

It is observed at this point that in order to produce constant slope curves for $\log(\Delta \epsilon^N/2)$ versus $\log t_f$ data, the

exponents on the strain amplitude on the left side of the equality (4.33) must be equal; i.e. $k(1-q) = n'(1-q)/\ell$. This produces a constraint based on micromechanical arguments, i.e.

$$k = \frac{n'}{\ell} \qquad (4.34)$$

Based on values of $k = 0.518$ and $\ell = 0.23$, a value for the cyclic strain hardening exponent is suggested as $n' = 0.12$. For the MAR-M 246 specimens tested, the average value for n' was equal to 0.18 (see Table 9a). This is within reasonable agreement with to $n' = 0.12$ produced by the above constraint, considering the amount of data available and the potential scatter therein.

Further Estimation of the Strain Amplitude Exponent

As mentioned, determinations of the exponent n were based on the assumption that the crack nucleation length and the macro-crack initiation length are constant at a given strain rate (see 4.28). With the consideration of the fatigue-environment couplings just discussed, it was determined to be more physically appealing to consider a_0 and a_i as dependent on inelastic strain amplitude. Therefore, the slopes of the $\log(\Delta\epsilon^N/2)$ versus $\log t_f$ curves do not define the value of n uniquely.

By taking the logarithm of both sides of equation (4.33) and incorporating the constraint $k = n'/\ell$, it is

observed that to produce linear $(\Delta\epsilon^{N}/2)$ versus t_f curves on a log-log scale,

$$-k(1-q) - n = N_{ave} \qquad (4.35)$$

where, N_{ave} = average value of the inverse of the slopes of parallel $\log(\Delta\epsilon^{N}/2)$ versus $\log t_f$ curves, which equals -1.03

Based on an average value of $n' = 0.18$ from the reduction of the low cycle fatigue data (to be discussed in a later section) and a value of 0.23 for the exponent ℓ, k is estimated to be $k = 0.78$. From the work of Shahinian [40], previously mentioned, the value of the Paris Growth Law exponent, M, for nickel-base superalloys was reported as $M = 3.5$. This would suggest a value for the exponent q of $q \geq M/2 \geq 1.75$ based on previous short crack arguments. With these calculations and using the minimum value of $q = 1.75$, an updated estimate of exponent n is given by,

$$n = -k(1-q) - N_{ave} = 1.62 \qquad (4.36)$$

Of course, n must be positive in order for expression (4.27) to make physical sense; i.e. increasing the inelastic strain amplitude increases the fatigue crack growth rate. This first order check is satisfied with the chosen value of q. As noted earlier, q can be dependent on oxygen penetration or other state variables and geometry.

Estimation of the Value of the Exponent m

From the $\log(\Delta\epsilon^N/2)$ versus $\log t_f$ curves, data for time to failure versus strain rate for a constant inelastic strain amplitude was obtained and plotted as shown in Figure 21. Again, taking the logarithm of both sides of (4.33) and considering the inelastic strain amplitude constant, the value of the strain rate exponent m was calculated from the inverse of the slopes shown in Figure 21. This was done at $(\Delta\epsilon^N/2) = 0.0060$ in/in and $(\Delta\epsilon^N/2) = 0.0009$ in/in, resulting in values of m = 0.94 and m = 0.98, respectively. This data corresponds to an average value of m = 0.96. It is important to note the closeness of the experimentally determined values for m to unity. This suggests a minimal strain rate dependence in the damage rate model; i.e. if the value of m was equal to unity, the explicit time-dependence found in the integrated form of the model (see 4.27) would cancel. This suggests that though this material, significantly rate-dependent at 900°C, experiences time-dependence of damage rate predominantly through environmental attack rather than rate-dependent plasticity effects. It is interesting that this conclusion may be drawn in the absence of vacuum tests eventhough such tests would be ultimately conclusive.

Environmental Effects Contained in Parabolic
Time-dependence

It is more physically appealing to include explicit dependence on environmental penetration than to assume that environmental interaction is implicitly contained in the strain rate dependence. Although a parabolic form of oxygen penetration is exhibited by many metals over some range of temperatures [48], it cannot be assumed that the fatigue crack growth rate equation (4.27) can be coupled with an explicit $t^{-1/2}$ dependence. Oxygen penetration is not necessarily related to crack propagation on a "one-to-one" basis; therefore, the time dependence describing environmental attack in the damage rate model may be expressed, in general, as

$$\frac{1}{a^q} \frac{da}{dt} = A(\sigma) \left(\frac{dC_{OX}}{dt}\right)^{-R} \left[1 + \alpha \ln \frac{D_c}{D_{co}}\right] |\dot{\epsilon}^N|^m \left(\frac{\Delta\epsilon^N}{2}\right)^n \tag{4.37}$$

where, C_{OX} = oxide concentration

R = constant

The expression (dC_{OX}/dt) is a description of the rate of build-up of oxidation; which is believed to be proportional to $t^{-1/2}$ (i.e. parabolic). At this point in the research program, it is not possible to determine further the nature of the environmental interaction in the fatigue

model. Future tests to be conducted in a vacuum environment will provide significant information as to the rate and severity of the oxidation process.

For completely reversed cycling at a constant strain rate and assuming, as in equation (4.33), that a_o and a_i are functions of $(\Delta\epsilon^N/2)$ and $(dC_{ox}/dt) \propto t^{-1/2}$, integrating (4.37) results in

$$G\left(\frac{\Delta\epsilon^N}{2}\right)^{-k(1-q)} = H\left(\frac{\Delta\epsilon^N}{2}\right)^n \cdot t_i^{\,1-R/2} \qquad (4.38)$$

where $\quad G = C_2^{\,(1-q)} - \left(\frac{C_1}{K'}\right)^{(1-q)/\ell} = $ constant

$$H = \frac{2(q-1)A'\,|\dot\epsilon|^m}{2-R} = \text{constant}$$

Taking the logarithms of both sides of equation (4.38), the following expression is obtained:

$$-k(1-q)\log\frac{\Delta\epsilon^N}{2} + \log G = \log H + n\cdot\log\frac{\Delta\epsilon^N}{2} + \left(\frac{2-R}{2}\right)\log t_i$$
$$(4.39)$$

Thus,

$$[-k(1-q)-n]\ \log\frac{\Delta\epsilon^N}{2} = \left(\frac{2-R}{2}\right)\log t_i + \text{constants}$$
$$(4.40)$$

Analogous to equation (4.35), in order to produce linear $(\Delta\epsilon^N/2)$ versus t_i curves on a log-log scale,

$$\frac{2[-k(1-q)-n]}{2-R} = N_{ave} \qquad (4.41)$$

where N_{ave} is, as before, the average value of the inverse of the slopes of the parallel $\log(\Delta\epsilon^N/2)$ versus $\log t_i$ curves (Re: $t_i = t_f$).

For tests performed in a vacuum environment at a constant strain rate, $R = 0$. This would result in the reduction of (4.41) to $-k(1-q)-n = N_{ave}$, which is identical to the result obtained by the assumption that all rate-type environmental effects are contained in the strain rate dependence. However, this expression allows for the determination of the exponent n once q is selected and k is specified. Recall that k may be determined from slip band measurements or from the constraint, $k = n'/\ell$, where $\ell = 0.23$.

For tests conducted at different, but uniform strain rates at a constant inelastic strain amplitude, taking the logarithm of both sides of equation (4.38) would yield the following:

$$K_1 = K_2 + m \log|\dot{\epsilon}| + \frac{2-R}{2} \log t_i \qquad (4.42)$$

where K_1 and K_2 are constants.

If N_R is defined as the slope of the $\log \epsilon$ versus $\log t_i$ curves (Figure 21), then

$$N_R = -2m/(2-R) \qquad (4.43)$$

Once q is selected (either as a constant such as q = M/2 or as a function of crack length and geometry), n is determined from vacuum test data. It follows that the exponent R is known from equation (4.41) and the exponent m is calculated with expression (4.43). Hence, the importance of conducting vacuum environment experiments to further characterize the parameters of the microcrack growth model is evident.

Metallographic Observations

Optical Microscopy

Following the procedures outlined in Chapter III, the tested MAR-M 246 specimens were sectioned and mounted (as shown in Figure 3) to facilitate a study of the micro-structure and failure characteristics of the superalloy.

From the samples sectioned horizontally, below the fracture surface, the grains were large enough to be discerned with the naked eye, on the order of millimeters in length for the longest dimension. The grains were radially elongated from the center of the specimen with an aspect ratio (length : height and width) of approximately 6:1. The shape and orientation of the grain structure is a direct consequence of the casting process. Non-uniform cooling of the molten material (i.e. surface solidifying before the core) produced the radial pattern described above. The relative size and shape of the grain structure can be seen

in Figure 23. (Note that this is a specimen sectioned
vertically through the fracture surface.)

Apparent in Figure 23 is evidence that specimen failure
occurred via intergranular primary cracking. All the samples
examined demonstrated this intergranular mode of failure. A
second example is shown in Figure 24. The overall
characteristics of the fracture surfaces will be described
in the next section.

Also observed on the longitudinally sectioned samples
was a varied amount of secondary cracking (see Figures 24
and 25). For the majority of the secondary cracks optically
inspected, initiation occurred at a grain boundary. This can
be explained in terms of environmental attack, i.e.
oxidation penetration along a grain boundary. As was
presented in equation (4.29), initiation of a macrocrack may
be expressed in terms of oxidation penetration depth,

$$\left(\frac{\Delta\sigma}{2}\right){l_i}^{\ell} = C_i$$

Assuming parabolic oxidation kinetics, Antolovich and
Jayaraman [28] proposed a model that relates the depth of an
oxide spike to the time of the test,

$$\frac{l_i}{{l_i}^{o}} = \left[\frac{t_{ci}}{{t_{ci}}^{o}}\right]^{1/2} \qquad (4.44)$$

where ${l_i}^{o}$ = initiation crack length for shortest test

l_i = oxygen penetration at initiation

t_{ci}° = time for shortest test

t_{ci} = time for crack initiation

For purposes of developing a correlation, l_i° is set equal to unity. Hence, the value of l_i can be calculated relative to the shortest test. Using time to failure data, the relative assumed oxide depth, l_i, was calculated using this parabolic relation. Then, these computed values were plotted against stress amplitude (log scale) as shown in Figure 22. From a linear regression of this data, the value of the exponent l in equation (4.29) was determined to be 0.19. The average value for l in the study by Antolovich and Jayaraman [28] was, as disussed previously, 0.23. Thus the assumption of parabolic oxidation kinetics is supported by the relative agreement of these results. It must be noted, however, that an appreciable amount of scatter exists in the MAR-M 246 stress amplitude versus relative oxide depth data; this must be taken into consideration when choosing a value of the exponent l in further computations. It is due to this uncertainty that the average value of $l = 0.23$, based on a relatively large data set, was incorporated into the fatigue characterization analysis (equations 4.29 to 4.36).

SEM : Fracture Surface Observations

Several specimens were prepared for analysis with the scanning electron microscope (SEM) as outlined in Chapter III. Immediately apparent, without magnification, was a radial pattern on all of the fracture surfaces. This pattern, also seen in the sub-fracture surface optical micograph specimens, suggests further evidence of an intergranular crack path. An example of this type of fracture is shown in Figure 26; which shows a grain partially dislocated at the edge of the fracture surface. This specimen (G-12) was tested at a high strain rate (10^{-2} sec^{-1}) and high strain amplitude (1.0%). Unfortunately, particular primary crack initiation sites were not determined due to the heavily oxidized condition of the fracture surfaces. Only general trends and features of the surfaces were discernable.

Although the radial characteristic was evident in all of the fracture surfaces, those specimens tested under conditions which led to relatively long cycling times produced somewhat less-featured fracture patterns. One example is shown in Figure 27. This specimen (G-4) was tested at a strain rate of 10^{-4} sec^{-1} and a strain amplitude of 0.4%; resulting in a time-per-cycle of 160 seconds. The duration of this cycle allowed for a great deal of time-dependent deformation, producing relatively smooth wave

fronts of inelastic deformation on parts of the fracture surface.

For all SEM-observed specimens, secondary cracking and slip band traces were present. The greatest degree of secondary cracking was observed on specimen G-12 (Figure 28); which was a high strain rate / high strain amplitude test. Tested at the same strain amplitude (1.0%) but at a lower strain rate (10^{-4} sec^{-1} versus 10^{-2} sec^{-1}), specimen G10 (Figure 29) produced a high intensity of slip bands but the secondary cracks were not as pronounced as those in specimen G-12. This fact can be attributed to the longer cycle time for specimen G-10; i.e. the "longer" test resulted in a greater degree of grain boundary oxidation and thus, smaller secondary crack openings prior to failure. At this amplitude it must be noted that the secondary cracking observed in these two specimens occurred along grain boundaries which ran parallel (Figure 28) and perpendicular (Figure 29) to the slip bands.

Along similar lines of discussion, specimen G-4, with a low strain rate (10^{-4} sec^{-1}) and a low strain amplitude (0.4%), did not produce as intense a degree of slip bands or secondary cracking as was observed in other specimens. However, the secondary cracks present were larger in magnitude, on average, than those of other specimens. The relatively long cycle time (160 seconds), as discussed

above, allowed for a considerable amount of deformation before failure. Figure 30 shows a large secondary crack produced along a grain boundary with intersecting slip bands (triple point) just below the fracture surface; which is visible at the top of the photograph.

Although less-featured and containing fewer slip band traces, specimen G-22 ($\dot{\epsilon} = 10^{-2}$ sec^{-1}, $\Delta\epsilon/2 = 0.4\%$) exhibited a considerable amount of secondary cracking. It was observed that, as with all other analyzed specimens, the secondary cracks led right up to the fracture surface. Also in accordance with previous observations, a large percentage of the secondary cracks formed at or along oxidized grain boundaries (see also Figure 31). The overall condition of the fracture surfaces and the location and intensity of the secondary cracks points towards the strong influence of environmental attack (i.e. grain boundary oxidation) of the MAR-M 246 low cycle fatigue specimens tested in a laboratory air environment at 900°C.

The SEM studies revealed that higher plastic strain ranges and rates lead to intense slip band traces at the surface and produce significant secondary cracking on intersecting grain boundaries. Lower strain amplitudes and rates lead to more time-dependent deformation. In all cases, the fatal crack appears to initiate and propagate in an intergranular fashion.

CHAPTER V

CONCLUSIONS AND INDICATIONS

The present study examined the feasibility of and developed the background for the formation of a thermomechanical fatigue model applicable to nickel-base superalloys. Through the use of a continuum damage approach and a modified damage rate method, some of the effects of creep, low cycle fatigue, and environment (along with interactions) were examined for cast MAR-M 246. Although the tests and analysis were performed at a single, elevated temperature, the initial investigation provided the framework for future development of a nonisothermal fatigue model.

Creep Damage Correlation

The Continuum Damage Approach, as detailed by Chaboche et al. [24], modeled creep damage accumulation with a relatively high degree of success; based on the limited amount of creep data generated. Methods for determining the parameters of the creep damage equation were established; eventhough the actual results are suspect due to the estricted data set. Two additional creep tests were repeated, after the initial numerical analysis was completed, under identical conditions as the original

constant stress tests in an attempt to estimate the scatter
in the creep rupture time data. The reduction of the
additional data suggested a value for the exponent on
stress, r, of r = 6.61 instead of r = 5.76 based on the
original two tests. Both of these results are close to those
obtained by Chaboche and associates [49] for IN 100 tested
at 900°C (r = 6.3) and at 1000°C (r = 5.2).

Obviously, additional creep tests will provide
increased accuracy and statistical support for the
determination of the creep model parameters. In addition,
detailed metallurgical examination of void growth would
yield a primary check to the numerical methods outlined
here.

Fatigue-Environment Characterization

Although it is not possible to rigorously quantify the
environmental effects on fatigue damage in the elevated
temperature testing of MAR-M 246 without performing
comparative tests in a vacuum environment, the analysis of
the existing low cycle fatigue and tensile data produced
several interesting findings.

First of all, based on short crack considerations, a
need for a nonlinear crack length dependence, i.e. the
$(1/a^q)$ term, in the fatigue crack growth law was established
for substructural crack propagation. However, the
determination of the value for this exponent for MAR-M 246

remained somewhat arbitrary due to the fact q may be variable and even geometry-dependent. Short crack considerations produced a lower bound for this parameter $(q \geq M/2)$ which was used in subsequent anayses.

Although a continuous environmental effect on fatigue damage where all rate-type effects are incorporated in the strain rate dependence of the micro-crack growth model did not include explicit dependence on environmental penetration, the considerations employed in its analysis provided a means for applying established micromechanical relationships to the hybrid damage rate model. Relationships between inelastic strain amplitude and slip band spacing and between stress amplitude and oxygen penetration depth were used for assumptions of crack nucleation length and macro-crack initiation length respectively. The resulting manipulations of the crack propagation model provided a method for estimating the values of the exponents n and m in the model based on the $(\Delta\epsilon^N/2)$ versus t_i data. Important to the determination of n and m was the development of the constraint, $k = n'/\ell$, which resulted from the micromechanical arguments mentioned above.

Of course, it is was more physically appealing to include an explicit dependence on environmental damage. An analysis was conducted assuming a parabolic-type oxygen penetration process in the crack growth model; i.e. $a \propto t^{-R/2}$

term was included. It was discovered the parameters of the model (n,m,R) could be determined from the comparison of the $(\Delta\epsilon^N/2)$ versus t_i curves for vacuum versus non-vacuum fatigue test data. The procedure for performing these computations was outlined and discussed.

It must be noted that the groundwork for the nonisothermal crack initiation model developed in this report does not include any physical investigation of creep-fatigue interaction. It is important for further improvement of the hybrid Damage Rate/Continuum Damage model that the confirmation of the creep-fatigue interaction proposed first by Majumdar and Maiya [27] (and adopted and modified in this study) be carried out. Experiments which combine fatigue with hold times should be undertaken to investigate the creep-fatigue characteristics of the MAR-M 246 superalloy and to determine the preictive capability of the crack growth model.

APPENDIX A

MECHANICAL TESTING PROCEDURE

Extensometry

Creep Testing

The apparatus used in the creep investigation was an ATS four arm extensometer for high temperature service. Four arms are used (two on both the top and bottom knife-edge brackets) to ensure completely vertical travel. Outside the furnace, a caliper was mounted to the extensomter for zeroing of the ATS capacitance gauge - also mounted outside of the furnace. The capacitance gauge has a resolution of $1x10^{-5}$ inches (0.01%) for a maximum amplified output of ten volts. This maximum reading, conditioned by a capacitance amplifier, corresponds to 0.2" of displacement.

A set of split-ring adapters were used to convert the 0.75" diameter specimen clamps to the 0.25" diameter gage section of the specimen. Since LCF type button-head specimens were used, a set of MAR-M 246 specimen adapters were required to attach the test sample to the 0.75" diameter pull rods. The pull rods attached to the adapters were also fabricated out of MAR-M 246 to ensure proper performance of the mechanical system at the operating temperature of 900°C.

Tensile and LCF Testing

The extensometer is extremely important in strain controlled testing. The extensometer used for the tensile and low cycle fatigue program was based on a modification of an MTS Model 632.11 clip gauge for isothermal high temperature application. The extensometer consisted of two 0.25" diameter alumina rods 3.5" in length connected to two 0.25" diameter stainless steel tubing (also 3.5" in length) split at one end to accomodate the rods. At the connection point, a Teflon hinge was clamped to secure the tube/rod joint and to provide flexure to the apparatus. Rectangular aluminum blocks with groves on one side and cyclindical plugs on the other were used for attachment between the clip gauge and the pivoting arms. The plugs were glued into the other ends of the stainless steel tubing and the knife edges on the clip gauge were fit into the grooves on the other side of the aluminum blocks. The knife-edges were held secure to the pivot arms by spring attachments. The opposite ends of the alumina rods were ground to a sharp wedge point using a diamond faced wheel. A bored and half-split aluminum block was clamped by a set screw to each alumina rod approximately 1.5" from the tips.

The complete extensometer assembly was suspended from a column of the load frame using an aluminum bracket with two pulleys. A counter-weight was tied to one end of a thread

and draped over the pulleys for connection to a wire loop at the center of gravity on the extensmeter. The alumina tips were held against the gage section of the specimen using a bracket on the opposite column of the load frame. On this bracket, two spring with glass hook assemblies were drawn in tension and hooked to looped wires secured to the aluminum half-split blocks described above. Spring tension was adjustable via a sliding action of the second bracket.

The calibration of the modified extensometer was accomplished with a precision INSTRON extensometer micrometer calibrator. After recording voltage output as a function of strain (compressive and tensile) as dictated by the micrometer, linear regression was performed on the data to determine the calibration correction for the MTS stain control electronics.

Data Aquisition and Reduction : Tensile and LCF Testing

Data aquisition for the tensile and low cycle fatigue testing was achieved with a NICOLET Model 2090:2B digital recording oscilloscope. Digitized strain gauge and load cell output voltages were written to floppy disks for processing. Digital data files for time versus load and time versus strain were converted to ASCII data via an S-CUBED 2090 access card installed in an IBM AT computer. This equipment was supported by a digital data processor software package, also manufactured by S-CUBED, named "Vu-Point". Basic

programs were used to convert and collate the separate data files to produce stress versus strain data - in a proper format for plotting.

In addition to the digital oscilloscope, a hardcopy X-Y recorder was used to produce hysteresis curves as backup to the NICOLET data. A strip-chart recorder was also facilitated to record load versus time data. This was especially useful when crack growth was initiated since the "load" would drop in magnitude, thus signaling imminent failure of the specimen.

APPENDIX B

Guide to Creep Analysis Numerical Procedures

Procedure I : Estimation of constants D_{INT}, B, $k(\sigma_{HI})$, and $k(\sigma_{LOW})$

STEP 1: Choose a value of D_{INT}. Based on studies of IN 100, the value of D_{INT} should be in the proximity of .10.

STEP 2: Choose a value for B.

STEP 3: With solutions to the creep continuum damage equation based on the constant stress 413 MPa test and the 300 MPa test, determine $k(\sigma_{HI})$ and $k(\sigma_{LOW})$ respectively, using equations (4.8) and (4.9).

STEP 4: Use the values of D_{INT}, B, $k(\sigma_{HI})$, and $k(\sigma_{LOW})$ determined in steps 1-3 in an iterative solution to the continuum damage equation based on the step stress sequence test. Use equations (4.7a) and (4.7b).

STEP 5: If the solution to STEP 4 converges for $k(\sigma_{HI})$ slightly greater than $k(\sigma_{LOW})$, go to STEP 6; else, return to STEP 2 and alter the value of B.

STEP 6: The values of B, $k(\sigma_{HI})$, and $k(\sigma_{LOW})$ are determined

for the value of D_{INT} chosen in STEP 1. These

results are recorded in Table 6. Use these results

of D_{INT} and B a final time in equations (4.8) and

(4.9) to determine a further estimation of $k(\sigma_{HI})$ and

$k(\sigma_{LOW})$ - also recorded (in parentheses) in Table 6.

STEP 7: Return to STEP 1 and repeat the process for another

value of D_{INT}.

Procedure II : Numerical solution to the coupled strain/damage

equations for two constant stress creep tests.

STEP 1: Numerically solve the set of two, nonlinear,

coupled differential equations (4.3) and (4.11) for

the higher stressed creep test. Use the most reason

-able value for $k(\sigma_{HI})$, and the corresponding value

of B from Table 6. Choose a value for ν.

STEP 2: Alter the value of B until the value of the creep

damage parameter, D, is equal to unity at the

experimental rupture time of the high stress level

test.

STEP 3: Without changing the parameter B, alter the value of ν until the numerical solution to nominal strain at rupture equals the experimental result.

STEP 4: Adjust the values of A and/or n from the results of equation (4.1) to improve the closeness of the numerical/experimental nominal creep strain data. This is done graphically; i.e. refer to Figure 6.

STEP 5: Using the values of B, A, n, and ν determined in steps 1-4, numerically solve equations (4.3) and (4.11) for the lower stressed creep test. Initially, use the value of $k(\sigma_{HI})$ as a first approximation to $k(\sigma_{LOW})$.

STEP 6: Do not change the value of B, but instead alter the value of $k(\sigma_{LOW})$ until D = 1 at the experimental time to rupture of the low stress level test.

STEP 7: Do not alter ν, but attempt to improve numerical and experimental correlation by changing the value of A.

(Results to these numercal solutions are shown in Figures 6 and 7 and in Table 7.)

APPENDIX C

TENSILE AND LCF RESULTS

Data Organization

All low cycle fatigue test data is shown in Table 5. Cyclically stable hysteresis loops for each strain amplitude at each strain rate tested are shown in Figures 11, 12, and 13. As described in Appendix A, stress-strain data was aquired via a digital recording oscilloscope. With this equipment, approximately 500 to 1000 data points were recorded per cycle (depending on the time-per-cycle for a given test and the available time-per-point sweep times on the oscilloscope). Observed in some instances, a low amplitude high frequency electrical signal was present in the test equipment electronics. In an attempt to reduce the noise in the stress-strain data, a five-point averaging of the data sets was performed during data reduction. The result of this procedure is shown in Figure 9. Note how the averaged data set represents the character of the hysteresis loop quite closely.

The data for the five tensile tests performed are shown in Figure 10 and the tensile properties are given in Table 4. Note that for the 10^{-3} $\sec^{-1}$ strain rate test, failure did not occur before unloading the specimen after 5% strain was

reached. The same procedures for "smoothing" the data with a five point averaging technique, as was performed on the LCF data, was carried out in this case as well.

Coffin-Manson Fatigue Life Behavior

Although the intention of this study was not to develop Coffin-Manson data, the low cycle fatigue data is presented in this form as a matter of convenience of comparison to other materials. Please note that in the MAR-M 246 data reduction, inelastic strain was used in all analyses; no attempts were made to remove creep strains from the fatigue data.

The inelastic strain amplitude may be related to fatigue life by the familiar expression,

$$\frac{\Delta\epsilon^N}{2} = \epsilon_f{}'(2N_f)^c \qquad (C.1)$$

where, $(\Delta\epsilon^N/2)$ = inelastic strain amplitude

$2N_f$ = number of reversals to failure

$\epsilon_f{}'$ = fatigue ductility coefficient

c = fatigue ductility exponent

The $(\Delta\epsilon^N/2)$ data points were determined from the relation,

$$\frac{\Delta\epsilon^N}{2} = \frac{\Delta\epsilon}{2} - \frac{\Delta\sigma}{2E} \qquad (C.2)$$

where the total strain amplitude and the stress amplitude

were determined directly from the hysteresis loop data. The value for the Young's Modulus, E, used here was the average value of those determined from each of the tensile tests (see Table 4). The linear regression of this data on a log-log basis is shown in Figure 14, and the resulting values for the parameters ϵ_f' and c are listed in Table 8 for each strain rate employed. An error analysis was not considered meaningful for this analysis (or for the other fatigue-life relationships) due to the limited number of data points obtained.

It is important to note that the use of this type of argument to explain fatigue behavior is clearly inappropriate. Plasticity varies continually throughout the life of a fatigue test and never stabilizes except in terms of the "rate" of increase. There is more contributing to fatigue damage (especially at elevated temperature) than inelastic strain, and this is in large, environment.

Life was also plotted and correlated against stress amplitude (Figure 15) and total strain amplitude (Figures 16, 17, and 18) for each strain rate using the following respective relations :

$$\frac{\Delta\sigma}{2} = \sigma_f' (2N_f)^b \qquad\qquad (C.3)$$

$$\frac{\Delta\epsilon}{2} = \frac{\sigma_f'}{E} (2N_f)^b + \epsilon_f' (2N_f)^c \qquad\qquad (C.4)$$

where, σ_f' = fatigue strength coefficient

b = fatigue strength exponent

E = average Young's Modulus = 145.5 GPa

The resulting parameters, σ_f' and b, for the stress amplitude versus fatigue life correlations are presented in Table 8. Note that in determining the total strain amplitude versus life curves, the average value of Young's Modulus was again used. The data represented by the solid line in the total strain versus life curves was generated from expression (C.4) with the parameters determined and recorded in Table 8. The lines represent approximately 100 data points each. The sets of three data points also on these curves were determined directly from the hysteresis loops themselves (see Table 5).

Monotonic and Cyclic Stress-Strain Behavior

The tensile behavior of the MAR-M 246 specimens may be described, from the onset of yielding to the ultimate load, by the stress-strain relation,

$$\sigma = K(\epsilon^N)^n \qquad (C.5)$$

where K is defined as the strength coefficient and n is the strain hardening exponent. These parameters were determined by a simple linear regression of the tensile data (stress versus inelastic strain up to the U.T.S) on a log-log scale.

The results are listed in Table 4.

The cyclic stress-strain behavior may be described similarly by the relation,

$$\Delta\sigma/2 = K'(\Delta\epsilon^N/2)^{n'} \qquad\qquad (C.6)$$

where K' is the cyclic strength coefficient and n' is the cyclic hardening exponent.

Two approaches were utilized for determining the parameters of equation (C.6) from stablized hysteresis loop data (see Figures 11-13). The first method used the hysteresis loop "shape". By this it is meant that a new coordinate system was set up at the lower (compressive) tip of a hysteresis loop for a given strain rate. Stress and inelastic strain data points were taken along the hystersis loop, measured relative to the new coordinate system's origin. These points defined a monotonic-type curve with stress-inelastic strain magnitudes double that of a similar tensile test. The data (divided by two) was then fit using a linear regression on a log scale to determine K' and n'. The calculations, performed at each strain rate, are shown in Figure 19a and the results are listed in Table 9a.

The second approach for determining K' and n' was accomplished by using the hysteresis loop tips. For a given strain rate, the tips of the stable hysteresis loops (tensile side) at each tested strain amplitude were fitted

on a log scale with a linear regression technique. These calculations are shown in Figure 19b and the results are given in Table 9b. When comparing the results of the two determinations of K' and n', it is important to note that the latter described calculations are based on a relatively small number of hysteresis loop tips and, hence, this procedure has a much lower confidence level that using the hysteresis loop shapes.

It is important to observe that the values of n' are greater than the values of n at each tested strain rate. This would imply that the MAR-M 246 specimens cyclically harden. This characterization is supported by the hysteresis loop data, although not to the degree suggested by the relative difference in the values mentioned above. The fatigue tested MAR-M 246 specimens demonstrated a small amount of cyclic hardening before cyclic stability was achieved relatively early in the fatigue life (i.e. well before the half-life of the specimens).

APPENDIX D

COMPUTER PROGRAMS

Program I : CREEPFIT.FOR

This FORTRAN program was developed to perform a Gauss-Seidel iteration of two equations derived from the creep damage rate equation. The number of iterations was variable. Constants D_{INT} and B were entered on-line. Constants $k(\sigma_{HI})$ and $k(\sigma_{LOW})$ were estimated via the iteration process initiated with guesses derived from two special-case solutions to the creep damage rate eqution (as explained in Chapter IV).

Program II : CREEPDE.FOR

This FORTRAN program was written to solve a set of two first order differential equations using a fourth order Runge-Kutta method. The equations themselves were used in functions - allowing for easy alteration. The application of the process to the creep strain rate and creep damage rate equations is outlined in the program documentation. The step size was adjusted in order to produce fifty data points of time versus creep strain and creep damage.

```
C Program : "CREEPIT.FOR"
C
C Program to perform a Gauss-Seidel iteration to solve two coupled
C non-linear equations to roughly determine acceptable ranges of four
C of the creep characterization parameters ( B, Dint, k(hi), k(low) ).
C
      IMPLICIT REAL(A-M,O-Z)
      INTEGER N
      DOUBLE PRECISION D,B,KHI,KLOW,C1,C2,C3,C4,XMPA
C
      PRINT *,'Enter initial guess for B and Dint :'
      READ *, B,D
C
      PRINT *,'Enter maximum number of iterations :'
      READ *, N
C
C Stresses are converted to MPa in this analysis.
C
      XMPA   = 6.895
      SIGHI  = 60.20*XMPA
      SIGLOW = 43.42*XMPA
C
C Time to failure of the creep tests.
C
      TRLOW     = 174.7
      TRHI      =  27.3
C
C Times of interupted creep test.
C
      TINTHI    =  13.8
      TINTLOW   = 140.0
C
C Calculate equation constants.
C
      R  = 5.76
      C1 = SIGHI**R  * TRHI
      C2 = SIGLOW**R * TRLOW
      C3 = SIGHI**R  * TINTHI
      C4 = SIGLOW**R * TINTLOW
C
C "Solve" equations for the non-interupted tests to obtain
C a first guess for parameters in the interupted equation analysis.
C
      KHI  = 1./(C1*B) - 1.
      KLOW = 1./(C2*B) - 1.
      PRINT *,'K(hi) implicit =',KHI
      PRINT *,'K(low)implicit =',KLOW
      PRINT *
C
```

```
C Iterate on the other two equations using the implicit
C calculations as a first guess.
C
      DO 10 I=1,N
         KHI  = (1.-(1.-D)**(KHI+1.))/(B*C3) - 1.
         KLOW = (1.-D)**(KLOW+1.)/(B*C4) - 1.
         PRINT *,'N =',I
         PRINT *,'K(hi) =',KHI
         PRINT *,'K(low)=',KLOW
   10    CONTINUE
C
      STOP
      END
```

```
C PROGRAM : "CREEPDE.FOR"
C
C Program to solve a 2 x 2 system of first order, non-linear differential
C equations using the fourth order Runge-Kutta method.
C
C The purpose of this program is to numerically fit experimental data
C from two creep tests (a high stress level test and a low stress level test)
C with a Creep Damage Rate equation coupled with a Creep Strain Rate equation.
C
C FITTING STRATEDGY :
C          1). The constants B and k in the Damage Rate Equation are manipulated
C              to produce a creep damage parameter of 1.0 at failure.
C          2). The non-linear creep parameter "NU" is adjusted until failure
C              occurs at the experimental value of e(failure).
C          3). The creep strain rate equation amplitude constant A is adjusted
C              to improve the analytical/numerical correlation. Close correlation
C              is stressed in the lower creep strain range.
C
C Results (time, creep strain, creep damage parameter) are written to FOR011.DAT
C
      IMPLICIT REAL (A-H,K-Z)
      INTEGER I,J
      DIMENSION YN(2),K0(2),K1(2),K2(2),K3(2)
      COMMON /BLK1/ NU
      COMMON /BLK2/ SIGMA
      COMMON /BLK3/ K,B
C
      PRINT *,'Enter stress level in ksi (59.96 or 43.46)...'
      READ *, STRESS
C
```

```
C Stress level is converted and used in Pascals in this analysis.
C
      STRESS = 59.96
      SIGMA = STRESS*6.895
C
      PRINT *,'Enter value for k(sigma)    :'
      READ *, K
      PRINT *,'Enter amplitude parameter B :'
      READ *, B
C
      PRINT *,'Enter guess for nu...'
      READ *, NU
C
C Set the step size.
C
      PRINT *,'Enter time to rupture of test (hours) :'
      READ *, DUR
      PRINT *,'Choose the number of points to be calculated :'
      READ *, STEPS
      H = (DUR-2.)/STEPS
C
C For both creep tests, secondary creep initiated at approximately two hours.
C Thus, t=2 is the "initial" time.
C
      T = 2.0


C Initial values:
C     For sigma = 60.0 ksi --> e(initial) = 0.00814 in/in.
C     For sigma = 43.5 ksi --> e(initial) = 0.00519 in/in.
C
      IF(SIGMA.EQ.59.96) YN(1) = 0.00814
      IF(SIGMA.EQ.43.46) YN(1) = 0.00519
      YN(2) = 0.0
C
C Open file to place data.
C
      OPEN(UNIT=11,STATUS='NEW')
C
C In "stepping" loop, increment time and place previous values
C of y1,y2 into the variables : Y1 , Y2 respectively.
C NOTE : Y1 -> Strain     Y2 -> Damage Parameter
C
      DO 20 I=1,NINT(STEPS)
         T  = T + H
         Y1 = YN(1)
         Y2 = YN(2)
C
         K0(1) = H*F(Y2)
         K0(2) = H*G(Y2)
C
```

```
        K1(1) - H*F(Y2+.5*K0(2))
        K1(2) - H*G(Y2+.5*K0(2))
C
        K2(1) - H*F(Y2+.5*K1(2))
        K2(2) - H*G(Y2+.5*K1(2))
C
        K3(1) - H*F(Y2+K2(2))
        K3(2) - H*G(Y2+K2(2))
C
        WRITE(11,*) ' '
        WRITE(11,*) 'Time -',T,' hours'
        DO 10 J-1,2
          YN(J) - YN(J) + (K0(J)+2.*(K1(J)+K2(J))+K3(J))/6.
          IF(J.EQ.1)THEN
            WRITE(11,*) 'e -',YN(1)
          ELSE
            WRITE(11,*) 'D -',YN(2)
          ENDIF
   10     CONTINUE
   20   CONTINUE
        CLOSE(UNIT-11)
        STOP
        END
C-------------------------------------------------------------
C Make the equations "FUNCTIONS".
C *  CREEP STRAIN RATE EQUATION  *
C
        REAL FUNCTION F(Y2)
        REAL Y2,A,SIGMA,XN,NU
        COMMON /BLK1/ NU
        COMMON /BLK2/ SIGMA
        A - 2.80E-21
        XN - 6.66
        F - A*SIGMA**XN * (1.-Y2)**(-NU)
        RETURN
        END
C
C *  CREEP DAMAGE PARAMETER EQUATION  *
C
        REAL FUNCTION G(Y2)
        REAL Y2,SIGMA,K,R,B
        COMMON /BLK2/ SIGMA
        COMMON /BLK3/ K,B
C
        IF(K.EQ.0.0)THEN
          PRINT *,'ERROR IN K'
        ENDIF
        R - 5.76
        G - B*SIGMA**R * (1.-Y2)**(-K)
        RETURN
        END
```

BIBLIOGRAPHY

1. Ross, E. W. and Sims, C. T.,"Nikel-Base Alloys,"
   Superalloys II, Sims, C. T., Stoloff, N. S., and Hagel,
   W. C., eds., John Wiley & Sons, N.Y., 1987, pp. 293-326.

2. Coffin, L. F.,"Fatigue at High Temperatures - Prediction
   and Interpretation," Proc. Inst. Mech. Eng., Vol. 188,
   1974.

3. Chaboche, J. L., Policella, H., and Kaczmarek, H.,
   "Applicability of the SRP Method and Creep-Fatigue Damage
   Approach to the LCHTF Life Prediction of IN 100 Alloy",
   AGARD SMP-243 Meeting on Strain Range Partitioning, April
   11-12, 1978, Aalborg, T. P. ONERA 1978 - 13.

4. Chaboche, J. L.,"Life Prediction in Structures: Present
   State of the Art and Future Trends," ONERA Conference
   invitee aux Journees Internationales de Printemps
   "Fatigue a Haute Temperature", Societe Francaise de
   Metallurgie, Paris, June 10-11, 1986.

5. Robinson, E. L., "Effect of Temperature Variation on the
   Creep Strength of Steels," Trans. ASME, Vol. 60, 1938,
   pp. 253-259.

6. Freeman, J. W., and Voorhees, H. R., "Creep Damage in
   Metals," ASTM, STP 391, 1965.

7. Code Case N-47, ASME Boiler and Pressure Vessel Code,
   ASME, New York, 1974.

8. Skelton, R. P., "The Prediction of Crack Growth Rates
   from Total Endurances in High Strain Fatigue," Fatigue of
   Engineering Materials and Structures, Vol. 2, 1979, p. 305

9. Wareing, J., "Creep-Fatigue Interaction in Austenitic
   Stainless Steels," Metallurgical Transactions, Vol. 8A
   (1977), pp. 711-721.

10. Plumbridge, W. J., Dean, M. S., and Miller, D. A.,"The
    Importance of Failure Mode in Fatigue-Creep Interactions,"
    Fatigue of Enginerring Materials and Structures, Vol. 5,
    No. 1 (1982), pp. 101-114.

11. Miller, D. A., Hamm, C. D., and Phillips, J. L., "A Mechanistic Approach to the Prediction of Creep-Dominated Failure During Simultaneous Creep-Fatigue," Materials Science and Engineering, Vol. 53, 1982, pp. 233-244.

12. Hirschberg, M. H., and Halford, G. R., "Strain Range Partitioning - A Tool for Characterizing High Temperature Low Cycle Fatigue," NASA TM X-71691, 1975.

13. Manson, S. S., "The Challenge to Unify Treatment of High Temperature Fatigue - A Partisan Proposal Based on Strain Range Partitioning," Fatigue at Elevated Temperatures, ASTM STP 520, 1973, pp. 744-782.

14. Manson, S. S., Halford, G. R., amd Hirschberg, M. H., "Creep-Fatigue Analysis by Strain Range Partitioning," NASA TM X-67838, 1971.

15. Saltsman, J. F., and Halford, G. R., "Strain Range Partitioning Life Predictions of the Long Time Metal Properties Council Creep-Fatigue Tests," Proc. Winter Annual Meeting of ASME, Dec. 2-7, 1979, pp. 101-132.

16. Coffin, L. F., "A Review of Fatigue Predictive Methods in the Regime Where Inelastic Strains Dominate," Proc. Winter Annual Meeting of ASME, Dec. 2-7, 1979, pp.1-24.

17. Coffin, L. F.,"Overview of Temperature and Environmental Effects on Fatigue of Structural Metals," Fatigue: Environment and Temperature Effects, J. J. Burke and V. Weiss, eds., Plenum Press, N.Y., 1983, pp. 1-40.

18. Ostergren, W. J., "A Damage Function and Associated Failure Equations for Predicting Hold Time and Frequency Effects in Elevated Temperature Low Cycle Fatigue," Jour. of Testing and Evaluation, Vol. 4, 1976, pp. 327-339.

19. Kachanov, L., Fundamentals of Fracture Mechanics, Nauka, Moscow, 1974.

20. Rabotnov, Y. N.,Creep Problems in Structural Members, North Holland Publishing Co., Amsterdam, 1969.

21. Chaboche, J. L., "Continuous Damage Mechanics - A Tool to Describe Phenomena Before Crack Initiation," Nuclear Engr. and Design, Vol. 64, 1981, pp. 233-247.

22. Lemaitre, J., and Chaboche, J. L., "A Non-Linear Model of Creep-Fatigue Damage Cumulation and Interaction," Mechanics of Visco-Plastic Media and Bodies, Jan Hult, Ed., Springer, Berlin, 1975, pp. 297-301.

23. Lemaitre, J., and Plumtree, A., "Application of Damage Concepts to Predict Creep-Fatigue Failures," ASME J. Eng. Materials and Technology, Vol. 101, 1979, pp. 284-292.

24. Lemaitre, J., and Chaboche, J. L., "Aspect Phenomeno-logique de la Rupture par Endommagement," Journal de Mecanique Appliquie, Vol. 2, No. 3, 1978, pp.317-363.

25. Manson, S. S., Freche, J. C., and Ensign, C. R., "Application of a Double Linear Damage Rule to Cumulative Fatigue," NASA TM D-3839, 1966.

26. Preist, R. H., and Ellison, E. G., "An Assessment of Life Analysis Techniques for Fatigue-Creep Situations," Res Mechanica, Vol. 4, 1982, pp. 127-150.

27. Majumdar, S.,and Maiya, P. S., "A Mechanistic Model for Time-Dependent Fatigue," ASME Journal of Engineering Materials and Technology, Vol. 102, Jan. 1980, pp.159-167.

28. Antolovich, S. D., and Jayaraman, N., "The Effect of Microstructure on the Fatigue Behavior of Ni Base Superalloys," Fatigue: Environment and Temperature Effects, J. J. Burke and V. Weiss, Eds., Plenum Press, N.Y., 1983, pp. 119-144.

29. TMF Workshop Abstracts, NASA LeRC, Nov. 15-16, 1984.

30. Woodford, D. A., "Creep Damage and the Remaining Life Concept," ASME J. Engr. Materials and Technology, Vol. 101, Oct. 1979, pp. 311-316.

31. Leckie, F. A., and Onat, E. T., "Tensorial Nature of Damage Measuring Internal Variables," Physical Non-Linearities in Structural Analysis, IUTAM, 1980, pp. 140-155.

32. Cailletaud, G., and Chaboche, J. L., "Macrscopic Description of the Microstructural Changes Induced by Varying Temperature: Example of IN 100 Behavior," ICM3 Cambridge, TP ONERA, 1979, p. 112.

33. Murakami, S., and Ohno, N., "A Continuum Theory of Creep and Creep Damage," Creep in Structures, IUTAM, 1980, pp. 422-444.

34. Ostergren, W. J., and Krempl, E., "A Uniaxial Damage Accumulation Law for Time-Varying Loading Including Creep-Fatigue Interaction," ASME Jour. of Pressure Vessel Tech., Vol. 101, 1979, pp. 118-124.

35. Harrison, G. F., and Tilly, G. P., "The Static and Cyclic Creep Properties of Three Forms of a Cast Nickel Alloy," Creep and Fatigue in Elevated Temperature Applications, International Conference of ASME, Phila. 1972, Vol. 1, 1975.

36. Lemaitre, J., "Damage Modelling for Prediction of Plastic or Creep-Fatigue Failure in Structures," Paper L5-1, SMIRT-5 Conference, Berlin, 1979.

37. Pedron, J. P., and Pineau, A., "Influence de L'Oxydation sur la Propagation des Fissures a Haute Temperature dans L'Alliage Inconel 718," Memoires et Etudes Scientifiques Revue de Metallurgie, Dec. 1983, pp. 665-674.

38. Cook, R. H., and Skelton, R. P., "Environment-Dependence of the Mechanical Properties of Metals at High Temperature," International Metallurgical Reviews, Vol. 19, 1974.

39. Smialek, J. L.,and Meier, G. H., "High-Temperature Oxidation," Superalloys II, Sims, C. T., Stoloff, N. S., and Hagel, W. C., Eds., John Wiley & Sons, N.Y., 1987, pp. 293-326.

40. Shahinian, P., "Fatigue Crack Growth Characteristics of High Temperature Alloys," Metals Technology, Nov. 1978, pp. 372-379.

41. Antolovich, S. D., and Campbell, J. E., "Fracture Properties of Superalloys," Superalloys Source Book, Matthew J. Donachie, Jr., Ed., American Society for Metals, Metals Park, Ohio, pp. 112-169.

42. Wareing, J., and Tomkins, B., "Creep-Fatigue Failure in High Temperature Alloys," Creep in Structures, 3rd IUTAM Symposium, Leicester, England, Sept. 1980, pp. 477-503.

43. Davidson, D. L., "A Model for Fatigue Crack Advance Based on Crack Tip Metallurgical and Mechanics Parameters," Acta Metall., Vol. 32, No. 5, 1984, pp. 707-714.

44. Carlson, R. L., and Saxena, A., "On the Analysis of Short Fatigue Cracks," International Journal of Fracture, Vol. 33 (1987), pp. R37-R39.

108

45. Diederich, D., Lerch, B., and Antolovich, S. D., "Observations of Low Cycle Fatigue and Fatigue Crack Propagation Substructures in Waspaloy," 8th Inter-American Conf. on Mat. Tech., San Juan, PR, June 1984, pp.7.1-7.6

46. Manson, S. S., "Interface between Fatigue, Creep and Fracture," International Journal of Fracture Mechanics, Vol. 2, No. 1, 1966, pp. 327-363.

47. Lerch, B. A., Jayaraman, N., and Antolovich, S. D., " A Study of Fatigue Damage Mechanisms in Waspaloy from 25 to 800°C," Materials Science and Engineering, Vol. 57 (1982), pp. L9-L12.

48. West, J. M., et al., Basic Corrosion and Oxidation, John Wiley & Sons, New York, 1986, pp. 179-184.

49. Chaboche, J. L., Policella, H., and Savalle, S., "Application of the Continuous Damage Approach to the Prediction of High Temperature Low-Cycle Fatigue," High Temperature Alloys for Gas Turbines, Liege, 1978, pp. 627-639.

50. Sims, C. T., Stoloff, N. S., and Hagel, W. C., Superalloys II, John Wiley & Sons, N.Y., 1987, p. 529.

Table 1 : Chemical Composition
of MAR-M 246

Element	Nominal * Composition	Material for this Study
Ni	Bal.	Bal.
W	10	9.13
Co	10	9.84
Cr	9	9.17
Al	5.5	5.17
Mo	2.5	2.38
Ti	1.5	1.47
Ta	1.5	1.33
Zr	0.05	0.02
B	0.015	<0.01
C		0.11
Fe		0.09
Mn		0.07
Cu		0.06
Si		0.03

All values are in weight percent.
* Ref. [50]

Table 2 : Test Matrices

a. Creep Tests

Specimen I.D.	Load (MPa)
G23	414
G21	300
G19	414 for half-life of G23 test then 300 until rupture

b. Tensile Tests

Specimen I.D.	Strain Rate	Maximum Allowable Strain
G13	10^{-1} sec^{-1}	10 %
G11	10^{-2}	10
G15	10^{-3}	5
G3	10^{-4}	10
G1	10^{-5}	10

c. Low Cycle Fatigue Tests

Specimen I.D.	Strain Rate	Strain Amplitude
G12	10^{-2} sec^{-1}	1.0 %
G5	10^{-2}	0.6
G22	10^{-2}	0.4
G16	10^{-3}	1.0
G18	10^{-3}	0.8
G6	10^{-3}	0.6
G7	10^{-3}	0.4
G14	10^{-3}	0.2
G10	10^{-4}	1.0
G8	10^{-4}	0.8
G4	10^{-4}	0.4

<div align="center">

Table 3 : Creep Test Data for MAR-M 246
in Air at 900°C

</div>

Specimen I.D.	Nominal Stress (MPa)	Nominal Strain to Failure (in/in)	Time to Failure (hours)	Steady-state Nominal Creep Strain Rate ($\dot{e}_{ss}$)	Monkman-Grant Strain ($\dot{e}_{ss} \cdot t_R$)
G23	413	0.0635	27.35	81.1×10^{-5} hr^{-1}	0.0222
S999-5 c.	413	0.0416	31.80	61.4×10^{-5}	0.0195
G21	300	0.0446	174.70	9.53×10^{-5}	0.0166
S999-4 c.	299	0.0492	300.30	7.25×10^{-5}	0.0218
G19 a.	415		13.80	54.6×10^{-5}	
G19 b.	299	0.0420	140.00	6.97×10^{-5}	

Notes : a. Test G19 was a step-stress sequence test; loaded to 415 MPa for one half of the time to rupture of test G23 and then,
       b. loaded until failure at the stress level of test G21
       c. After the initial creep analysis was completed, tests were performed to aquire an indication of the scatter in the constant stress creep test data.

Table 4 : Tensile Test Data for MAR-M 246
in Air at 900°C

Specimen I.D.	Strain Rate (sec^{-1})	Strain to Failure (%)	Young's Modulus (GPa) b.	0.2% Yield Strength (MPa)	U.T.S. (MPa) c.	K (MPa) d.	n e.
G13	10^{-1}	5.9	156.41	814	1051	1332.97	0.06991
G11	10^{-2}	7.2	161.00	851	950	1049.93	0.02666
G15	10^{-3}	a.	140.40	729	821	907.21	0.02589
G3	10^{-4}	4.3	146.62	611	706	885.83	0.05446
G1	10^{-5}	3.2	123.14	570	695	899.72	0.06186

NOTES : a. Specimen strained to 5% strain and then unloaded.
b. Average Young's modulus = 145.51 GPa.
c. Ultimate Tensile Strength
d. K = Strength coefficient
e. n = Strain hardening exponent

Table 5 : LCF Test Data for MAR-M 246
in Air at 900°C

Specimen I.D.	Strain Rate (sec^{-1})	Total Strain Amplitude (in/in)	Inelastic Strain Amplitude (in/in)	Stress Amplitude (MPa)	Reversals to Failure	Cycle Analyzed
G12	10^{-2}	0.010143	0.003163	1015.25	48	16
G5	10^{-2}	0.006387	0.001057	775.52	236 c.	64
G22 b.	10^{-2}	0.003801	0.000162	529.48	2576 c.	600
G16	10^{-3}	0.009824	0.003834	871.60	36 c.	8
G18	10^{-3}	0.007158	0.002227	717.51	90 c.	16
G6	10^{-3}	0.006058	0.001087	723.34	192 c.	32
G7	10^{-3}	0.003968	0.000142 a.	556.69	1166 c.	200
G14	10^{-3}	–	–	–	144724 d.	–
G10	10^{-4}	0.009967	0.004537	746.94	28	8
G8	10^{-4}	0.008121	0.002872	763.79	50 c.	8
G4	10^{-4}	0.004024	0.000514	510.83	748 c.	128

NOTES : a. The use of this small strain amplitude data point resulted in unreasonable values for the fatigue life constants. Therefore, it was not used in the determination of those values.
b. A tensile mean stress of 86.65 MPa was present in this test. Since this was on the order of only 10% of the yield stress, it was felt that a correction on the strain/life parameters was unnecessary.
c. Specimens failed outside the gage length of the extensometer.
d. After 143644 reversals, it became evident that this small strain amplitude (0.2%) test was in the HCF regime. The strain amplitude was changed to 0.4% and failure occurred 1080 reversals later.

Table 6 : Estimated Values of Constants for
Creep Damage Rate Equation

D_{INT}	B	$k(\sigma_{HI})$	$k(\sigma_{LOW})$
.05	2.43×10^{-18}	8.76 (11.53)*	8.74 (11.86)*
.07	3.43×10^{-18}	5.97 (7.87)	5.89 (8.11)
.10	4.98×10^{-18}	3.80 (5.11)	3.75 (5.27)
.12	6.05×10^{-18}	2.93 (4.03)	2.91 (4.16)
.15	7.70×10^{-18}	2.08 (2.95)	2.07 (3.06)
.17	8.82×10^{-18}	1.70 (2.45)	1.68 (2.54)
.20	10.55×10^{-18}	1.26 (1.89)	1.24 (1.96)

D_{INT} : Creep damage parameter.

B : Temperature dependent constant.

$k(\sigma_{HI})$: Stress-dependent constant for high stress level
creep test.

$k(\sigma_{LOW})$: Stress-dependent constant for low stress level
creep test.

NOTE: Values in parentheses are determined from the
solution of the continuum damage equations for
constant stress creep (equations 4.8 and 4.9) with
the B values given in the table. Values beside the
$k(\sigma_{HI})$ estimates are based on the 413 MPa creep test,
and those next to the $k(\sigma_{LOW})$ estimates are based on
the 300 MPa test.

Table 7 : Creep Characterization Constants

Constant		413 MPa Test	300 MPa Test	
$k(\sigma)$	:	5.11	4.72	
A	:	2.8×10^{-21}	2.4×10^{-21}	a.
n	:	6.66	6.66	
r	:	5.76	5.76	
B	:	5.51×10^{-18}	5.51×10^{-18}	b.
ν	:	3.9	3.9	

NOTES: a). Original calculation of A, based on
       n = 6.66 and equation (4.1), was 3.0×10^{-21}.
       b). Original estimate of B was 4.98×10^{-18}.

Table 8 : Coffin-Manson Fatigue Life Constants

Strain Rate (sec^{-1})	σ_f' (MPa)	b	ϵ_f' (in/in)	c
10^{-2}	1902.48	−0.1632	0.05963	−0.7492
10^{-3}	1314.17	−0.1212	0.05836	−0.7475
10^{-4}	1186.53	−0.1260	0.03879	−0.6029

σ_f' : Fatigue strength coefficient.

b   : Fatigue strength exponent.

ϵ_f' : Fatigue ductility coefficient.

c   : Fatigue ductility exponent.

Table 9 : Cyclic Constants for MAR-M246
Tested in Air at 900°C

a. Constants calculated using hysteresis loop shape :

Strain Rate	K'	n'
10^{-2} sec^{-1}	2016.04 MPa	0.1187
10^{-3}	2906.50	0.2290
10^{-4}	2231.98	0.2037

b. Constants calculated using hysteresis loop tips :

Strain Rate	K'	n'	
10^{-2} sec^{-1}	3505.67 MPa	0.2174	*
10^{-3}	1630.01	0.1219	*
10^{-4}	2194.27	0.1908	*

K' : Cyclic strength coefficient.

n' : Cyclic hardening exponent.

* NOTE: These calculations are based on a relatively small
number of hysteresis loop tips and, hence, this
procedure has a much lower confidence level than
using the hysteresis loop shapes.

Surfaces A,B,C, and D must be parallel within .001
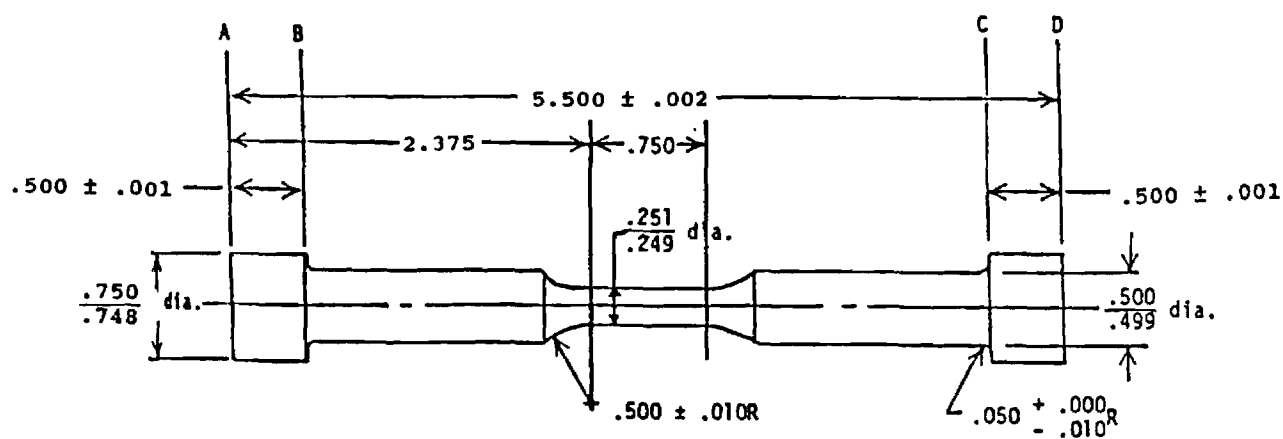
All dimensions are in inches.

Figure 1. Tensile and low cycle fatigue specimen dimensions.

INDUCTION COIL
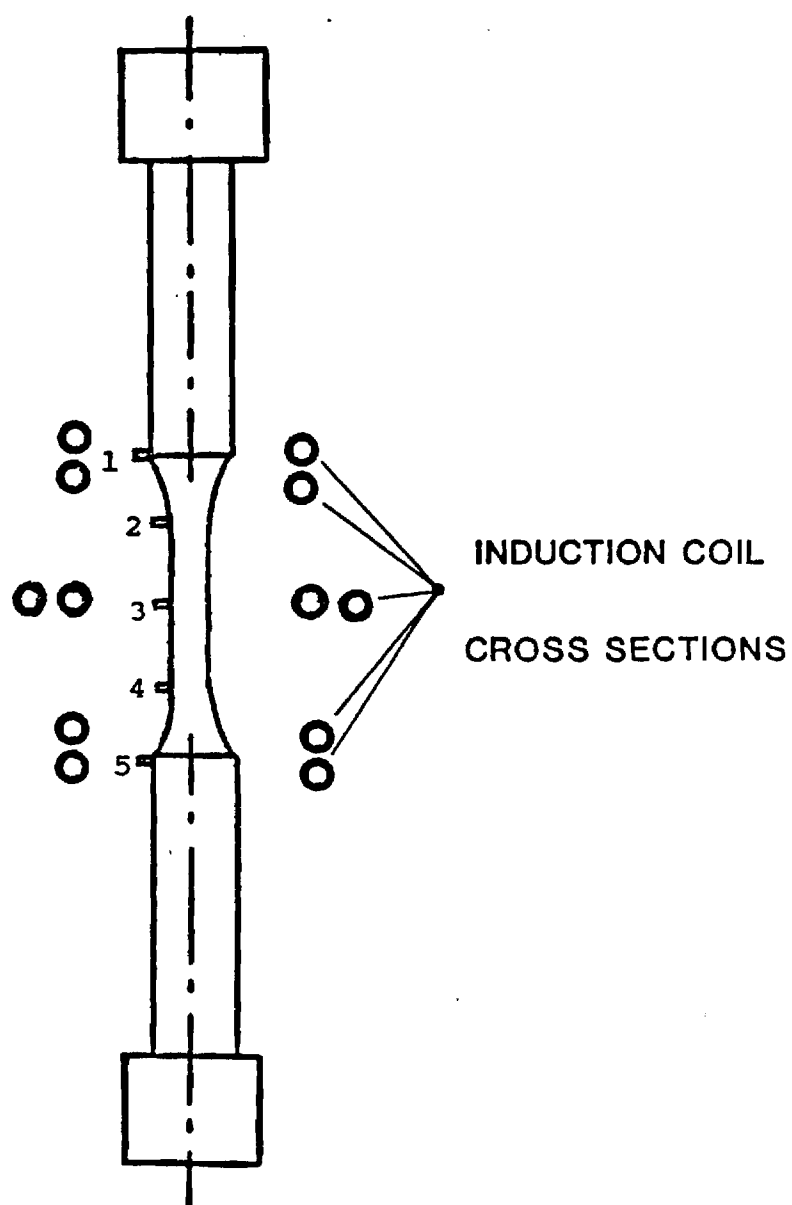
CROSS SECTIONS

Figure 2. Schematic of the calibration specimen for tensile and LCF testing in air at 900°C. Thermocouple #1 was used for control.
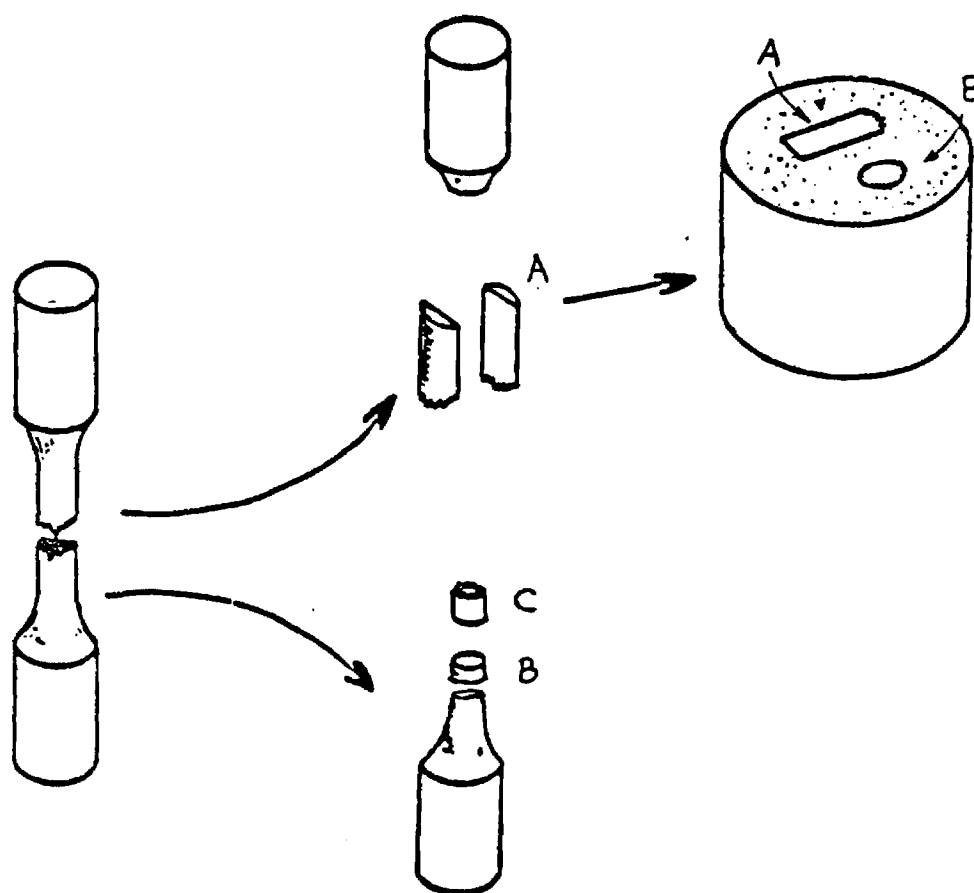
Figure 3. Schematic of sectioning techniques in preparation for optical observation (A and B) and electron microscopy (C). Optical segments were mounted in diallyl phthalate.

Nominal Creep Strain (in/in)
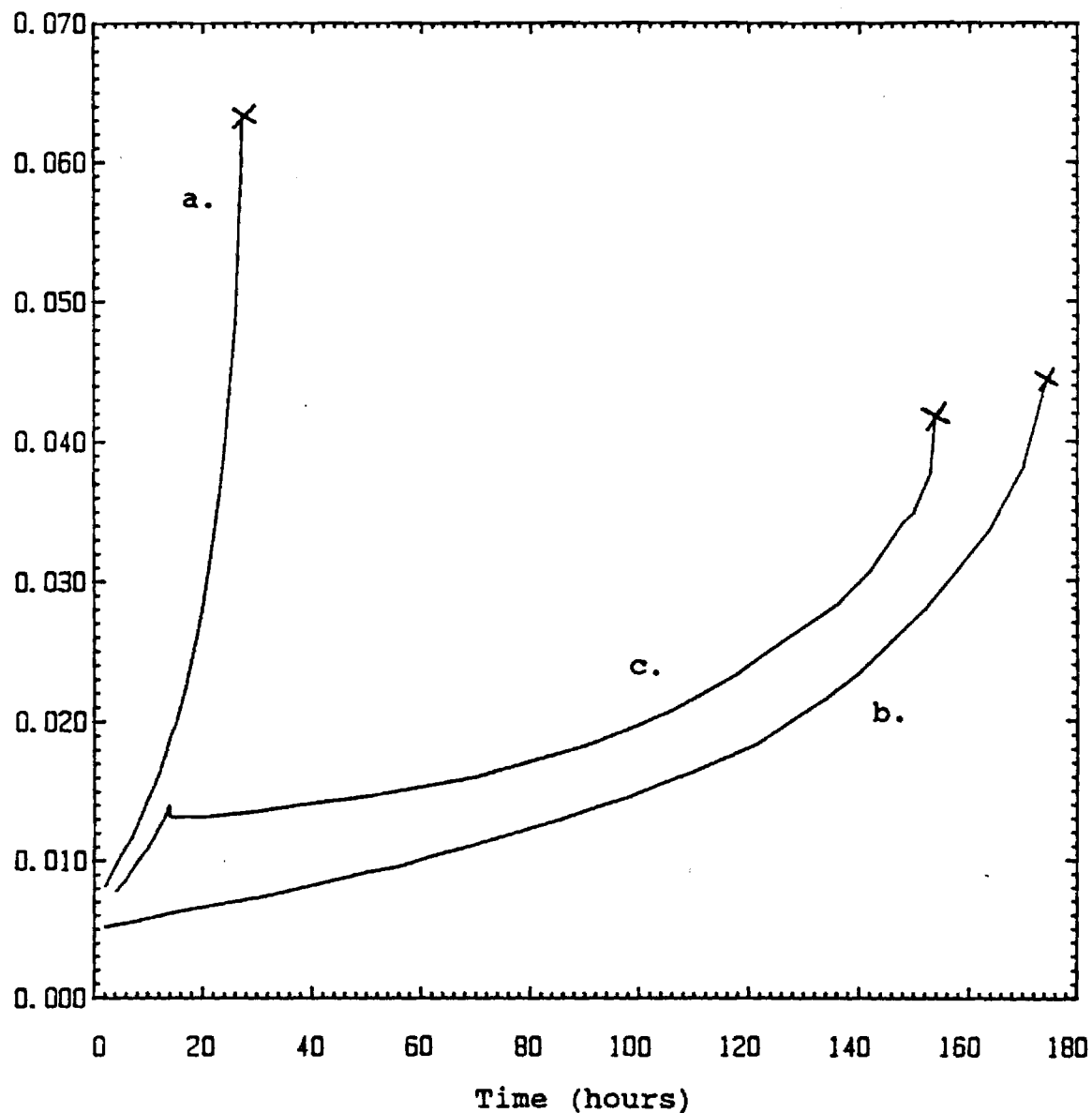
Figure 4. Nominal creep data for MAR-M 246 tested in
air at 900°C.
a). σ = 413 MPa   b). σ = 300 MPa
c). σ = 415 / 299 MPa step
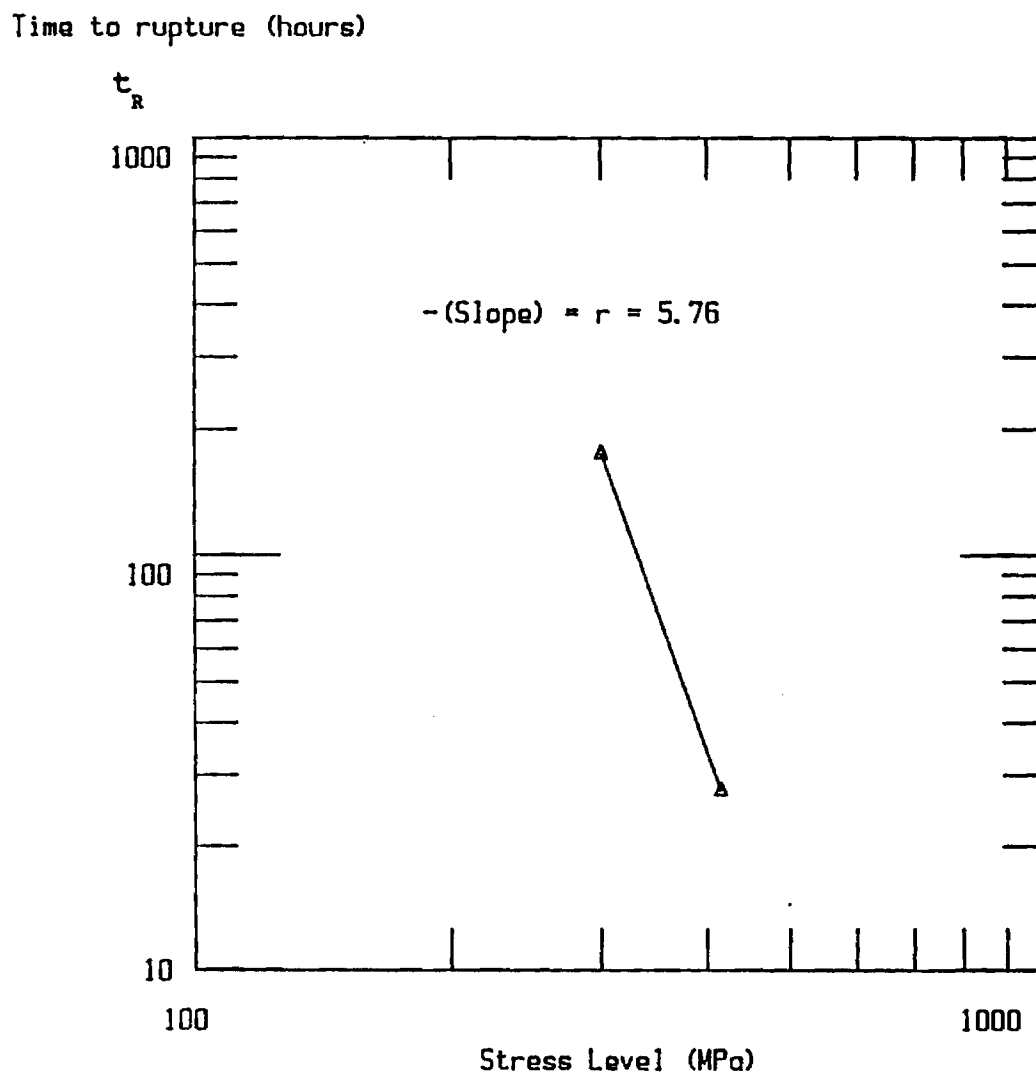
Figure 5. Determination of the creep damage constant r.

Nominal Creep Strain (in/in)
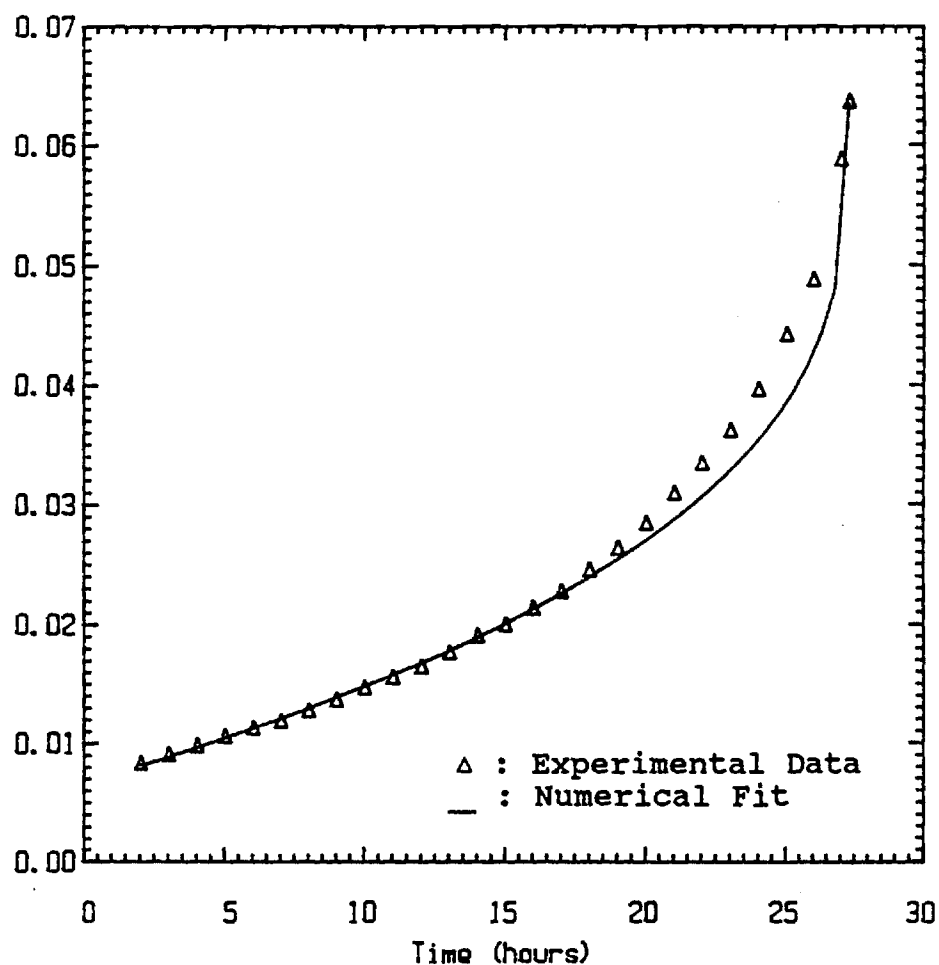
Figure 6. Numerical analysis of creep strain rate equation
versus experimental creep strain data for MAR-M 246
tested in air at 900°C under a stress of 413 MPa.

Nominal
Creep Strain (in/in)
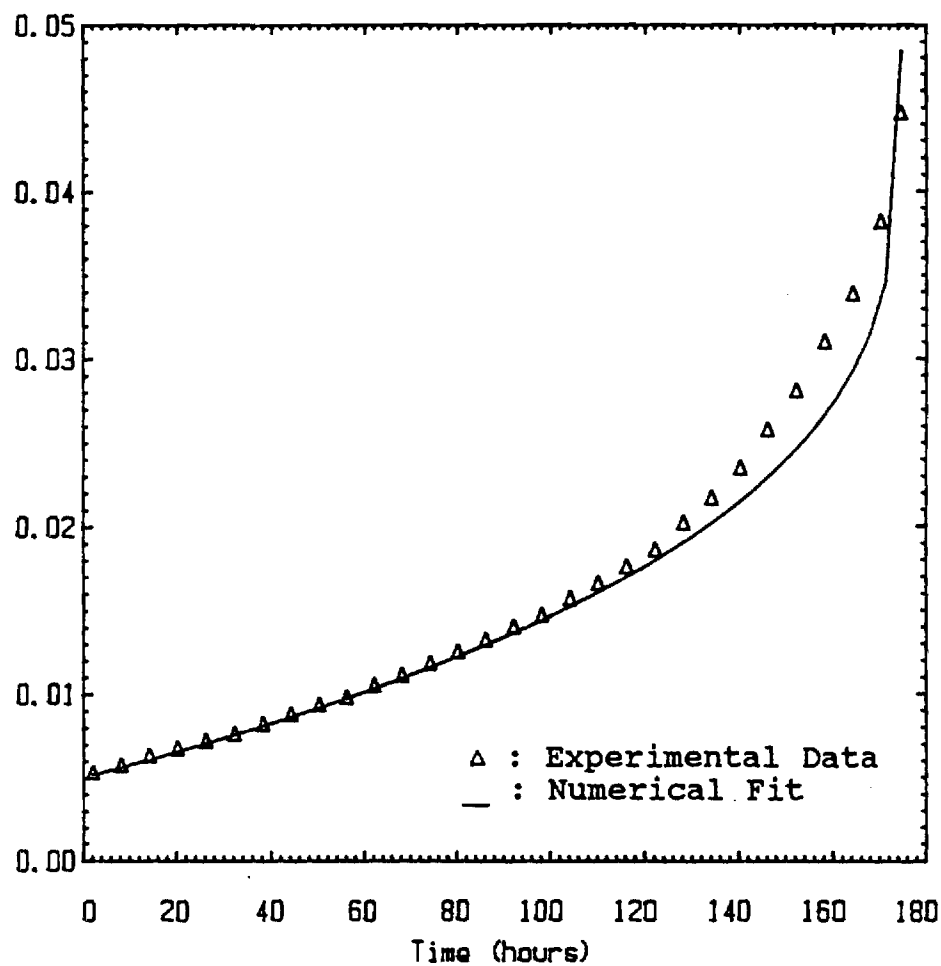
Figure 7. Numerical analysis of creep strain rate equation
versus experimental creep strain data for MAR-M 246
tested in air at 900°C under a stress of 300 MPa.
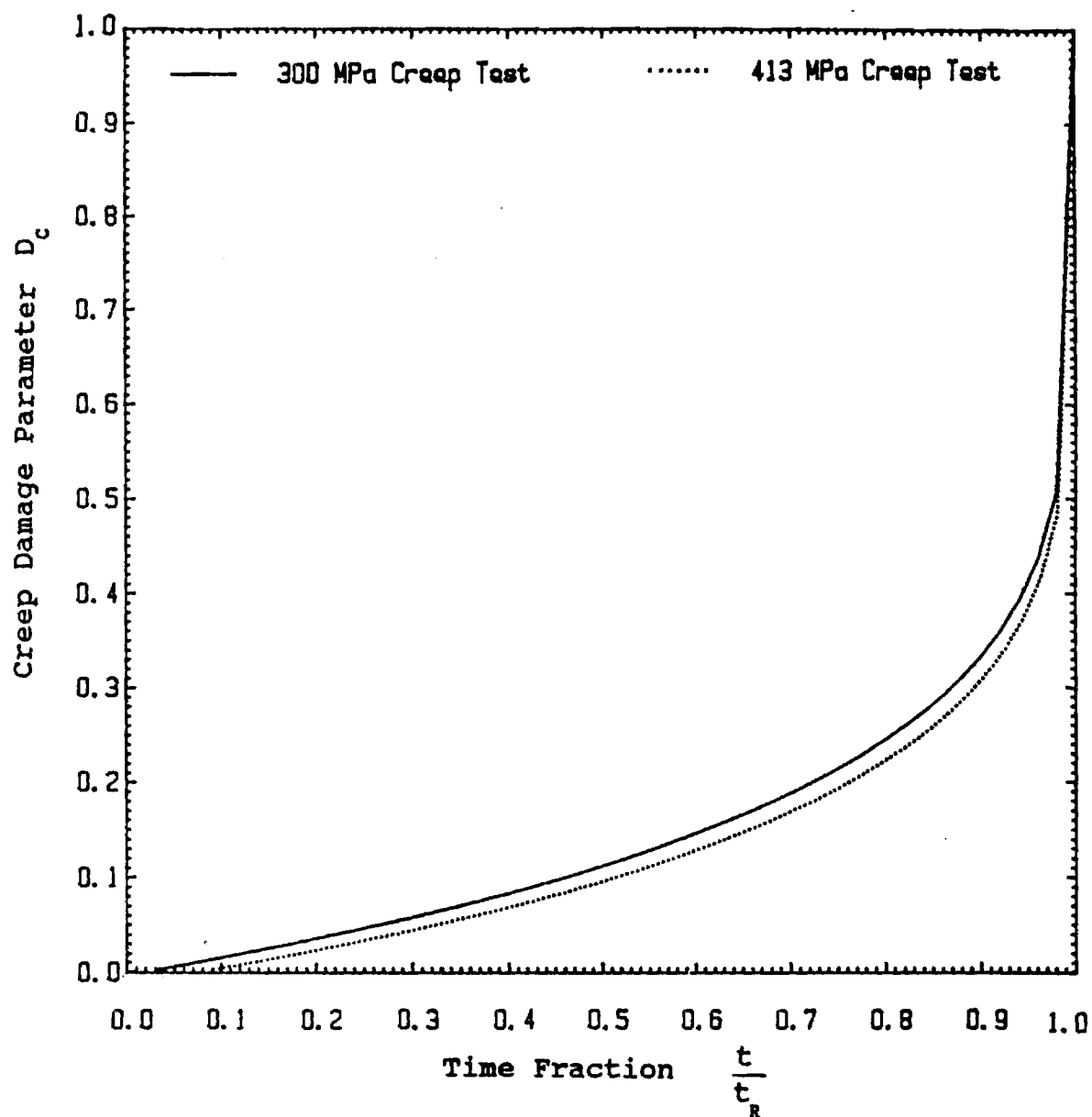
Figure 8. Creep damage parameter versus normalized time for
two constant-stress creep tests of MAR-M 246 in
air at 900°C.

STRESS   (MPa)
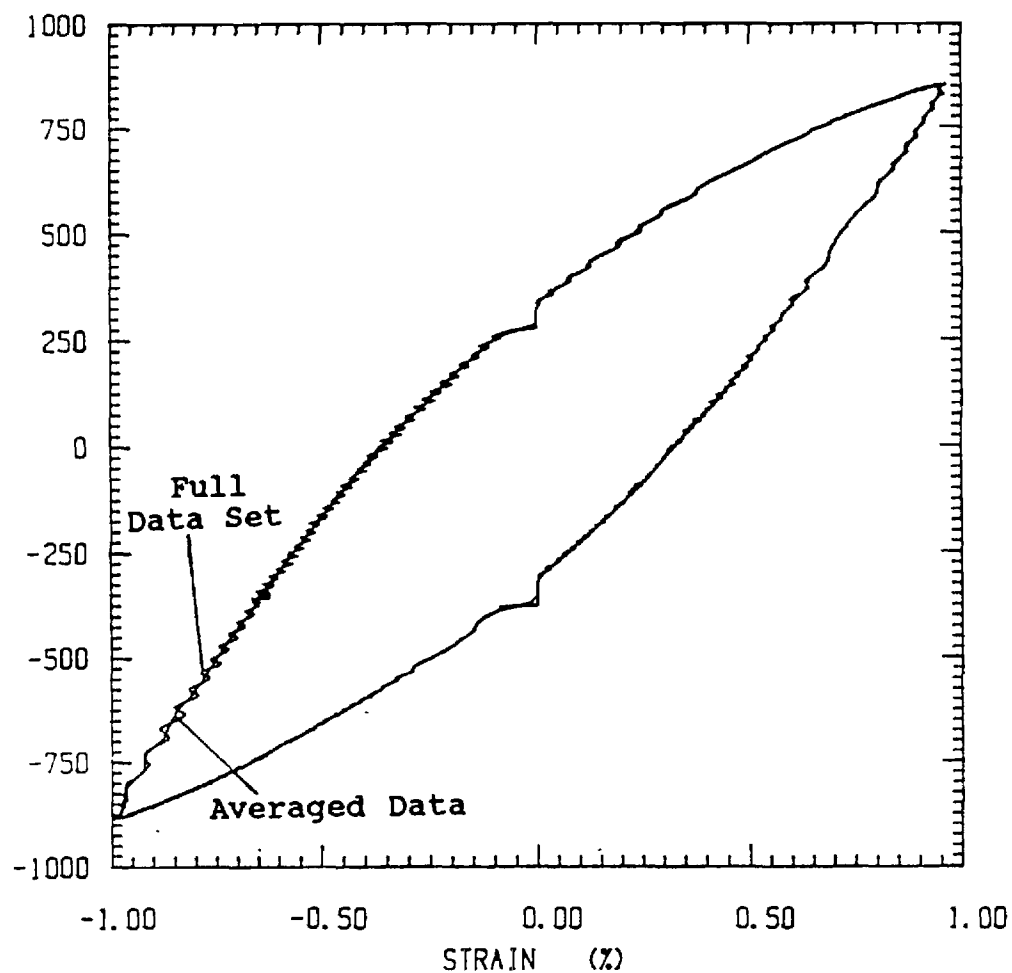
Figure 9. Hysteresis loop with 5-point averaging of the data compared with complete data set. Data is from a MAR-M 246 test in air at 900°C with a strain rate of 10^{-3} sec^{-1} and a strain amplitude of 1.0%.

STRESS   (MPa)
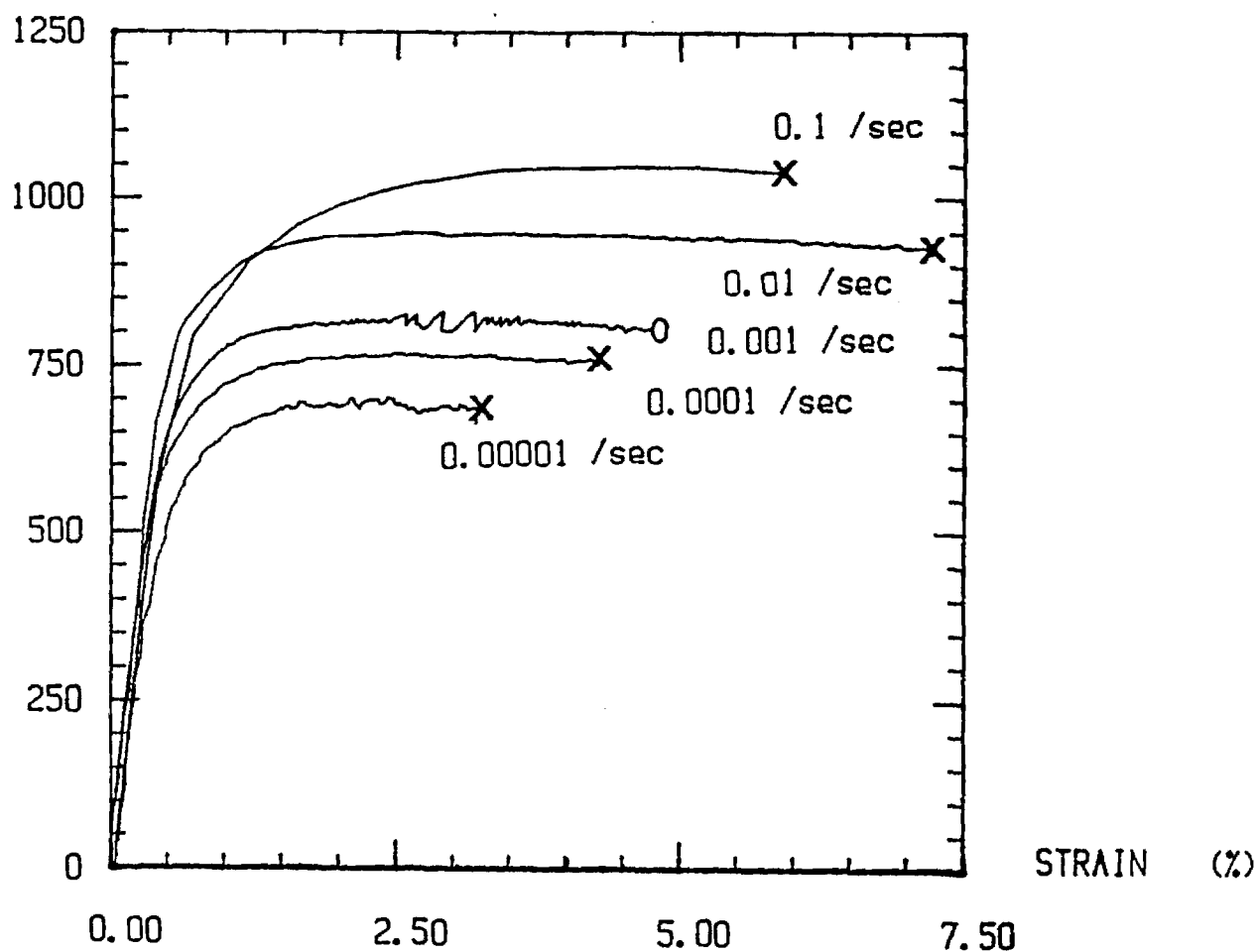
Figure 10. Tensile test data for MAR-M 246 tested in air at 900°C. Strain rates are as indicated.

STRESS (MPa)
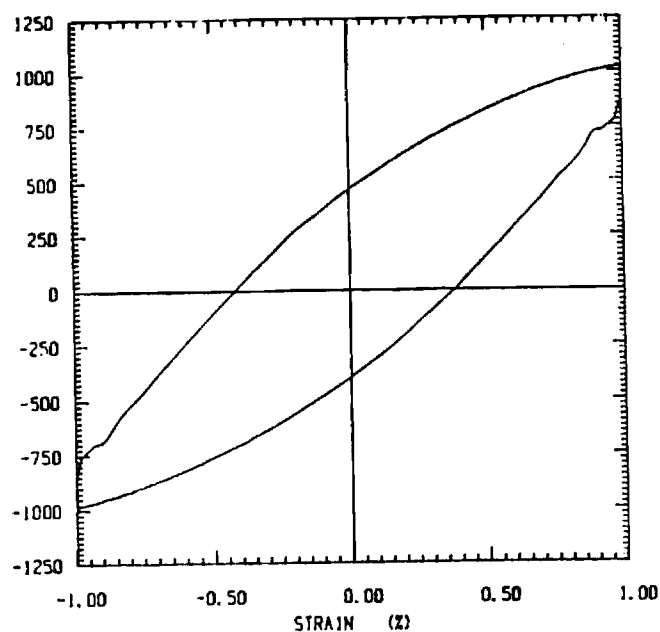
a.

STRESS (MPa)

b.
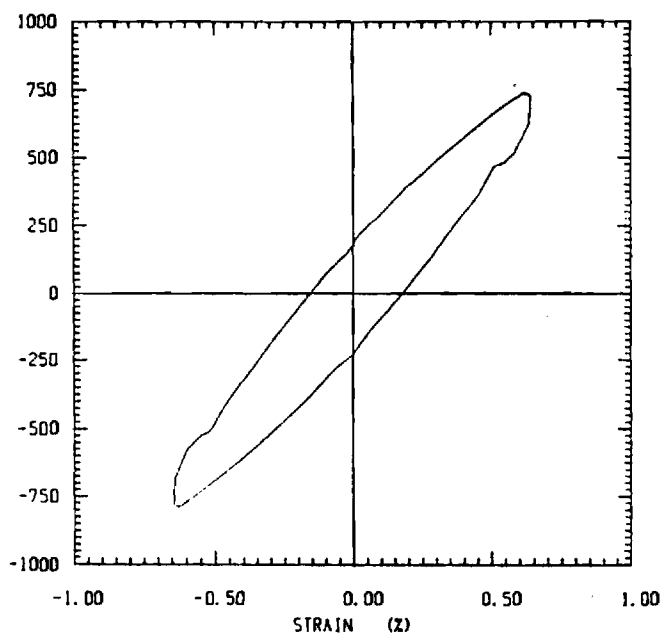
STRESS (MPa)

$\sigma_a = 86.65$ MPa
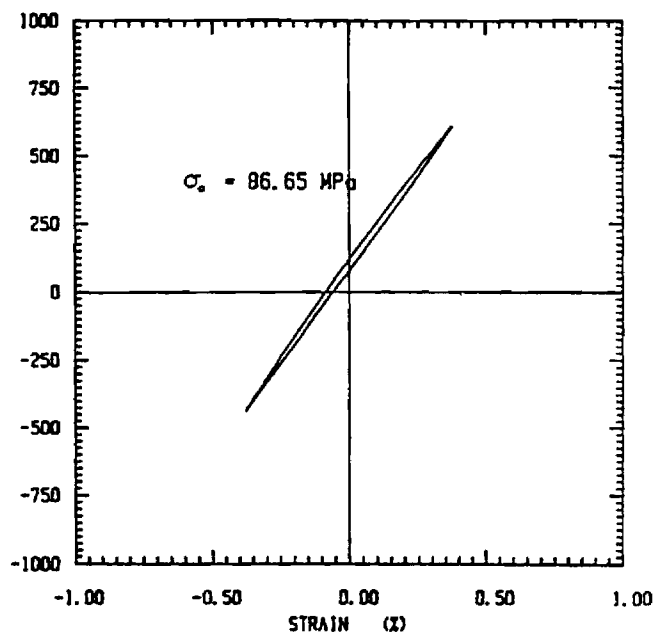
c.

Figure 11. Cyclically stable hysteresis loops for LCF tests at 900°C in air at a strain rate of 10^{-2} sec^{-1}. Strain amplitudes are :

a). 1.0%   b). 0.6%   c). 0.4%
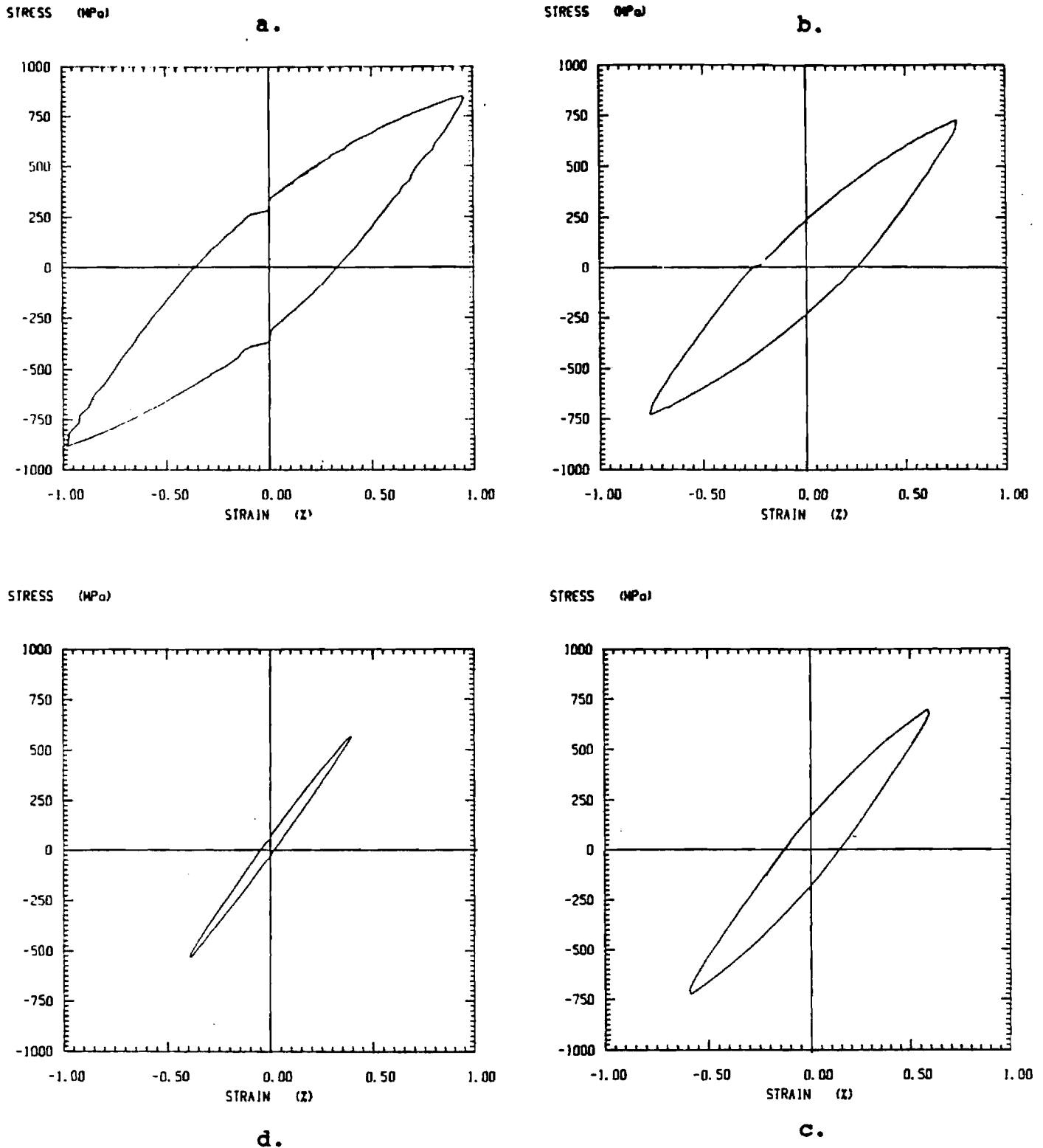
Figure 12. Cyclically stable hysteresis loops for LCF tests at 900°C in air at a strain rate if 10^{-3} sec^{-1}. Strain amplitudes are a). 1.0% b). 0.8% d). 0.4% c). 0.6%
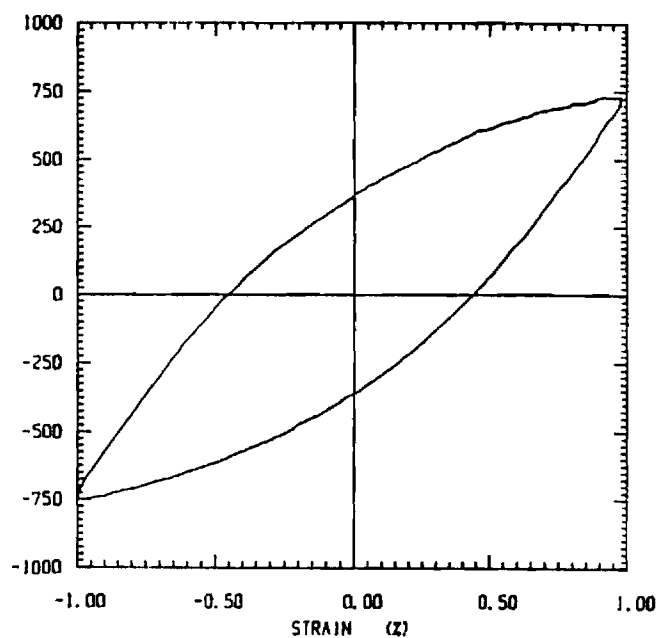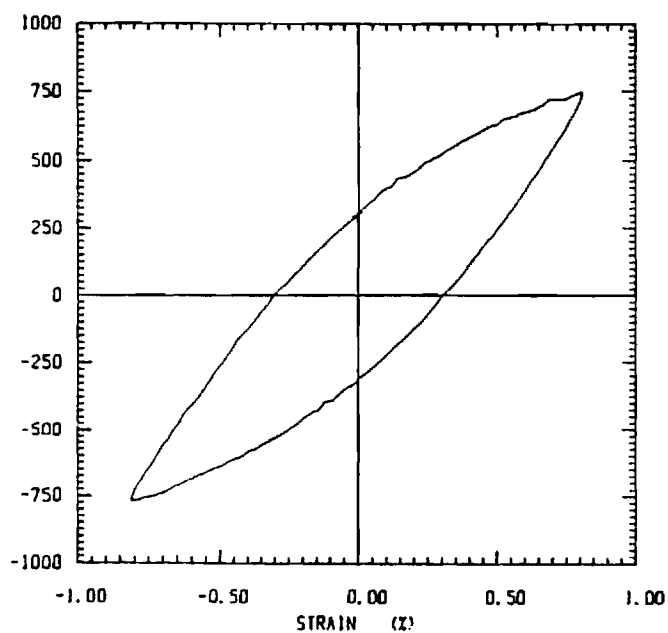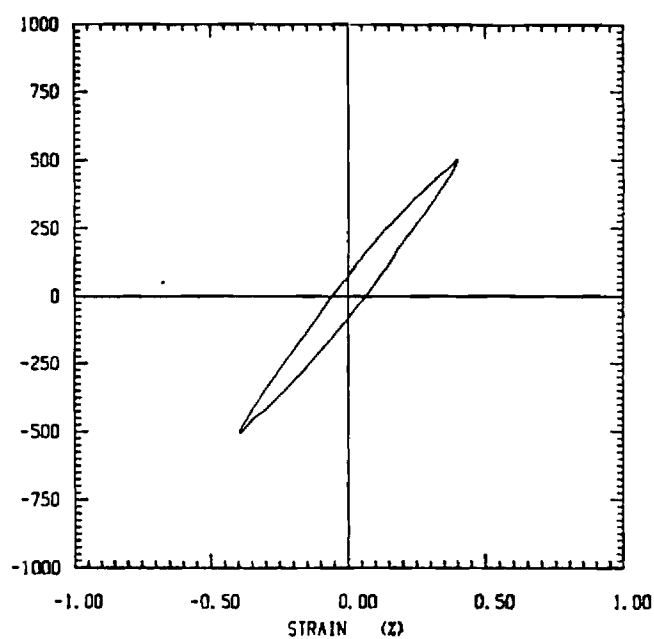
Figure 13. Cyclically stable hysteresis loops for LCF tests at 900°C in air at a strain rate of 10^{-4} sec^{-1}. Strain amplitudes are :
a). 1.0%   b).0.8%   c). 0.4%
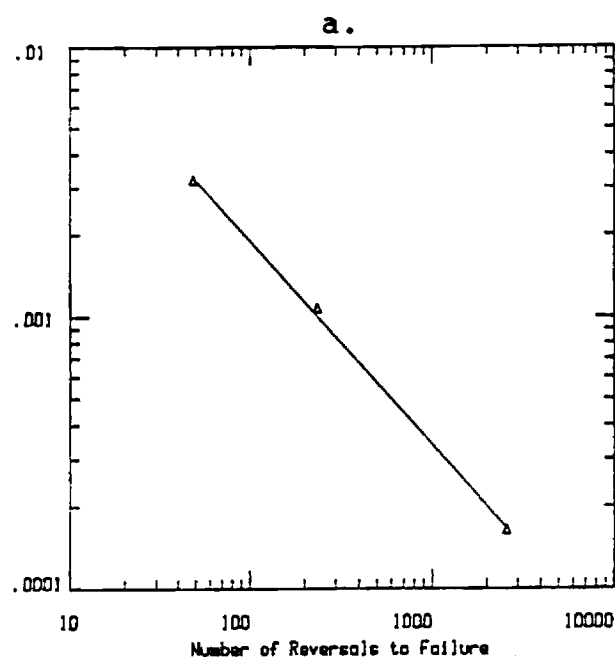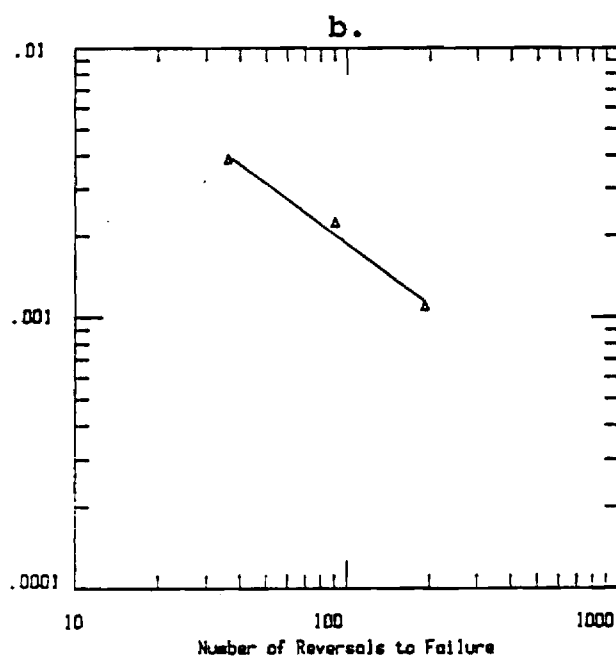
Inelastic Strain Amplitude (in/in)
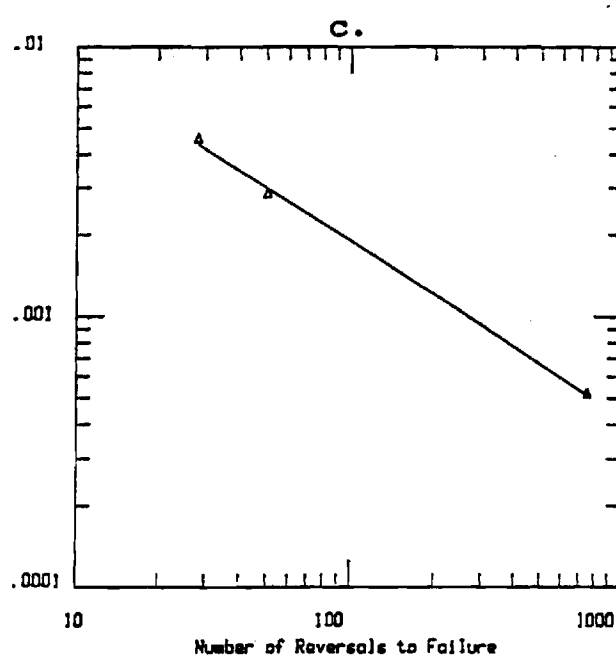
Figure 14. Inelastic strain amplitude versus number of reversals
to failure for MAR-M 246 tested in air at 900°C.
Strain amplitudes are:
a). 1.0% b). 0.8% c). 0.4%

Stress Amplitude (MPa)
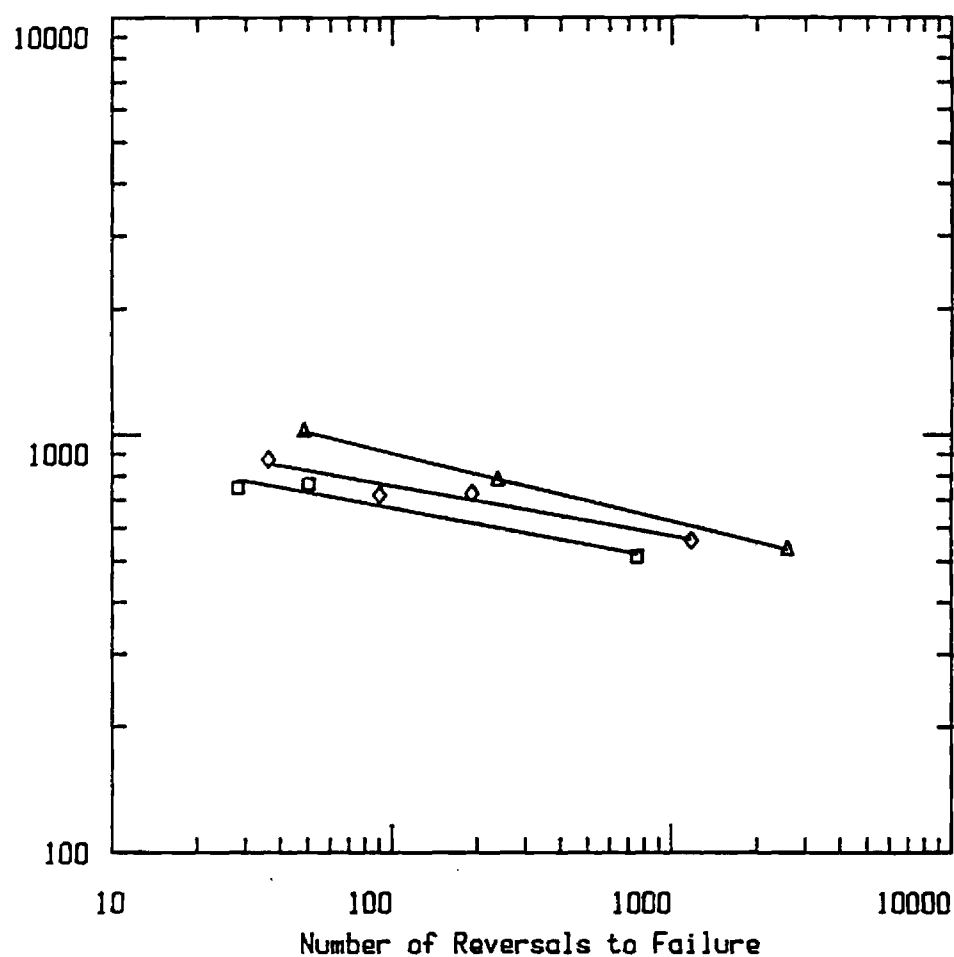
$$\triangle = 10^{-2} \text{ sec}^{-1} \text{ Strain Rate}$$
$$\diamond = 10^{-3} \text{ sec}^{-1} \text{ Strain Rate}$$
$$\square = 10^{-4} \text{ sec}^{-1} \text{ Strain Rate}$$

Figure 15. Stress amplitude versus number of reversals to failure for MAR-M 246 tested in air at 900°C.

Total Strain Amplitude (in/in)
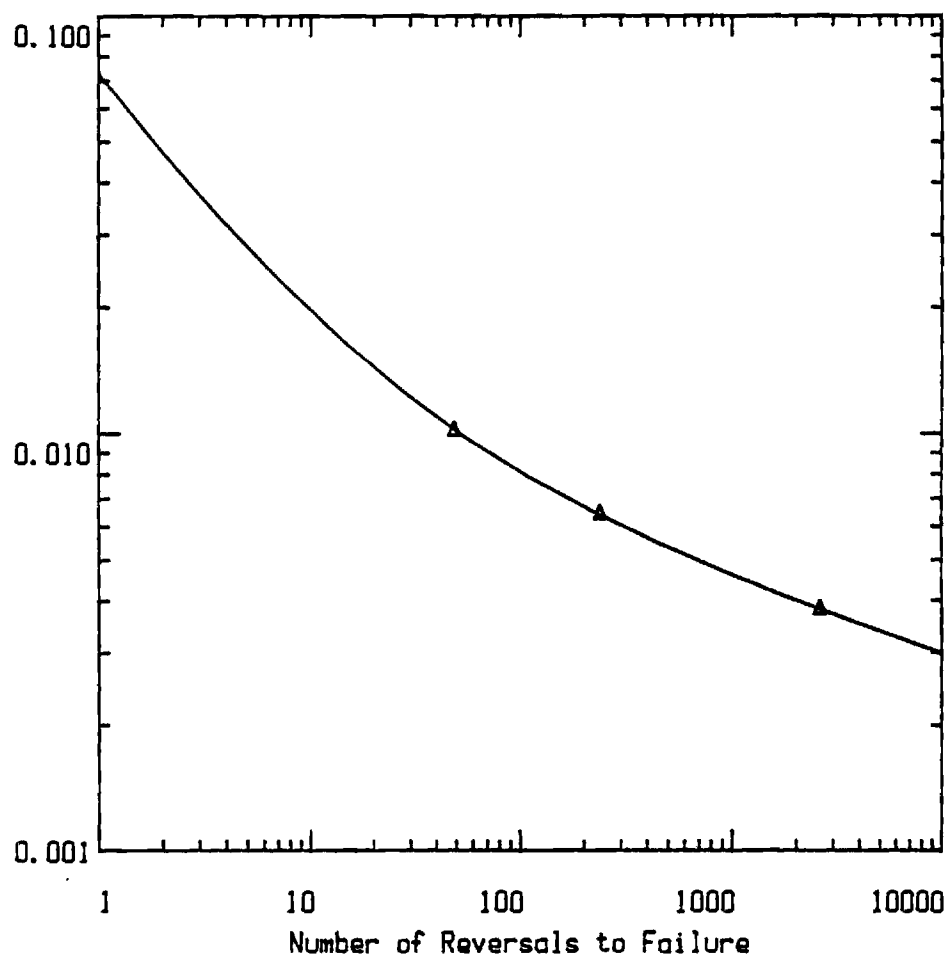
Δ : Total strain amplitude data points.
(Ref. Table 5)

Figure 16. Coffin-Manson strain-life curve for MAR-M 246 tested
in air at 900°C at a strain rate of 10^{-2} sec^{-1}.

Total Strain Amplitude (in/in)
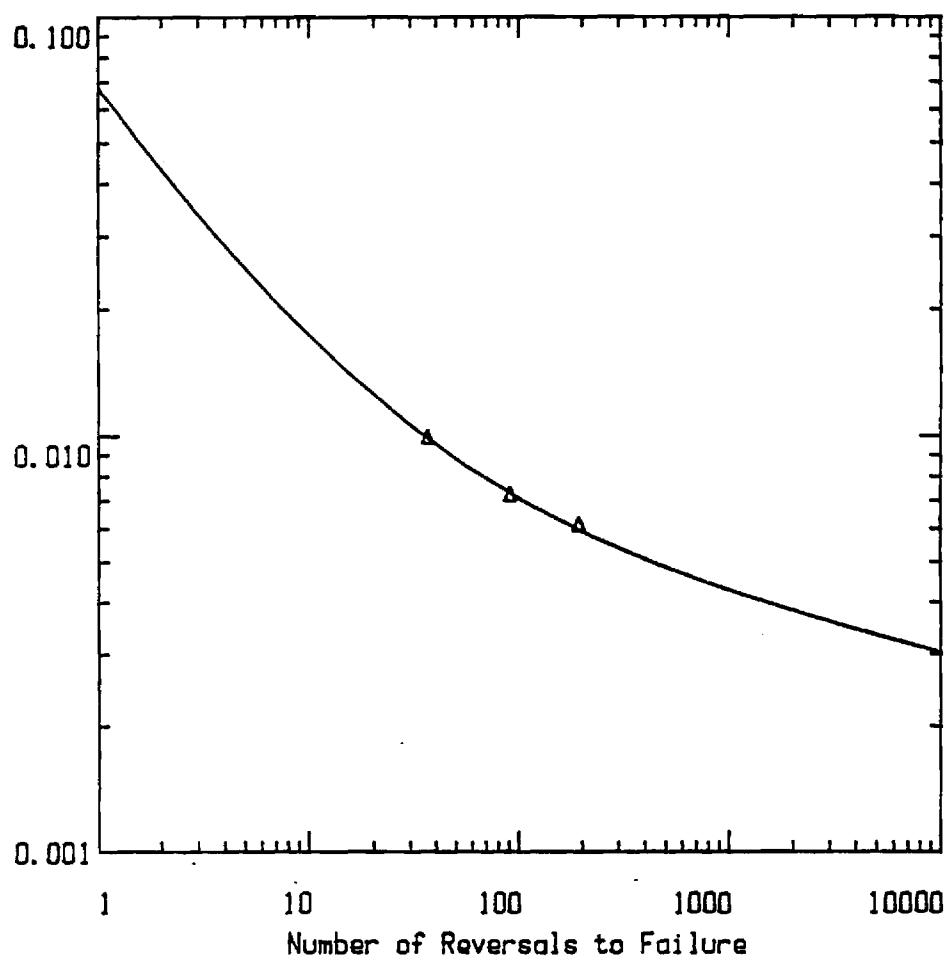
Δ : Total strain amplitude data points.
(Ref. Table 5)

Figure 17. Coffin-Manson strain-life curve for MAR-M 246 tested
in air at 900°C at a strain rate of 10^{-3} sec^{-1}.

Total Strain Amplitude (in/in)
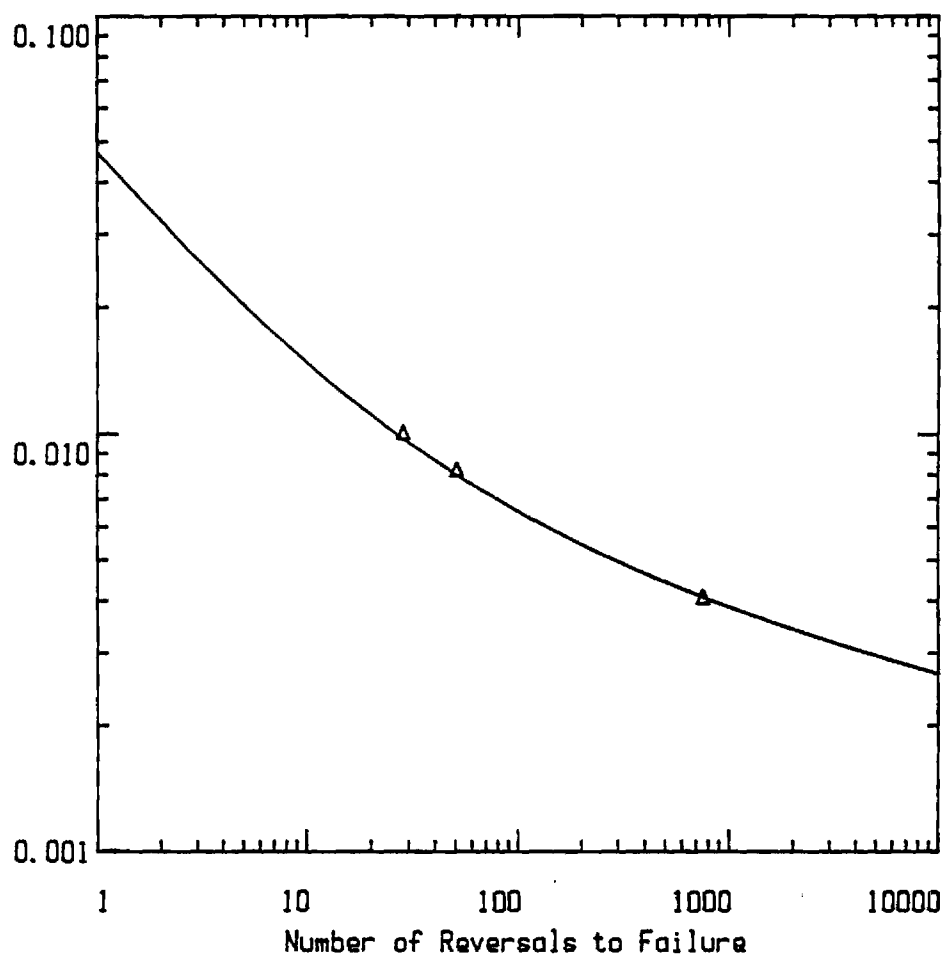
$\triangle$: Total strain amplitude data points.
(Ref. Table 5)

Figure 18. Coffin-Manson strain-life curve for MAR-M 246 tested in air at 900°C at a strain rate of 10^{-4} sec^{-1}.

Stress Amplitude (MPa)

a.

Inelastic Strain Amplitude (in/in)

Stress Amplitude (MPa)

b.
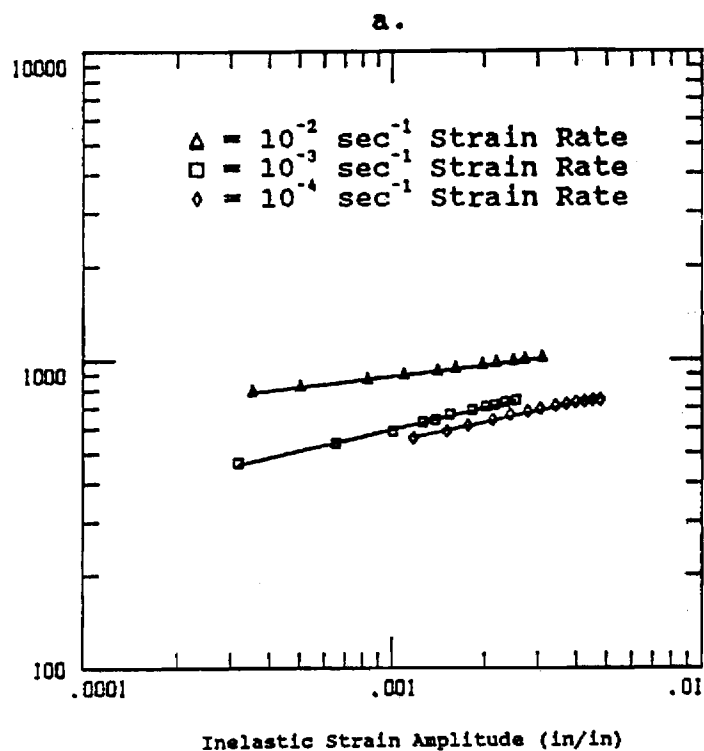
Inelastic Strain Amplitude (in/in)
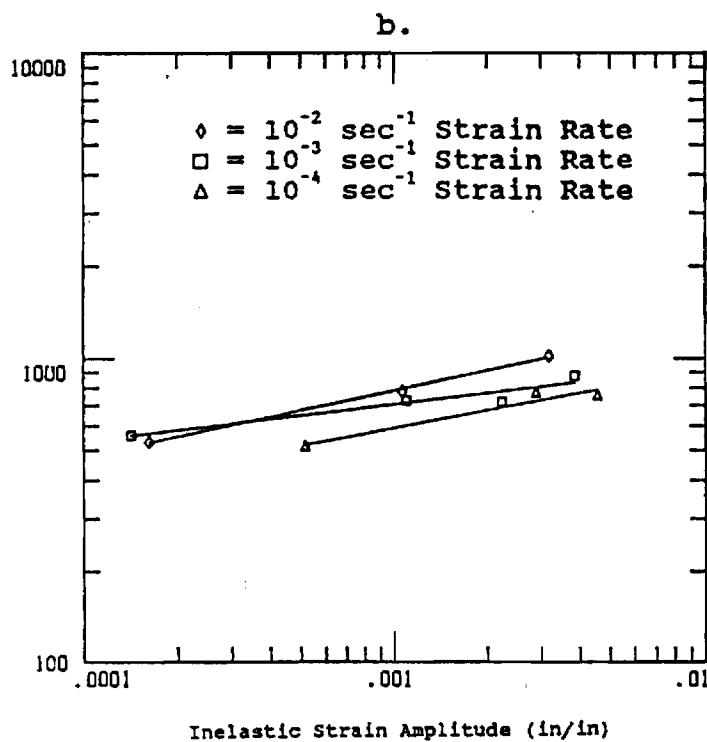
Figure 19. Determination of cyclic constants for MAR-M 246 tested
in air at 900°C using,
a.) hysteresis loop shape
b.) hysteresis loop tips.

Inelastic Strain Amplitude (in/in)

Figure 20. Inelastic strain amplitude versus time to failure
for MAR-M 246 tested in air at 900°C.

Strain Rate (sec^{-1})
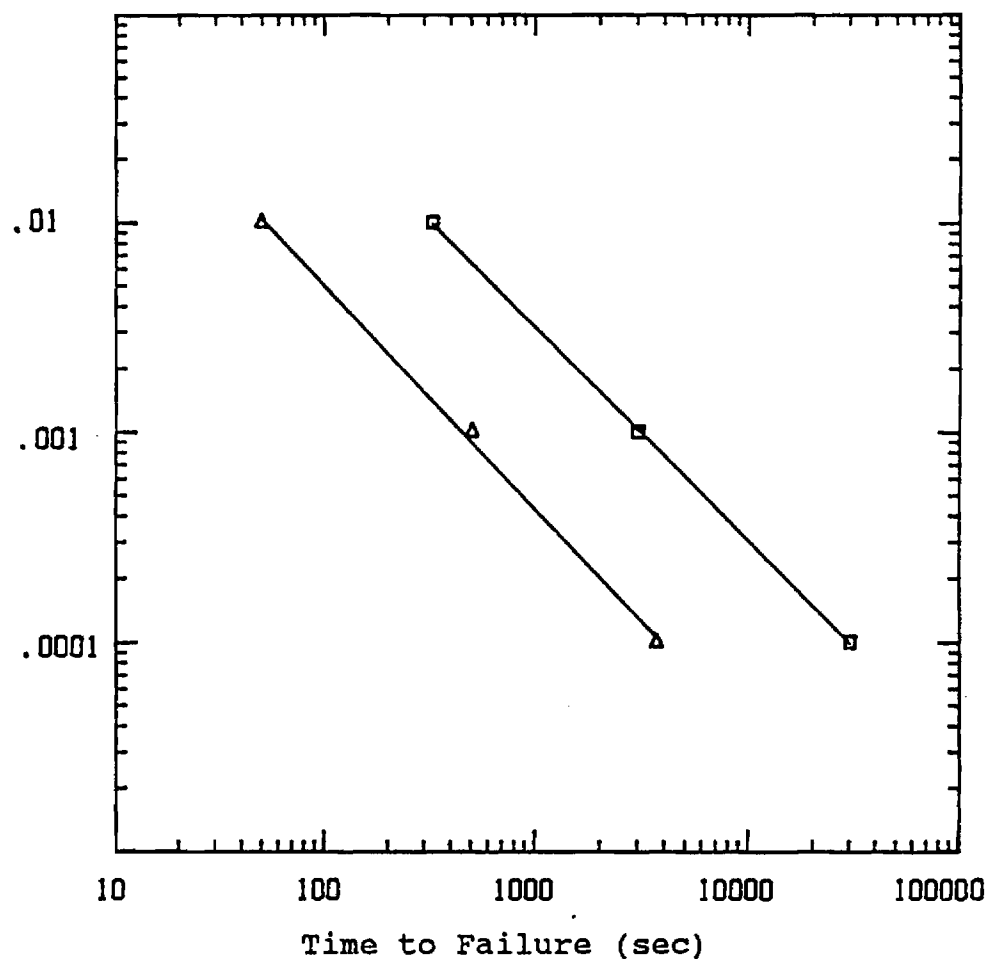
□ Inelastic Strain Amplitude = 0.0060 in/in , Slope = -1.06
△ Inelastic Strain Amplitude = 0.0009 in/in , Slope = -1.02

Figure 21. Strain rate versus time to failure for MAR-M 246
             tested in air at 900°C.

Stress Amplitude (MPa)

Slope = -0.19
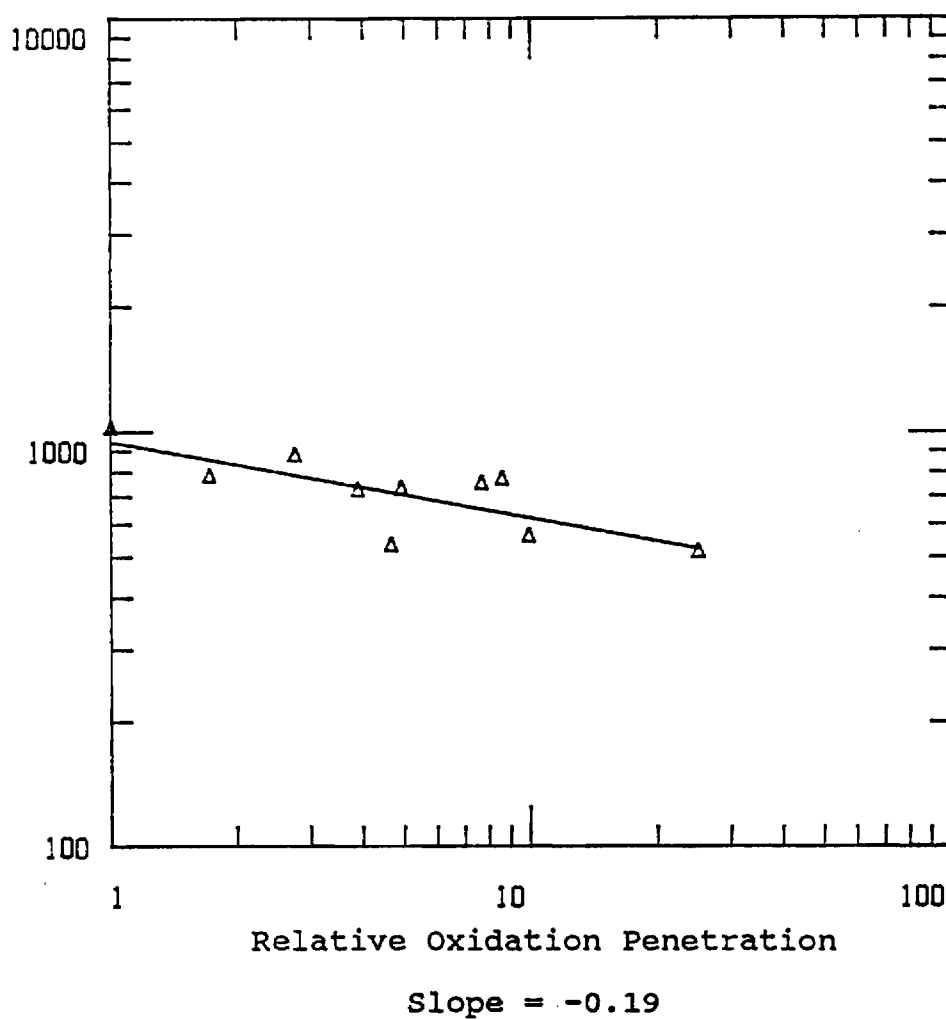
Figure 22. Stress amplitude versus relative oxidation depth
for MAR-M 246 in air at 900°C. Parabolic kinetics
assumed, as outlined by Antolovich [Ref. 28].

1.0 mm
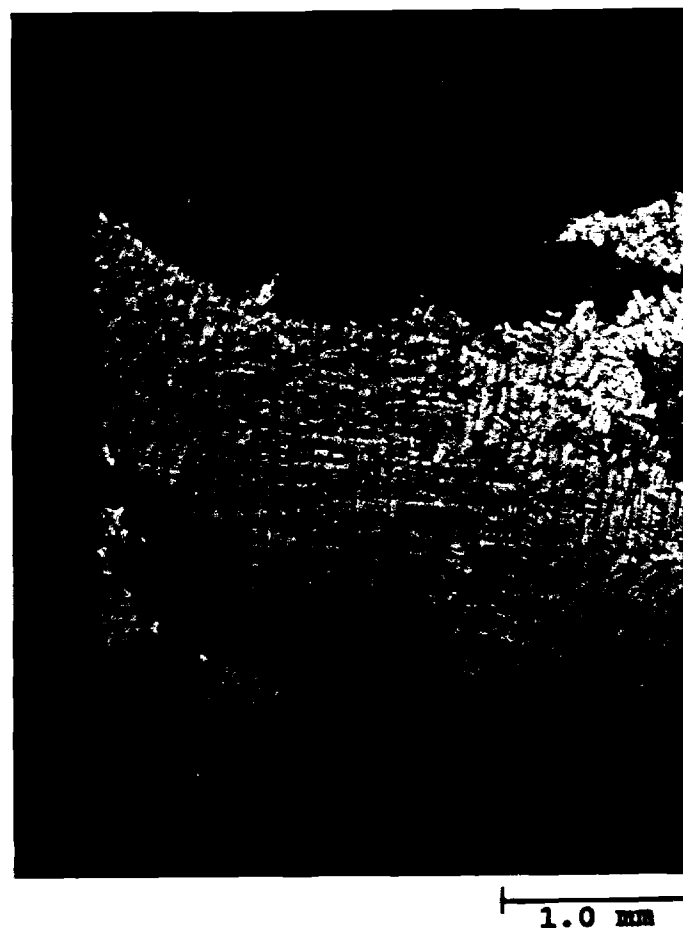
Figure 23. Longitudinal section through fracture surface of specimen G-12. Clearly seen is intergranular failure. Note aspect ratio and orientation of grains. TEST: $\dot{\epsilon} = 10^{-2}$ sec^{-1} $\Delta\epsilon/2 = 1.0\%$
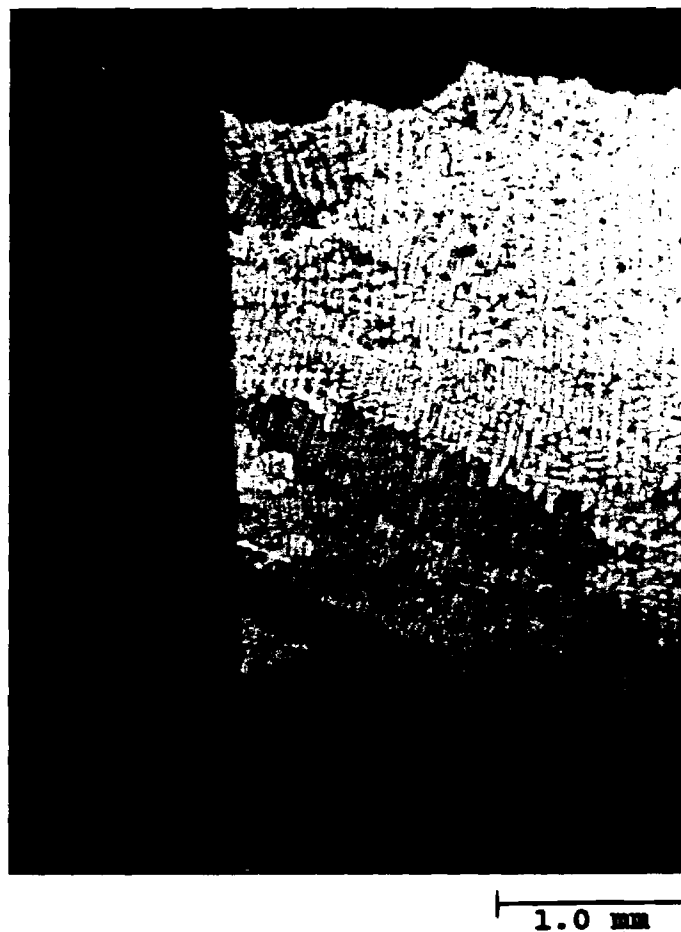
1.0 mm

Figure 24. Longitudinal section through fracture suface of
specimen G-8. Secondary cracking initiating at
grain boundaries is evident.
TEST: $\dot{\epsilon} = 10^{-4}$ sec^{-1} $\Delta\epsilon/2 = 0.8\%$

0.2 mm

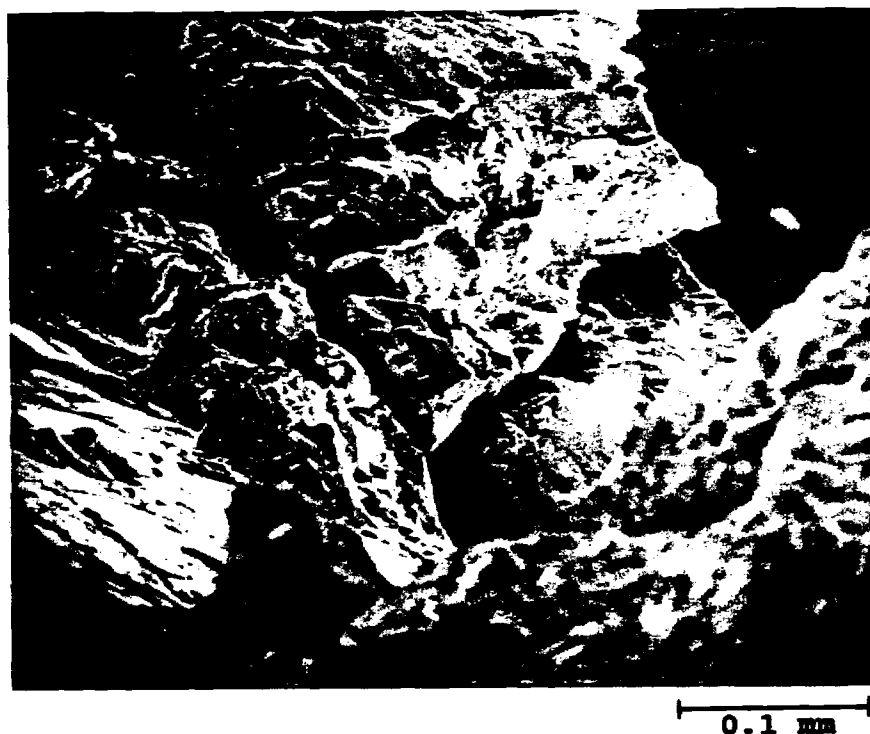Figure 25. Detail of secondary cracking of specimen G-8
(Ref. Figure 24)

0.1 mm

Figure 26. SEM micrograph of fracture surface of specimen
G-12. Grain dislocation is shown near the edge
of the fracture surface. Note the intergranular
failure.
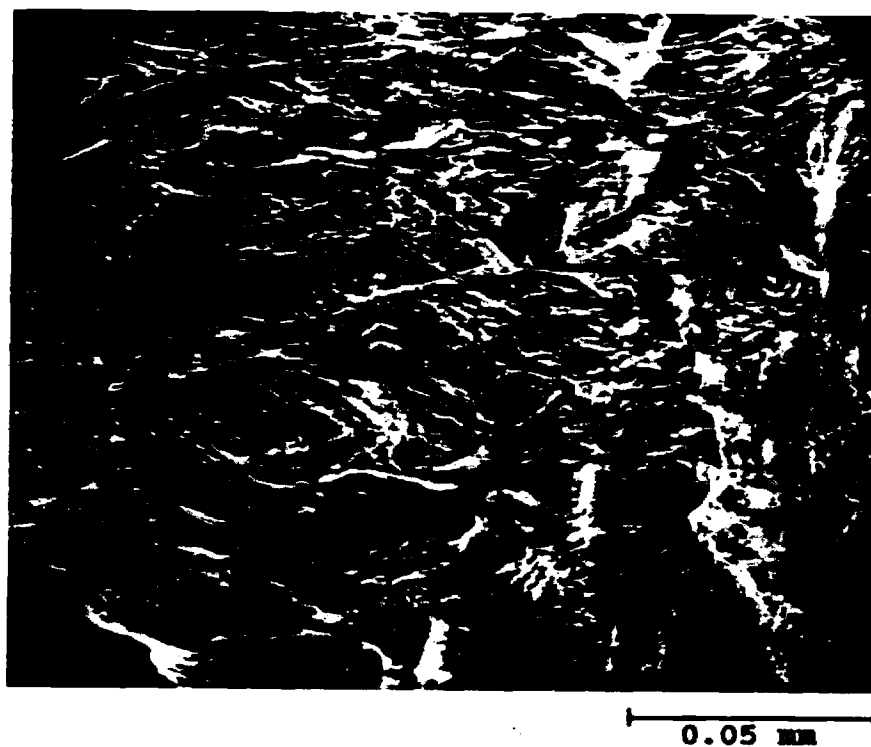TEST PARAMETERS: $\dot{\epsilon} = 10^{-2}$ sec^{-1} $\Delta\epsilon/2 = 1.0\%$

0.05 mm

Figure 27. SEM micrograph of fracture surface of specimen
G-4. Surface is planar with wave fronts of
time-dependent deformation evident.
TEST PARAMETERS: $\dot{\epsilon} = 10^{-4}$ sec^{-1} $\Delta\epsilon/2 = 0.4\%$

0.05 mm

Figure 28. SEM micrograph of secondary cracking and
intense slip band traces along specimen G12
gage section just below the fracture surface.
TEST PARAMETERS: $\dot{\epsilon} = 10^{-2}$ sec^{-1} $\Delta\epsilon/2 = 1.0\%$
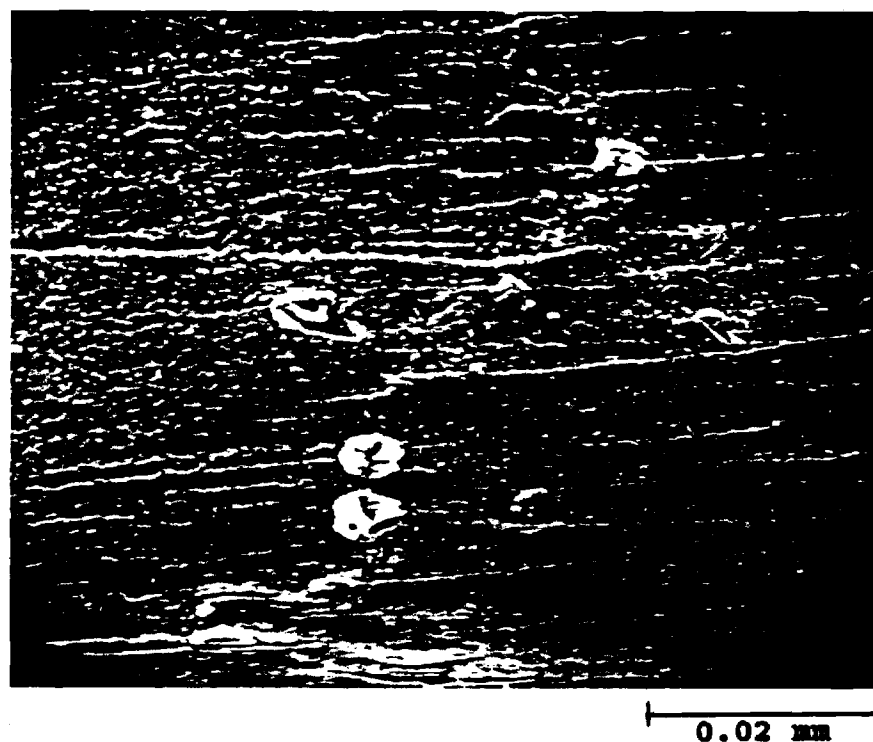
0.02 mm

Figure 29. SEM microgaph of grain boundary (verticle) with
intersecting slip bands (horizontal) on
specimen G8.
TEST PARAMETERS: $\dot{\varepsilon} = 10^{-4}$ sec^{-1} $\Delta\varepsilon/2 = 1.0\%$

0.05 mm

Figure 30. SEM micrograph of specimen G4. Secondary crack
along grain boundary at a triple point. Note
fracture surface at top of photograph.
TEST PARAMETERS: $\dot{\epsilon} = 10^{-4}$ sec^{-1} $\Delta\epsilon/2 = 0.4\%$
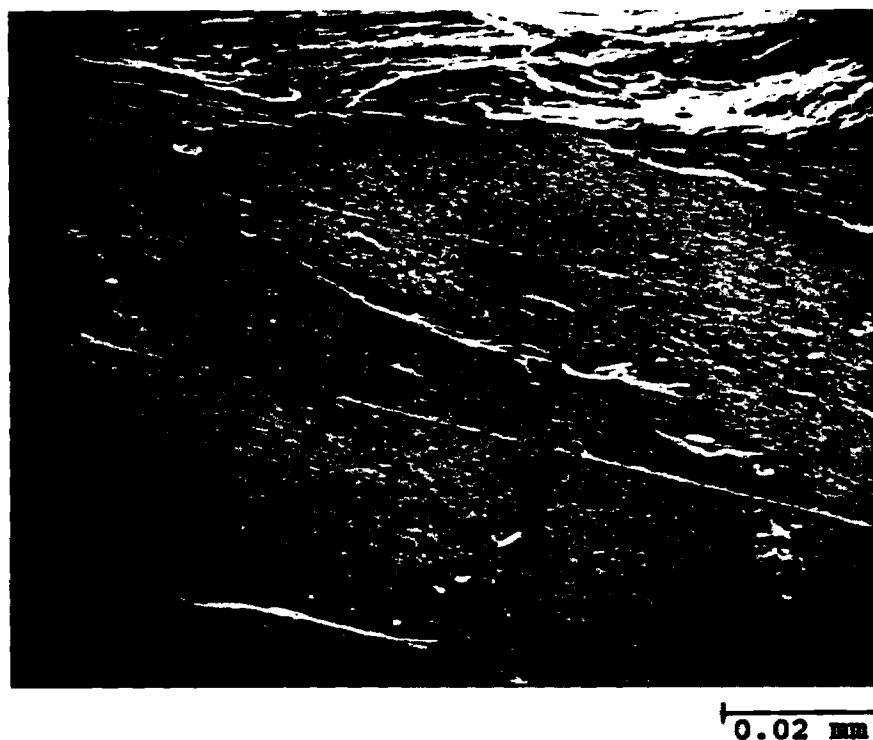
0.02 mm

Figure 31. SEM micrograph of gage section of specimen
G22. Secondary cracking initiated at grain
boundaries. A relatively low intensity of slip
bands present.
TEST PARAMETERS: $\dot{\epsilon} = 10^{-2}$ sec^{-1} $\Delta\epsilon/2 = 0.4\%$